SYNTHESIS OF OLIGO(P-PHENYLENE VINYLENE)S AND FUNCTIONALIZATION OF SI(100) AND/OR SI(111) SURFACES WITH OLIGO(P-PHENYLENE VINYLENE)S

by

CHIVIN SUN

A dissertation submitted to the Graduate Faculty in Chemistry in partial fulfillment of the requirements for the degree of Doctor of Philosophy, The City University of New York

2009

This manuscript has been read and accepted for the
Graduate Faculty in Chemistry in satisfaction of the
dissertation requirement for the degree of Doctor of Philosophy.

Prof. Ralf M. Peetz

Date	Chair of Examining Committee

Prof. Mahesh K. Lakshman

Date	Executive Officer

Prof. Shi Jin

Prof. Glen R. Kowach

Prof. Ralf M. Peetz
Supervision Committee

THE CITY UNIVERSITY OF NEW YORK

Abstract

SYNTHESIS OF OLIGO(P-PHENYLENE VINYLENE)S AND FUNCTIONALIZATION OF SI(100) AND/OR SI(111) SURFACES WITH OLIGO(P-PHENYLENE VINYLENE)S.

by

Chivin Sun

Adviser: Professor Ralf M. Peetz

This doctoral thesis focuses firstly on the step-wise synthesis of a library of rigid-rod-type conjugated difunctional oligo(*p*-phenylene vinylene)s (OPVs) with varying chain lengths of the main chain and side chain substitution, i.e., monomer, dimer, and trimer units with chain end - terminal alcohol, aldehyde, vinyl, and alkyne functionality. All oligomers are soluble and show trans configuration at the internal vinylene bonds. The solublizing side-chains are of the alkyloxy type, i.e. heptyloxy ($-OC_7H_{15}$), butyloxy ($-OC_4H_9$), and methyloxy ($-OCH_3$). All OPVs were characterized by means of ATR-FTIR, ^{1}H-NMR (200 or 600 MHz) and ^{13}C-NMR (50 or 150 MHz), 2D-NMR (HMBC, HSQC experiments), and optical spectroscopy.

In subsequent steps, the OPVs were used as “building blocks”. One application involved using a Cu(1)-catalyzed [3+2] Huisgen “click” cycloaddition to connect biotin ligands to both ends of the OPV, using spacer chains of varying length, consisting of oligo(ethylene glycol). Combining the valuable electro-optical properties of conjugated organic molecules with the biological recognition capability of biotin, the latter can be placed at variable distances via choosing an

appropriate length of the hydrophilic spacer, which also serves to regulate the binding capabilities of the two terminal biotin units. To demonstrate this binding potential, networks were formed with streptavidin-coated quantum dots. The synthetic conditions are presented, together with representative optimizations of the key reactions. The organic compounds were analyzed by means of ATR-FTIR, ^{1}H-NMR (200 or 600 MHz), ^{13}C-NMR (50 or 150 MHz), 2D-NMR (HMBC, HMQC experiments), MS (ESI or MALDI-TOF), and optical spectroscopy. Networks were imaged with TEM.

Another application involved templated grafting of the rigid-rod-type OPVs to flat surfaces of Si(100) and Si(111) via covalent Si(100)/Si(111)-O-C or Si(100)/Si(111)-C bonds. OPVs with terminal hydroxide (–OH), aldehyde (-CHO), alkyne (-C≡CH), and vinyl (-CH=CH_2) functionalities were used.

One approach involved the reaction of –OH, –CHO, and –CH=CH_2 functional OPVs with Si(100)/Si(111)-H and/or Si(100)/Si(111)-Cl functionalized surfaces. Subsequent reaction of resulting the Si(100)/Si(111)-OPV-OH surfaces with p-tolyl isocyanate produced urethane containing monolayers in a "click like" approach. The monolayers were characterized by means of XPS, ATR-FTIR, AFM, and confocal fluorescence laser scanning microscopy (CFLSM).

A second approach involved synthesizing Si(100)/Si(111)-$OCH_2CH_2N_3$ functional surfaces from the Si(100)/Si(111)-H and/or Si(100)/Si(111)-Cl with $HOCH_2CH_2N_3$, then using a “click reaction” to attach -C≡CH functional OPV to the surface-bound N_3. The resulting monolayers were characterized by means of XPS, ATR-FTIR, AFM, and CFLSM.

A third approach involved the synthesis of Si(111)-OCH_2CH_2OH functional surfaces from Si(111)-H and/or Si(111)-Cl with $HOCH_2CH_2OH$, and then using a "click like" reaction between the Si(111)-OCH_2CH_2OH functionalized surfaces and 1,4-phenylene diisocyanate (OCN-Ph-NCO) to afford Si(111)-U-Ph-NCO surfaces. Subsequent reaction of these with the –OH functional OPVs produced urethane containing OPV monolayers. The latter were characterized by means of XPS, ATR-FTIR, AFM, and CFLSM.

The combined results presented in this thesis represent a further major advance in the controlled functionalization of Si-surfaces and herald a variety of potential applications that use such a combination of inorganic and organic semiconductors.

Acknowledgements

The author gratefully acknowledges all those people who so efficiently taught him at The College of Staten Island (CSI) and Graduate Center at The City University of New York (CUNY). He also would like to acknowledge the financial support from different sources- CUNY, CSI, RF-CUNY, NSF, CUNY-Collaborative Incentive, and NYSTAR-CePM. He also would like to thank Professor Bhanu Chauhan for providing an initial Si(100) wafer. The author wishes to acknowledge funding for the confocal microscope from the National Science Foundation (DBI 04210460).

The author greatly appreciates his Ph.D. supervisor, Professor Ralf M. Peetz, for his constructive criticism, recommendations, suggestions, discussions, encouragement, and problem solving which have resulted in this thesis.

He is grateful to Professors Shi Jin and Glen R. Kowach for serving as thesis committee members and their suggestions and criticism during this work.

Professor Qiao-Sheng Hu provided valuable advice in the organic synthesis part.

The author also wishes to thank Dr. Hsin Wang and Dr. Boris Arshava for their help and advice with NMR experiments, Dr. Yalin Wang for his help with the AFM experiments, Mr. Tai Park for his help with thermal characterization, and Professor William J. L'Amoreaux for his help with confocal fluorescence laser scanning microscopy (CFLSM) and scanning electron microscope (SEM).

He also wishes to thank Dr. Neeraja Vundyala for collaborating with the biotin-functional oligo(*p*-phenylene vinylene)s project.

The author was able to train and work with several undergraduate students, including especially Ms. Carliann Castanzo, Mr. Cole Oluwaseun, Ms. Faizah Qadri, and Mr. Bilal Marie. He would like to thank them for their contributions.

Moreover, the author would like to thank all his colleagues, friends, and other people whose names are not mentioned above for their help and providing facilities during the academic years.

Finally, acknowledgement is gratefully extended to his family (wife Kong Hiek CHEA and sons Kim, Kenny, and Kevin), parents, and parent's in-law for their love, understanding, encouragement, and financial support, which has been a constant source of inspiration.

He would like to dedicate this thesis his family.

Table of contents

1. Introduction **1**

1.1. Silicon surfaces **1**

1.1.1. Hydrogen-terminated Si surfaces: Si-H surfaces **2**

1.1.2. Chloride-terminated Si surfaces: Si-Cl surfaces **3**

1.1.3. Formation of Si-CH_2-R surfaces **4**

1.1.3.1. Thermal hydrosilylation **4**

1.1.3.2. Photochemical hydrosilylation **5**

1.1.3.3. Grignard and alkyllithium reactions **6**

1.1.3.4. Electrochemical grafting **7**

1.1.4. Formation of Si-O-CH_2-R surfaces **8**

1.1.5. Functional monolayers **10**

1.2. Poly(*p*-phenylene vinylene)s and oligo(*p*-phenylene vinylene)s **13**

1.3. Biomolecule-polymer conjugates **17**

1.4. Click chemistry **17**

2. Synthesis and characterization of homologous oligo(*p*-phenylene vinylene)s (OPVs) **19**

2.1. Method 1: Monomers, dimers, trimers **19**

2.1.1. Overview **19**

2.1.2. Results and discussion **19**

2.1.2.1. Synthesis of monomer OPVs **20**

2.1.2.2. Synthesis of dimer OPVs **21**

2.1.2.3. Synthesis of trimer OPVs **22**

2.1.2.4. Side chain variation **22**

2.1.3. Spectroscopic characterization **23**

2.1.3.1. Nuclear magnetic resonance (NMR) **23**

2.1.3.2. Attenuated total reflection fourier transform infrared (ATR-FTIR) **34**

2.1.3.3. UV/Vis absorption and emission **37**

2.1.4. Experimental **40**

2.2. Method 2: Monomers, trimers **60**

2.2.1. Overview **60**

2.2.2. Results and discussion **60**

2.2.3. Experimental **61**

3. Biotin-functional oligo(*p*-phenylene vinylene)s synthesized using click chemistry **70**

3.1. Overview **70**

3.2. Results and discussion **70**

3.3. Experimental **78**

4. Functionalization of Si(100) and Si(111) surfaces with oligo(*p*-phenylene vinylene)s **103**

4.1. Overview **103**

4.2. Surfaces: Results and discussion **104**

4.2.1. Si-H and Si-Cl **104**

4.2.2. Dihydroxy-functional OPVs on Si(100)-H **107**

4.2.3. Si(100)-OPV-CH_2OH **111**

4.2.4. Si(100)-OPV-U-Ph **114**

4.2.5. Si(111)-OPV-CH_2OH **117**

4.2.6. Si(111)-OPV-U-Ph **121**

4.2.7. Optical properties **123**

4.3. Experimental **126**

5. Stepwise functionalization of Si-H/Si-Cl surfaces using click chemistry **132**

5.1. Overview **132**

5.2. Surfaces: Results and discussion **133**

5.2.1. Si(100) **133**

5.2.1.1. Si(100)-H and Si(100)-Cl **133**

5.2.1.2. Si(100)~N_3 **134**

5.2.1.3. Si(100)-Click-Br **135**

5.2.1.4. Si(100)-Click-OPV-alkyne **137**

5.2.2. Si(111) **140**

5.2.2.1. Si(111)-H and Si(111)-Cl **140**

5.2.2.2. Si(111)-N_3 **140**

5.2.2.3. Si(111)-Click-OPV-alkyne **143**

5.2.2.4. Si(111)-Click-NH_2 **146**

5.2.2.5. Si(111)-Click-OPV-CHO **147**

5.2.3. DSi(111): Double side polished Si(111) **148**

5.2.3.1. DSi(111)O_x **148**

5.2.3.2. DSi(111)-H and DSi(111)-Cl **149**

5.2.3.3. DSi(111)~N_3 **149**

5.2.3.4. DSi(111)-Click-Br **152**

5.2.3.5. DSi(111)-Click-OPV-alkyne **153**

5.3. Experimental **158**

6. Stepwise functionalization of Si-H/Si-Cl surfaces using urethane chemistry ("click-like") **170**

6.1. Overview **170**

6.2. Surfaces: Results and discussion **171**

6.2.1. Si(111)-H and Si(111)-Cl **171**

6.2.2. Si(111)-EG-OH **171**

6.2.3. Si(111)-U-Ph-NCO **174**

6.2.4. Si(111)-U-Ph-U-OPV-CH_2OH **174**

6.3. Experimental **179**

7. References **184**

Table of schemes

Scheme 1.1.	Hydride-terminated Si(100) and Si(111) surfaces	**3**
Scheme 1.2.	Chloride-terminated Si(100) and Si(111) surfaces	**4**
Scheme 1.3.	Proposed radical mechanism for Si-H reacting with alkenes using dibenzoyl peroxide	**5**
Scheme 1.4.	UV-irradiation in hydrosilylation of Si-H surfaces with alkenes and alkynes	**6**
Scheme 1.5.	Reaction of alkyl-lithium or Grignard-compounds on Si-Cl surfaces	**7**
Scheme 1.6.	Functionalization of Si-H surfaces using arene diazonium salts	**7**
Scheme 1.7.	Functionalization of Si-H or Si-Cl surfaces with alcohols and/or aldehydes	**8**
Scheme 1.8.	Proposed reaction mechanism for Si(111)-H reacting with alcohols	**9**
Scheme 1.9.	Reaction of alkyl functional surfaces with organic and bioorganic compounds	**12**
Scheme 1.10.	Poly(*p*-phenylene vinylene)s	**14**
Scheme 1.11.	Poly(2-methoxy-5-(2′-ethyl-hexyloxy)-1,4-phenylene vinylene)	**16**
Scheme 1.12.	α,ω-dimethyl-oligo(2,5-bis[2-(S)-methylbuthyloxy]-*p*-phenylene vinylene)s	**16**
Scheme 2.1.	Method 1: Overall synthetic approach for monomers, dimers, and trimers	**20**
Scheme 2.2.	Building blocks with various end group functionalities	**21**
Scheme 2.3.	Dihydroxy functional OPVs with varying side-chain lengths e.g. monomer **6**, dimer **11**, and trimer **17**: Carbon assignments	**32**
Scheme 2.4.	Method 2: Overall synthetic approach for monomers and trimers	**62**

Scheme 3.1.	“Click” functionalization of oligo(*p*-phenylene vinylene)	**71**
Scheme 3.2.	Quantum dot/ OPV network formation via biotin	**71**
Scheme 4.1.	Dihydroxy functional OPVs with varying side-chain lengths	**104**
Scheme 4.2.	Reactions of OPVs with Si-H and/or Si-Cl surfaces	**104**
Scheme 4.3.	Synthesis of model surface Si-OPV-U-Ph	**128**
Scheme 5.1.	Reactions of OPVs on Si-H and/or Si-Cl surfaces via click chemistry	**132**
Scheme 5.2.	Synthesis of model surface Si-Click-OPV-alkyne	**161**
Scheme 6.1.	Reactions of OPVs on Si-H and/or Si-Cl surfaces using ethylene glycol and 1,4-phenylene diisocyanate as linkers via “click-like” chemistry	**170**
Scheme 6.2.	Synthesis of model surface Si-U-Ph-U-OPV-CH_2OH	**181**

Table of figures

Figure 2.1.	^{1}H-NMR (600Hz, $CDCl_3$) spectrum of OPV **16** with complete assignments	**23**
Figure 2.2.	HSQC spectrum (600 Hz, $CDCl_3$) of OPV **16** (Select region)	**25**
Figure 2.3.	HMBC spectrum (600 Hz, $CDCl_3$) of OPV **16** (Select region)	**26**
Figure 2.4.	^{1}H-NMR (600 Hz, $CDCl_3$) spectra of dihydroxy OPVs with different chain lengths e.g. monomer **6**, dimer **11**, and trimer **17**	**28**
Figure 2.5	End-group dependent ^{1}H NMR spectra (600 Hz, $CDCl_3$) of trimer OPVs **16**, **17**, **18**, and **19**, (Select regions)	**29**
Figure 2.6.	^{13}C-NMR (50 and 150 Hz, $CDCl_3$) spectra of dihydroxy OPVs with different chain lengths e.g. monomer **6** (red), dimer **11** (blue), and trimer **17** (black)	**32**
Figure 2.7.	End-group dependent ^{13}C-NMR (150 Hz, $CDCl_3$) spectra of trimer building blocks **16** (black), **17** (green), **18** (blue), and **19** (red)	**34**
Figure 2.8.	ATR-FTIR spectra of trimer OPVs **16**, **17**, **18**, and **19**	**36**
Figure 2.9.	ATR-FTIR spectra of dihydroxy OPVs with different chain lengths e.g. monomer **6**, dimer **11**, and trimer **17** (select regions)	**37**
Figure 2.10.	Normalized UV/visible absorption (left) and emission (right) spectra of dihydroxy-functional OPVs **5** (black), **11** (red), and **17** (blue) in $CHCl_3$	**38**
Figure 2.11.	UV/visible absorption (left) and emission (right) spectra (normalized) of trimer OPVs **16** (green), **17** (black), **18** (red), and **19** (blue) in $CHCl_3$	**38**
Figure 3.1.	UV/Vis absorption and emission (normalized) of OPVs **19**, **29**, and **30** (left), concentration dependent emission of **30** solutions in DMF, excitation at 438 nm	**77**

Figure 3.2. TEM images of (a) Streptavidin Qdot control, (b) network of streptavidin Qdots and 18µM biotin-OPV **30**, (c) network of streptavidin Qdots and 1 µM biotin-OPV **30** **78**

Figure 4.1. XPS spectra overlaid; survey scan (top) and narrow scan (bottom) of Si(100)-H and Si(111)-H surfaces **106**

Figure 4.2. AFM images of Si(100)-H (top) and Si(111)-H (bottom) surfaces **107**

Figure 4.3. XPS spectra overlaid; survey scans of silicon wafer with SiO_x, Si(100)-H, Si(100)-**5**, Si(100)-**11** and Si(100)-**17** surfaces **109**

Figure 4.4. ATR-FTIR spectra overlaid; silicon wafer with SiO_x, Si(100)-H, Si(100)-**5**, Si(100)-**11**, and Si(100)-**17** surfaces **110**

Figure 4.5. Representative XPS spectra overlaid; survey scans (top) of Si(100)-T-OPV-CH_2OH and Si(100)-H surfaces and narrow scan (bottom) spectrum of Si(100)-T-OPV-CH_2OH surface **113**

Figure 4.6. AFM image of Si(100)-OPV-CH_2OH surface (entries **2**) **114**

Figure 4.7. Representative XPS spectra overlaid; survey scans (top) and narrow scans (bottom) spectra of Si(100)-T-OPV-U-Ph and Si(100)-T-OPV-CH_2OH surfaces **116**

Figure 4.8. ATR-FTIR spectrum of Si(100)-OPV-U-Ph surface **117**

Figure 4.9. Representative XPS spectra overlaid; survey scans (top) of Si(111)-T-OPV-CH_2OH and Si(111)-H surfaces and narrow scan (bottom) of Si(111)-T-OPV-CH_2OH surface **120**

Figure 4.10. AFM images of Si(111)-T-OPV-CH_2OH surfaces (entry **2** and **3**) **121**

Figure 4.11. Representative XPS spectra overlaid; survey scans of Si(111)-OPV-CH_2OH and Si(111)-OPV-U-Ph surfaces **122**

Figure 4.12. Representative XPS spectra overlaid; narrow scans of Si(111)-OPV-CH_2OH and Si(111)-OPV-U-Ph surfaces **122**

Figure 4.13.	AFM image of Si(111)-OPV-U-Ph surface	**123**
Figure 4.14.	Normalized emission spectra of T-OPV-CH_2OH in solution ($CHCl_3$), T-OPV-CH_2OH spin-cast on SiO_x wafer, and Si(111)-T-OPV-CH_2OH surfaces	**124**
Figure 4.15.	Normalized emission spectra of a T-OPV-CH_2OH in solution ($CHCl_3$), Si(111)-T-OPV-CH_2OH, a Si(111)-T-OPV-U-Ph, and control in a spin-cast surfaces	**125**
Figure 5.1.	Representative XPS spectra overlaid; survey scans of Si(100)-H and Si(100)~N_3 surfaces	**134**
Figure 5.2.	Representative XPS spectra overlaid; survey scans (top) and narrow scans (bottom) of Si(100)~N_3 and Si(100)-Click-Br surfaces	**136**
Figure 5.3.	AFM image of Si(100)-Click-Br surface	**137**
Figure 5.4.	Representative XPS spectra overlaid; survey scans of Si(100)~N_3 and Si(100)-Click-OPV-alkyne surfaces	**138**
Figure 5.5.	Representative XPS spectra overlaid; narrow scans of Si(100)~N_3 and Si(100)-Click-OPV-alkyne surfaces	**139**
Figure 5.6.	AFM image of Si(100)-Click-OPV-alkyne surface	**140**
Figure 5.7.	Representative XPS spectra overlaid; survey scans of Si(111)-H, Si(100)~N_3 and Si(111)~N_3 surfaces	**141**
Figure 5.8.	Representative XPS spectra overlaid; survey scans of Si(111)~N_3 from Si(111)-Cl and Si(111)-H surfaces	**143**
Figure 5.9.	Representative XPS spectra overlaid; survey scans of Si(111)-H, Si(111)~N_3, and Si(111)-Click-OPV-alkyne surfaces	**144**
Figure 5.10.	Representative XPS spectra overlaid; narrow scans of Si(111)~N_3 and Si(111)-Click-OPV-alkyne surfaces	**145**
Figure 5.11.	Normalized UV/Vis absorption spectrum of T-OPV-dialkyne in solution ($CHCl_3$, red) and normalized emission spectra of T-OPV-dialkyne in solution ($CHCl_3$, blue) and Si(111)-T-OPV-alkyne surface (black)	**146**

Figure 5.12. Representative XPS spectra overlaid; survey scans of Si(111)-Click-NH_2 and Si(111)~N_3 surfaces **147**

Figure 5.13. Representative XPS spectra overlaid; survey scans of Si(111)-Click-OPV-CHO and Si(111)-Click-NH_2 surfaces **148**

Figure 5.14. Representative XPS spectra overlaid; survey scans of DSi(111)-H and DSi(111)~N_3 surfaces **150**

Figure 5.15. ATR-FTIR spectra of $DSiO_x$ (black), DSi~N_3 (17hours, green), and DSi~N_3 (24hours, purple) surfaces **151**

Figure 5.16. Representative XPS spectra overlaid; survey scans of DSi(111)~N_3 surfaces (from Si-H for 48h at 80^{o}C and from Si-Cl for 24h at 50^{o}C) **152**

Figure 5.17. ATR-FTIR spectra of $HOCH_2CH_2N_3$ (bulk, red), and surfaces DSi(111)~N_3 (from Si-Cl for 17h at 80^{o}C, green), DSi(111)~N_3 (from Si-Cl for 24h at 80^{o}C, purple), and DSi(111)-Click-Br (blue) **153**

Figure 5.18. Representative XPS spectra overlaid; survey scans of DSi(111)-Click-OPV-alkyne and DSi(111)~N_3 (from Si-Cl for 24h at 80^{o}C) surfaces **155**

Figure 5.19. Representative XPS spectra overlaid; narrow scans of DSi(111)~N_3 and DSi(111)-Click-OPV-alkyne surfaces **156**

Figure 5.20. ATR-FTIR spectra of trimer-OPV-alcohol (bulk), and surfaces DSi(111)O_x, DSi(111)~N_3 surface (from Si-Cl for 24h at 80^{o}C), and DSi(111)-Click-OPV-alkyne **157**

Figure 5.21. AFM image of DSi(111)-Click-OPV-alkyne surface **158**

Figure 6.1. Representative XPS spectra overlaid; survey scans (top) and narrow scans (bottom) of Si(111)-EG-OH (green: without Me_3SiCl, blue: with Me_3SiCl with additional degassing, and red: with Me_3SiCl) and Si(111)-H surfaces (black) **173**

Figure 6.2. AFM image of Si(111)-EG-OH surface **174**

Figure 6.3. Representative XPS spectra overlaid; survey scans (top) and narrow scans (bottom) of Si(111)-U-Ph-U-OPV-CH_2OH, Si(111)-EG-OH, and Si(111)-H surfaces **176**

Figure 6.4. AMF images of Si(111)-U-Ph-U-OPV-CH_2OH surface (entry **1**) with different scan angles relative to x-axis **177**

Figure 6.5. AFM image of Si(111)-U-Ph-U-OPV-CH_2OH surface (entry **2**) **178**

Tables

Table 2.1.	Observed single bond C-H couplings in T-OPV-CHO **16** (HSQC-experiment)	**25**
Table 2.2.	Observed multiple bond C-H couplings in **16** (HMBC-experiment)	**27**
Table 2.3.	Select chemical shifts (^{1}H-NMR) in trimer OPVs **16**, **17**, **18**, and **19**	**30**
Table 2.4.	Summarized 13C NMR shifts with assignments of **6**, **11**, and **17**	**33**
Table 2.5.	Summarized ^{13}C-NMR assignments of **16**, **18**, and **19**	**35**
Table 2.6.	The absorption and emission wavelengths of the depicted spectra of OPVs	**39**
Table 3.1.	Representative synthesis results of biotin-PEG-N_3's **27** and **28**	**73**
Table 3.2.	Representative click reactions of OPV dialkyne **19**	**74**
Table 4.1.	Representative reaction conditions for Si(100)-OPV-CH_2OH surfaces	**111**
Table 4.2.	Representative reaction conditions for Si(100)-OPV-U-Ph surfaces	**115**
Table 4.3.	Representative reaction conditions for Si(111)-OPV-CH_2OH surfaces	**118**
Table 6.1.	Representative reaction conditions for Si(111)-U-Ph-U-OPV-CH_2OH surfaces	**175**

1. Introduction

1.1. Silicon surfaces

Results of rapidly growing interest in the surface chemistry of silicon, in particular in the controlled formation of organic monolayers, offer the promise of enhancing the functionality of many technological applications presently in use and envisioned for the future - as well as a fundamental perspective in the understanding of such surfaces.[1,2,3a,3e] High purity single-crystal silicon wafers are commercially available and relatively inexpensive due to their wide-spread use in microelectronic applications. The most common surface orientations are Si(100) and Si(111).[1,2,4] Depending on the desired electronic properties, silicon wafers are doped in a controlled fashion with electron-donating (n-type: P, As, Sb) or electron-withdrawing (p-type: B) elements to render the material more intrinsically conducting.

Specifically the modification of the Si semiconductor surface via stable Si-CH_2-R /Si-OCH_2-R linked organic monolayers is currently an area of intensive research. Potential applications include bio-functionalized semiconductor devices. Detailed studies focus on fundamental chemical and electronic processes at these semiconductor surfaces.[3] Many silicon chip - based device applications demand precise control over several interfacial properties. Examples include micro-array technology for applications in genomics, proteomics, and sensing,[5-9] lab-on-chip and total automated systems (μ-TAS),[10,11] as well as micro- and nano-electromechanical systems (MEMS and NEMS).[12]

1.1.1. Hydrogen-terminated Si surfaces: Si-H surfaces

Upon exposure to air, single-crystal silicon wafers rapidly become covered with a thin native oxide layer, which can be removed either chemically with the help of fluoride ions, or thermally under ultra high vacuum conditions. The hydride-terminated silicon wafer surfaces offer many advantages with excellent chemical homogeneity (i.e., >99% H termination) which can be potentially easily assessed analytically due to strong IR-active stretching modes at ~2100 cm^{-1}, providing additional information on surface flatness.[13-16] Long-term use of native Si-H-terminated surfaces is not practical for any applications due to their propensity to oxidize. However, Si-H-terminated surfaces can be handled in air without measurable degradation for periods of minutes to tens of minutes.[13,14] Atomically flat areas of monohydride ≡Si-H termination can be achieved on commercial silicon wafers of the (111) orientation after treatment with degassed 40% aqueous NH_4F for 4-6 minutes (Scheme 1.1a).[13-16] Such Si(111)-H monohydride surfaces feature a sharp-IR stretching mode ν(Si-H) at 2084 cm^{-1}, as indicated above. In this case atomically smooth surfaces can extend over nanometer-scale distances.[13] Atomic resolution in the imaging of the surface silicon atoms can be achieved by scanning tunneling microscopy (STM), confirming the flat and ordered surface produced by NH_4F etching.[14] Allongue et al. showed that polished silicon wafers are reasonably stable and atomically flat on the tens-of-microns scale, and of high quality, both structurally and electronically. STM images are able to show the three-fold symmetrical arrangement of silicon atoms, separated by 3.84 Å, each atom capped with one hydrogen atom.[17] No

reports are found on atomically flat Si(100) surfaces produced by chemical etching methods, due to the anisotropic nature of the etching process by fluoride ions in the case of Si(100). The chemical etching of Si(100) surfaces tends to roughen the surface (Scheme 1.1b). Arima[18] and Chabal[19] showed that under certain conditions it is possible to produce relatively flat surfaces with small-sized, atomically resolved domains. But the structures of the hydrogenated surfaces produced are not uniform. Although the surfaces are predominantly SiH_2-terminated, they do contain significant amounts of SiH and SiH_3 termini.

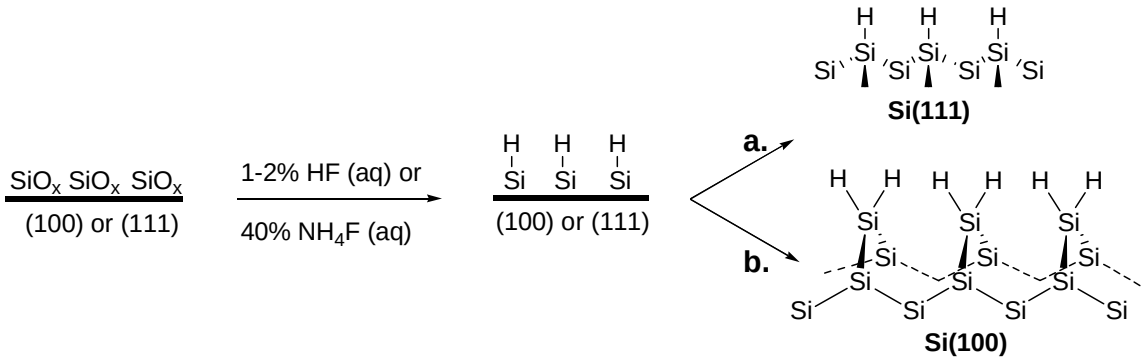

Scheme 1.1. Hydride-terminated Si(100) and Si(111) surfaces.

1.1.2. Chloride-terminated Si surfaces: Si-Cl surfaces

Compared to Si(100)-H , the Si(111)-H surface has only one reactive Si-H bond and less free space around the individual Si-atoms at the surface for any further reaction. Therefore, a more reactive Si(111)-Cl surface was also used to attach organic molecules. The Si-Cl terminated surfaces are very reactive and need to be handled under an inert atmosphere at all stages of the respective reactions. Si-Cl surfaces are prepared by treating the respective Si-H surface with PCl_5 in chlorobenzene, using benzoyl peroxide as a radical initiator (Scheme 1.2).[20] Alternatively, Cl_2 gas can be used to convert the Si-H surface to Si-Cl surface

with either photochemical or thermal activation (Scheme 2).[21-23] Although using Si-Cl surface requires one more synthetic step and the use of inert-gas atmosphere at all stages, compared to Si-H surfaces,this proves to be the most effective approach to synthesize reproducible and homogenous surfaces. Literature reports tend to support this observation.[21,24,25,26]

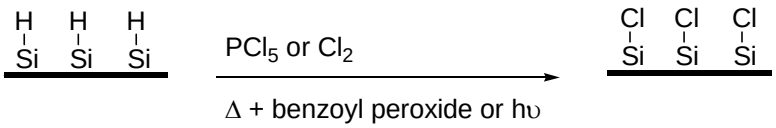

Scheme 1.2. Chloride-terminated Si(100) and Si(111) surfaces.

1.1.3. Formation of Si-CH_2-R surfaces

1.1.3.1. Thermal hydrosilylation

Linford and Chidsey observed the formation of monolayers consisting of long alkyl chain molecules directly attached to Si surfaces (Si-CH_2-R) covalently after reacting Si(111)-H with alkenes in the presence of dibenzoyl peroxide.[27,28] scheme 1.3 shows a radical mechanism that has been proposed for the monolayer formation. First, the diacyl peroxide (initiator) undergoes a homolytic cleavage to form two acyloxy radicals, which further decompose to carbon dioxide and alkyl radicals ($R^{\bullet}$-radical). A $R^{\bullet}$-radical can abstract a $H^{\bullet}$-radical from the Si-H surface, leaving a silicon radical $Si^{\bullet}$ behind. This $Si^{\bullet}$-radical then reacts with an alkene (either neat or in solution) to form a secondary alkyl radical, which then subsequently abstracts hydrogen from a vicinal Si-H bond. The atom transfer of the hydrogen yields a saturated organic molecule attached to the surface and a new $Si^{\bullet}$-radical on the surface which can propagate the sequence

of events ending in the formation of a monolayer.[28] The Si•-radicals are known to react rapidly with olefins to form Si-C bonds.[29] In an alternative method, also reported by Linford and Chidsey, the monolayer formation (via Si-C bond) can be achieved at higher temperatures (≥150 ^{o}C) in the absence of diacyl peroxide initiator. Thermally induced through homolytic Si-H cleavage (Si-H → Si• + H•), yielding the surface-bound Si•-radical with subsequent monolayer formation.[30]

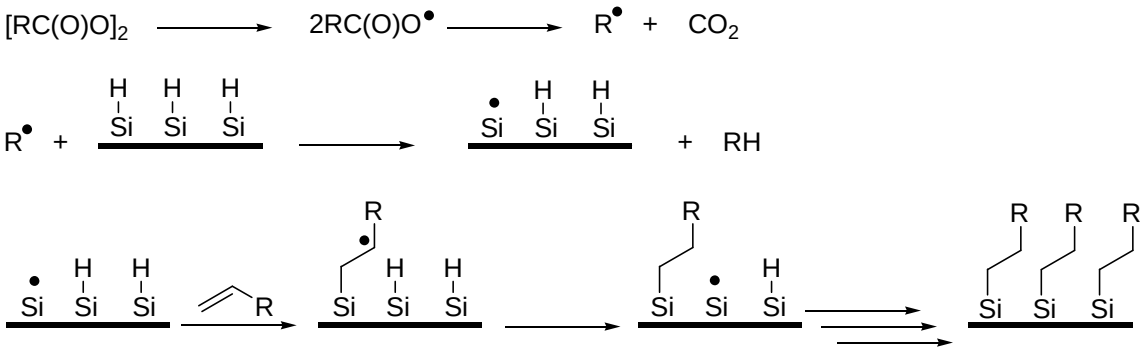

Scheme 1.3. Proposed radical mechanism for Si-H reacting with alkenes using dibenzoyl peroxide.

1.1.3.2. Photochemical hydrosilylation

UV-irradiation can also promote hydrosilylation of unsaturated compounds,[31] due to photochemically induced homolytic cleavage of surface-Si-H bonds to (Scheme 1.4). This approach requires only ambient temperatures and provides a way to avoid thermal conditions that could be harmful to organic molecules and delicate or small features on a silicon chip. Terry[32] and Cicero[33] showed the irradiation of a Si(111)-H surface with UV light (wavelengths used: 185 and 253.7 nm) at room temperature for 2 hours in the presence of aliphatic alkenes (reported examples: 1-pentene and 1-octadecene) results in hydrosilylation.

Sieval[34,35] and Zhang[36] successfully reacted both alkenes (reported examples: 1-octene, 1-octadecene, and styrene) and alkynes (reported examples: 1-octyne and phenylacetylene) were with Si-H surfaces using UV light, yielding alkyl (Si-C-C bond) and alkenyl (Si-C=C bond) monolayers, respectively.

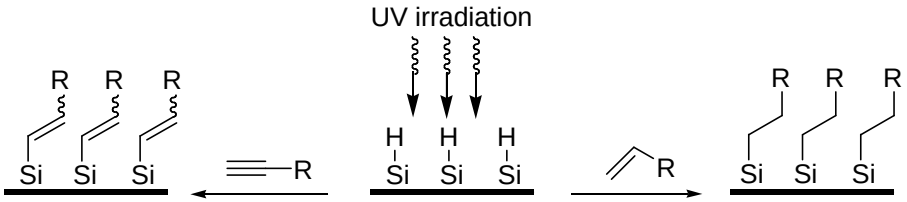

Scheme 1.4. UV-irradiation in hydrosilylation of Si-H surfaces with alkenes and alkynes.

1.1.3.3. Grignard and alkyllithium reactions

Bansal *et al.,* functionalized flat, single-crystal silicon with carbanions using a two-step halogenation / alkylation route.[24,25] First, the chlorination of a Si(111)-H surface with PCl_5 produced a Si(111)-Cl surface. Then, a trans-metallation with alkyl-lithium or Grignard-compounds yielded alkyl groups bound to the silicon surface through a Si-C linkage with LiCl or MgXCl as byproducts (Scheme 1.5). Of such surfaces, those with long alkyl termination were more resistant to oxidation under ambient conditions and to boiling in aerated chloroform and water, compared to those with shorter alkyl chains.

He *et al.,* reported that this two-step approach (halogenation followed by alkylation) can also produce monolayers of oligothiophenes on Si(111) surfaces.[21] Boukherroub *et al.*[26] showed the direct reaction of a Grignard reagent with the Si(111)-X (where X = Cl, Br, or H) surface to form monolayers similar to those of He *et al*.

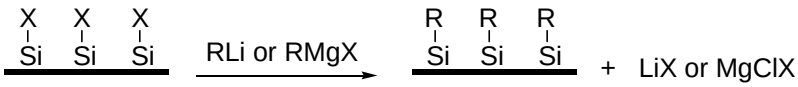

X = Cl, Br, H

Scheme 1.5. Reaction of alkyl-lithium or Grignard-compounds on Si-Cl surfaces.

1.1.3.4. Electrochemical grafting

Electrochemical approaches have also been reported - Henry *et al.*[37] and Allongue *et al.*[38,39] observed close-packed phenyl monolayers starting from flat hydride-terminated n-type Si(111) surfaces. The key step was the reduction of an arene diazonium salt to form an aryl radical (Ar• radical), which then directly bonded to the surface by forming a silicon-carbon bond (Scheme 1.6). One advantage of this approach involving arene diazonium salts is the compatibility with a significant number of substitution patterns on the aromat that is to be bonded to the surface, such as molecules featuring Br, NO_2, CN, NH_2, COOH, or alkyl group, thus providing synthetic flexibility. Moreover, the electron rich surfaces are less susceptible to nucleophilic attack by water, therefore minimizing oxidation of the functional surfaces.

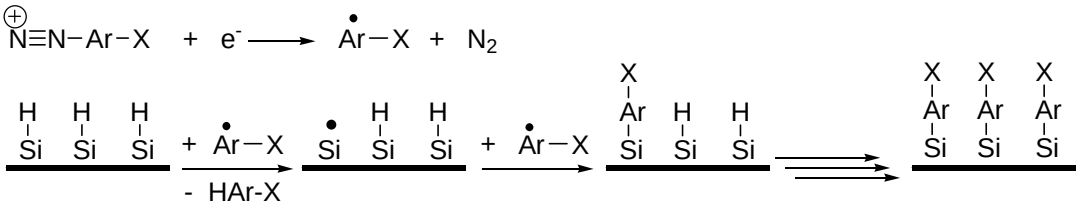

X= Br, NO_2, CN, NH_2, COOH, or alkyl group

Scheme 1.6. Functionalization of Si-H surfaces using arene diazonium salts.

1.1.4. Formation of Si-O-CH_2-R surfaces

The Si-C bond is both thermodynamically and kinetically stable due to the high bond strength and low polarity.[40,41] Alkyl layers attached to Si surfaces through Si-C bonds become unstable at ~ 250-300 ^{o}C, due to desorption.[42,43] Dusciac *et al*., showed that the covalent Si-O-C bond can display a more robust behavior than the corresponding Si-C linkage to the bulk silicon.[44]

In 1995 Cleland *et al.,* reported the direct functionalization of Si(111)-H by the thermal reaction with alcohols to form Si(111)-OCH_2R modified monolayers (Scheme 1.7a).[45]

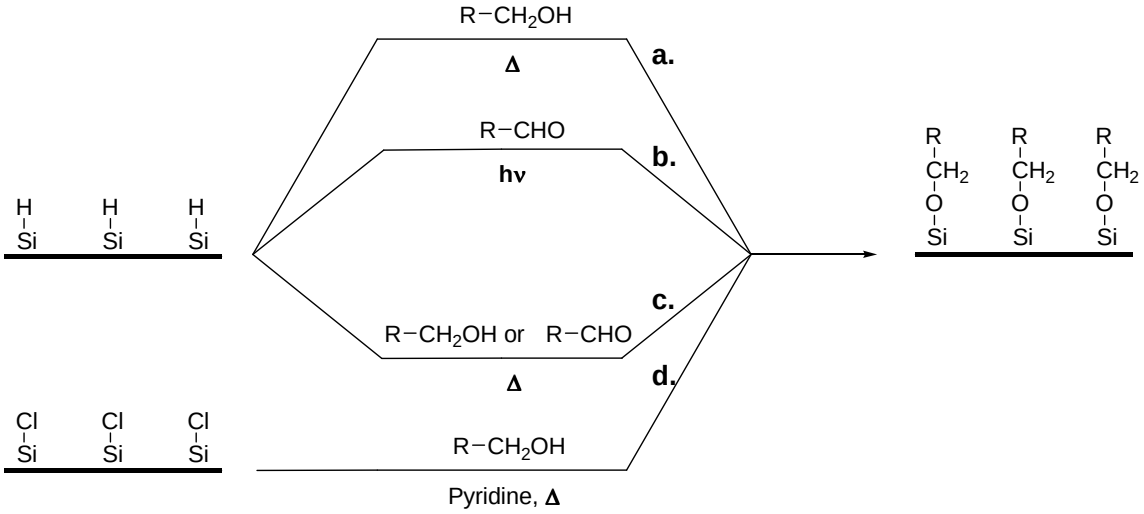

Scheme 1.7. Functionalization of Si-H or Si-Cl surfaces with alcohols and/or aldehydes.

In 1998 Effenberger *et al.,* reported on the photochemical hydrosilylation of aldehydes (RCHO) in a reaction with Si(111)-H to form Si(111)-OCH_2R surfaces (Scheme 1.7b).[46] In 2000 Boukherroub *et al.,* reported thermal reaction of neat alcohols and aldehydes to form Si(111)-OR surfaces (Scheme 1.7c), complementing the photochemical approach.[47] The reaction mechanism

proposed for alcohols reacting with the surface (Si-H) is similar to the oxidation of silicon by water.[48] But alcohols do not etch the silicon surface, while water does. Boukherroub *et al.,* also illustrated that traces of water that are not removed from the alcohols used in functionalization reactions result in significant etch pits on the surfaces.[47] To remove such trace amounts of water a reactive chemical can be added to the alcohol solution, such as trimethylsilyl chloride. [47]

The thermal reaction of aldehydes with Si(111)-H surfaces was observed to be similar to alkenes, however, the reaction occured at much lower temperatures than those of the corresponding alkenes scheme 1.3.[47] There are two proposed mechanisms for this reaction. The first involves a nuleophilic attack of the carbonyl group on the silicon surface, followed by a 1,2-hydride shift. The second mechanism is similar to the radical mechanism proposed for the alkenes (see above).[27, 28]

In 2000 Zhu *et al.,* reported a simple and novel process for the formation of organic monolayers on silicon via Si-O-CH_2R linkages by reacting an alcohol with chlorine-terminated Si(100) or Si(111) in the presence of pyridine (base catalyzed) (Scheme 1.7d).[22]

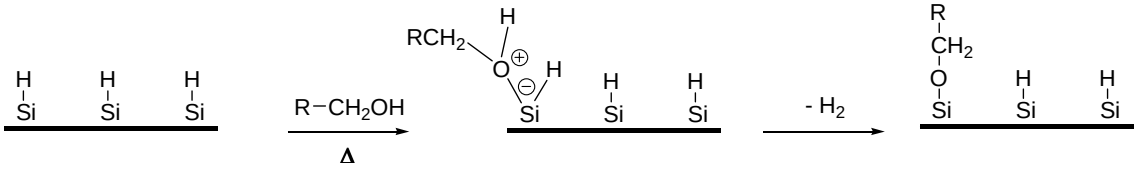

Scheme 1.8. Proposed reaction mechanism for Si(111)-H reacting with alcohols.

The thermal reaction of alcohols with Si(111)-H surfaces simply involves a nuleophilic attack of the hydroxy group on the silicon surface (Scheme 1.8).

1.1.5. Functional monolayers

In most examples discussed above, the surface reactions of alkyl chains lead to organic monolayers bearing terminal methyl groups. Methyl terminated monolayers can be useful for mechanical studies as well as for passivation and chemical stabilization. However, the low reactivity of this terminal group makes further manipulation of the surface's physical or chemical properties difficult.

Wagner *et al.,*[49] and Cicero *et al.,*[50] reported on C-H bond activation in terminal methyl groups of an octadecyl monolayer on Si(111). In one approach, a Si(111)-$C_{18}H_{37}$ surface was broadband-illuminated at 350 nm in the presence of 4'-[3-trifluoromethyl-3H-diazirin-3-yl]-benzoic acid *N*-hydroxysuccinimide ester (TBDA-OSu), affording a hydrophobic surface containing a reactive terminal *N*-succinimide group (Scheme 1.9a). This group could be further functionalized with nucleophiles. In another approach, a Si(111)-$C_{18}H_{37}$ surface was illuminated at ~351 nm in the presence of chlorine gas in sulfur dioxide, affording a chlorosulfonyl-terminated octadecyl monolayer surface. The latter could subsequently be substituted with nucleophiles (i.e., with primary and secondary amines including ethylene diamine) (Scheme 1.9b).

The incorporation of more complex organic and bioorganic structures at the interface requires other strategies for coupling such molecules to the surfaces. An example is the reaction of bifunctional molecules, in which one group binds to the surface and the other is available for further reaction.

Sieval *et al.*[51] thermally reacted alkenes that were terminated with ester groups, forming an ester terminated Si(100) surface. This surface could be either

hydrolyzed to form a modified carboxylic acid or reduced with $LiAlH_4$ to form an alcohol modified surface (Scheme 1.9c). Boukherroub *et al.*[52] reported the photochemical reaction of ethyl undecylenate with Si(111)-H to afford Si(111)-$C_{10}H_{20}COOEt$ surface with subsequent further functionalizations (Scheme 9d).

Strother *et, al.* showed two approaches to modify silicon surfaces with DNA. The first approach,[53] a Si(111)-$(CH_2)_{10}C(O)OCH_2CF_3$ surface was prepared from 2,2,2-trifluoroethyl undec-10-enoate and Si(111)-H using photoinitiation. The Si(111)-$(CH_2)_{10}C(O)OCH_2CF_3$ surface was then hydrolyzed to afford a negatively charged undecylenate surface. This surface served as a substrate for the attachment of DNA through an electrostatically adsorbed layer of polylysine and subsequent attachment to a thiol-modified DNA using heterobifunctional cross-linkers. In another approach,[54] a Si(100)-$(CH_2)_nNHC(O)OBu^t$ surface was prepared from $CH_2=CH(CH_2)_{n-2}NHC(O)OBu^t$ and Si(100)-H. The Si(100)-$(CH_2)_nNHC(O)OBu^t$ surface was hydrolyzed to afford a Si(100)-$(CH_2)_nNH_2$ surface. To theamine terminated monolayer then were attached thiol-modified DNA oligomers using a heterobifunctional cross-linker.

Alkene acids, esters, and epoxides do not require protection during the surface attachment. These bifunctional molecules appear to react primarily via the alkene end, leaving the terminal group available for further reaction.[51,52,55] Voicu *et al.*[56] observed photochemical modification of Si(111)-H with undecylenic acid without detectable reaction of the carboxylic acid group. The acid monolayer could be activated with N-hydroxysuccinimide, which was then coupled with amine tagged molecules, e.g., with oligonucleotides and methoxytetraethyleneglycol.

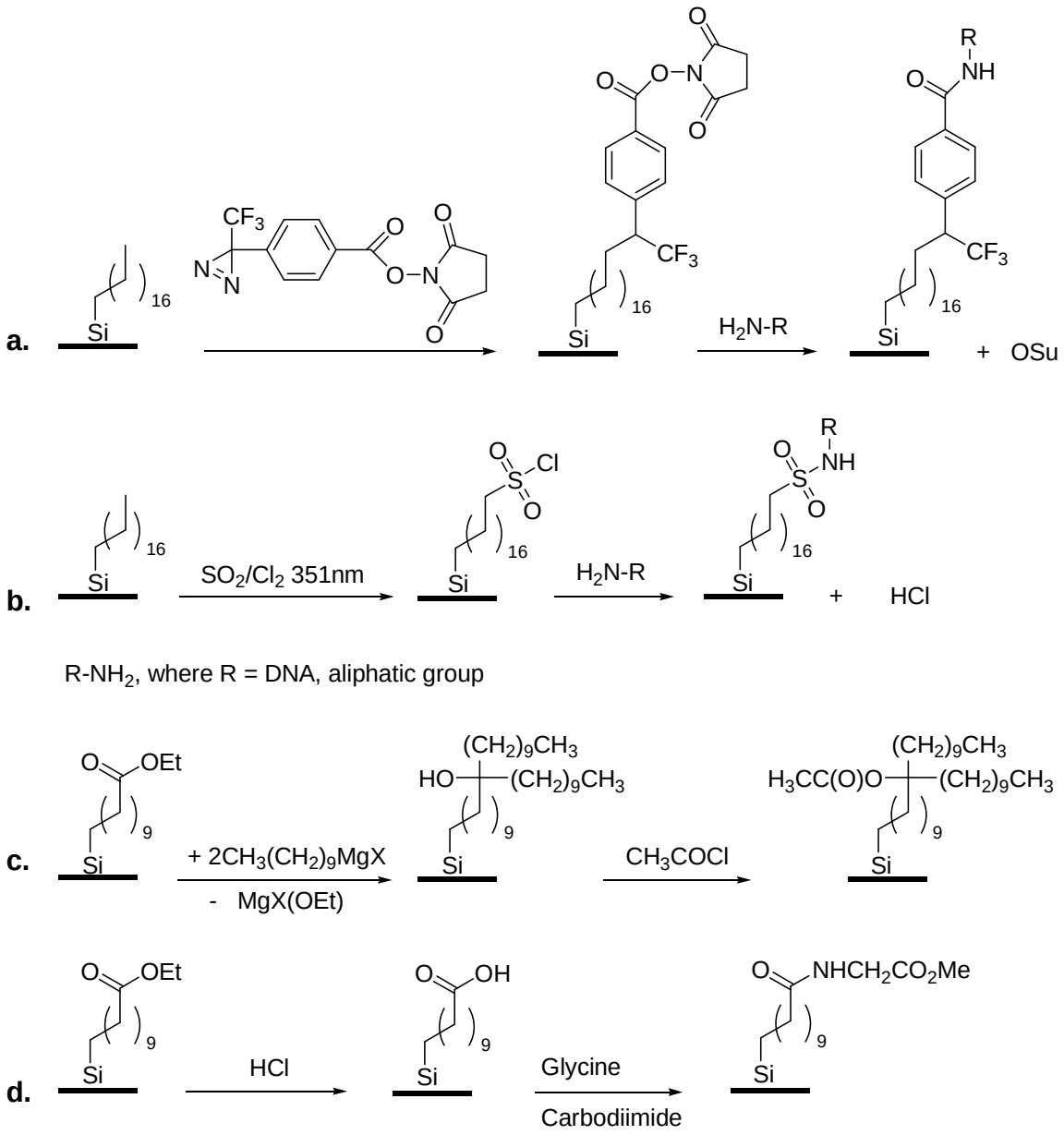

Scheme 1.9. Reaction of alkyl functional surfaces with organic and bioorganic compounds.

However, in these approaches it proved difficult to control the concentration of reagents and the intensity and spectrum of the light source.

The bifunctional molecules usually have two similarly reactive functional sites, and the formation of the recpective monolayer can lead to mixed terminations. In

addition, in most cases these molecules were flexible chains. In such cases, the reaction of both terminal groups of one chain with the surface is possible via a back-biting process, leading to the formation of monolayers with saturated terminal group. However, protections and deprotections involve a variety of additional functional groups and reaction steps, potentially harmful to delicate or small features on a silicon chip. Therefore, using rigid-rod-type conjugated difunctional oligo(*p*-phenylene vinylene)s (OPVs) with varying chain lengths and chain end functionality, e.g. monomer, dimer, and trimer with terminal dialcohol, dialdehyde, divinyl, and dialkyne functionality were used in the presented work.

1.2. Poly(*p*-phenylene vinylene)s and oligo(*p*-phenylene vinylene)s

Organic conjugated polymers and oligomers feature alternating single and double (multiple) bonds along the polymer/oligomer backbone. The conjugated π-electrons lead to semiconductor properties that can be rendered conducting after appropriate doping.

Unsubstituted poly(*p*-phenylene vinylene)s (PPVs) are insoluble, infusible, and cannot be processed (Scheme 1.10a). In 1961 Drefahl and Plötner[57] synthesized the first soluble oligo(*p*-phenylene vinylene)s (OPVs), however the number of reports on the optical and electronic properties of such oligomers remained limited.[58] In 1990, Burroughes et al., reported electroluminescent polymer-based devices using unsubstituted PPVs synthesized via a modified sulfonium precursor technique.[59] After this first report on electroluminescence from conjugated organic polymers, the number of reports on new conjugated

molecules with electroluminescence (EL) properties has grown exponentially.[3] This is due partly to the inherent flexibility of organic synthesis in general, which can be conveniently adapted in order to tune the optical and electronic properties of the materials of interests by making use of a myriad of possible molecular architectures. Many methods have been reported to prepare PPVs and OPVs suitable for EL applications, i.e. light emitting diodes. Seeking optimum luminescence efficiency and lifetime of the EL devices, these PPVs and OPVs are synthesized by various routes to target different molecular weights, molecular weight distributions, and molecular architecture. Principle challenges include controlling structural defects and impurities in the final materials.

In 1991 Müllen *et al.,* reported a more extensive study on a series of OPVs with n = 2-7, where n is the number of aromatic rings.[60] In 1991 Braun and Heeger showed that polymer-based light-emitting diodes (pLED's) can be reasonably efficient.[61] In 1994 Sakamoto *et al.,*[62] reported ultraviolet to infrared absorption measurements with positively charged unsubstituted PV oligomers.

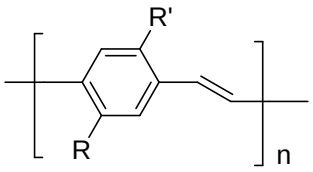

a. R' = R = H: Unsubstituted poly(*p*-phenylene vinylene)s

b. R' = R or R' ≠ R: Alkyl substituents poly(*p*-phenylene vinylene)s

c. R' = R or R' ≠ R: Alkyloxy substituents poly(*p*-phenylene vinylene)s

Scheme 1.10. Poly(*p*-phenylene vinylene)s.

Laterally attached alkyl or alkyloxy substituents (Scheme 1.10b-c) not only help solubilize the polymers, which can then easily be processed. These substituents also modify the electronic properties of the polymers, leading to changes in the optical absorption and emission spectra[63,64] and as such an increase of the luminescence yield.[65,66] Alkyloxy substituents are known to cause a bathochromic shift in the UV/Vis absorption of PPV (smaller band gap than in unsubstituted PPV). These properties make them valuable candidates for numerous applications that depend on efficient luminescence,[67-69] low weight, flexibility, and low cost.

In 1995, Thorn-Csányi *et al.,*[70] reported on an olefin metathesis synthesis of soluble PPV derivatives, using 2,5-diheptyl-1,4-divinylbenzene as substrate (Scheme 1.10c). Soluble products with chain lengths up to 12 could be obtained and showed nearly the same electro-optical properties as unsubstituted PPV. In 1996 Meier *et al.,* described the synthesis and optical properties of a series of oligo(2,5-dipropyloxy-*p*-phenylene vinylene)s with n = 2-12.[71,72] Functionalization of the polymeric homologue PPV has commonly been used to tune properties, such as Electron Affinity (EA). It should also be mentioned that side-chain substitutions may also have unfavorable consequences for the electronic properties in term of energy gap, electron affinity, and ionization potential (IP). However, in 1998 Chua *et al.,*[73] successfully synthesized PPV with two alkoxy substituting side-chains on adjacent carbon atoms (Scheme 1.11) to yield higher electron affinity and a red-shifted energy gap. In 2000 Peeters *et al.,* investigated a series of α,ω-dimethyl-oligo(2,5-bis[2-(S)- methylbuthoxy]-*p*-phenylene

vinylene)s with n = 2-7 (Scheme 1.12).[74] In 2000 Hal *et al.,*[75] measured cation spectra of dialkoxy-substituted OPVs by photoinduced absorption spectroscopy. In 2002, using pulse radiolysis with time-resolved spectrophotometric detection, Grozema *et al.*[76] measured the optical absorption spectra of radical cations of partially dialkoxy-substituted PV oligomers.

Due to their attractive electroluminescence properties, PPVs and their substituted derivatives are now accessible and reasonably well-studied systems.[77-81] Other valuable opto-electronic properties[82] of PPVs and OPVs currently receiving significant attention apart from electroluminescence,[59,61,83] are photo-conductivity,[84] photoluminescence, nonlinear optical response,[85] and electrical conductivity after doping.[86]

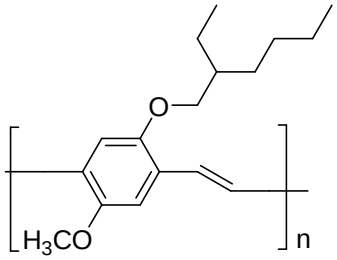

Scheme 1.11. Poly(2-methoxy-5-(2′-ethyl-hexyloxy)-1,4-phenylene vinylene).

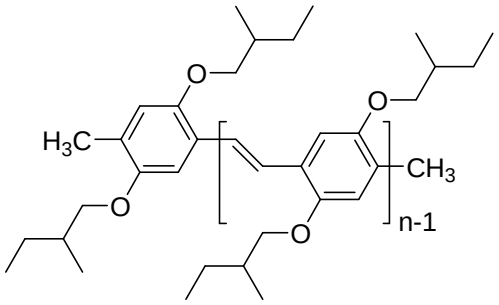

Scheme 1.12. α,ω-dimethyl-oligo(2,5-bis[2-(S)-methylbuthyloxy]-*p*-phenylene vinylene)s.

Well-defined and soluble OPVs cannot only be used as active materials in various applications mentioned above but serve as model compounds to approximate properties for the more complex polymer homologues. In addition, they have the advantage of being soluble and inherently easier to process, making them attractive alternatives to homologous polymers and very useful as versatile electronic building blocks for organic functionalization.

1.3. Biomolecule-polymer conjugates

Biomolecule-polymer conjugates are widely used in medicine and biotechnology[87-89], the biomolecule being either a macromolecule (e.g. protein), lipid, or ligand, such as sugar or biotin. Biotin binds the protein avidin with Ka = 10^{15}. As a consequence, the strong biotin-avidin interaction has been extensively utilized in the life sciences.[90-92] Biotinylated polymers and copolymers of poly(ethylene oxide) (PEO), poly(2-(diethylamino)ethyl methacrylate) (PDEAEMA), poly(ethylene glycol) (PEG), and poly(lactic acid) (PLA) have been studied for various biotechnological applications. PEG has been used as a variable spacer for biotin conjugates with avidin binding capability.[93-95]

1.4. Click Chemistry

The copper catalyzed azide-alkyne 1,2,3–triazole forming “click” reaction[96-100] is a popular coupling reaction that utilizes the general concept of click chemistry. The reaction has been used in a variety of fields, e.g. drug discovery,[101] materials science,[102] and biology.[103] The chemoselective “click” reaction is tolerant to the

presence of a wide range of functional groups; it has been used to label cells,[104] synthesize dendrimers,[105] conducting polymers,[106-112] polymer modified viruses,[113] and gold nanoparticle-enzyme conjugates.[114] Recently, azide-functionalized biotinylated haptens and mannose-derivitized azide have been synthesized using a Kenner-type linker for the preparation of small-molecule-arrays.[115]

2. Synthesis and characterization of homologous oligo(*p*-phenylene vinylene)s (OPVs)

2.1. Method 1: Monomers, dimers, trimers

2.1.1. Overview

The design and synthesis of a library of homologous oligo(p-phenylene vinylene)s (OPVs) is reported. All OPVs are characterized by means of ATR-FTIR, ^{1}H-NMR (200 or 600 MHz) and ^{13}C-NMR (50 or 150 MHz), 2D-NMR (HMBC, HSQC experiments), and optical spectroscopy.

2.1.2. Results and discussion

We report on the design and synthesis of a library containing homologous trimeric, dimeric, and monomeric of dialkyloxy-substituted oligo(p-phenylene vinylene)s (OPVs). The oligomers have been end-group functionalized, making them available to a variety of further derivatization reactions. Specifically, linear n-heptyloxy, n-butyloxy, and methyloxy side chains, and vinyl-, aldehyde-, hydroxy-, and alkyne-end groups are used. The mulit-step synthetic approach starts from commercially available 1,4-hydroquinone toward the monomeric blocks that also serve as intermediates toward the higher homologs. The overall approach is summarized in scheme 2.1. Homologous key intermediates can be identified as oligomers with diacetal-functional chain ends (**4**, **9**, and **15**).

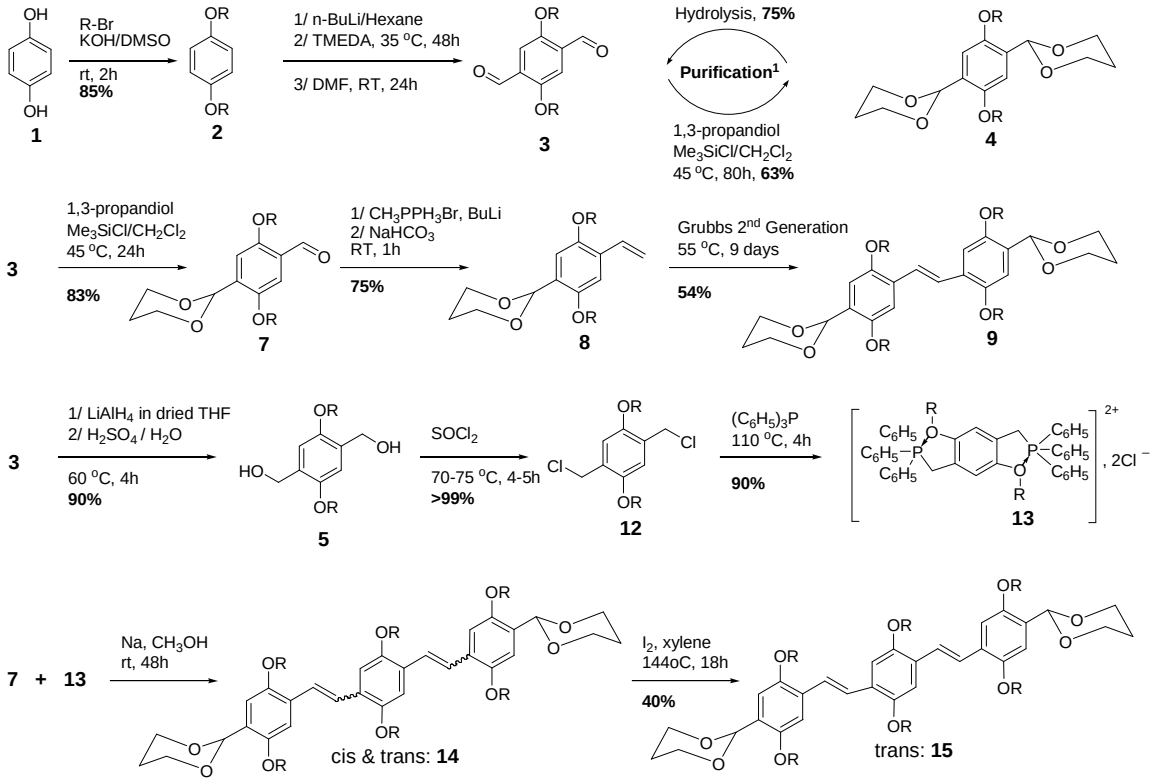

R = (a) -C_7H_{15}, (b) -C_4H_9, and (c) -CH_3

Scheme 2.1. Method 1: Overall synthetic approach for monomers, dimers, and trimers.

2.1.2.1. Synthesis of monomer OPVs

Commercially available 1,4-hydroquinone **1** is converted into 1,4-diheptyloxybenzene **2** with 1-bromoheptane. **2** is ortho-metallated with butyl-Lithium (BuLi) and then reacted with dimethyl formamide (DMF) to yield the dialdehyde-functional monomer **3**. Due to partially incomplete di-lithiation, **3** usually contains 5-10 % (by weight) of the monoaldehyde-functional monomer. Attempts to separate the mono- and difunctional aldehydes via column chromatography or re-crystallization fail. After conversion of all aldehyde functionality of the impure **3** into diacetals in **4**, mono- and bisacetal functional

monomers can be separated via column chromatography. Subsequently, the diacetal functional **4** is quantitatively converted back into the now pure dialdehyde functional **3** (Scheme 2.1, purification). **3** serves as a key intermediate; via reduction with $LiAlH_4$ it affords the dihydroxy-functional monomer **5**. Alternatively, **3** can be converted into the divinyl-functional monomer homologue **6** via a standard Wittig reaction (Scheme 2.2).

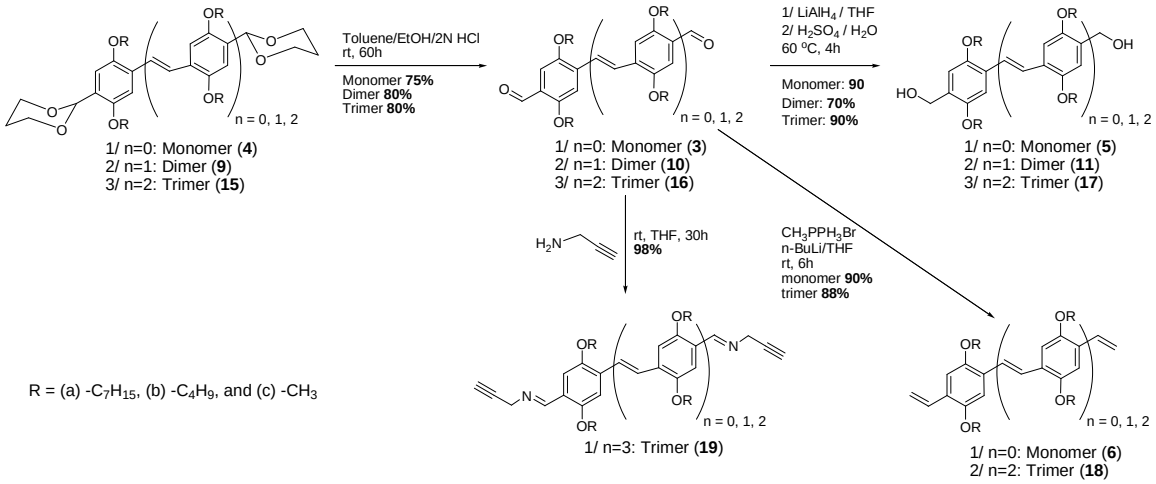

Scheme 2.2. Building block with various end group functionalities.

2.1.2.2. Synthesis of dimer OPVs

As mentioned, monomer **3** also serves as key intermediate in the synthesis of the dimer homologues. To this end, first, one aldehyde function of **3** is converted into an acetal, affording **7**. Secondly, **7** is converted into **8** via a standard Wittig reaction. Subsequently, two molecules of **8** are coupled via olefin metathesis using a Grubbs 2nd generation catalyst, selectively yielding **9**. Hydrolysis of **9** affords yellow-orange crystals of the dialdehyde-functional OPV dimer **10**

(Scheme 2.2). In analogy to the monomer homologue, **10** can be converted either into a divinyl functional or a dialcohol functional OPV dimer **11**.

2.1.2.3. Synthesis of trimer OPVs

The trimer building block is assembled via coupling reaction of **7** and **13**, which originate from intermediates used in the dimer and monomer synthesis respectively. First, **13** is synthesized starting from **5** via chlorination followed by reaction of **12** with triphenylphosphine. Compounds **7** and **13** couple to yield **14**, which features both cis- and trans-configured vinylene bonds. An isomerization of **14** to the all-trans configured **15** is carried out using iodine. **15** is subsequently hydrolyzed to the dialdehyde-functional OPV-trimer **16** (Scheme 2.2). In analogy to the monomer and dimer homologues, **16** is transformed into the respective di-vinyl and di-hydroxy functional trimer OPVs **18** and **17**. Even the dialkyne functional **19** proves accessible via coupling with propargyl amine (Chapter 3).[116]

2.1.2.4. Side chain variation

Representatively, the general synthetic approach has been described in detail for the example of a heptyloxy side chain. A series of homologs using a butyloxy side chain was syntesized accordingly. Attempts using methyloxy side chain substitution did not prove feasible beyond the monomeric unit due to limited solubility of even the dimeric OPVs and beyond in particular.

2.1.3. Spectroscopic characterization

2.1.3.1. Nuclear magnetic resonance (NMR)

NMR confirms the target structures. Representatively, a complete assignment of a trimer-OPV with dialdehyde endgroups **16** is shown in figure 2.1.

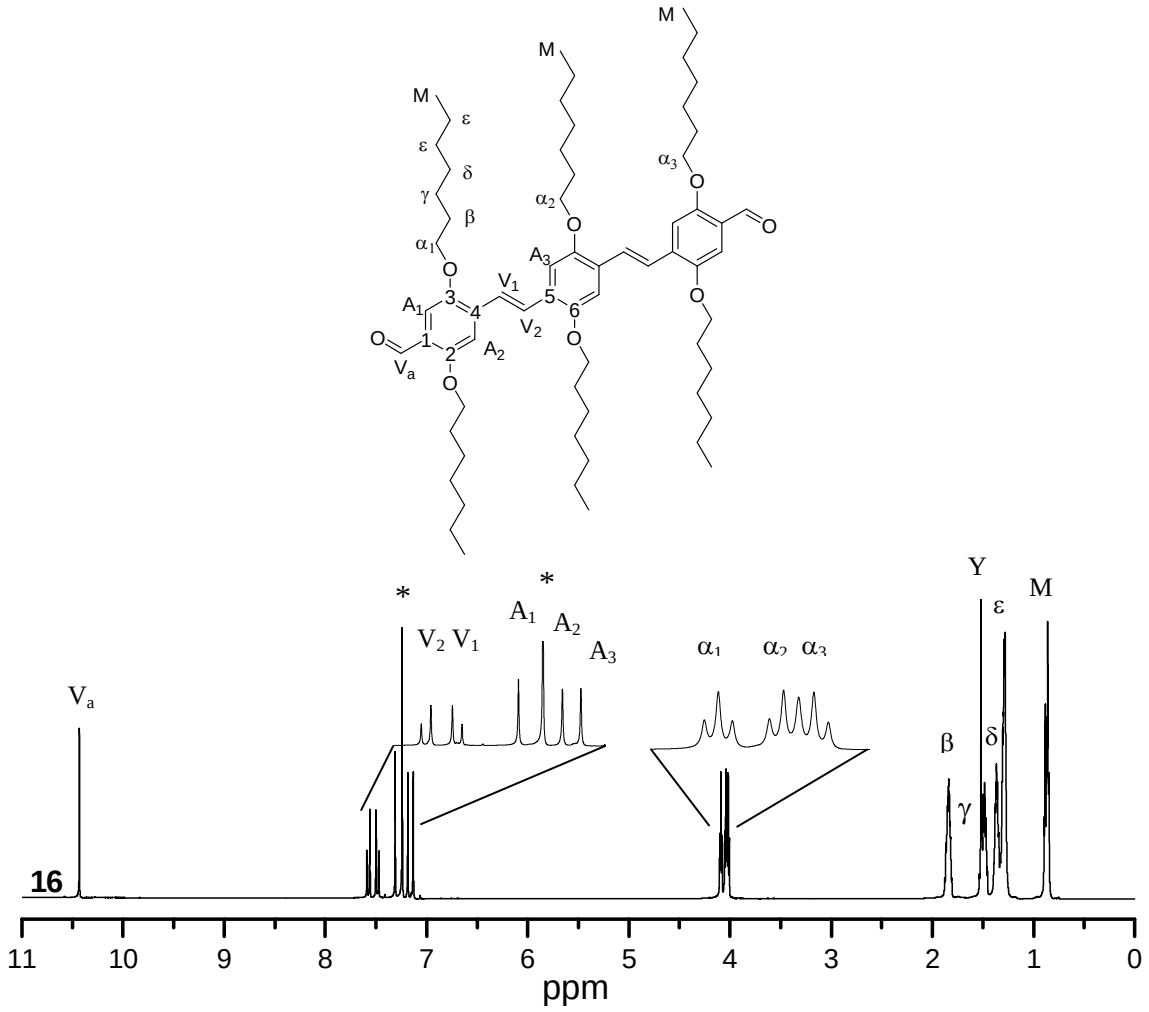

Figure 2.1. ^{1}H-NMR (600Hz, $CDCl_3$) spectrum of OPV 16 with complete assignments.

All OPV homologues feature a centro-symmetry, enabling resolved ^{1}H-NMR spectra in which resonances from the different functional units of the oligomer can be systematically analyzed in regard to chain-length, side-chain substitution,

and end-group functionalization. In all cases the terminal methyl protons M from the heptyloxy side chains are resolved at ~0.8 – 0.9 ppm. The alkyl CH_2 protons β through ε are observed at ~1.8 – 1.3 ppm respectively. The CH_2 protons next to O are shifted to ~4.0 – 4.1 ppm and resolve into three triplets (in the case of the OPV trimers) with different chemical shifts, depending on their position in the molecule. α_1 and α_3 are connected to the lateral phenylene rings and pointed toward the outside or inside of the molecule respectively. α_2 marks the resonances from the -OCH_2 protons on the medial phenylene ring. The aromatic protons A_1, A_2, and A_3 show resonances at ~7.31, 7.18, and 7.13 ppm respectively. The vinylene protons V_1 and V_2 cause resonances centered at ~7.50 and 7.56 ppm respectively, and the aldehyde protons V_a show a resonance at ~ 10.43 ppm.

The resonances from the aromatic and vinylene protons proved highly dependent on the end-group (aldehyde, hydroxy, vinyl, and alkyne). Two-dimensional NMR, i.e. heteronuclear single quantum correlation (HSQC) and heteronuclear multiple bond correlation (HMBC), enabled the exact assignment of every single resonance. Figure 2.2 examplarily illustrates the single bond C-H correlation via the HSQC experiment of T-OPV-CHO **16**. All the carbons with show cross peaks directly bonded protons, e.g., the H_{A1} is coupling with C_{A1}, while quaternary carbons do not show any crosspeaks in this experiment. Table 2.1 details the observed single bond C-H correlations of a select region.

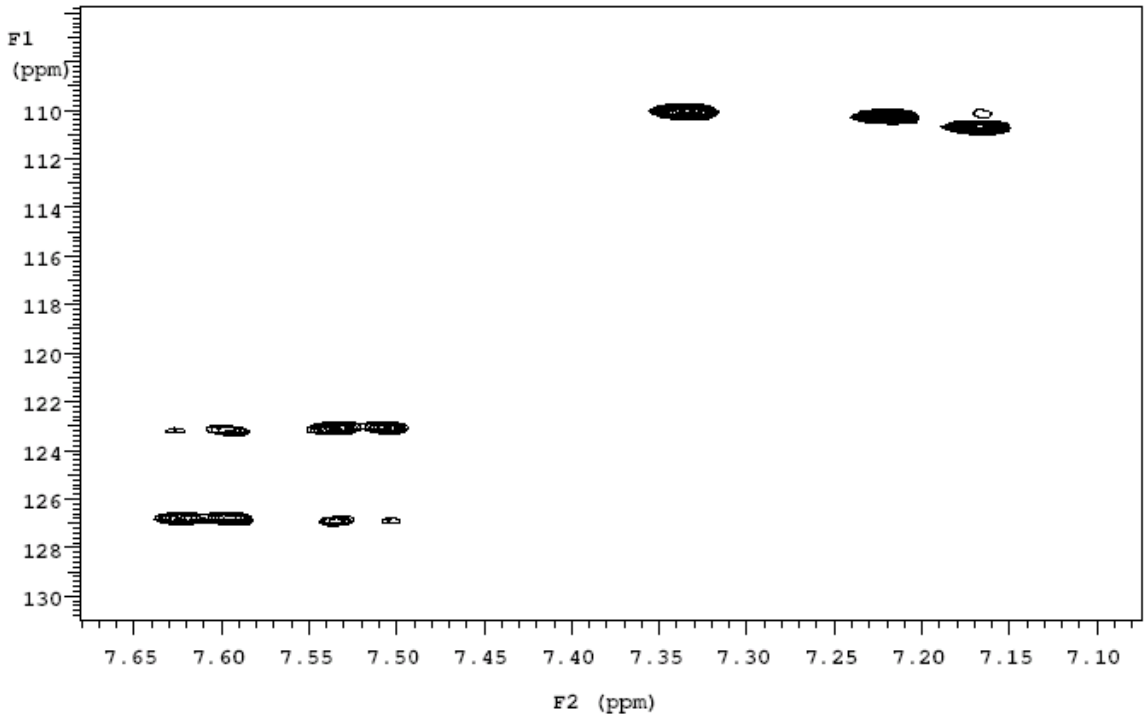

Figure 2.2. HSQC spectrum (600 Hz, $CDCl_3$) of OPV **16** (Select region).

Table 2.1. Observed single bond C-H couplings in T-OPV-CHO **16** (HSQC-experiment).

HSQC	H_{A1}	H_{A2}	H_{V1}	H_{V2}	H_{A3}	$H_{\alpha1}$	$H_{\alpha2}$	$H_{\alpha3}$
C_{A1}	√							
C_{A2}		√						
C_{V1}			√					
C_{V2}				√				
C_{A3}					√			
$C_{\alpha1}$						√		
$C_{\alpha2}$							√	
$C_{\alpha3}$								√

Figure 2.3 examplarily illustrates the HMBC of **16** (select region). This experiment enables the analysis of long-range correlations between carbons and protons that are two (J2) or three (J3) bonds apart. The H_{Va} proton shows a cross peak correlating via J2 to C_1 and via J3 to C_{A1} and C_2. Table 2.2 details the observed multiple bond C-H correlations of a select region of **16**.

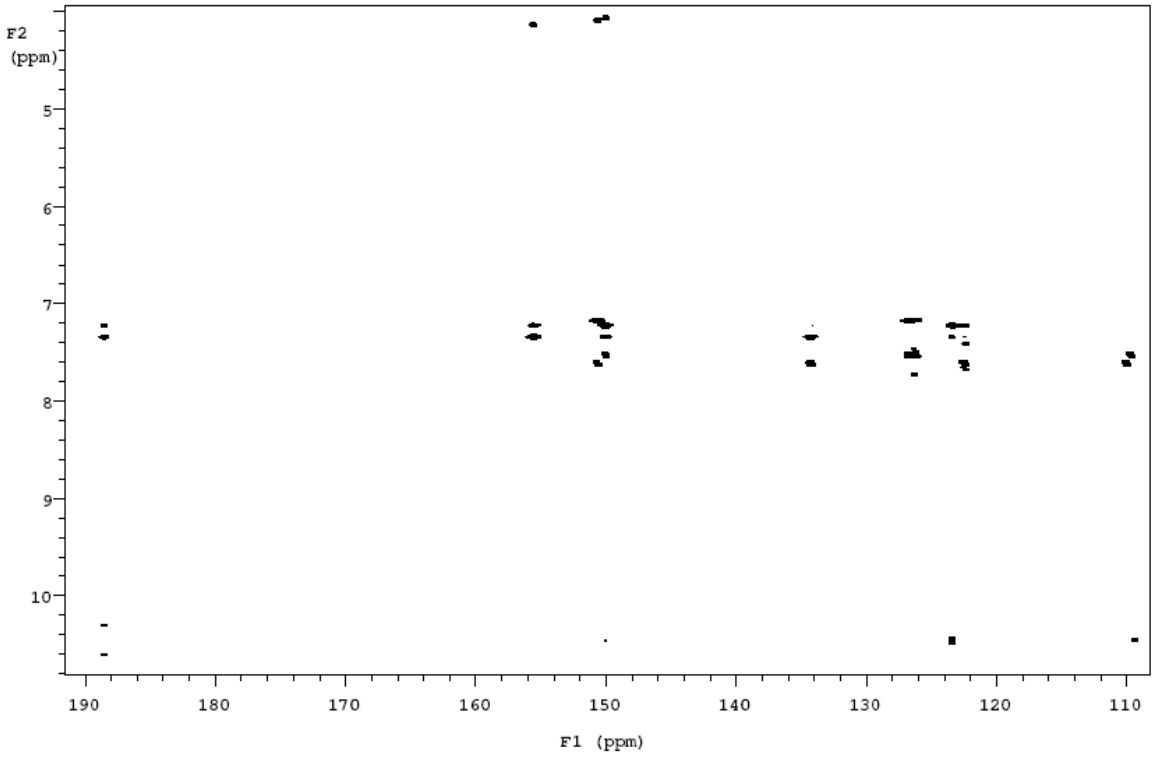

Figure 2.3. HMBC spectrum (600 Hz, $CDCl_3$) of OPV **16** (Select region).

Table 2.2. Observed multiple bond C-H couplings in **16** (HMBC-experiment).

HMBC	H_{Va}	H_{A1}	H_{A2}	H_{V1}	H_{V2}	H_{A3}	$H_{\alpha1}$	$H_{\alpha2}$	$H_{\alpha3}$
C_{Va}		√							
C_1	√	√	√						
C_{A1}	√								
C_3		√	√	X			√		
C_4		√	√	√	√				
C_{A2}				√					
C_2	√	√	√						√
C_{V1}			√		√				
C_{V2}				√		√			
C_5				√	X	√			
C_{A3}					√	√			
C_6					√	√		√	

√ : coupling expected and observed

x : coupling expected and no significant coupling observed

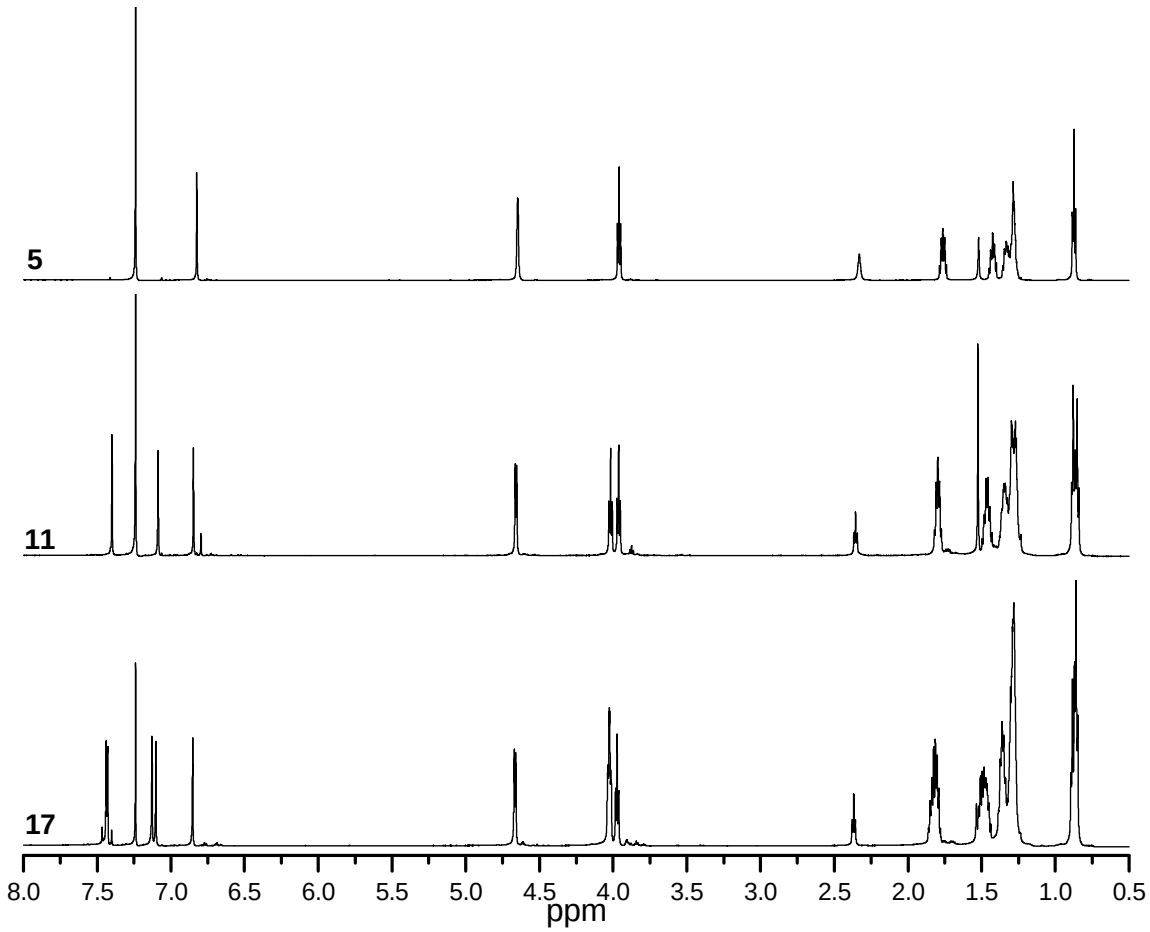

Figure 2.4. ^{1}H-NMR (600 Hz, $CDCl_3$) spectra of dihydroxy OPVs with different chain lengths e.g. monomer **6**, dimer **11**, and trimer **17**.

Figure 2.4 illustrates the chain-length dependent ^{1}H-NMR spectra by overlaying dihydroxy-functional monomer, dimer, and trimer OPV homologues **6**, **11**, **17**. The monomer spectrum of **6** shows a resonance of the aromatic proton from the phenylene ring at ~6.8 ppm. In the case of the dimer **11**, two resonances from aromatic protons are observed with an integral ratio 1:1. One signal is caused by the aromatic protons near the terminal hydroxyl groups (~6.85 ppm) and the other by the aromatic protons next to the newly formed vinylene bond (~7.09 ppm). In the case of the trimer **17** a third resonance from an aromatic proton is

caused by the protons from the central phenylene ring at~7.15 with the same integral intensity. The respective resonances from the outer rings are slightly shifted to 7.13 and ~6.88 ppm due to the increased electronic system. Resonances from protons at the internal vinylene bonds in the dimer are observed at ~7.4 ppm. The trimer shows two vinylene resonances at ~7.46 and ~7.45 ppm. These were assigned to the inner and outer vinylene protons V_2 and V_1 respectively.

Just as the resonances from the aromatic and vinylene protons, the resonances from protons in the OCH_2-units highly dependent on the chain end functionality. To illustrate this, figure 2.5 shows overlaid end-group dependent NMR spectra of trimer OPVs for two select regions.

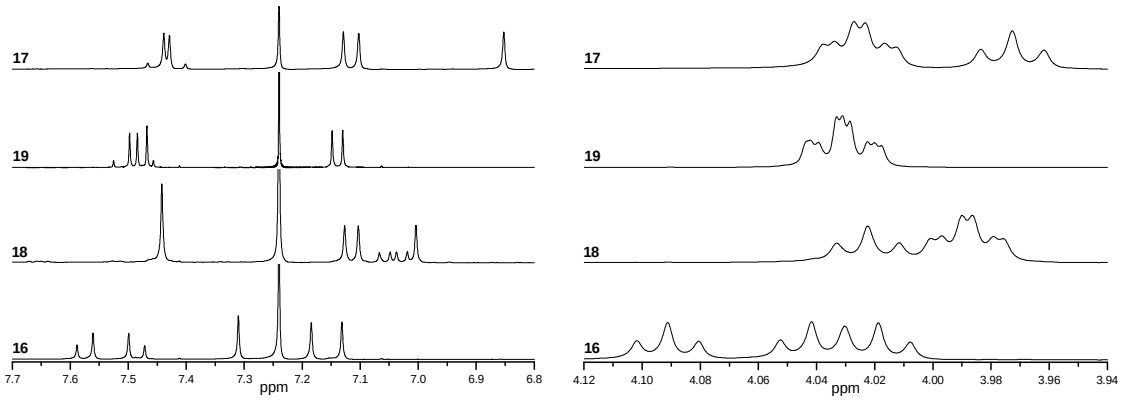

Figure 2.5 End-group dependent ^1H NMR spectra (600 Hz, $CDCl_3$) of trimer OPVs **16**, **17**, **18**, and **19**, (Select regions).

The dihydroxy functional trimer OPV **17** shows characteristic triplet resonance at ~2.40 ppm from –O<u>H</u>, and a doublet from C<u>**H$_2$**</u>-OH at 4.69 ppm (not shown). The dialkyne functional trimer OPV **19** features a singlet at ~2.47 ppm from the alkyne C≡C<u>H</u>, a singlet at ~4.50 ppm for the N-C<u>H$_2$</u>, and a singlet at ~8.99 ppm from

C<u>H</u>=N. The divinyl OPV **18** causes two doublets of doublets at ~5.25 and ~5.74 ppm for the trans- and cis-vinyl protons respectively, and a doublet of doublets centered at ~7.05 ppm from C<u>**H**</u>=CH_2 (V_a). The dialdehyde **16** features a singlet at 10.43 ppm from the aldehyde proton.

The end-groups are directly connected to the aromatic system, resulting in very characteristic chemical shifts of homologous protons A, V, and α. Table 2.3 details characteristic chemical shifts for the trimer OPV homologues.

Table 2.3. Select chemical shifts (^{1}H-NMR) in trimer OPVs **16**, **17**, **18**, and **19.**

trimer OPV	Chemical Shift δ (ppm)							
	A_1	A_2	A_3	V_1	V_2	α_1	α_2	α_3
19	7.47	7.15	7.13	7.48	7.50	4.08	4.07	4.06
18	7.00	7.10	7.13	7.44		3.99	4.02	4.00
17	6.88	7.13	7.15	7.45	7.46	4.00	4.06	4.04
16	7.31	7.18	7.13	7.50	7.56	4.10	4.06	4.04

In the case for aromatics protons A_1, A_2, A_3 the respective resonances are found as three singlets at ~6.88, 7.13, and 7.15ppm for the trimer dialcohol **17**, at ~7.00, 7.10, and 7.13ppm for the timer divinyl **18**, at ~7.47, 7.15, and 7.13ppm for the trimer dialkyne **19**, and at ~7.31, 7.18, and 7.13ppm for trimer dialdehyde **16**, respectively. The vinylene protons resonate as one singlet (V_1=V_2 ~7.44ppm) in the case of trimer divinyl, as two singlets (V_1 ~7.48, V_2 ~7.50ppm) in the trimer-dialkyne, and as two singlets (V_1 ~7.50, V_2 ~7.56ppm) in the trimer–dialdehyde.

This distinct behavior is likely due to the high electronegativity of terminal aldehydes compare to the other homologues. The trimer-dialcohol shows two singlets for the vinylene protons $V_1$and V_2 at ~7.45 and: ~7.46ppm respectively.

The overlaid spectra on the right side of figure 2.5 show end-group dependent H-NMR spectra for the α-methylene proton region. The end-groups also have strong influence on the α-methylene region (α_1, α_2, and α_3). The α- protons show three resolved triplets at ~4.10, 4.06, and 4.04ppm in trimer-dialdehyde **16**, at ~4.00, 4.06, and 4.04ppm in the trimer-dialcohol **17**, at ~3.99, 4.02, and 4.00ppm in the trimer-divinyl **18**, and at ~4.08, 4.07, and 4.06ppm in the trimer-dialkyne **19**.

Figure 2.6 exemplarily illustrates the chain-length dependent ^{13}C-NMR spectra by overlaying dihydroxy -functional monomer, dimer, and trimer OPV homologues **6**, **11**, and **17**. ^{13}C assignments are detailed in scheme 2.3. The monomer spectrum of **6** shows aromatic carbon resonances from the phenylene ring at ~112.1 (3), 128.8 (2), and 150.4 (4) ppm. The dimer **11** shows aromatic carbon resonance at ~129.4 (2), 114.0 (3), 150.6 (4), 127.1 (5), 109.1 (6), and 151.1 (7) ppm. In the case of the trimer **17** the aromatic carbon resonances are observed at ~129.33 (2), 113.97 (3), 150.63 (4), 127.18 (5), 109.05 (6), 151.05 (7), 127.37 (10), 110.64 (11), and 151.07 (12) ppm. The internal vinylene carbon resonances in the dimer are observed at ~123.5 (8, 9) ppm. The trimer shows two internal vinylene carbon resonances at ~123.48 (8) and 123.34 (9) ppm. Table 2.4 details the respective chemical ^{13}C-shifts in the dihydroxy -functional OPV homologues **6**, **11**, and **17**.

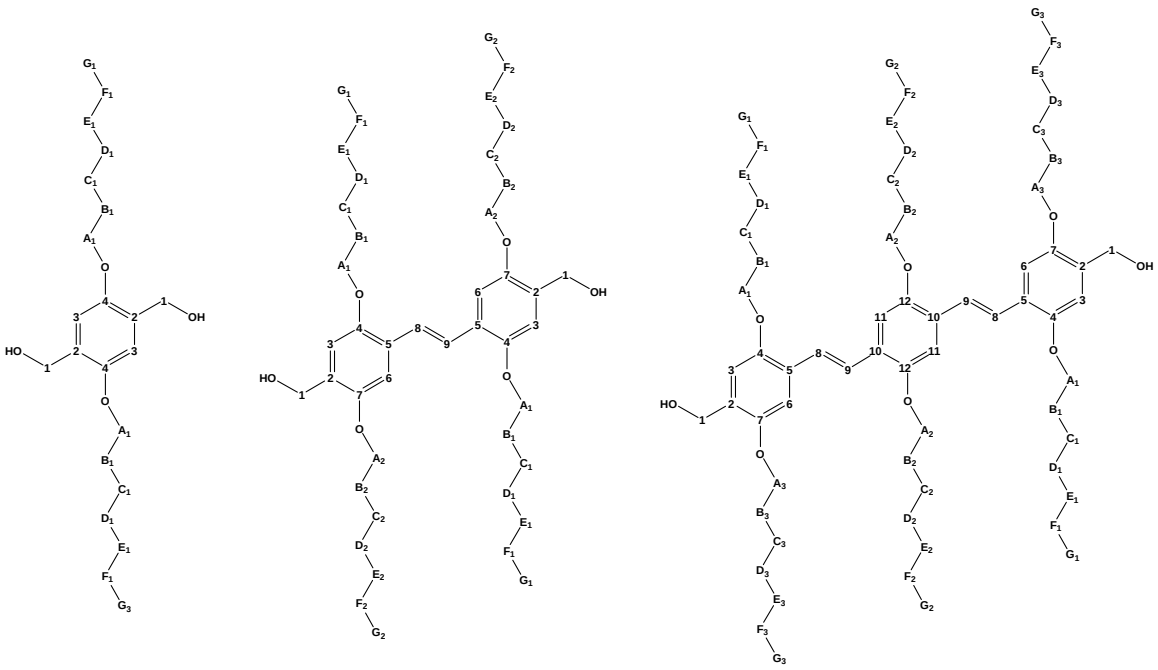

Scheme 2.3. Dihydroxy functional OPVs with varying side-chain lengths e.g. monomer **6**, dimer **11**, and trimer **17**: Carbon assignments.

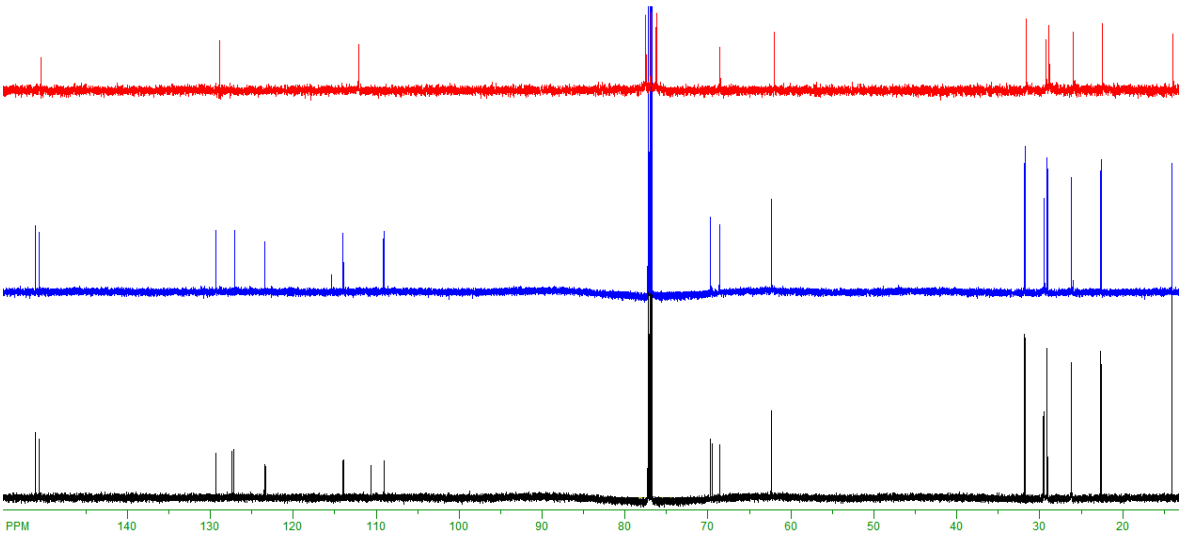

Figure 2.6. ^{13}C-NMR (50 and 150 Hz, $CDCl_3$) spectra of dihydroxy OPVs with different chain lengths e.g. monomer **6** (red), dimer **11** (blue), and trimer **17** (black).

Table 2.4. Summarized ^{13}C NMR shifts with assignments of **6**, **11**, and **17**.

Carbon assignment	**6**[a)]	**11**[b)]	**17**[b)]
Methyl	13.9 (G)	14.07-14.08 (G_1-G_2)	14.08-14.09 (G_1-G_3)
Methylene	22.4 (F) 31.6 (E) 28.9 (D) 25.9 (C) 29.2 (B) 68.5 (A) 62.0 (1)	22.64-22.62 (F_1-F_2) 31.85-31.79 (E_1-E_2) 29.10-29.08 (D_1-D_2) 26.2-26.1 (C_1-C_2) 29.50-29.46 (B_1-B_2) 68.6-69.7 (A_1-A_2) 62.3 (1)	22.66-22.62 (F_1-F_3) 31.88-31.79 (E_1-E_3) 29.17-29.09 (D_1-D_3) 26.23-26.16 (C_1-C_3) 29.56-29.47 (B_1-B_3) 69.68-68.55 (A_1-A_3) 62.33 (1)
Aromatic	128.8 (2) 112.1 (3) 150.4 (4)	129.4 (2) 114.0 (3) 150.6 (4) 127.1 (5) 109.1 (6) 151.1 (7)	129.33 (2) 113.97 (3) 150.63 (4) 127.18 (5) 109.05 (6) 151.05 (7) 127.37 (10) 110.64 (11) 151.07 (12)
Vinylene (V)	n.a.	123.5 (8 & 9)	123.48 (8) 123.34 (9)

[a)] 50MHz [b)] 150 MHz

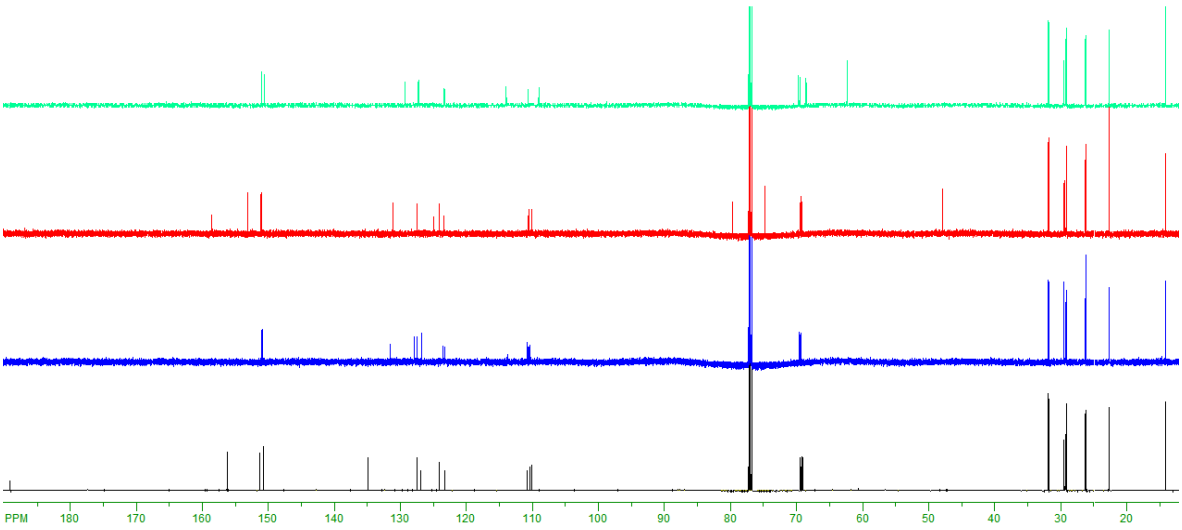

Figure 2.7. End-group dependent ^{13}C-NMR (150 Hz, $CDCl_3$) spectra of trimer building blocks **16** (black), **17** (green), **18** (blue), and **19** (red).

Table 2.5. details the respective chemical ^{13}C-shifts in the different-functional OPV homologues **16**, **18**, and **19**.

2.1.3.2. Attenuated total reflection fourier transform infrared (ATR-FTIR)

Figure 2.8 shows end-group dependent ATR-FTIR spectra of trimer building blocks, the analysis of which confirms observations from NMR studies. The trimer dialdehyde shows aromatic aldehyde end-functional (C=O) stretching vibrations with extended conjugation at 1674 cm^{-1}. The trimer dialcohol shows hydroxy end-functional (OH) stretching vibration at 3319 cm^{-1}. The trimer divinyl shows terminal vinylene end-functional group (-CH=CH_2) out of plane deformation at 994 and 913 cm^{-1}. The trimer dilakyne shows alkyne end-

functional group stretching vibration (≡C-H) at 3307 cm^{-1} and C=N stretching at 1639 cm^{-1}.

Table 2.5. Summarized ^{13}C-NMR assignments of **16**, **18**, and **19**.

Carbon assignment	**16**[b)]	**18**[b)]	**19**[b)]
Methyl	14.1 (G_1-G_3)	14.1-14.07 (G_1-G_3)	14.1-14.08 (G_1-G_3)
Methylene	22.64-22.61 (F_1-F_3) 31.90-31.77 (E_1-E_3) 29.14-29.06 (D_1-D_3) 26.2-26.1 (C_1-C_3) 29.5-29.27 (B_1-B_3) 69.4-69.04 (A_1-A_3)	22.65-22.63 (F_1-F_3) 31.86-31.82 (E_1-E_3) 29.14-29.12 (D_1-D_3) 26.23-26.18 (C_1-C_3) 29.6-29.17 (B_1-B_3) 69.6-69.3 (A_1-A_3)	22.65-22.63 (F_1-F_3) 31.86-31.83 (E_1-E_3) 29.16-29.10 (D_1-D_3) 26.23-26.14 (C_1-C_3) 29.52-29.42 (B_1-B_3) 69.44-69.16 (A_1-A_3)
Aromatic	110.1-110.8 (3, 6, & 11) 135.0, 127.5, & 124.1 (2, 5, & 10) 150.6-156.3 (4, 7, & 12)	110.8-110.4 (3, 6, & 11) 127.9-126.8 (2, 5, & 10) 151.1-150.8 (4, 7, & 12)	110.7-110.1 (3, 6, & 11) 131.1, 125, & 124.2 (2, 5, & 10) 151.0-153.1 (4, 7, & 12)
Vinylene (V)	123.2 & 127.0 (8 & 9)	123.3-123.5 (8 & 9)	123.4 & 127.4 (8 & 9)
End-group	189.2 (1)	131.6 (1) 113.8 (=CH_2)	158.7 (1) 79.7 (-C≡) 74.8 (≡CH) 47.9 (N-CH_2-)

[a)] 50MHz [b)] 150 MHz

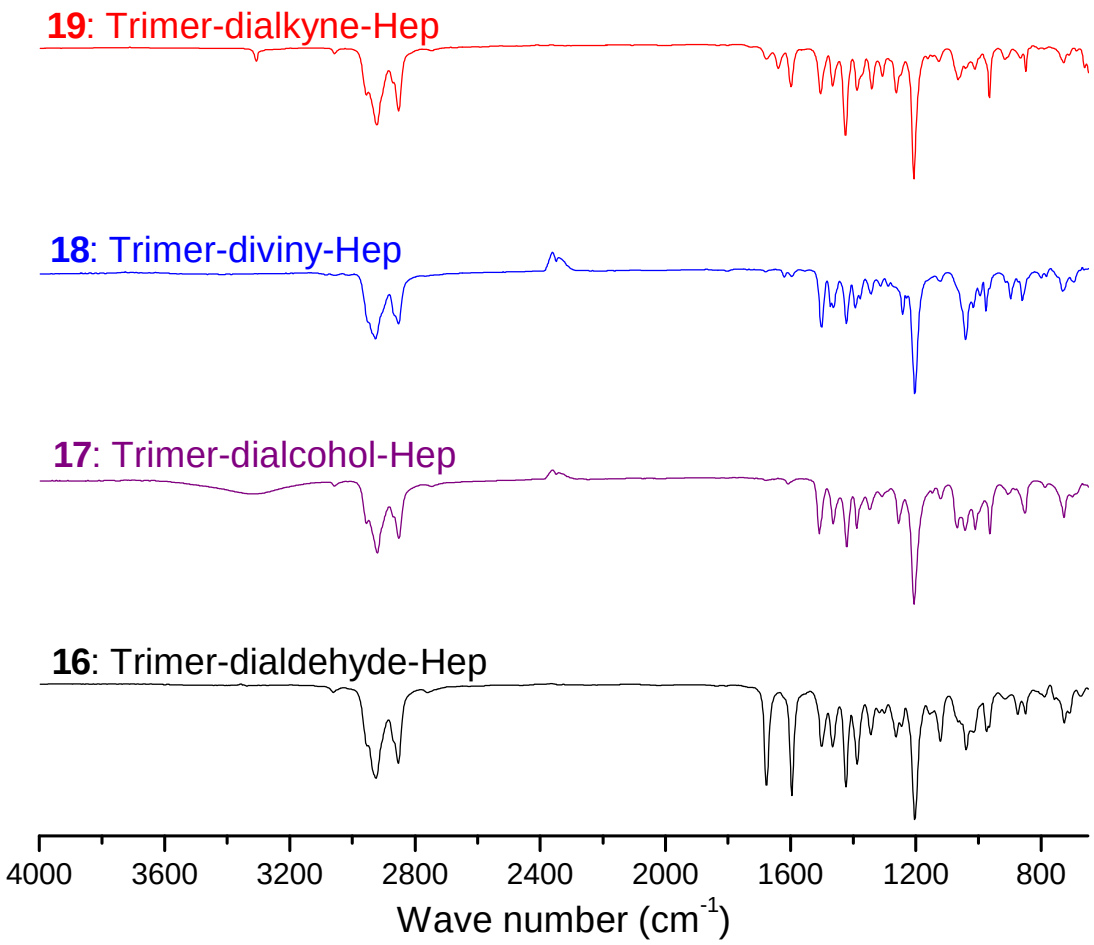

Figure 2.8. ATR-FTIR spectra of trimer OPVs **16**, **17**, **18**, and **19**.

The chain length dependent ATR-FTIR spectra (Figure 2.9) are representatively illustrated for dihydroxy end-functional oligomers with lateral heptyloxy side-chain substitution (Select region 650-1600cm^{-1}). The monomer shows no absorptions from any vinylene group, while dimer and trimer show vinylene (CH=CH) out of plane deformations at 964cm^{-1}.

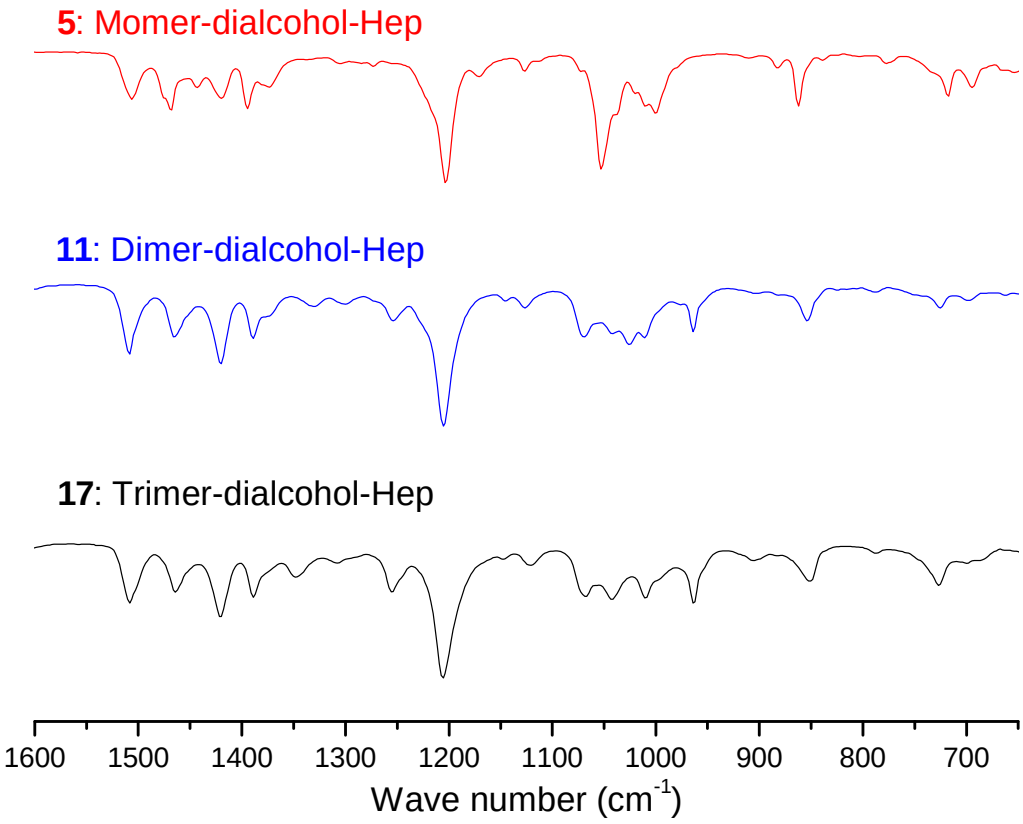

Figure 2.9. ATR-FTIR spectra of dihydroxy OPVs with different chain lengths e.g. monomer **6**, dimer **11**, and trimer **17** (select regions).

2.1.3.3. UV/Vis absorption and emission

Figure 2.10 shows normalized chain-length dependent UV/Vis absorption (left) and emission (right) spectra of dihydroxy functional building blocks with lateral diheptyloxy side chain substitution.

As expected, a bathochromic shift in the absorption maximum is observed with increasing chain length. λ_{max} for the monomer, dimer, and trimer (**5**, **11**, and **17)** are observed at 296, 361, and 410 nm respectively. When excited in their respective absorption maxima, **5**, **11**, and **17** display emission maxima λ_{max} at 334, 410, and 462 nm respectively. All emission spectra contain long wavelength

components at ~ 440, 465, and 485 nm, respectively, due to aggregation via hydrogen bonding of the terminal hydroxy groups.[117]

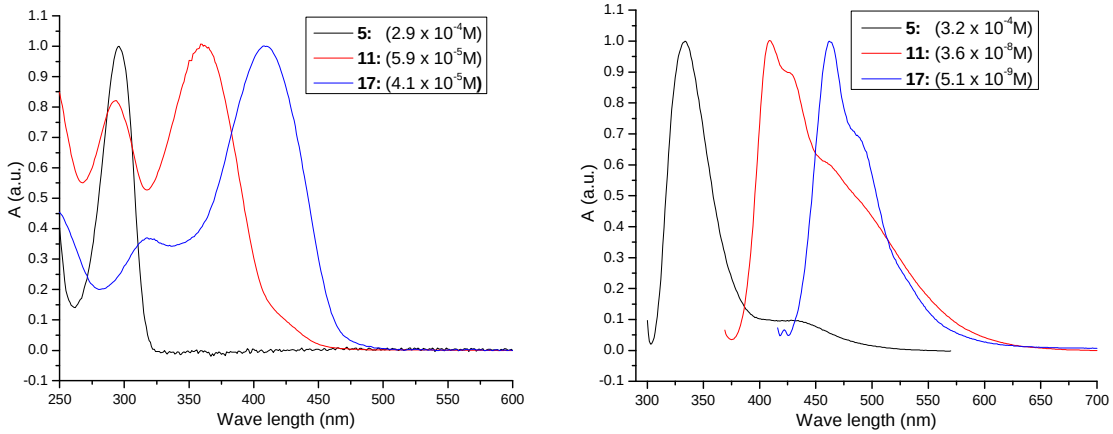

Figure 2.10. Normalized UV/visible absorption (left) and emission (right) spectra of dihydroxy-functional OPVs **5** (black), **11** (red), and **17** (blue) in $CHCl_3$.

The end group has a strong influence on the optical characteristics also. Representatively, figure 2.11 compares the normalized UV/Vis absorption (left) and emission (right) spectra of OPV-trimers with different end groups (**16**, **17**, **18**, and **19**).

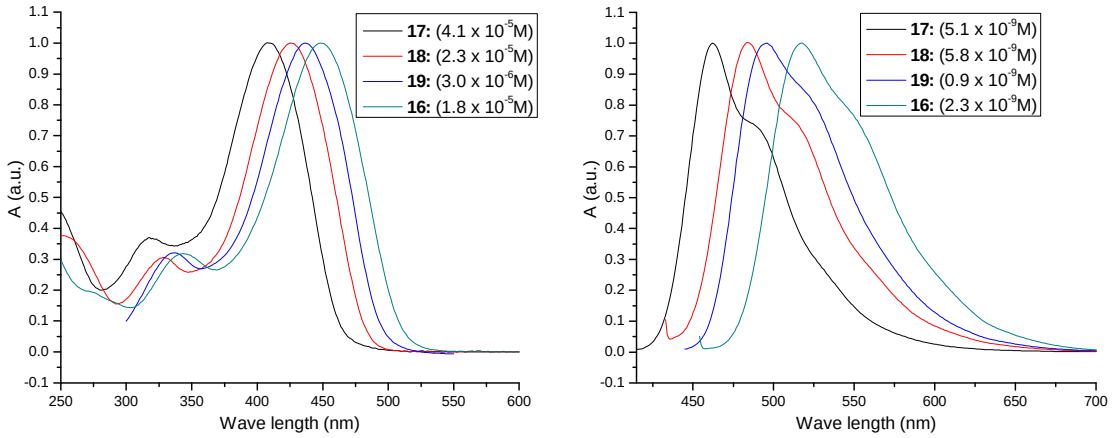

Figure 2.11. UV/visible absorption (left) and emission (right) spectra (normalized) of trimer OPVs **16** (green), **17** (black), **18** (red), and **19** (blue) in $CHCl_3$.

The values for the absorption maximum λ_{max} increase in the order dialcohol **17**, divinyl **18**, dialkyne **19**, dialdehyde **16** with λ_{max} = 410, 426, 437, 449 nm respectively. The same order is observed for the emission maxima with λ_{max} = 461, 484, 496, 517 nm respectively. The trimer dialcohol shows lowest wavelength absorption and emission maxima due to high electronegativity of the chain end –OH, and the fact that these O are not in conjugation with the aromat. The absorption and emission show an increase in the maximum wavelength from divinyl to dialkyne to dialdehyde, probably due to the increase in electronegativity from C to N to O, respectively.

Varying the alkyloxy sidechain (heptyloxy, buthyloxy, and methyloxy) does not significantly influence the optical properties in solution. The absorption and emission wavelengths of the depicted spectra are summarized in table 2.6.

Table 2.6. The absorption and emission wavelengths of the depicted spectra of OPVs.

OPV	λ_{max} Absorption (nm)	λ_{max} Emission (nm)
17	410	461
18	426	484
19	437	496
16	449	517
16b		
11	361	410
5a	296	334
5b		
5c		
6c	344	391
3c	399	456

R = (a) $–C_7H_{15}$, (b) $–C_4H_9$, and (c) $–CH_3$

2.1.4. Experimental

2.1.4.1. General information

All experiments using air/moisture sensitive materials were carried out under an atmosphere of high purity argon using standard Schlenk techniques. All glass-ware was cleaned and dried for at least 24h in an oven at 120^{o}C prior to use.

2.1.4.2. Chemicals

Hydroquinone 90+%, 1-bromoheptane 90%, 1-bromobutane 99%, dimethyl sulfoxide (DMSO) 99.9%, 1,4-dimethoxy benzene 99%, n-butyl lithium (^{n}Bu-Li: 2.5M or 1.6M solution in hexane), tetramethylethylenediamine (TMEDA) 99.5%, triphenylphosphine 99%, 1,3-propandiol 99.6%, chlorotrimethylsilane redistilled 99+%, iodine 99.9%, methyl-triphenyl-phosphoniumbromid 98%, Grubbs 2nd generation, thionyl chloride ($SOCl_2$) 97%, and propargylamine 98% were purchased from Sigma-Aldrich. Xylenes certified ACS, chloroform HPLC grade, ethanol, methanol, acetone were purchased from Fisher Scientific. Dimethylformamide (DMF) 99.8% was purchased from Acros. Hexane, THF, methylenechloride and toluene, all are HPLC grade, were purchased from Fisher Scientific and were dried and degassed, using a “Pure Solv” solvent purification system (using activated alumina, copper catalyst, molecular sieves columns) by Innovative Technology Inc. before use. All other chemicals were used as received. Column chromatography was carried out on silica gel 60 (particle size: 0.063-0.200nm) from VWR. Intermediates and products were analyzed by means

of FTIR/ATR, ^{1}H-NMR(200 or 600Hz), and ^{13}C-NMR (50 or 150Hz) in regard to size, microstructure, and purity.

2.1.4.3. Instrumentation

^{1}H NMR (200 or 600Hz) and ^{13}C NMR (50 or 150Hz) spectra were recorded on Varian spectrometers in $CDCl_3$ or DMSO as an internal deuterium lock for ^{1}H-NMR. Heteronuclear single quantum correlation (HSQC) and heteronuclear multiple bond correlation (HMBC) experiments were done on 600MHz spectrometer. ATR-FTIR spectra were recorded on Bruker Tensor 27 spectrometer using a Pike ATR accessory for characterizing samples. All data were processed and analyzed by OPUS software. UV-Visible absorption spectra were recorded using a Perkin Elmer Lambda 650 Spectrophotometeter with 1-cm path length cells. Solvents for optical property investigations were Spectrasolv from Fisher Scientific. Photoluminescence spectra were recorded using a Horiba Jobin Yvon Fluoromax-3 spectrofluorometer with 1-cm path length cells. The cells were cleared and samples were prepared with spectroscopic grade chloroform and hexanes.

2.1.4.4. Synthesis of OPVs with heptyloxy as side chain

2.1.4.4.1. Synthesis of 1,4-diheptyloxybenzene (2a)

80.16g of potassium hydroxide (pellets) and 400mL dimethylsulfoxide (DMSO) were stirred for 30 min under argon. 18.7g (170mmol) of hydroquinone (**1**) was added and stirred for other 30 min and then added 100mL (640mmol) of 1-

bromoheptane. The reaction mixture was stirred at room temperature for 2 hours and then poured into 1.5L ice-bath. The precipitate was filtered and recrystallized with 100ml ethanol three times to yield 1,4-diheptyloxybenzene (**2a**, 44.0g, 85%).

^{1}H-NMR ($CDCl_3$, 600MHz): [ppm] 6.81 (4H, s, CH-aromatic), 3.89 (4H, t, α-CH_2-), 1.74 (4H, m, β-CH_2-), 1.43 (4H, m, γ-CH_2-), 1.34 (4H, m, δ-CH_2-), 1.30 (8H, m, ε-CH_2-), and 0.88 (6H, t, -CH_3). ^{13}C-NMR ($CDCl_3$, 50MHz): [ppm] 153.2, 115.4, 68.6, 31.8, 29.4, 29.1, 26.0, 22.6, and 14.1.

2.1.4.4.2. Synthesis of 2,5-diheptyloxyterephthalaldehyde (3a before purification)

15g (49mmol) of **2a** was dissolved in 200mL dried hexane under argon. 22.1mL (148mmol) of tetramethylethylenediamine (TMEDA) was added into it and cooled down to 0^0C. 59mL (148mmol, 2.5M in hexane) of n-buthylithium was added dropwise for 45min under continuous stirring. The reaction flask was heated at 35 ^{o}C for 48 hours and cooled down to 0 ^{o}C. 13.3mL (173mmol) of dimethylformamide (DMF) was added and stirred at room temperature for another of 24 hours. The reaction mixture was hydrolized by pouring into 1L HCl-icebath. The precipitate was filtered. The water phase was extracted with 100ml toluene for several times. The precipitate was dissolved with 50mL toluene and washed with 100mL water for several times. Combined toluene phases were dried over Na_2SO_4 overnight and filtered. The solvent was evaporated out to yield a mixture of mono- and di-aldehyde (**3a** before purification 13.43g, 80%).

2.1.4.4.3. Synthesis of 1,4-diheptyloxyterephthalaldehyd-(1,3-propandiol)acetal (4a)

12.5g (34.7mmol) of 2,5-diheptyloxyterephthalaldehyde (mixture of mono- and di-aldehyde) were dissolved in 180mL dried dichloromethane under argon. 10.1mL (139mmol) of 1,3-propandiol was added and followed by 35.5mL (280mmol) of chlorotrimethylsilane. The reaction solution was refluxed at 45 ^{o}C for 80 hours. The mixture was hydrolyzed by 24g $NaHCO_3/H_2O$. Column chromatography (Silica gel 60: Hexane/toluene-toluene-toluene/chloroform) was used to yield 1,4-diheptyloxy terephthalaldehyd-(1,3-propandiol)acetal (**4a**, 10.45g, 63%).

^{1}H-NMR ($CDCl_3$, 200MHz): [ppm] 7.11 (2H, s, CH-aromatic), 5.80 (2H, s, CH-acetal), 4.20 (8H, t, α-CH_2-acetal) 3.96 (4H, t, α-CH_2-alkyl), 2.18 (4H, m, β-CH_2-acetal), 1.75 (4H, m, β-CH_2-alkyl) 1.36 (16H, m, -CH_2-alkyl), and 0.88 (6H, t, -CH_3).

2.1.4.4.4. Synthesis of 2,5-diheptyloxyterephthalaldehyde (3a purified)

10.5g (22mmol) of **4a** was dissolved in 250mL toluene. Then, 200mL ethanol and 200mL 2M HCl were added into it. The reaction mixture was stirred vividly for 60 hours at room temperature. The toluene phase was separated and the water phase was extracted with 20mL toluene for several times. The combined organic solvent was dried over Na_2SO_4 and solvent was evaporated off. Column chromatography (Al_2O_3 basic type II, toluene-toluene/chloroform) was used to yield 2,5-diheptyloxyterephthalaldehyde (**3a**, 5.97g, 75%).

^{1}H-NMR ($CDCl_3$, 600MHz): [ppm] 10.50 (2H, s, -CHO), 7.41 (2H, s, CH-aromatic), 4.06 (4H, t, J=6.47Hz, α-CH_2-), 1.88 (4H, m, β-CH_2-), 1.45 (4H, m, γ-CH_2-), 1.34 (4H, m, δ-CH_2-) 1.29 (8H, m, ε-CH_2-), and 0.87 (6H, t, J=6.95Hz, -CH_3). ^{13}C-NMR ($CDCl_3$, 50MHz): [ppm] 189.2, 155.1, 129.1, 111.4, 69.1, 31.6, 28.93, 28.88, 25.9, 22.5, and 13.9. ATR-FTIR [cm^{-1}]: 3055, 2953, 2930, 2862, 2870, 2854, 1681, 1489, 1472, 1429, 1395, 1288, 1217, 1140, 857, 746, 720, and 695.

2.1.4.4.5. Synthesis of 2,5-diheptyloxy-4-(1,3-propandiol)acetal-1-carbaldehyde-benzene (7a)

6.0g (16.58mmol) of **3a** was dissolved in 168mL dried dichloromethane under argon. 1.33mL (18.40mmol) of 1,3-propandiol was added and followed by 4.64mL (36.72mmol) of chlorotrimethylsilane. The reaction mixture was refluxed at 45 ^{o}C for 24 hours. The reaction mixture was hydrolyzed with 4.8g $NaHCO_3$/H_2O. Column Chromatography (Silica gel 60: Hexane/toluene-toluene-toluene/chloroform) was used to yield 2,5-diheptyloxy-4-(1,3-propandiol)acetal-1-carbaldehyde-benzene (**7a**, 5.78g, 83%)

^{1}H-NMR ($CDCl_3$, 200MHz): [ppm] 10.44 (1H, s, -CHO) 7.27 (1H, s, CH-aromatic), 7.26 (1H, s, CH-aromatic) 5.82 (1H, s, -CH-acetal), 4.22 (2H, t, α-CH_2-alky), 4.22 (2H, m, α-CH_2-alky), 4.06 (4H, m, α-CH_2-acetal), 2.22 (2H, m, β-CH_2-acetal), 1.81 (4H, m, β-CH_2-alkyl) 1.39 (16H, m, -CH_2-alkyl), and 0.89 (6H, m, -CH_3).

2.1.4.4.6. Synthesis of 2,5-diheptyloxy-1-(1,3-propanediol)acetal-4-vinyl-benzene (8a)

12.46g (29.67mmol) of methyl-triphenyl-phosphoniumbromid was dissolved in 56mL dried THF. 11mL (27.61mmol, 2.5M in hexanes, less than stochiometry) of n-butyl lithium was added and the reaction solution was stirred at room temperature for 20 min. 6.2g (14.47mmol) of **7a** was dissolved in 31mL dried THF and added to the reaction vessel slowly. The reaction mixture was stirred for 1 hour and then added to ice-cold 50mL $NaHCO_3$. The water phase was extracted with 40mL toluene for several times. The combined organic solvent was washed one time with NaCl solution and then twice with 30mL water. The toluene phase was dried over Na_2SO_4 and concentrated to yield 2,5-diheptyloxy-1-(1,3-propanediol)acetal-4-vinyl-benzene (**8a**, 9.3g, 75%) as colorless to slightly yellow highly viscous liquid.

^{1}H-NMR ($CDCl_3$, 200MHz): [ppm] 7.12 (1H, s, CH-aromatic), 6.97 (1H, s, CH-aromatic) 5.82 (1H, s, CH-acetal), 5.74 (1H, dd, vinylene, -CH=C), 5.26 (2H, dd, vinylene, -C=CH_2), 4.25 (2H, t, α-CH_2-alky), 4.21 (2H, t, α-CH_2-alky), 4.06 (4H, t, α-CH_2-acetal), 2.60 (2H, m, β-CH_2-acetal), 1.77 (4H, m, β-CH_2-alkyl) 1.39 (16H, m, -CH_2-alkyl), and 0.89 (6H, m, -CH_3).

2.1.4.4.7. Synthesis of trans-DHepO-PV-dimer-diacetal (9a)

100 mg (0.239mmol) of **8a** was dissolved in 4mL dried CH_2Cl_2 and then added 3.0mg (0.0048mmol) of Grubbs 2nd generation catalyst in reduce pressure vessel. The reaction was heated at 55 ^oC for 9 days and vented several times

per day to release ethylene occurred as byproduct. The solution was quenched by added $CHCl_3$ and solvent was evaporated off. Column chromatography (Silica gel 60: Hexane-toluene-chloroform-ether by increasing solvent slowly) was used to yield trans-DHepO-PV-dimer-diacetal (**9a**, 50mg, 54%).

^{1}H-NMR ($CDCl_3$, 200MHz): [ppm] 7.40 (2H, s, vilylene trans-CH=CH-), 7.12 (2H, s, CH-aromatic), 7.09 (2H, s, CH-aromatic) 5.82 (2H, s, CH-acetal), 4.22 (8H, t, α-CH_2- acetal), 3.99 (8H, t, α-CH_2-alky), 2.28 (4H, m, β-CH_2-acetal), 1.75 (8H, m, β-CH_2-alkyl) 1.37 (32H, m, -CH_2-alkyl), and 0.85 (12H, m, -CH_3).

2.1.4.4.8. Synthesis of trans-DhepO-PV-dimer-dialdehyde (10a)

The hydrolysis of **9a** was performed in analogy to the hydrolysis of the DHepO-PV-Monomer-Diacetal (**4a**). 250mg (0.309mmol) of **9a** was dissolved in 35mL toluene under argon. Then, 35mL ethanol and 35mL 2M HCl were added into it. The mixture was stirred intensively (emulsion was formed) for three days. The toluene phase was separated and water phase was extracted with 20mL toluene for several times. The combined organic solvent was dried over Na_2SO_4 and solvent was evaporated to yield trans-DhepO-PV-dimer-dialdehyde (**10a**, 171mg, 80%) as yellow/yellow-orange crystals. In this particular case, no further purification was necessary.

^{1}H-NMR ($CDCl_3$, 200MHz): [ppm] 10.44 (2H, s, aldehyde) 7.56 (2H, s, vinylene trans-CH=CH), 7.32 (2H, s, CH-aromatic), 7.17 (2H, s, CH-aromatic), 4.08 (4H, t, J=6.3Hz, α_1-CH_2-), 4.02 (4H, t, J=6.3Hz, α_2-CH_2-), 1.83 (8H, m, β-CH_2-), 1.40 (32H, m, -CH_2-), and 0.88 (12H, m, -CH_3).

2.1.4.4.9. Synthesis of trans-DhepO-PV-dimer-dialcohol (11a)

80mg (0.116mmol) of $LiAH_4$ was mixed with 20mL dried THF under argon in two necks 100mL round bottom flask. 0.09g of **10a** was dissolved in 15mL dried THF in dropping funnel. The solution was added dropwise into reaction flask. The reaction mixture was refluxed at 60 ^{o}C for 4 hours. The mixture was cooled down to room temperature and ice-water was added until end of hydrogen gas. The dilute (10mL, 10% H_2SO_4) were added to dissolved $Al(OH)_3$. Product was isolated by dissolved in $CHCl_3$ and dried over Na_2SO_4 to yield trans-DhepO-PV-dimer-dialcohol (**11a**, 70mg, 77%) as a yellow solid.

^{1}H-NMR ($CDCl_3$, 600MHz): [ppm] 7.40 (2H, s, vinylene trans-CH=CH), 7.09 (2H, s, CH-aromatic), 6.85 (2H, s, CH-aromatic), 4.65 (4H, d, J=6.6Hz, CH_2-(*OH*)), 4.02 (4H, t, J=6.5Hz, -α_2-CH_2-), 3.96 (4H, t, J=6.5Hz, -α_1-CH_2-), 2.36 (2H, t, J=6.6Hz, -OH), 1.80 (8H, m, β-CH_2-), 1.47 (8H, m, γ-CH_2-), 1.35 (8H, m, δ-CH_2-) 1.29 (16H, m, ε-CH_2-), 0.88 (6H, t, J=7.0Hz, -CH_3), and 0.85 (6H, t, J=7.0Hz, -CH_3). ^{13}C-NMR ($CDCl_3$, 150MHz): [ppm] 151.1, 150.6, 129.4, 127.1, 123.5, 114.0, 109.1, 69.7, 68.6, 62.3, 31.85, 31.79, 29.50, 29.46, 29.10, 29.08, 26.2, 26.1, 22.64, 22.62, 14.08, and 14.07. ATR-FTIR [cm^{-1}]: 3325, 3058, 2957, 2923, 2855, 2749, 1511, 1466, 1422, 1391, 1332, 1302, 1256, 1207, 1147, 1128, 1071, 1044, 1028, 966, 856, 790, 727, 701, and 664.

2.1.4.4.10. Synthesis of 1,4-diheptyloxy-2,5-bis(hydroxymethyl)benzene (5a)

2.0g (5.52mmol) of $LiAlH_4$ was mixed with 130mL dried THF under argon in three necks 500mL round bottom flask. 4g (11mmol) of **3a** was dissolved in dried THF in a dropping funnel. The solution was added dropwise into reaction flask. The reaction mixture was refluxed at 60 ^{o}C for 4 hours. The mixture was cooled down to room temperature and ice-water was added until end of hydrogen gas. The dilute (100mL, 10% H_2SO_4) was added to dissolve $Al(OH)_3$. Product was isolated as a white solid by dissolved in $CHCl_3$ and dried over Na_2SO_4 to yield 1,4-diheptyloxy-2,5-bis(hydroxymethyl)benzene (**5a**, 1.82g, 90%).

^{1}H-NMR ($CDCl_3$, 600MHz): [ppm] 6.82 (2H, s, CH-aromatic), 4.65 (4H, s, -CH_2-(*OH*)), 3.96 (4H, t, J=6.48Hz, α-CH_2-), 2.33 (2H, s, -OH) 1.76 (4H, m, β-CH_2-), 1.43 (4H, m, γ-CH_2-), 1.33 (4H, m, δ-CH_2-) 1.29 (8H, m, ε-CH_2-), and 0.92 (6H, t, J=7.01Hz, -CH_3). ^{13}C-NMR ($CDCl_3$, 50MHz): [ppm] 150.4, 128.8, 112.1, 68.5, 62.0, 31.6, 29.2, 28.9, 25.9, 22.4, and 13.9. ATR-FTIR [cm^{-1}]: 3285, 2934, 2917, 2851, 1505, 1469, 1443, 1420, 1395, 1374, 1203, 1171, 1053, 1000, 882, 862, 778, 718, and 695.

2.1.4.4.11. Synthesis of 2,5-diheptyloxy-1,4-bis(chloromethyl)benzene (12a)

10mL of thoinyl chloride ($SOCl_2$) was added into 25mL two necks round bottom flash under stream of argon. 2.65g (7.24mmol) of **5a** was added slowly (Careful HCl gas released during the reaction). The reaction mixture was heated at 70-75

^{o}C for 4-5 hours. The solution was cooled down and the volatiles were removed. A solid formed to yield 2,5-diheptyloxy-1,4-bis(chloromethyl)benzene (**12a**, 2.92g, >99%).

^{1}H-NMR ($CDCl_3$, 200MHz): [ppm] 6.89 (2H, s, CH-aromatic), 4.61 (4H, t, -CH_2Cl), 3.96 (4H, t, α-CH_2-), 1.78 (4H, m, β-CH_2-), 1.35 (16H, m, -CH_2-), and 0.88 (6H, t, -CH_3).

2.1.4.4.12. Synthesis of 2,5-diheptyloxy-1,4-bis(triphenylphosphonium-methylchloride) benzene (13a)

2.92g (7.24mmol) of **12a** was mixed with 5.69g (21.7mmol) of triphenylphosphine in 40mL dried toluene under argon gas in 100mL two neck vessel. The reaction mixture was refluxed at 110 ^{o}C for 4 days. The precipitation was filtered as gray precipitation and washed with ether to yield 2,5-diheptyloxy-1,4-bis(triphenylphosphonium-methylchloride) benzene (**13a,** 6.04g, 90%).

^{1}H-NMR ($CDCl_3$, 200MHz): [ppm] 7.71-7.59 (30H, m, CH-aromatic-Ph_3P^+-group), 6.68 (2H, s, CH-aromatic), 5.43 (4H, s, Ph-CH_2-P^+Ph_3), 2.96 (4H, t, α-CH_2-), 1.89 (4H, s, β-CH_2-), 1.15 (16H, m, -CH_2-), and 0.87 (6H, t, -CH_3).

2.1.4.4.13. Synthesis of DhepO-PV-trimer-diacetal (14a)

82.2mg (3.57mmol) of Na metal was dissolved in 50mL of dried CH_3OH. 1.103g (1.190mmol) of **13a** was added and stirred for 30 min. Then, 2.0g (4.755mmol) of 2,5-diheptyloxy-4-(1,3-propandiol) acetal-1-carbaldehyde-benzene was added onto it. The reaction mixture was refluxed for 48 hours. The solution was cooled

down to room temperature and concentrated. 100mL of H_2O was added and then the watery phase was extracted with 20mL toluene for several times. The toluene phase was dried over Na_2SO_4, filtered, and concentrated to yield a mixture of cis and trans configured DhepO-PV-trimer-diacetal (**14a**).

2.1.4.4.14. Synthesis of DhepO-PV-trimer-diacetal via isomerization (15a)

393mg (0.345mmol) of **14a** was dissolved in 100mL xylene (oxygen-free). 10-15mg of I_2 was added and refluxed for 18 hours at 144 ^oC. The reaction mixture was concentrated and column chromatography (Al_2O_3 Basic type II, toluene-toluene/chloroform-chloroform/toluene) was used to yield all trans DhepO-PV-trimer-diacetal (**15a**, 157mg, 40%).

^{1}H-NMR ($CDCl_3$, 200MHz): [ppm] 7.45 (4H, s, vinylene trans-CH=CH), 7.16 (2H, s, CH-aromatic), 7.14 (2H, s, CH-aromatic), 7.12 (2H, s, CH-aromatic), 5.86 (2H, s, -CH-acetal) 4.25 (8H, m, α-CH_2-acetal), 4.03 (12H, m, α-CH_2-alkyl) 2.23 (4H, m, β-CH_2-acetal), 1.85 (12H, m, β-CH_2-alkyl), 1.47 (48H, m, -CH_2-alkyl), and 0.88 (18H, m, -CH_3).

2.1.4.4.15. Synthesis of DhepO-PV-trimer-dialdehyde (16a)

400mg (0.351mmol) of **15a** was dissolved in 40mL toluene. Then, 40mL ethanol and 40mL 2M HCl were added into it. The reaction mixture was stirred vividly for 60 hours at room temperature. The toluene phase was separated and extracted the water phase with 20mL toluene for several times. The combined organic solvent was dried over Na_2SO_4 and solvent was evaporated off. Column

chromatography (Al_2O_3 basic type II, toluene-toluene/chloroform) was used to yield DhepO-PV-trimer-dialdehyde (IUPAC: 2,5-bis(heptyloxy)-1,4-bis[2,5-bis(heptyloxy)-4-formyl-phenylenevinylene]benzene (**16a**, 287mg, 80%).

^{1}H-NMR ($CDCl_3$, 600MHz): [ppm] 10.43 (2H, s, aldehyde) 7.56 (2H, s, vinylene trans-CH=CH), 7.50 (2H, s, vinylene trans-CH=CH), 7.31 (2H, s, CH-aromatic), 7.18 (2H, s, CH-aromatic), 7.13 (2H, s, CH-aromatic), 4.10 (4H, t, J=6.4Hz, α_1-CH_2-), 4.05 (4H, t, J=6.4Hz, α_2-CH_2-), 4.04 (4H, t, J=6.4Hz, α_3-CH_2-), 1.84 (12H, m, β-CH_2-), 1.50 (12H, m, γ-CH_2-), 1.37 (12H, m, δ-CH_2-), 1.29 (24H, m, ε-CH_2-), and 0.87 (18H, m, -CH_3). ^{13}C-NMR ($CDCl_3$, 150MHz): [ppm] 189.2, 156.3, 151.3, 150.7, 135.0, 127.5, 127.0, 124.1, 123.2, 110.8, 110.4, 110.1, 69.4, 69.14, 69.04, 31.9, 31.84, 31.77, 29.5, 29.29, 29.27, 29.14, 29.08, 29.06, 26.2, 26.1, 22.64, 22.61, and 14.1. ATR-FTIR [cm^{-1}]: 3060, 2955, 2924, 2871, 2853, 1677, 1596, 1500, 1465, 1423, 1387, 1283, 1203, 1146, 1066, 965, 849, 789, 726, and 709

2.1.4.4.16. Synthesis of DhepO-PV-trimer-dialcohol (17a)

80mg (0.078mmol) of $LiAH_4$ was mixed with 20mL of dried THF under argon in two necks 100mL round bottom flask. 0.31g of **16a** was dissolved in 15mL of dried THF in dropping funnel. The solution was added dropwise into a reaction flask. The reaction mixture was refluxed at 60 ^{o}C for 4 hours. The mixture was cooled down to room temperature and ice-water was added until end of hydrogen gas evolution. 10mL 10% H_2SO_4 was added to dissolve $Al(OH)_3$. The product was isolated as a yellow solid, dissolved in $CHCl_3$ and dried over Na_2SO_4 to yield DhepO-PV-trimer-dialcohol (**17a**, 72mg, 90%) as a light yellow fluorescent solid.

^{1}H-NMR ($CDCl_3$, 600MHz): [ppm] 7.46 (2H, s, vinylene trans-CH=CH), 7.45 (2H, s, vinylene trans-CH=CH), 7.15 (2H, s, CH-aromatic), 7.13 (2H, s, CH-aromatic), 6.88 (2H, s, CH-aromatic), 4.69 (4H, d, J=6.33Hz, CH_2-(*OH*)), 4.06 (4H, t, J=2.3Hz α_2-CH_2-), 4.04 (4H, t, J=4.2Hz, α_3-CH_2-), 4.00 (4H, t, J=6.52Hz, α_1-CH_2-), 2.40 (2H, t, J=6.52Hz, -OH), 1.84 (12H, m, β-CH_2-), 1.51 (12H, m, γ-CH_2-), 1.39 (12H, m, δ-CH_2-), 1.31 (24H, m, ε-CH_2-), and 0.88 (18H, m, -CH_3). ^{13}C-NMR ($CDCl_3$, 150MHz): [ppm] 151.07, 151.05, 150.63, 129.3, 127.37, 127.18, 123.48, 123.35, 114.0, 110.6, 109.1, 69.7, 69.5, 68.6, 62.33, 31.88, 31.85, 31.79, 29.56, 29.51, 29.47, 29.17, 29.12, 29.09, 26.23, 26.2, 26.16, 22.66, 22.65, 22.62, 14.09, and 14.08. ATR-FTIR [cm^{-1}]: 3319, 3058, 2955, 2920, 2852, 2747, 1508, 1464, 1421, 1389, 1348¸ 1308, 1255, 1206, 1147, 1121, 1068, 1043, 1010, 964, 906, 852, 787, 727, and 700.

2.1.4.4.17. Synthesis of DhepO-PV-trimer-dialcohol (17a, 2nd method)

Bisaldehyde (**16a**, 204.4mg, 0.2mmol) was dissolved in a mixture of 10mL methanol and 35mL of dichloromethane. Sodium borohydride (15.2mg, 0.4mmol) was added and stirred at room temperature for 1 hour. The reaction mixture was poured into water and extracted with dichloromethane twice. The dichloromethane phase was dried over Na_2SO_4 and concentrated to yield DhepO-PV-trimer-dialcohol (**17a**, 184.7mg, 90%) as a light yellow fluorescent solid.

2.1.4.4.18. Synthesis of DhepO-PV-trimer-divinyl (18a)

To a suspension of methytriphenylphosphonium bromide (532mg, 1.448mmol) in 2.4mL dried THF, 0.536mL (2.5M in hexane) n-Bu-Li was added via dropwise. The reaction mixture was stirred at room temperature for 2 hours. Then bisaldehyde **16a** (254g, 0.248mmol) was added slowly to the mixture. The resulting mixture was stirred for another 4 hours at room temperature and hydrolyzed with ice-cold water. Chloroform was added to collect the organic layer and dried over Na_2SO_4. Silica gel column chromatography was used to purifiy DhepO-PV-trimer-divinyl (**18a**, 222mg, 88%), yeilded as a light yellowish fluorescent solid.

^{1}H-NMR ($CDCl_3$, 600MHz): [ppm] 7.44 (4H, s, internal vinylene trans-CH=CH-), 7.13 (2H, s, CH-aromatic), 7.10 (2H, s, CH-aromatic), 7.05 (2H, dd, J=6.6Hz, J=11.11Hz, terminal vinylene trans-CH=C-), 7.00 (2H, s, CH-aromatic), 5.74 (2H, d, J=17.68Hz, terminal vinylene cis-C=CH_2), 5.25 (2H, d, J=11.82Hz, terminal vinylene trans-C=CH_2), 4.02 (4H, t, J=6.5Hz, α_2-CH_2-), 4.00 (4H, t, J=6.5Hz, α_3-CH_2-), 3.99 (4H, t, J=6.5Hz, α_1-CH_2-), 1.83 (12H, m, β-CH_2-), 1.50 (12H, m, γ-CH_2-), 1.36 (12H, m, δ-CH_2-), 1.29 (24H, m, ε-CH_2-), and 0.87 (18H, m, -CH_3). ^{13}C-NMR ($CDCl_3$, 150MHz) [ppm] 151.1, 150.9, 150.8, 131.6, 127.9, 127.4, 126.8, 123.5, 123.3, 113.8, 110.8, 110.6, 110.4, 69.6, 69.5, 69.3, 31.86, 31.85, 31.82, 29.6, 29.5, 29.17, 29.14, 29.12, 26.23, 26.18, 22.65, 22.63, 14.1, and 14.07. ATR-FTIR [cm^{-1}]: 3084, 3057, 3011, 2926, 2853, 1501, 1465, 1422, 1393, 1378, 1343, 1313¸ 1289, 1242, 1230, 1203, 1121, 1041, 1016, 994, 976, 913, 897, 860, 799, 783, 731, and 694.

2.1.4.4.19. Synthesis of DhepO-PV-trimer-dialkyne (19a)

To a solution of propargylamine (0.33g, 6mmol) in 10mL of THF, 2g of anhydrous magnesium sulfate and the DhepO-PV-trimer-dialdehyde **16a** (0.51g, 0.5mmol,) were added at -15 ^{o}C with stirring. The mixture was allowed to stir at room temperature under argon atmosphere for 30 h. The magnesium sulfate filtration and solvent evaporation yielded **19a** (0.53g, 98%) as a yellowish orange solid.

^{1}H NMR (600 MHz, $CDCl_3$): [ppm] 8.99 (2H, s), 7.50 (2H, s, vinylene trans-CH=CH), 7.48 (2H, s, vinylene trans-CH=CH), 7.47 (2H, s, CH-aromatic), 7.15 (2H, s, CH-aromatic), 7.13 (2H, s, CH-aromatic), 4.49 (4H, s), 4.08 (4H, t, α_1-CH_2-), 4.07 (4H, t, α_2-CH_2-), 4.06 (4H, t, α_3-CH_2-), 2.47 (2H, s, -C≡CH), 1.81 (12H, m, -CH_2), 1.29 (48H, m, -CH_2-), and 0.85 (18H, m, -CH_3). ^{13}C-NMR ($CDCl_3$, 150MHz): [ppm] 158.7, 153.1, 151.2, 151.0, 131.1, 127.4, 125, 124.2, 123.4, 110.7, 110.5, 110.1, 79.7, 74.8, 69.44, 69.38, 69.16, 47.9, 31.864, 31.856, 31.826, 29.52, 29.44, 29.42, 29.16, 29.11, 29.10, 26.23, 26.15, 26.14, 22.65, 22.63, 14.1, 14.08, and 14.075. ATR-FTIR [cm^{-1}]: 3307, 3057, 2955, 2922, 2853, 2746, 1725, 1678, 1639, 1599, 1504, 1465, 1424, 1387, 1341, 1306, 1262, 1206, 1162, 1147, 1127, 1065, 1041, 1011, 965, 916, 866, 849, 807, 792, 726, 711, and 686.

2.1.4.5. Synthesis of OPVs with butyloxy as side chain

The syntheses of OPVs with butyloxy as side chain were performed in analogy to the syntheses of OPVs with heptyloxy as side chain.

2.1.4.5.1. Synthesis of 1,4-dibutyloxybenzene (2b)

^{1}H-NMR ($CDCl_3$, 200MHz): [ppm] 6.81 (4H, s, CH aromatic), 3.89 (4H, t, α-CH_2-), 1.73 (4H, m, β-CH_2-), 1.48 (4H, m, γ-CH_2-), and 0.95 (6H, t, -CH_3). ^{13}C-NMR ($CDCl_3$, 50MHz): [ppm] 153.2, 115.3, 68.3, 31.4, 19.2, and 13.9. Yield 91%.

2.1.4.5.2. Synthesis of 1,4-dibutyloxyterephthalaldehyde-(1,3-propandiol)acetal (4b)

^{1}H-NMR ($CDCl_3$, 200MHz): [ppm] 7.26 (2H, s, CH-aromatic), 5.83 (2H, s, CH-acetal), 4.23 (8H, t, α-CH_2-acetal) 3.99 (4H, t, α-CH_2-alkyl), 2.28 (4H, m, β-CH_2-acetal), 1.78 (4H, m, β-CH_2-alkyl) 1.46 (4H, m, -CH_2-alkyl), and 0.93 (6H, t, -CH_3). Yield 60%.

2.1.4.5.3. Synthesis of 2,5-dibutyloxyterephthalaldehyde (3b purified)

^{1}H-NMR ($CDCl_3$, 600MHz): [ppm] 10.50 (2H, s, (V_a) -CHO), 7.41 (2H, s, CH-aromatic), 4.07 (4H, t, J=6.43Hz, α-CH_2-), 1.80 (4H, m, β-CH_2-), 1.48 (4H, m, γ-CH_2-), and 0.97 (6H, t, J=7.4Hz, -CH_3). ^{13}C-NMR ($CDCl_3$, 50MHz): [ppm] 189.2, 155.1, 129.1, 111.5, 68.8, 30.9, 19.1, and 13.6. ATR-FTIR [cm^{-1}]: 3055, 2954, 2875, 1681, 1486, 1464, 1428, 1391, 1284, 1214, 1171, 1121, 1069, 1027, 1008, 981, 919, 890, 840, 744, and 692. Yield 70%.

2.1.4.5.4. Synthesis of 2,5-dibutyloxy-4-(1,3-propandiol)acetal-1-carbaldehyde-benzene (7b)

^{1}H-NMR ($CDCl_3$, 200MHz): [ppm] 10.44 (1H, s, -CHO) 7.27 (1H, s, CH-aromatic), 7.26 (1H, s, CH-aromatic) 5.82 (1H, s, CH-Acetal), 4.22 (2H, t, α-CH_2-alky), 4.07 (2H, t, α-CH_2-alky), 3.97 (4H, t, α-CH_2-acetal), 2.26 (2H, m, β-CH_2-acetal), 1.78 (4H, m, β-CH_2-alkyl) 1.46 (4H, m, -CH_2-alkyl), and 0.95 (6H, t, -CH_3). Yield 75%.

2.1.4.5.5. Synthesis of 1,4-dibutyloxy-2,5-bis(hydroxymethyl)benxene (5b)

^{1}H-NMR ($CDCl_3$, 600MHz): [ppm] 6.83 (2H, s, CH-aromatic), 4.66 (4H, d, J=5.83Hz, -CH_2-(OH)), 3.97 (4H, t, J=6.44Hz, α-CH_2-), 2.36 (2H, t, J=6.1Hz, -OH), 1.75 (4H, m, β-CH_2-), 1.47 (4H, m, γ-CH_2-), and 0.96 (6H, t, J=7.4Hz, -CH_3). ^{13}C-NMR ($CDCl_3$, 50MHz): [ppm] 150.5, 128.9, 112.2, 68.4, 62.0, 31.4, 19.3, and 13.8. ATR-FTIR [cm^{-1}]: 3316, 3250, 3241, 3069, 2957, 2933, 2916, 2870, 1507, 1469, 1447, 1416, 1392, 1366, 1316, 1298, 1282, 1229, 1203, 1174, 1145, 1123, 1070, 1035, 1001, 982, 909, 864, 815, 799, 783, and 740. Yield 87%.

2.1.4.5.6. Synthesis of 2,5-dibutyloxy-1,4-bis(chloromethyl)benxene (12b)

^{1}H-NMR ($CDCl_3$, 600MHz): [ppm] 6.89 (2H, s, CH-aromatic), 4.61 (4H, t, -CH_2Cl), 3.97 (4H, t, α-CH_2-), 1.77 (4H, m, β-CH_2-), 1.51 (4H, m, γ-CH_2-), and 0.97 (6H, t, -CH_3). Yiled 94%.

2.1.4.5.7. Synthesis of 2,5-dibutyloxy-1,4-bis(triphenylphosphonium-methylchloride) benxene (13b)

^{1}H-NMR ($CDCl_3$, 200MHz): [ppm] 7.75-7.62 (30H, m, CH-aromatic-Ph_3P^+-group), 6.88 (2H, s, CH-aromatic), 5.53 (4H, s, Ph-CH_2-P^+Ph_3), 2.98 (4H, t, α-CH_2-), 1.89 (4H, s, β-CH_2-), 1.18 (4H, m, γ-CH_2-), and 0.89 (6H, t, -CH_3). Yield 89%.

2.1.4.5.8. Synthesis of DbuO-PV-trimer-diacetal via isomerization (15b)

^{1}H-NMR ($CDCl_3$, 200MHz): [ppm] 7.45 (4H, s, vinylene trans-CH=CH), 7.16 (2H, s, CH-aromatic), 7.14 (2H, s, CH-aromatic), 7.12 (2H, s, CH-aromatic), 5.87 (2H, s, -CH-acetal) 4.27 (8H, m, α-CH_2-acetal), 4.04 (12H, m, α-CH_2-alkyl) 2.23 (4H, m, β-CH_2-acetal), 1.88 (12H, m, β-CH_2-alkyl), 1.47 (12H, m, γ-CH_2-alkyl), and 0.89 (18H, m, -CH_3). Yield 47%.

2.1.4.5.9. Synthesis of DbuO-PV-trimer-dialdehyde (16b)

^{1}H-NMR ($CDCl_3$, 600MHz) [ppm] 10.43 (2H, s, aldehyde), 7.57 (2H, s, vinylene trans-CH=CH), 7.51 (2H, s, vinylene trans-CH=CH), 7.31 (2H, s, CH-aromatic), 7.19 (2H, s, CH-aromatic), 7.14 (2H, s, CH-aromatic), 4.105 (4H, t, J=6.4Hz, α_1-CH_2-), 4.056 (4H, t, J=6.4Hz, α_2-CH_2-), 4.028 (4H, t, J=6.4Hz, α_3-CH_2-) 1.854 (12H, m, β-CH_2-), 1.57 (12H, m, γ-CH_2-), and 1.011 (18H, m, -CH_3). ^{13}C-NMR ($CDCl_3$, 150MHz): [ppm] 189.1, 156.2, 151.3, 150.7, 134.9, 127.4, 126.9, 124.1, 123.1, 110.7, 110.4, 110.1, 69.1, 68.8, 68.75, 31.5, 31.34, 31.31, 19.5, 19.4, 19.3, 13.96, 13.93, and 13.84. ATR-FTIR [cm^{-1}]: 3060, 2954, 2935, 2869, 2764,

1674, 1594, 1501, 1467, 1421, 1389, 1343, 1262, 1246, 1202, 1159, 1120, 1066, 1036, 1025, 1010, 970, 919, 887, 854, 784, 742, 708, 678, and 667. Yield 80%.

2.1.4.5.10. Synthesis of DbuO-PV-trimer-dialcohol (17b)

^{1}H-NMR ($CDCl_3$, 600MHz): [ppm] 7.45 (2H, s, vinylene trans-CH=CH), 7.44 (2H, s, vinylene trans-CH=CH), 7.14 (2H, s, CH-aromatic), 7.11 (2H, s, CH-aromatic), 6.86 (2H, s, CH-aromatic), 4.67 (4H, d, J=6.48Hz, CH_2-(OH)), 4.04 (8H, m, $\alpha_{2\text{-}3}$-CH_2-), 3.99 (4H, t, J=6.4Hz, α_1-CH_2-) 2.35 (2H, t, J=6.5Hz, -OH), 1.81 (12H, m, β-CH_2-), 1.56 (12H, m, γ-CH_2-), and 0.99 (18H, m, -CH_3). ^{13}C-NMR ($CDCl_3$, 50MHz): [ppm] 151.015-150.583, 129.3, 127.1, 123.2, 114.0, 110.5, 108.9, 69.4, 68.2, 62.3, 31.6, 19.4, and 13.9. ATR-FTIR [cm^{-1}]: 3354, 3059, 2953, 2906, 2868, 1508, 1467, 1421, 1389, 1344, 1254, 1204, 1147, 1121, 1070, 1043, 1027, 981, 964, 909, 859, 742, and 701. Yield 85%.

2.1.4.6. Synthesis of OPVs with metyloxy as side chain

The syntheses of OPVs with metyloxy side chain were performed in analogy to the syntheses of OPVs with heptyloxy and butyloxy side chain. However, attempts using methyloxy side chain substitution did not prove feasible beyond the monomeric unit due to very limited solubility of the dimeric OPVs and beyond.

2.1.4.6.1. Synthesis of 2,5-dimetyloxyterephthalaldehyde (3c)

It is worth to note that when the side chain is methoxy, these purification steps were not necessary. The purification was done by washing with toluene to yield pure monomer dialdehyde.

13.524g (98mmol) 1,4-dimetyloxybenzene were dissolved in dried 400mL hexane under argon. 44.2mL (296mmol) tetramethylethylenediamine (TMEDA) were added and cooled down to 0 ^{o}C. 185mL (296mmol) of 1.6M n-buthylithium in hexane were added dropwise for 45min. The solution flask was heated to 35 ^{o}C for 48 hours and room temperature for 24 hours and cooled down to 0 ^{o}C. 26.6mL (346mmol) dimethylformamide (DMF) were added and stirred at room temperature for 24 hours. The solution was poured into 2L HCl - icebath. Precipitation occurred was dissolved with 100mL chloroform and washed with 100mL water several times. The solvent phase was dried over Na_2SO_4 and filtered. Then, solvent was evaporated out under vacuum at 45 ^{o}C, and washed with 100mL toluene to yield pure 2,5-dimetyloxyterephthalaldehyde (**3c**, 11.98g, 63%).

^{1}H-NMR ($CDCl_3$, 600MHz): [ppm] 10.47 (2H, s, -CHO), 7.43 (2H, s, CH-aromatic), and 3.92 (6H, s, -OCH_3). ^{13}C-NMR ($CDCl_3$, 50MHz): [ppm] 189.2, 155.7, 129.1, 110.8, and 56.2. ATR-FTIR [cm^{-1}]: 3049, 2981, 2953, 2870, 1677, 1481, 1409, 1396, 1301, 1211, 1192, 1163, 1129, 1022, 876, 786, 744, 701, and 658.

2.1.4.6.2. Synthesis of 1,4-dimetyloxy-2,5-bis(hydroxymethyl)benxene (5c)

^{1}H-NMR ($CDCl_3$, 600MHz): [ppm] 6.86 (2H, s, CH-aromatic), 4.66 (4H, s, -CH_2-(*OH*)), 3.82 (6H, s, -OCH_3), 2.24 (2H, s, OH). ^{13}C-NMR ($CDCl_3$, 150MHz): [ppm] 151.2, 128.9, 111.4, 61.9, and 55.9. ATR-FTIR [cm^{-1}]: 3283, 3001, 2933, 2856,

2830, 1504, 1460, 1405, 1374, 1274, 1212, 1184, 1169, 1044, 1021, 863, 786, 722, 668, and 655. Yield 90%.

2.1.4.6.3. Synthesis of 1,4-dimetyloxy-2,5-divinylbenxene (6c)

^{1}H-NMR ($CDCl_3$, 600MHz): [ppm] 7.03 (2H, dd, J=6.6Hz, J=11.14Hz, -CH=C-), 6.98 (2H, s, CH-aromatic), 5.73 (2H, d, J=17.73Hz, cis-C=CH_2), 5.27 (2H, d, J=12.09Hz, trans-C=CH_2), and 3.83 (6H, s, -OCH_3). ATR-FTIR [cm^{-1}]: 3087, 3007, 2961, 2835, 1496, 1465, 1404, 1310, 1277, 1206, 1183, 1053, 1036, 997, 912, 864 826, 724, and 695. Yield 90%.

2.2. Method 2: Monomers, trimers

2.2.1. Overview

A second approach is presented with a different synthetic strategy in analogy to existing literature,[118] providing faster synthetic access to monomers and trimers blocks. The time and chemicals (especially solvent for purification) were save and the overall yield was higher. All OPVs were characterized by means of ATR-FTIR, ^{1}H-NMR (200 or 600 MHz) and ^{13}C-NMR (50 or 150 MHz), 2D-NMR (HMBC, HSQC experiments), and optical spectroscopy.

2.2.2. Results and discussion

The synthetic sequence starts from commercially available 1,4-hydroquinone **1** toward monomeric intermediates. Derivatives of the monomer are then further

combined into the respective trimer synthesis. The overall approach is outlined scheme 2.4.

Bromo-methylation of compound **2** affords key intermediate **20**. ^{1}H-NMR and ^{13}C-NMR spectra confirm the presence of the two bromomethylene groups at 2- and 5-positions at the aromatic core. Acetylation of **20** with potassium acetate in the presence of tetrabutyl-ammonium bromide affords **21**. Reduction of **21** with $LiAlH_4$ affords **5**. **5** is oxidized with pyridinium chlorochromate to yield key intermediate **3**. A short silica gel column yields pure **3** directly from the reaction mixture. **22** is synthesized starting from **20** with triphenylphosphine. Compounds **3** and **22** couple to yield **16'**, which features a mixture of cis- and trans-configured vinylene bonds. Isomerization of **16'** to the all-trans configured **16** is carried out using iodine.

2.2.3. Experimental

2.2.3.1. General information

All experiments using air/moisture sensitive materials were carried out under an atmosphere of high purity argon using standard Schlenk techniques. All glass-ware was cleaned and dried for at least 24h in an oven at 120^{o}C prior to use.

2.2.3.2. Chemicals

Paraformaldehyde powder 95%, hydrogen bromide (33 wt. % solution in acetic acid), tetrabutylammonium bromide, pyridinium chlorochromate 98%, lithium ethoxide (1.0M solution in ethanol), sodium borohydride 99% were purchased

from Sigma-Aldrich. Glacial Acetic acid 99.9%, potassium acetate 99%, acetonitrile 99.9% were purchased from VWR.

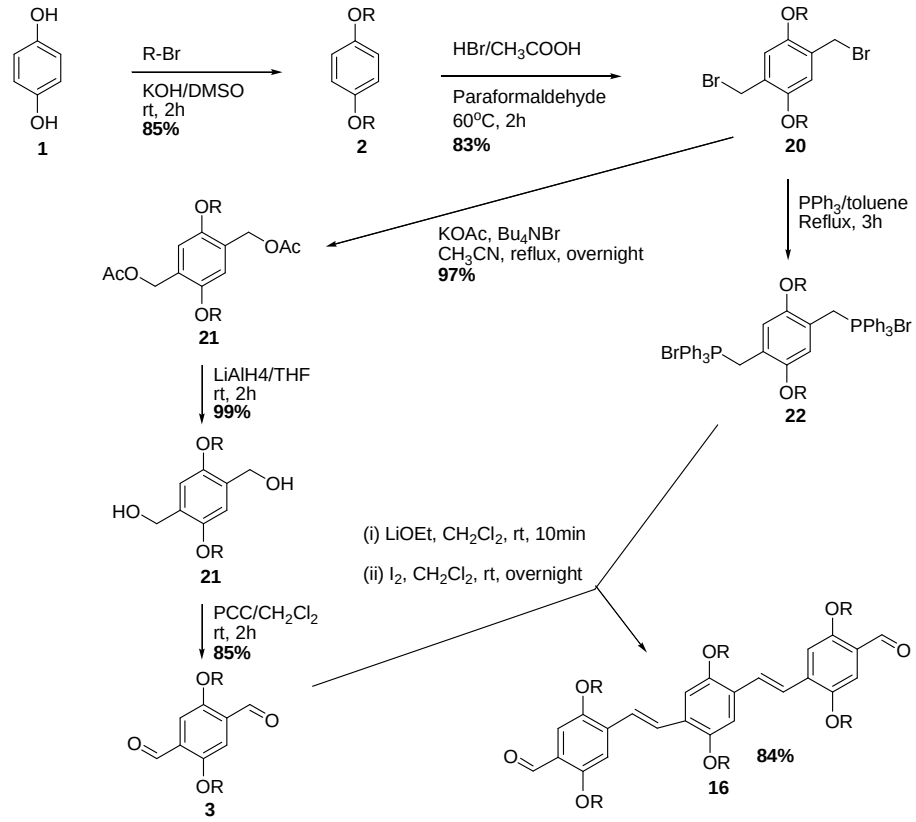

R = (a) -C_7H_{15}, (b) -C_4H_9, and (c) -CH_3

Scheme 2.4. Method 2: Overall synthetic approach for monomers and trimers.

2.2.3.3. Instrumentation

^{1}H NMR (200 or 600Hz) and ^{13}C NMR (50 or 150Hz) spectra were recorded on Varian spectrometers in $CDCl_3$ or DMSO as an internal deuterium lock for ^{1}H-NMR. ATR-FTIR spectra were recorded on Bruker Tensor 27 spectrometer using a Pike ATR accessory for characterizing samples. All data were processed and analyzed by OPUS software. UV-Visible absorption spectra were recorded using

a Perkin Elmer Lambda 650 Spectrophotometeter with 1-cm path length cells. Solvents for optical property investigations were Spectrasolv from Fisher Scientific. Photoluminescence spectra were recorded using a Horiba Jobin Yvon Fluoromax-3 spectrofluorometer with 1-cm path length cells. The cells were cleared and samples were prepared with spectroscopic grade chloroform and hexanes.

2.2.3.4. Synthesis of OPVs with heptyloxy side chains

2.2.3.4.1. Synthesis of 1,4-bis(heptyloxy)benzene (2a)

The synthesis of 1,4-diheptyloxybenzene **2a** was performed as described above (Scheme 2.1, Chapter 2).

2.2.3.4.2. Synthesis of 2,5-bis(bromomethyl)-1,4-bis(heptyloxy)benzene (20a)

A mixture of compound **2a** (9.24g, 30.2mmol), paraformaldehyde (1.86g, 32.0mmol) in acetic acid (100mL), and HBr (12.0mL, 33 wt % in acetic acid) were added. The mixture was heated to 60-70 ^{o}C for 2 hours, then cooled down to room temperature and poured into 600mL water. The precipitate was isolated and re-dissolved in hot chloroform. Re-precipitation into methanol yielded 2,5-bis(bromomethyl)-1,4-bis(heptyloxy)benzene as a white loose solid (**20a**, 12.35g, 83%).

^{1}H-NMR ($CDCl_3$, 200MHz): [ppm] 6.83 (s, 2H, aromatic), 4.51 (s, 4H, CH_2Br), 3.96 (t, 4H, α-CH_2-), 1.81 (q, 4H, β-CH_2-), 1.49 (m, 4H, γ-CH_2-), 1.28 (m, 12H, -

CH_2-), and 0.88 (t, 6H, -CH_3). ^{13}C-NMR ($CDCl_3$, 50MHz): [ppm] 150.6, 127.4, 114.5, 68.9, 31.8, 29.3, 29.0, 28.7, 26.0, 22.6, and 14.1.

2.2.3.4.3. Synthesis of 2,5-bis(acetylmethyl)-1,4-bis(heptyloxy)benzene (21a)

20a (10.24g, 20.8mmol), potassium acetate (6.2g, 63.2mmol), and tetra-n-butyl ammonium bromide (1.0g) were added to a mixture of acetonitrile (200mL) and chloroform (100mL). The reaction mixture was refluxed overnight and then poured into 300mL water. Extraction with 200mL chloroform (three times) followed. The combined chloroform fractions were washed with 200mL water twice. The organic phase was dried over anhydrous sodium sulfate. The solvent was removed in vacuo to yield 2,5-bis(acetylmethyl)-1,4-bis(heptyloxy)benzene (**21a**, 9.08 g, 97%).

^{1}H-NMR ($CDCl_3$, 200MHz): [ppm] 6.85 (s, 2H, CH-aromatic), 5.11 (s, 4H, -CH_2OAc), 3.92 (t, 4H, α-CH_2-), 2.08 (s, 6H, OAc), 1.76 (quintet, 4H, β-CH_2-), 1.44 (m, 4H, γ-CH_2-), 1.27 (m, 12H, -CH_2-), and 0.87 (t, 6H, CH_3).

^{13}C-NMR ($CDCl_3$, 50MHz): [ppm] 170.6, 150.6, 124.9, 113.5, 68.8, 61.4, 31.6, 29.2, 28.9, 25.8, 22.4, 20.8, and 13.9.

2.2.3.4.4. Synthesis of 2,5-bis(hydroxymethyl)-1,4-bis(heptyloxy) benzene (5a)

$LiAlH_4$ (3.24g, 80.71mmol) was suspended in dry THF (150mL) under argon. A solution of **21a** (9.08g, 20.18mmol) in dry THF (100mL) was added drop wise.

The resulting reaction mixture was stirred at room temperature for 2 hours. Cold ethyl acetate was used to quench excess $LiAlH_4$. Water was added to the resulting suspension. Extraction with 150mL chloroform (three times) followed. The combined chloroform fractions were washed with 200mL water three times. The organic phase was dried over anhydrous sodium sulfate. The solvent was removed to yield 2,5-bis(hydroxymethyl)-1,4-bis(heptyloxy)benzene as a white solid (**5a**, 6.65g, 99 %).

^{1}H-NMR ($CDCl_3$, 600MHz): [ppm] 6.82 (2H, s, CH-aromatic), 4.65 (4H, s, -CH_2-(*OH*)), 3.96 (4H, t, J=6.48Hz, α-CH_2-), 2.33 (2H, s, -OH) 1.76 (4H, m, β-CH_2-), 1.43 (4H, m, γ-CH_2-), 1.33 (4H, m, δ-CH_2-) 1.29 (8H, m, ε-CH_2-), and 0.92 (6H, t, J=7.01Hz, -CH_3). ^{13}C-NMR ($CDCl_3$, 50MHz): [ppm] 150.4, 128.8, 112.1, 68.5, 62.0, 31.6, 29.2, 28.9, 25.9, 22.4, and 13.9. ATR/FTIR [cm^{-1}]: 3285, 2934, 2917, 2851, 1505, 1469, 1443, 1420, 1395, 1374, 1203, 1171, 1053, 1000, 882, 862, 778, 718, and 695.

2.2.3.4.5. Synthesis of 2,5-bis(heptyloxy)benzene-1,4-dialdehyde (3a)

A mixture of **5a** (5.82g, 15.9mmol) and pyridinium chlorochromate (PCC) (13.8g, 63.9mmol) in 500mL dichloromethane was stirred at room temperature for 2 hours. The reaction mixture was poured to a short silica gel column (chloroform as solvent) for purification to yield yellow-orange 2,5-bis(heptyloxy)benzene-1,4-dialdehyde (**3a**, 4.89 g, 84.9%).

^{1}H-NMR ($CDCl_3$, 600MHz): [ppm] 10.50 (2H, s, -CHO), 7.41 (2H, s, CH-aromatic), 4.06 (4H, t, J=6.47Hz, α-CH_2-), 1.88 (4H, m, β-CH_2-), 1.45 (4H, m, γ-

CH_2-), 1.34 (4H, m, δ-CH_2-) 1.29 (8H, m, ε-CH_2-), and 0.87 (6H, t, J=6.95Hz, -CH_3). ^{13}C-NMR ($CDCl_3$, 50MHz): [ppm] 189.2, 155.1, 129.1, 111.4, 69.1, 31.6, 28.93, 28.88, 25.9, 22.5, and 13.9. ATR/FTIR [cm^{-1}]: 3055, 2953, 2930, 2862, 2870, 2854, 1681, 1489, 1472, 1429, 1395, 1288, 1217, 1140, 857, 746, 720, and 695.

2.2.3.4.6. Synthesis of 2,5-diheptyloxy-1,4-bis(triphenylphosphonium-methylbromide) benzene (22a)

A mixture of **20a** (1.968g, 4.0mmol) and triphenylphosphine (2.2g, 8.4mmol) in 100mL toluene was refluxed for 3 h. After solvent removal compound **22a** was yielded as a solid. Purification was not necessary.

2.2.3.4.7. Synthesis of 2,5-bis(heptyloxy)-1,4-bis[(2,5-diheptyloxy-4-formyl)phenylene vinylene] benzene 16a

A mixture of solid **22a** (from above) and compound **3a** (2.896g, 8.0mmol) was dissolved in 150mL methylene chloride. Lithium ethoxide solution (10mL, 1.0M in ethanol) was added drop wise at room temperature unstill the red-purple color produced disappeared. The mixture was stirred for 10 min after completion of base addition. Dilute aqueous HCl was then added, the organic layer separated and subsequently washed with water several times and finally dried over anhydrous sodium sulfate. The residue was isolated after solvent removal. To this E- and Z-isomer mixture in 200mL of methylene chloride were added 2g (7.87mmol) of iodine, and the mixture was stirred at room temperature overnight.

Then 200mL of methylene chloride were added to the now dark brown solution. The resulting solution was washed consecutively with aqueous $Na_2S_2O_3$ solution (1.0M, 150mL) three times, and finally with water several times. After silica gel column using toluene as eluent, compound **16a** was isolated as a red orange fluorescent solid (3.43g, 84%).

^{1}H-NMR ($CDCl_3$, 600MHz): [ppm] 10.43 (2H, s, aldehyde) 7.56 (2H, s, vinylene trans-CH=CH), 7.50 (2H, s, vinylene trans-CH=CH), 7.31 (2H, s, CH-aromatic), 7.18 (2H, s, CH-aromatic), 7.13 (2H, s, CH-aromatic), 4.09 (4H, t, J=6.4Hz, α_1-CH_2-), 4.04 (4H, t, J=6.4Hz, α_2-CH_2-), 4.02 (4H, t, J=6.4Hz, α_3-CH_2-), 1.84 (12H, m, β-CH_2-), 1.50 (12H, m, γ-CH_2-), 1.37 (12H, m, δ-CH_2-), 1.29 (24H, m, ε-CH_2-), and 0.87 (18H, m, -CH_3). ^{13}C-NMR ($CDCl_3$, 150MHz): [ppm] 189.2, 156.3, 151.3, 150.7, 135.0, 127.5, 127.0, 124.1, 123.2, 110.8, 110.4, 110.1, 69.4, 69.14, 69.04, 31.9, 31.84, 31.77, 29.5, 29.29, 29.27, 29.14, 29.08, 29.06, 26.2, 26.1, 22.64, 22.61, and 14.1. ATR/FTIR [cm^{-1}]: 3060, 2955, 2924, 2871, 2853, 1677, 1596, 1500, 1465, 1423, 1387, 1283, 1203, 1146, 1066, 965, 849, 789, 726, and 709.

2.2.3.5. Synthesis of OPVs with butyloxy side chains

The syntheses of OPVs with butyloxy side chains were performed in analogy to the syntheses of OPVs with heptyloxy side chains.

2.2.3.5.1. Synthesis of 1,4-bis(butyloxy)benzene (2b)

The synthesis of 1,4-dibutyloxybenzene **2b** was performed as described above (Scheme 2.1, Chapter 2).

2.2.3.5.2. Synthesis of 2,5-bis(bromomethyl)-1,4-bis(butyloxy)benzene (20b)

^{1}H-NMR ($CDCl_3$, 200MHz): [ppm] 6.84 (s, 2H, CH-aromatic), 4.514 (s, 4H, CH_2Br), 3.97 (t, 4H, α-CH_2-), 1.79 (q, 4H, β-CH_2-), 1.50 (m, 4H, γ-CH_2-), and 0.97 (t, 6H, -CH_3). ^{13}C-NMR ($CDCl_3$, 50MHz): [ppm] 150.6, 127.5, 114.6, 68.7, 31.4, 28.8, 19.3, and 13.9. Yield 77%.

2.2.3.5.3. Synthesis of 2,5-bis(acetylmethyl)-1,4-bis(butyloxy)benzene (21b)

^{1}H-NMR ($CDCl_3$, 200MHz): [ppm] 6.86 (s, 2H, CH-aromatic), 5.11 (s, 4H, -CH_2OAc), 3.93 (t, 4H, α-CH_2-), 2.08 (s, 6H, OAc), 1.73 (q, 4H, β-CH_2-), 1.48 (m, 4H, γ-CH_2-), and 0.94 (t, 6H, -CH_3). ^{13}C-NMR ($CDCl_3$, 50MHz): [ppm] 170.7, 150.7, 125.1, 113.6, 68.5, 61.4, 31.2, 20.7, 19.0, and 13.6. Yield 99%.

2.2.3.5.4. Synthesis of 2,5-bis(hydroxymethyl)-1,4-bis(butyloxy)benzene (5b)

^{1}H-NMR ($CDCl_3$, 600MHz): [ppm] 6.83 (2H, s, CH-aromatic), 4.66 (4H, d, J=5.83Hz, -CH_2-(OH)), 3.97 (4H, t, J=6.44Hz, α-CH_2-), 2.36 (2H, t, J=6.1Hz, -OH), 1.75 (4H, m, β-CH_2-), 1.47 (4H, m, γ-CH_2-), and 0.96 (6H, t, J=7.4Hz, -CH_3). ^{13}C-NMR ($CDCl_3$, 50MHz): [ppm] 150.5, 128.9, 112.2, 68.4, 62.0, 31.4, 19.3, and 13.8. ATR/FTIR [cm^{-1}]: 3316, 3250, 3241, 3069, 2957, 2933, 2916, 2870, 1507,

1469, 1447, 1416, 1392, 1366, 1316, 1298, 1282, 1229, 1203, 1174, 1145, 1123, 1070, 1035, 1001, 982, 909, 864, 815, 799, 783, and 740. Yield 83%.

2.2.3.5.5. Synthesis of 2,5-bis(butyloxy)benzene-1,4-dialdehyde (3b)

^{1}H-NMR ($CDCl_3$, 600MHz): [ppm] 10.50 (2H, s, -CHO), 7.41 (2H, s, CH-aromatic), 4.07 (4H, t, J=6.43Hz, α-CH_2-), 1.80 (4H, m, β-CH_2-), 1.48 (4H, m, γ-CH_2-), and 0.97 (6H, t, J=7.4Hz, -CH_3). ^{13}C-NMR ($CDCl_3$, 50MHz): [ppm] 189.2, 155.1, 129.1, 111.5, 68.8, 30.9, 19.1, and 13.6. ATR/FTIR [cm^{-1}]: 3055, 2954, 2875, 1681, 1486, 1464, 1428, 1391, 1284, 1214, 1171, 1121, 1069, 1027, 1008, 981, 919, 890, 840, 744, and 692. Yield 82%.

2.2.3.5.6. Synthesis of 2,5-bis(butyloxy)-1,4-bis[(2,5-diheptyloxy-4-formyl)phenylene vinylene]benzene (16b)

^{1}H-NMR ($CDCl_3$, 600MHz) [ppm] 10.43 (2H, s, aldehyde), 7.57 (2H, s, vinylene trans-CH=CH), 7.51 (2H, s, vinylene trans-CH=CH), 7.31 (2H, s, CH-aromatic), 7.19 (2H, s, CH-aromatic), 7.14 (2H, s, CH-aromatic), 4.105 (4H, t, J=6.4Hz, α_1-CH_2-), 4.056 (4H, t, J=6.4Hz, α_2-CH_2-), 4.028 (4H, t, J=6.4Hz, α_3-CH_2-) 1.854 (12H, m, β-CH_2-), 1.57 (12H, m, γ-CH_2-), and 1.011 (18H, m, -CH_3). ^{13}C-NMR ($CDCl_3$, 150MHz): [ppm] 189.1, 156.2, 151.3, 150.7, 134.9, 127.4, 126.9, 124.1, 123.1, 110.7, 110.4, 110.1, 69.1, 68.8, 68.75, 31.5, 31.34, 31.31, 19.5, 19.4, 19.3, 13.96, 13.93, and 13.84. ATR/FTIR [cm^{-1}]: 3060, 2954, 2935, 2869, 2764, 1674, 1594, 1501, 1467, 1421, 1389, 1343, 1262, 1246, 1202, 1159, 1120, 1066, 1036, 1025, 1010, 970, 919, 887, 854, 784, 742, 708, 678, and 667. Yield 74%.

3. Biotin-functional oligo(*p*-phenylene vinylene)s synthesized using click chemistry[116]

3.1. Overview

The design and synthesis of biotin functionalized oligo(*p*-phenylene vinylene) (OPV) using the Cu(1)-catalyzed [3+2] Huisgen “click” cycloaddition is presented. Biotin is placed at variable distances from the oligomer via appropriate length of a hydrophilic spacer, which also serves to regulate the binding capabilities of the two terminal biotin units. Streptavidin-coated quantum dots are used to demonstrate the binding potential. The organic compounds are analyzed by means of ATR-FTIR, ^{1}H-NMR (200 or 600 MHz), ^{13}C-NMR (50 or 150 MHz), 2D-NMR (HMBC, HMQC experiments), MS (ESI or MALDI-TOF), and optical spectroscopy. Networks were imaged with TEM.

3.2. Results and discussion

Specifically, the copper catalyzed azide-alkyne “click” cycloaddition reaction is used to functionalize alkyne modified OPV oligomers with biotin-PEG-azides. The syntheses of the respective dialkyne functional OPVs and azide-terminated biotin-PEG derivatives are also described and discussed. The luminescence properties of the resulting biotin-“clicked”-OPV conjugates are probed. In a prototype reaction, networks with streptavidin coated quantum dots (Qdots) are formed and characterized using transmission electron microscopy (TEM) (Scheme 3.2 ans 3.3).

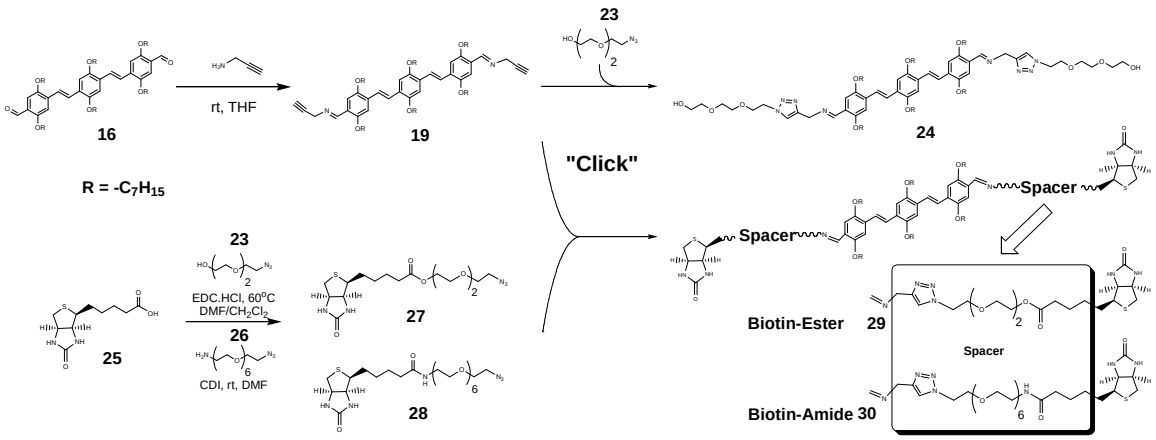

Scheme 3.1. "Click" functionalization of oligo(*p*-phenylene vinylene).

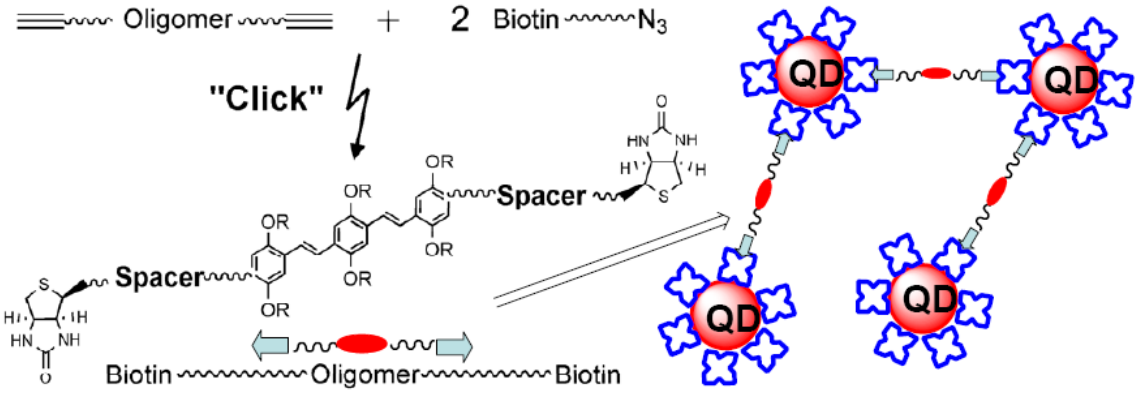

QD = Streptavidin coated quantum dot

Scheme 3.2. Quantum dot / OPV network formation via biotin.

The general synthetic strategy involves preparing two intermediates first, dialkyne functional oligomer **19** and azide functional biotin-PEG units **27** or **28** (Scheme 3.1), which then are subsequently combined by means of "click"-chemistry. The approach incorporates flexibility: the conjugated oligomer can be chosen from a large library of oligomers or other molecules, depending on the desired electro-optical characteristics and the targeted aggregation behavior. Compounds **27** and **28** represent a second platform for a library of potentially

valuable reactions, involving a straightforward functionalization with biotin or other ligand segments of varying hydrophilicity via “click”-chemistry; biotin may be placed at a defined distance from the conjugated oligomer by simply choosing a PEG segment of the desired chain length, depending on the specific requirements of the potential application. The chain length of the PEG segment also controls the biotin binding capability as well as the overall hydrophobic (conjugated oligomer)/ hydrophilic (biotin-PEG spacer) balance of the building blocks.

Specifically, the conjugated oligomer OPV, trimer dialdehyde **16**, is synthesized and characterized in analogy to chapter 2 and literature,[118-119] and subsequently reacted with propargylamine under Schiff base formation conditions to produce dialkyne functional trimer OPV **19** in quantitative yields (Scheme 3.1).

In a next step, the azide functional biotin-PEG conjugates **27** and **28** (biotin-PEG-N_3) are synthesized with different PEG spacers using either 1,3-dicyclohexyl-carbodiimide (DCC), carbonyldiimidazole (CDI), or 1-[3-(dimethylamino) propyl]-3-ethylcarbodiimide hydrochloride (EDC.HCl) mediated coupling. Two coupling reactions, that is, esterification and amidation, are alternatively employed. In order to vary the distance of biotin from the conjugated oligomer and overall hydrophobic/ hydrophilic balance (see above), PEG segments of different lengths are used for the esterification and amidation, the latter using four additional repeat units in the PEG segment. Representative optimization reactions are summarized in table 3.1 and show satisfactory yields.

Table 3.1. Representative synthesis results[a] of biotin-PEG-N_3's **27** and **28**[c]

Entry	Coupling reagent/ Catalyst	Solvent	T(^{o}C)/t(h)	Yield[b] (%)
1	EDC.HCl/DMAP	DMF	rt/ 18	20
2		DMF / CH_2Cl_2	60/24	65
3			rt/ 48	60
4				80[c]
5	CDI	DMF	rt/ 18	30
6				65[c]
7			80/24	40

[a] Conditions: [Biotin] = 80mM; [PEG-N_3] = 100mM; [1-(3-(dimethylamino) propyl)-3-ethylcarbodiimide hydrochloride : EDC.HCl] = 100mM; [Carbonyldiimidazole : CDI] = 234 mM; rt = ambient temperature; [b] Isolated Yield; [c] Isolated Yield of **28**

Using DCC in DMF or DMSO/CH_2Cl_2 results in no reaction or trace yields of the biotin-ester **27** after about 20 h at room temperature, as do attempts using EDC.HCl in DMF or CDI in DMSO under similar conditions (not shown in table 3.1). The reaction works when CDI or EDC.HCl together with 4-dimethylaminopyridine (DMAP) in DMF is employed; modest yields of **27** can be achieved after 18 h at ambient conditions using table 3.1 (Entries 5 and 1 respectively). The coupling reagent EDC.HCl produces the water soluble urea byproduct, enabling facile purification of the target ester. The reaction conditions have been further optimized: increased yields can be obtained at higher reaction temperatures and longer reaction times, and/or with the solvent mixture DMF/CH_2Cl_2 (Table 3.1, entries 2, 3 and 7).

The amidation proves more successful than the esterification and proceeds smoothly at ambient temperatures to give **28** with significantly higher yields than ester **27** under analogous conditions (Table 3.1, entries 4 and 6), using a commercial NH_2-functional PEG azide, and making further optimizations unnecessary. It should be noted that the commercial NH_2-functional PEG azide (~90% purity) is used without any further purification.

Finally, in the key step, intermediate azide functional PEG-biotins **27** and **28** are "clicked" onto the dialkyne functional OPV **19**, yielding the target conjugates **29** and **30** (Scheme 3.1). Representative synthesis results are summarized (Table 3.2).

Table 3.2. Representative click reactions of OPV dialkyne **19**[a]

Entry	Azide	Product	$Cu(CH_3CN)_4PF_6$ (mol equiv.)	T (h)	Yield [b] (%)
1	**23**	**24**	1	8	80
2	**23**	**24**	0.2	10	90
3	**23**	**24**	0.2	18	95
4	**27**	**29**	0.5	18	70
5	**27**	**29**	0.2	18	85
6	**28**	**30**	0.5	18	85
7	**28**	**30**	0.2	18	95

[a] Conditions: [**19**] **=** 5.7mM; [**23**], [**27**] and [**28**] **=** 13.8mM; ambient temperature; solvent CH_2Cl_2; [b] Yields based on ^1H NMR.

Initial “clicking”attempts using $CuSO_4.5H_2O$/sodium ascorbate mixtures were unsuccessful in various solvent mixtures (not shown in Table 3.2), resulting in the degradation of the two imine functions in **19** and the re-formation of the corresponding aldehyde functional **16**. Model reactions of alkyne **19** and PEG-azide **23** via [3+2] Huisgen cycloaddition in the presence of commercially available $Cu(CH_3CN)_4PF_6$ resulted in very good yields of the corresponding PEG-functional OPV **24** (Scheme 3.1, Table 3.2, entries 1–3). Incidentally, **24** represents a potentially valuable material in its own rights.

The dialkyne-functional OPV **19** and the azide-terminated biotin conjugates **27** and **28** are “clicked” under similarly mild reaction conditions. The reactions are performed in CH_2Cl_2 using 0.2 - 0.5 equivalents of Cu(I) catalyst to give the 1,4-triazoles in good to very good yields (Table 3.2, entries 4 – 7). The main challenge consists in finding conditions, under which the formation of the by-product OPV (di)aldehyde (see above) is minimized, as it can not be avoided entirely (~5% by ^{1}H-NMR). When larger amounts of Cu catalyst are used, more aldehyde byproduct is produced (Table 3.2, entries 1, 4, and 6 versus the respective other entries). Also, the ester **27** produces more aldehyde than the amide **28**, resulting in overall lower yields in **29** versus **30**. After workup, the compound purity is ~95%; this level of purity is quite reasonable if one takes into account the fact that these molecules are oligomers with molecular weights over 1500 D. Attempts to purify the samples further via column chromatography lead to no additional improvement. The best and most consistent results are obtained after 18 h using 0.2 equiv of catalyst (Table 3.2, entries 2, 5, and 7).

The compounds synthesized were analyzed by means of ATR-FTIR, ^{1}H-NMR (200 or 600 MHz), ^{13}C-NMR, and MS (ESI or MALDI-TOF). The Cu-catalyzed cycloaddition typically leads to exclusively 1,4 product, heteronuclear NMR-coupling experiments confirmed this in the cases of **24**, **29,** and **30** (See experimental). The electro-optical properties of the OPV are retained after the attachment of the biotin-spacer elements, as can be observed from the very similar absorption and photoluminescence characteristics of **19, 29,** and **30** in DMF solution (Figure 3.1, left). Due to the high fluorescence quantum efficiency of the trimeric OPV moiety,[120] the biotin OPV conjugates show fluorescence even at very low concentrations. Together with a high molar extinction coefficient,[120] the optical properties make these materials attractive candidates for imaging / biosensing applications. A broadening of the fluorescence in the longer wavelengths in the cases of **29** and **30** is most probably a consequence of enhanced aggregation of the fluorophore moieties in the polar solvent DMF, and supported by concentration-dependent emission spectra (Figure 3.1, right**).**

One objective for synthesizing soluble biotin-OPV derivatives was to see if they can be used as “adaptors” to connect streptavidin coated quantum dots (Qdots). Preliminary studies were performed to evaluate the abilities of **29** and **30** to bind the biotin binding sites on commercially available streptavidin Qdots 655 nm by incubating the (biotin-OPV-biotin)s **29** and **30** with the Qdots. The Qdots polyvalently display biotin binding sites; the addition of bivalent biotin-OPV results in a network of Qdots connected by OPV linkers. The network formation are observed using TEM (Figure 3.2). The Qdot control sample (Figure 3.2a)

shows no aggregation. Samples with combined streptavidin-Qdots and biotin-OPV-biotin **30** clearly display network formation (Figure 3.2b and c). In contrast, multiple attempts with biotin-OPV-biotin **29** (not shown) yielded inconclusive results. A tentative explanation could be that the longer PEG spacer in the case of **30** is necessary for the biotin moieties to access the streptavidin binding sites.

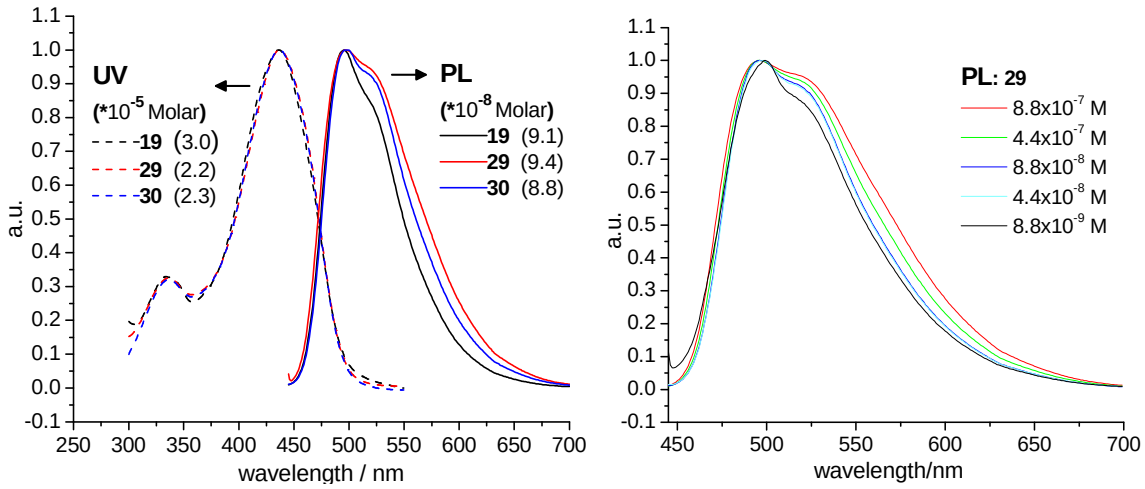

Figure 3.1. UV/Vis absorption and emission (normalized) of OPVs **19**, **29**, and **30** (left), concentration dependent emission of **30** solutions in DMF, excitation at 438 nm.

The electro-optical properties of **29**, **30**, as well as the networks with two interacting electronic systems are currently under further investigation. Also, the fabrication of biotin-OPV monolayers on silica chips is underway for arraying Qdots in two dimensions for bio-sensing applications.

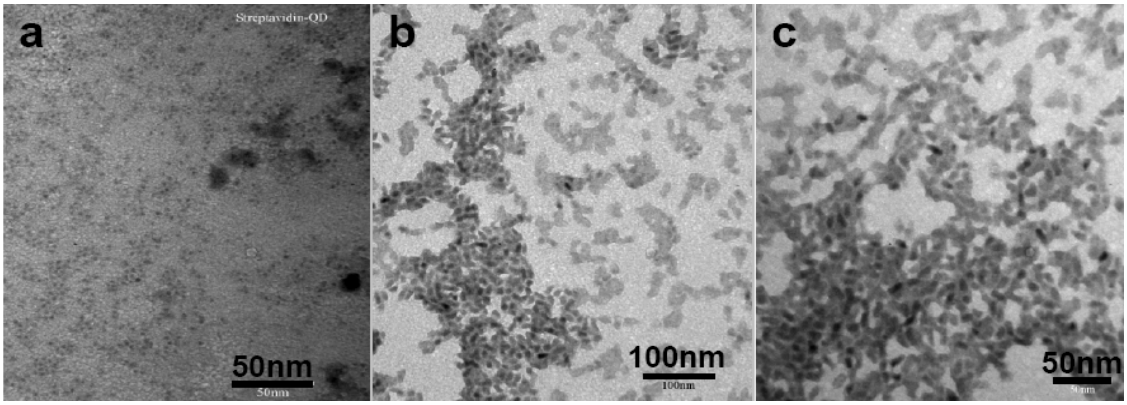

Figure 3.2. TEM images of (a) Streptavidin Qdot control, (b) network of streptavidin Qdots and 18μM biotin-OPV **30**, (c) network of streptavidin Qdots and 1 μM biotin-OPV **30**.

3.3. Experimental

3.3.1. General information

All experiments using air/moisture sensitive materials were carried out under an atmosphere of high purity argon using standard Schlenk techniques. All glass-ware was cleaned and dried for at least 24h in an oven at 120^{o}C prior to use.

3.3.2. Chemicals

D(+)-Biotin (98%) was obtained from Acros Chemicals. 1,3 dicyclohexylcarbodiimide (DCC), 1,1-carbonyldiimidazole (CDI), 4-(dimethyl-aminopyridine) (DMAP) were purchased from Sigma-Aldrich. The azido-PEG-amine and *O*-(2-Aminoethyl)-*O′*-(2-azidoethyl)pentaethylene glycol ≥90% (oligomer purity) (Mw 350.41g/mol) were obtained from Fluka. 1-ethyl-3-(3-dimethylaminopropyl)carbodiimide hydrochloride (EDC.HCl) was purchased from Pierce Chemicals. Propargylamine (98%) and $Cu(CH_3CN)_4PF_6$ catalyst were obtained from Aldrich. Solvents, e.g. dimethyl sulfoxide (99.9%),

dichloromethane, chloroform and methanol were purchased from Fisher scientific. *N*,*N*-dimethylformamide (DMF), anhydrous (99.8%) was obtained from Acros Organics. All other solvents were dried and degassed, using a “Pure Solv” solvent purification system (activated alumina, copper catalyst, molecular sieves columns) by Innovative Technology Inc. before use. All other chemicals were used as received. Column chromatography was carried out on silica gel 60 (70-230 mesh) from EMD Chemicals Inc.

3.3.3. Instrumentation

^{1}H and ^{13}C NMR spectra were recorded on Varian 200 MHz or 600 MHz spectrometers in $CDCl_3$. Heteronuclear multiple quantum correlation (HMQC) and heteronuclear multiple bond correlation (HMBC) experiments were done on 600 MHz spectrometer. FTIR-ATR spectra were recorded on Bruker Tensor 27 spectrometer using a Pike ATR accessory. UV-Vis spectra were recorded using a Perkin Elmer Lambda 650. Solvents for optical property investigations were Spectrasolv from Fisher. Photoluminescence spectra were recorded using a Horiba Jobin Yvon Fluoromax-3 spectrofluorometer. Elemental analysis data were obtained from Atlantic Microlab Inc. (Norcross, GA), and CHNS analysis was done on a LECO 932 instrument and are performed by combustion using automatic analyzers. Oxygen analysis was performed by pyrolysis. Mass spectrometry was carried out at Hunter College (New York). The mass spectra were obtained on an Agilent 1100 LC/MSD using Electrospray (ESI) ionization in methanol. MALDI-TOF was carried out at Carnegie Mellon University, the matrix-

assisted laser desorption ionization time-of-flight mass spectrometer (MALDI-TOF) was a PerSeptive Biosystems VoyagerSTR and the matrix used was Dithranol. ^{1}H- and ^{13}C-NMR assignment of OPV are according to literature.[121]

3.3.4. Synthesis of biotin-OPV (30) – streptavidin Qdots 655nm and TEM thereof

TEM images were recorded using a Phillip CM 100 microscope at 60 kV. OPV-Biotin conjugate **30** in DMF 4 µM, and 89 µM respectively were used. 2 µL of the OPV (**30**) solutions were added to 8 µL of streptavidin quantum dots 655 nm (supplied by Chemicon International, SA306) to study the network formation at two different ratios of Qdot: OPV. The OPV quantum dot mixtures were applied to carbon coated copper grids 200 mesh and observed, negative staining was unnecessary for visualization.

3.3.5. Synthesis of N_3-PEG-OH (23)

The azido PEG-OH, 2-(2-(2-azidoethoxy)ethoxy)ethanol was synthesized according to literature.[122]

3.3.6. Synthesis of biotin- PEG-N_3 ester (27)

In a 50 mL round bottom flask, D (+)-Biotin (0.24 g, 1 mmol,) was added under argon in 2 mL of DMF and was heated at 80 ^{o}C until the biotin was dissolved. Then EDC.HCl (0.23 g, 1.2 mmol) in 10 mL of dry CH_2Cl_2 and DMAP (0.027 g, 0.223 mmol) and azido-PEG-OH **23** (0.21 g, 1.2 mmol,) were added and the

mixture was stirred at 60 ^{o}C for 24 h. The solvents were evaporated under reduced pressure and the reaction mixture was then extracted with saturated aqueous $NaHCO_3$ and the product was extracted with $CHCl_3$ (2 x 5 mL). The organic layer was washed with water, dried over anhydrous Na_2SO_4 and concentrated under reduced pressure. The crude product was purified by column chromatography (silica gel 60-120 mesh, $CHCl_3$/methanol: 95/5 v/v) (Yield: 0.26 g, 65%). FTIR-ATR: v_{max}/ cm^{-1} 3258, 3079 (NH), 2930, 2868 ($CH_{aliphat}$), 2107 (N_3), 1732, 1695 (CO), 1466, 1336, 1261 (C-N), 1212, 1155 (C-O-C), 937, 759, 688. ^{1}H NMR (200 MHz, $CDCl_3$): δ 1.36-1.64 (6H, m), 2.33 (2H, t, J = 7 Hz), 2.66-2.73 (1H, d, J = 12.6 Hz)), 2.82-2.90 (1H, dd, J = 4.6 Hz), 3.12 (1H, m), 3.35 (2H, t, J = 5.2 Hz), 3.62-3.68 (8H, m), 4.19 (2H, t, J = 4.4 Hz), 4.22-4.49 (2H, m), 5.52 (1H, s, NH), 6.07 (1H, s, NH). ESI-MS: calcd for $C_{16}H_{27}N_5O_5S$: 402.2 $[M+H]^+$, found: 402.1 $[M+H]^+$, 424.2 $[M+Na]^+$, found: 424.2 $[M+Na]^+$.

3.3.7. Synthesis of biotin- PEG-N_3 amide (28)

In a 50 mL round bottom flask, D(+)-Biotin (0.24 g, 1 mmol) was added under argon in 5 mL of DMF and was heated at 80 ^{o}C until the biotin was dissolved. Then carbonyldiimidazole (CDI) (0.19 g, 1.2 mmol,) was added and the mixture was stirred at room temperature for 4 h to activate the carboxyl group of the biotin. Finally DMF solution containing azido-PEG-amine **26** (0.42 g, 1.2 mmol,) was added and the mixture was stirred at room temperature for 18 h. The solvents were evaporated under reduced pressure and the reaction mixture was then extracted with saturated aqueous $NaHCO_3$ and the product was extracted

with $CHCl_3$ (2 x 5 mL). The organic layer was washed with water, dried over anhydrous Na_2SO_4 and concentrated under reduced pressure. The crude product was purified by column chromatography (silica gel 60-120 mesh, $CHCl_3$/methanol: 95/5 v/v) (Yield: 0.46 g, 80%). FTIR-ATR: ν_{max}/cm^{-1} 3305, 3232 (N-H), 2925, 2864, 2100 (N_3), 1702 (CO), 1643 (amide I), 1549 (amide II) 1459, 1425, 1348, (C-N), 1205, 1101 (C-O-C). ^{1}H NMR (200 MHz, $CDCl_3$): δ 1.34-1.65 (6H, m), 2.17 (2H, t, J = 7.2 Hz), 2.65-2.72 (1H, d, J = 12.4 Hz), 2.80-2.89 (1H, dd, J = 4.6 Hz), 3.09 (1H, m), 3.32-3.64 (28H, m), 4.26-4.48 (2H, m), 5.81 (1H, s, NH), 6.7 (1H, s, NH), 7.0 (1H, t, J = 5 Hz, amide-NH). ESI-MS: calcd for $C_{24}H_{44}N_6O_8S$: 577.3; $[M+H]^+$, found: 577.3 $[M+H]^+$, 594.3 $[M+NH_4]^+$, found: 594.3 $[M+NH_4]^+$.

3.3.8. Synthesis of PEG functional OPV (24)

To a solution of **19** (25 mg, 0.023 mmol) and azido-PEG **23** (9.6 mg, 0.055 mmol) in 4 mL of CH_2Cl_2 was added $Cu(CH_3CN)_4PF_6$ (1.7 mg, 0.0046 mmol) and the solution stirred at room temperature overnight. The excess copper was removed using the commercial copper binding resin Cuprisorb^{TM} and the resulting solution was filtered and concentrated under reduced pressure to give the triazole **24** as an orange solid (Yield: 27.8 mg, 95%). ^{1}H NMR (600 MHz, $CDCl_3$): δ 8.85 (2H, s), 7.84 (2H, s, triazole-H), 7.49 (4H, s, *trans*-CH=CH), 7.48 (2H, s, CH-aromatic), 7.12-7.13 (4H, s, CH-aromatic), 4.93 (4H, s), 4.52 (4H, t, J = 4.8 Hz), 4.05 (12H, m, -α-CH_2), 3.87 (4H, t, J = 4.8 Hz), 3.66-3.59 (12H, m), 3.50 (4H, t, J = 4.2 Hz), 1.80 (12H, m, β-CH_2), 1.28 (48H, m, -CH_2-), 0.84 (18H, m, -CH_3).

3.3.9. Synthesis of OPV-biotin (29)

To a solution of **19** (25 mg, 0.023 mmol) and biotin PEG N_3 ester **27** (22 mg, 0.055mmol,) in 4 mL of CH_2Cl_2 was added $Cu(CH_3CN)_4PF_6$ (1.7 mg, 0.0046 mmol) and the solution stirred at room temperature overnight. The excess copper was removed using the commercial copper binding resin Cuprisorb^{TM} and the resulting solution was filtered and concentrated under reduced pressure to give the triazole **29** as an orange solid (Yield: 38 mg, 85%). ^{1}H NMR (600 MHz, $CDCl_3$): δ 8.84 (2H, s), 7.64 (2H, s, triazole-H), 7.48 (4H, s, *trans*-CH=CH), 7.47 (2H, s, CH-aromatic) 7.13-7.12 (4H, s, CH-aromatic), 5.32 (2H, s, NH-Biotin), 5.28 (2H, s, NH-Biotin), 4.92 (4H, s), 4.52 (4H, t, J = 4.8 Hz), 4.48-4.18 (8H, m), 4.01(12H, m, -α-CH_2), 3.86 (4H, t, J = 4.8 Hz), 3.72-3.38 (12H, m), 3.10 (2H, m), 2.89-2.83 (2H, dd, J = 4.8 Hz), 2.73-2.63 (2H, d, J = 12 Hz), 2.30 (4H, t, J = 7.2 Hz), 1.80 (12H, m, β-CH_2), 1.62-1.42 (12H, m), 1.28 (48H, m, -CH_2-), 0.84 (18H, m , -CH_3). MALDI-TOF: characteristic ion $[M+H]^+$: calcd 1899, found 1899.9570.

3.3.10. Synthesis of OPV-biotin (30)

To a solution of **19** (25 mg, 0.023 mmol) and biotin-PEG-N_3-amide **28** (32 mg, 0.055 mmol) in 4 mL of CH_2Cl_2 was added $Cu(CH_3CN)_4PF_6$ (1.7 mg, 0.0046 mmol) and the solution stirred at room temperature overnight. The excess copper was removed using the commercial copper binding resin Cuprisorb^{TM} and the resulting solution was filtered and concentrated under reduced pressure to give the triazole **30** as an orange solid (Yield: 48.6 mg, 95%). ^{1}H NMR (600 MHz,

$CDCl_3$): δ 8.82 (2H, s), 7.64 (2H, s, triazole-H), 7.48 (4H, s, *trans*-CH=CH), 7.47 (2H, s, CH-aromatic), 7.12-7.11 (4H, s, CH-aromatic), 6.82 (2H, s, NH), 6.52 (2H, s, NH-Biotin), 5.63 (2H, s, NH-Biotin), 4.90 (4H, s), 4.50 (4H, t, J = 4.8 Hz), 4.44-4.24 (4H, m), 4.01(12H, m, -α-CH_2), 3.85 (4H, t, J = 4.8 Hz), 3.62-3.35 (48H, m), 3.09 (2H, m), 2.82-2.88 (2H, dd, J = 4.8 Hz), 2.64-2.71 (2H, d, J = 12 Hz), 2.18 (4H, t, J = 7.2 Hz)), 1.80 (12H, m, β-CH_2), 1.64-1.42 (12H, m), 1.28 (48H, m, -CH_2-), 0.87 (18H, m, -CH_3).. MALDI-TOF: characteristic ion $[M+H]^+$: calcd 2251.4194, found 2251.0535.

3.3.11. Analytical detail of di(biotin-PEG-amide)OPV (30)

3.3.11.1. ^{1}H-NMR (600 MHz, $CDCl_3$) of 30 with assignments

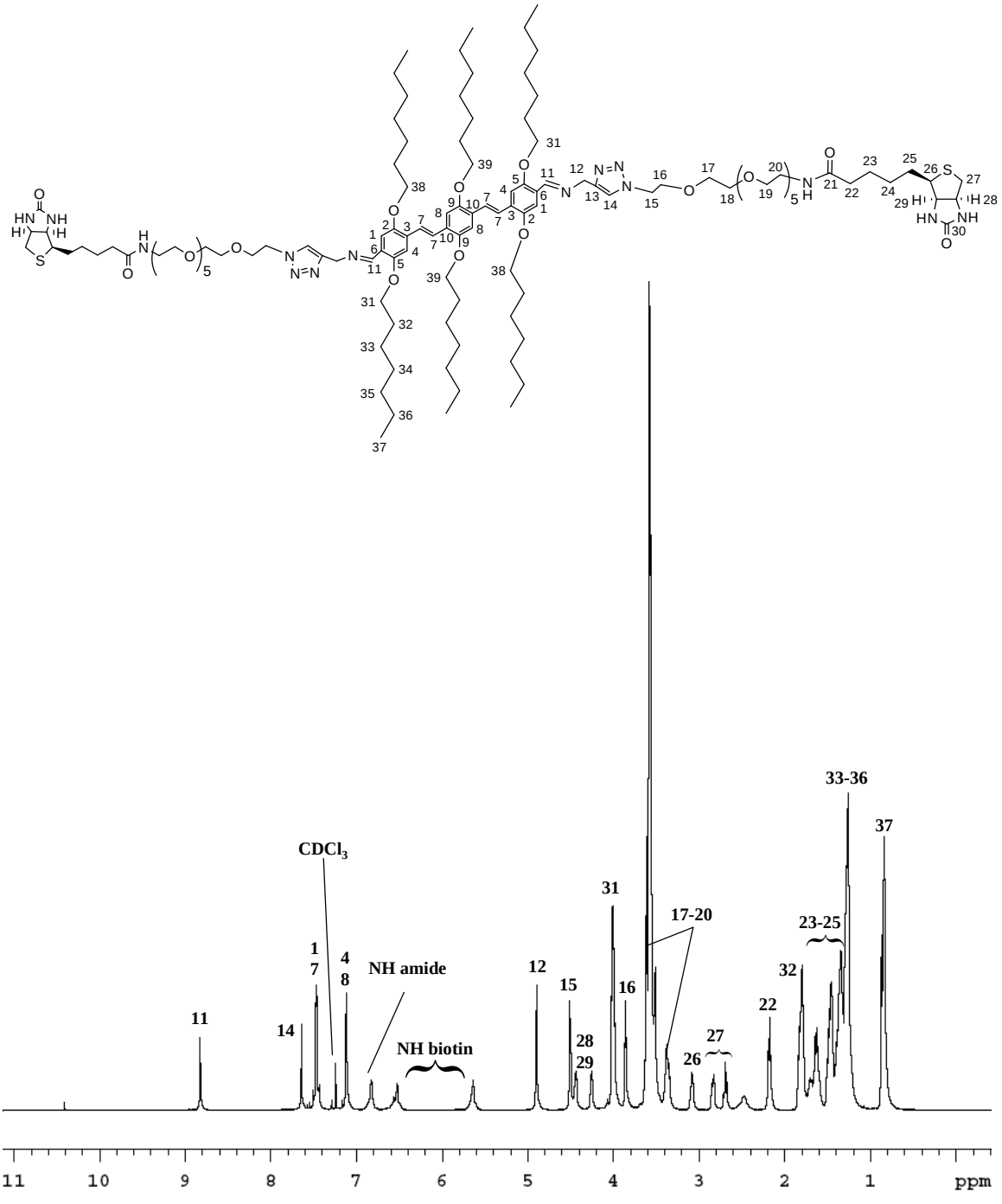

3.3.11.2. ^{13}C-NMR (150 MHz, $CDCl_3$) of 30 with assignments

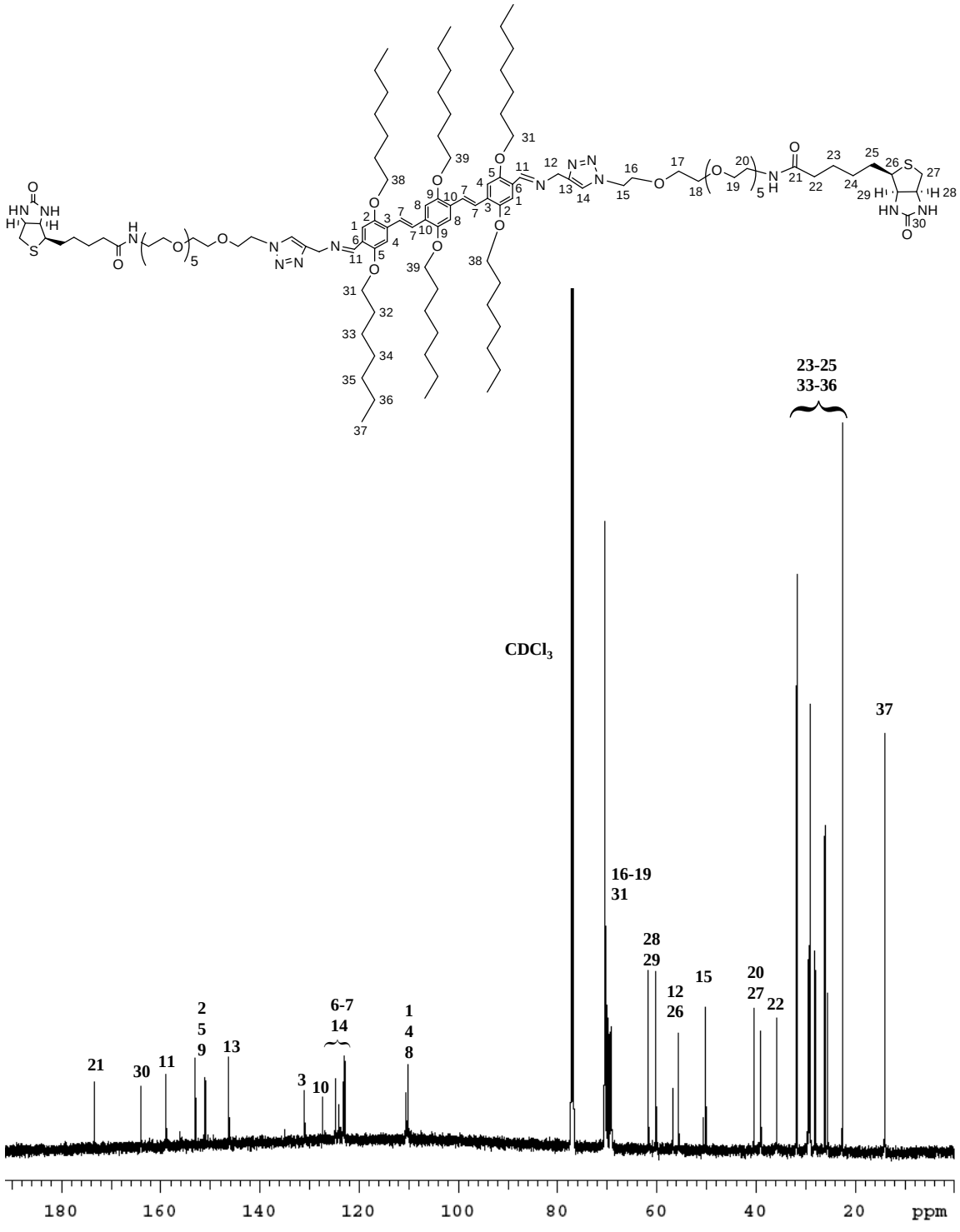

3.3.11.3. Table with summarized NMR assignments of 30

Assignment	^{1}H (ppm)	^{13}C (ppm)
1	7.47 (s, 2H)	110.12
2		151.07
3		130
4	7.13 (s,2H)	110.49
5		150.84
6		122.93
7	7.48 (s, 4H)	124.81, 124.04
8	7.12 (s, 2H)	110.49
9		153
10		127.29
11	8.83 (s, 2H)	158.89
12	4.9 (s, 4H)	57
13		146.25
14	7.65 (s, 2H)	122.93
15	4.51(t, 4H)	50.14
16	3.85 (t, 4H)	69.91
17-20	3.63-3.35 (m, 48H)	70.45-69.99, 39.06 (C20)
21		173.29
22	2.19 (t, 4H)	35.83
23-25	1.64-1.42 (m,12H)	
26	3.09 (m, 2H)	55.5
27	2.87-2.88 (dd, 2H) 2.71-2.64 (d, 2H)	40.46
28	4.46 (m, 2H)	61.66
29	4.26 (m, 2H)	60.09
30		163.83
31	4.01(t, 12H)	69.52, 69.32, 69.20
32	1.80 (m, 12H)	
33-36	1.28 (m, 48H)	31.80-22.60 (32, 23-25 also)
37	0.87 (t, 18H)	14.07
NH-amide	6.98 (t, 2H)	
Biotin-NH	6.43 (s, 2H)	
Biotin-NH	5.53 (s, 2H)	

3.3.11.4. HMQC and HMBC spectra of 30

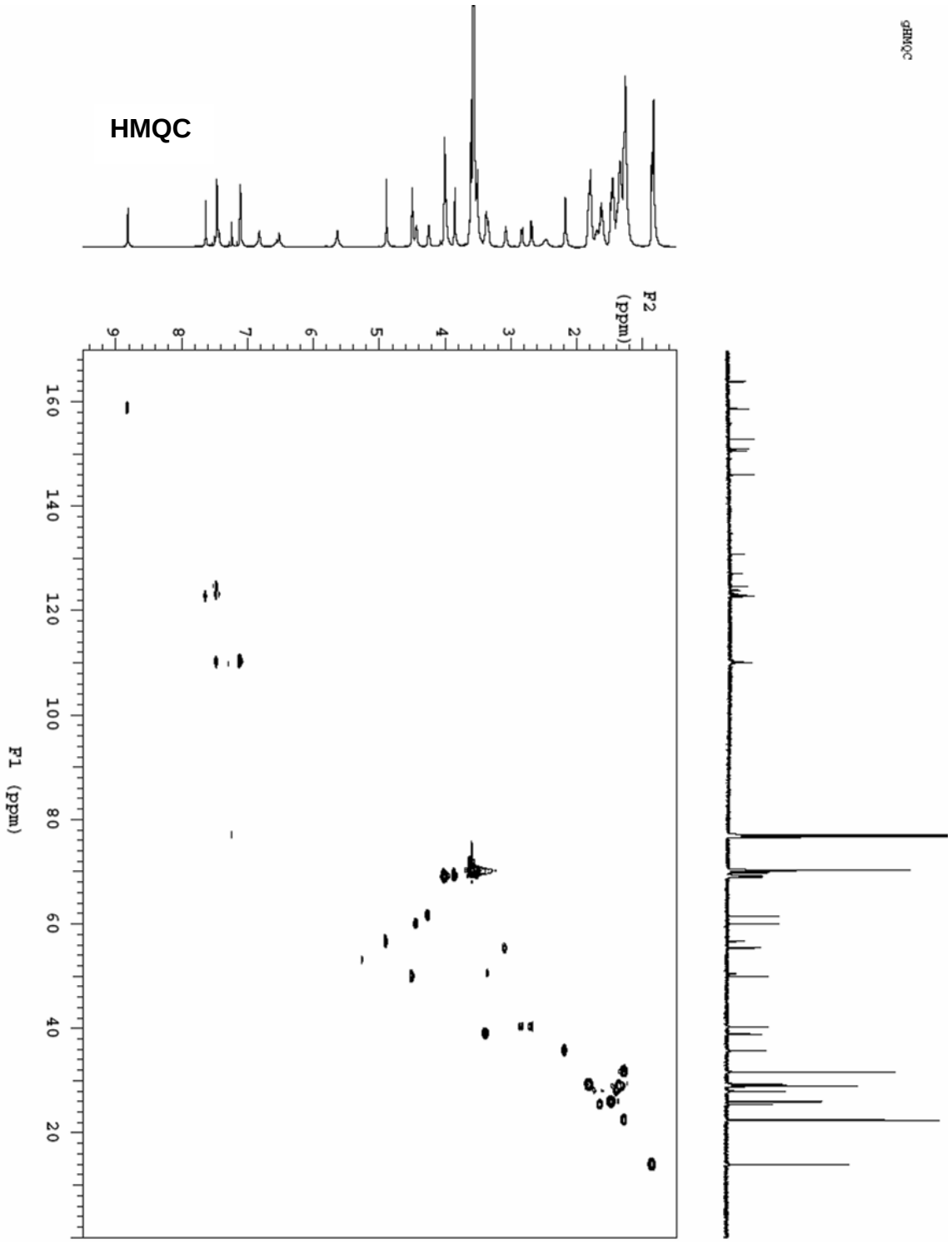

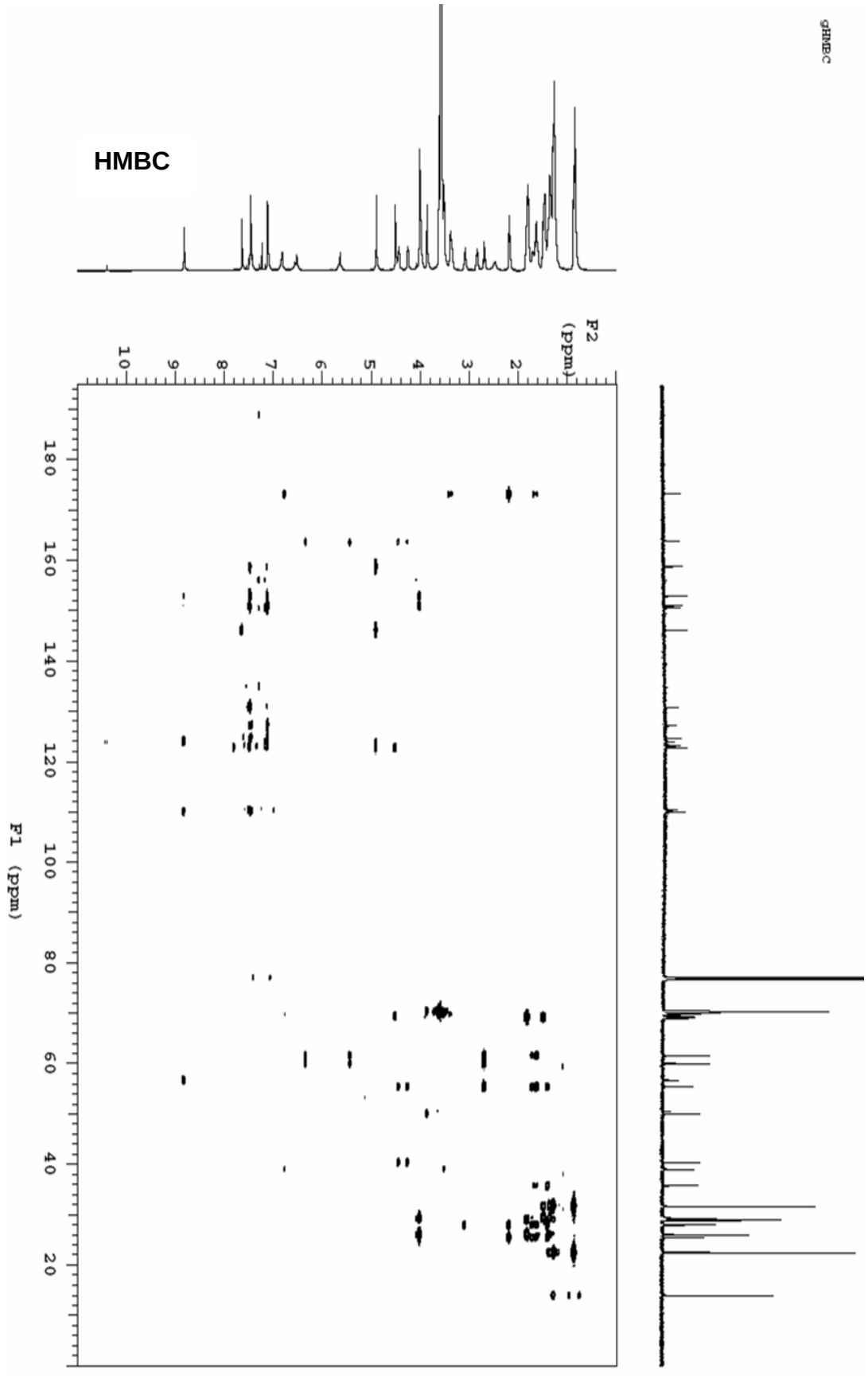
HMBC
gHMBC
F2 (ppm)
F1 (ppm)

3.3.11.5. Table with observed H-C couplings relevant to assigning the *anti-* geometry of the triazole ring

HMBC	OPV 30			
	$C12_{57}$	$C13_{146.25}$	$C14_{123}$	$C15_{50}$
H12	x	√	√	x
H14	x	√	x	x
H15	x	x	√	x

√ : coupling expected and observed

x : no significant coupling observed

3.3.12. Analytical detail of di(biotin-PEG-ester)OPV (29)

3.3.12.1. ^{1}H-NMR (600 MHz, $CDCl_3$) of 29 with assignments

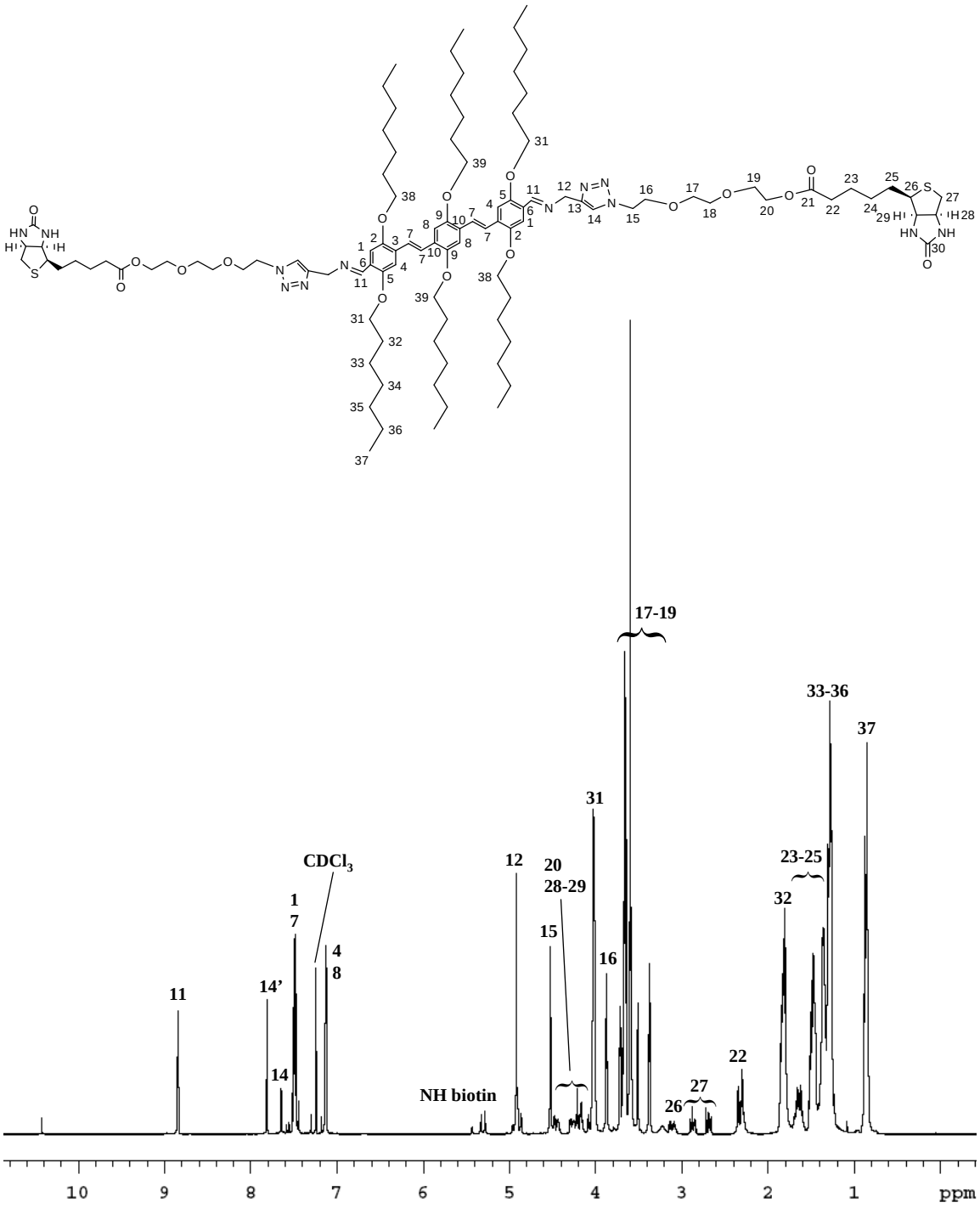

3.3.12.2. ^{13}C-NMR (150 MHz, $CDCl_3$) of 29 with assignments

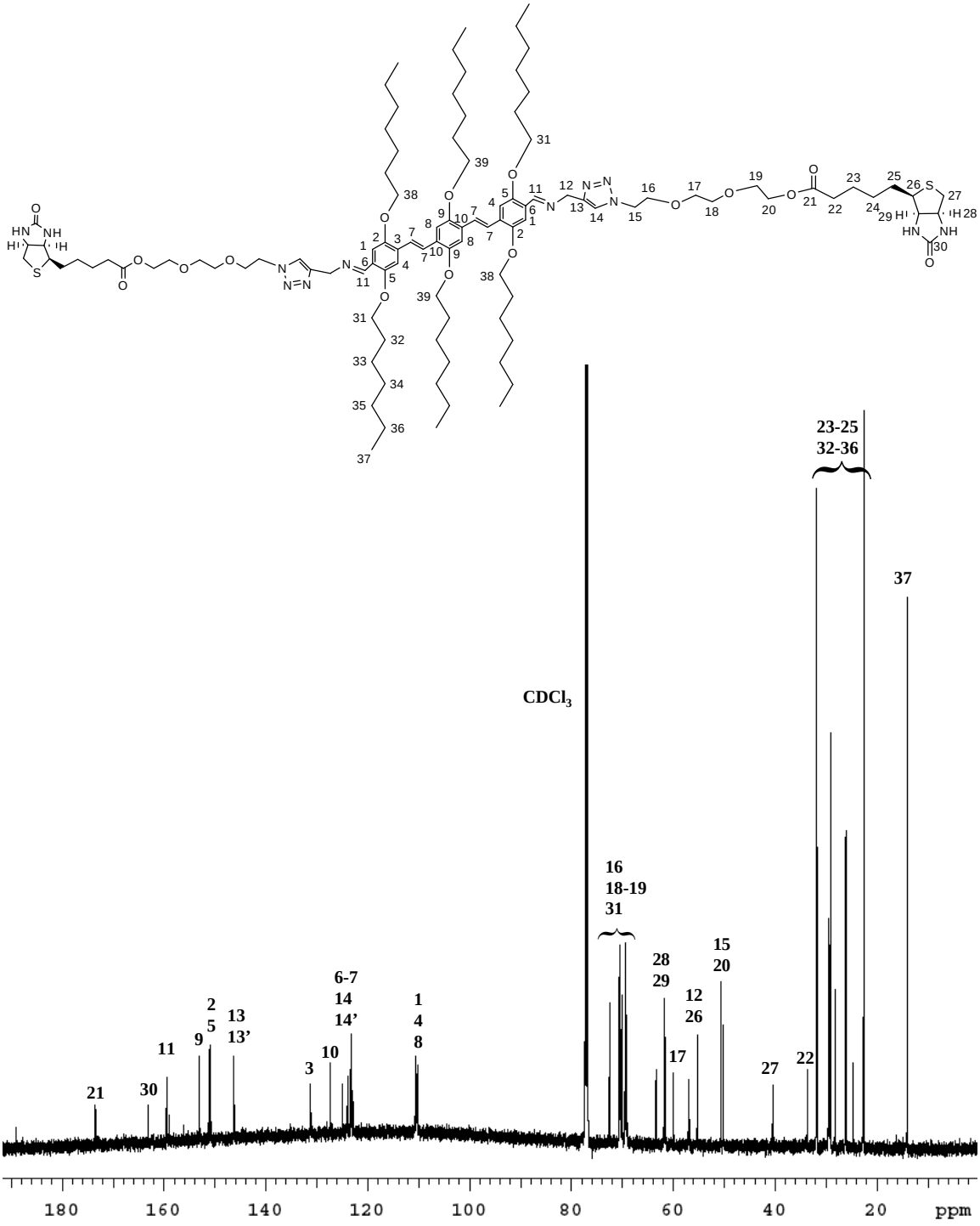

3.3.12.3. Table with NMR assignments of 29, comments on degradation products

Assignment	^{1}H (ppm)	^{13}C (ppm)
1	7.47 (s, 2H)	110.19
2		150.89
3		131.22
4	7.13 (s, 2H)	110.61
5		151.14
6		123.29
7	7.48 (s, 4H)	124.96, 124.04
8	7.12 (s, 2H)	110.41
9		153.12
10		127.39
11	8.84 (s, 2H)	158.89
12	4.92 (s, 4H)	56.98
13, 13'		146.18,146.34
14,14'	7.64 (s, 2H), 7.81 (s)	123.21, 122.88
15	4.51 (t, 4H)	50.13
16	3.87 (t, 4H)	69.58
17-20	4.18-3.38 (m,16H)	61.82 (C17), 72.45-70.02, 50.62 (C20)
21		173.52
22	2.30 (t, 4H)	33.69
23-25	1.62-1.42 (m,12H)	
26	3.10 (m, 2H)	55.29
27	2.89-2.83 (dd, 2H) 2.73-2.63 (d, 2H)	40.49
28	4.51 (m, 2H)	63.38
29	4.43 (m, 2H)	63.21
30		163.1
31	4.02(t, 12H)	69.38, 69.28, 69.20
32	1.80 (m, 12H)	
33-36	1.28 (m, 48H)	31.81-22.60 (C32, C23-25 also)
37	0.84 (t, 18H)	14.03
Biotin-NH	5.32 (s, 2H)	
Biotin-NH	5.28 (s, 2H)	

Note: H14', C13', C14' relate to the analogous nuclei of the byproduct that is formed when an ester group of **29** is cleaved. The resulting byproduct shows the same resonances as are observed in PEG-OPV **24**.

3.3.12.4. HMQC and HMBC spectra of 29

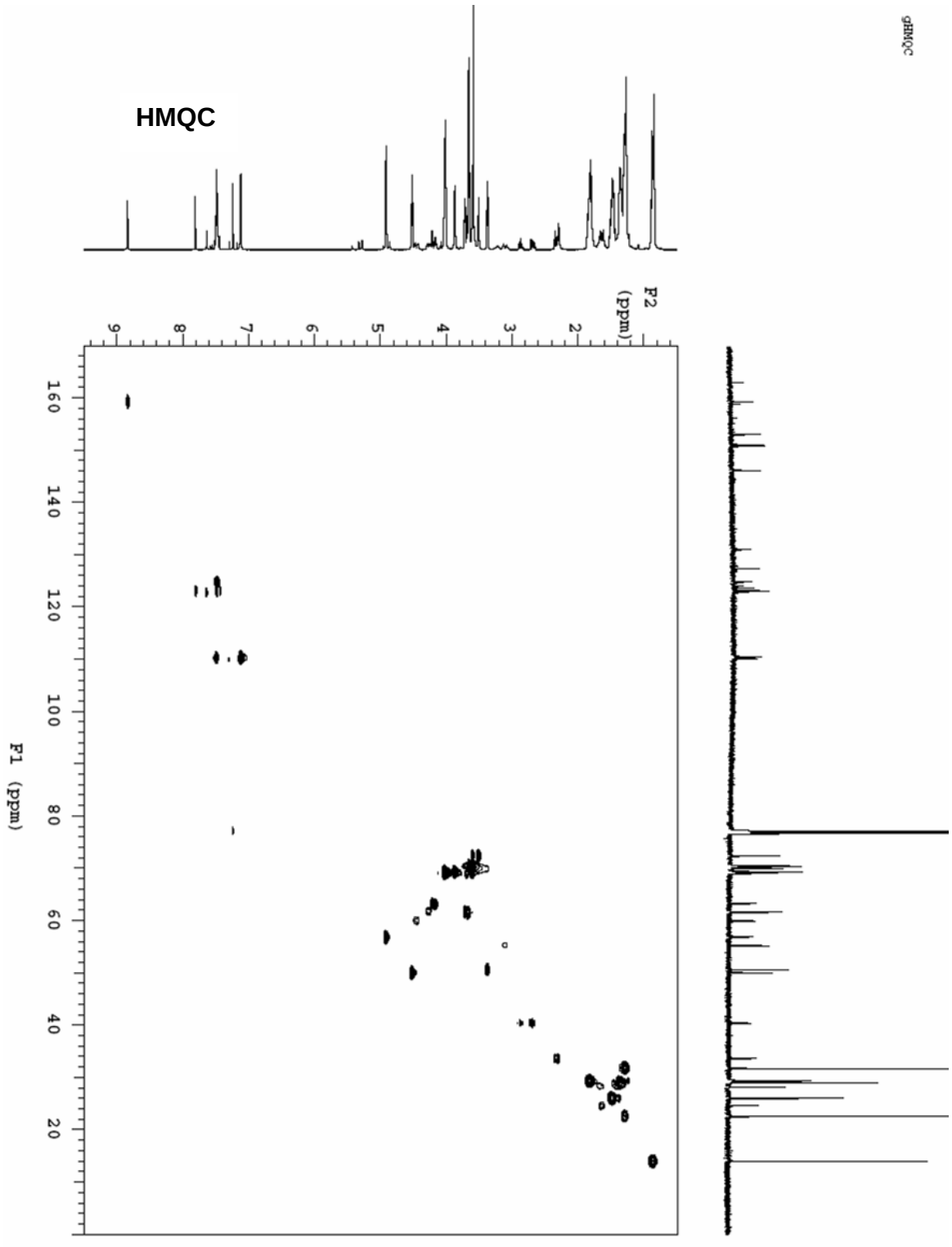

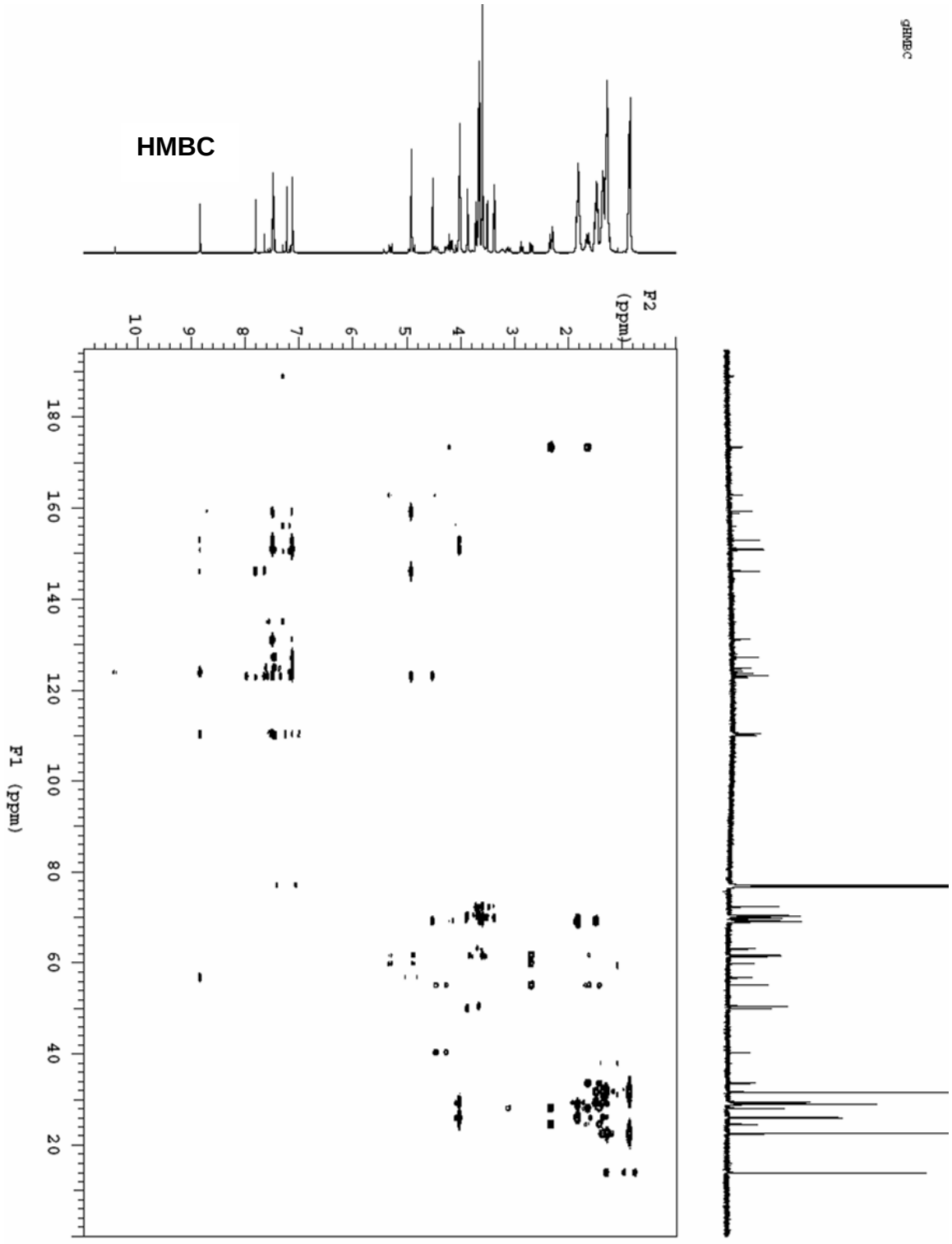
HMBC
gHMBC
F2 (ppm)
F1 (ppm)

3.3.12.5. Table with observed H-C couplings relevant to assigning the *anti-* geometry of the triazole ring

HMBC	OPV 29					
	$C12_{57}$ $C15_{50}$	$C13_{146.18}$	$C13'_{146.34}$	$C14_{123.21}$	$C14'_{122.88}$	
H12	x	√	x	√	x	x
H14	x	√	x	x	x	x
H14'	x	x	√	x	x	x
H15	x	x	x	√	x	x

Note: H14', C13', C14' relate to the ester cleaved product of **29** (comment see above)

√ : coupling expected and observed

x : no significant coupling observed

3.3.13. Analytical detail of PEG-functional OPV (24)

3.3.13.1. ^{1}H-NMR (600 MHz, $CDCl_3$) of 24 with assignments

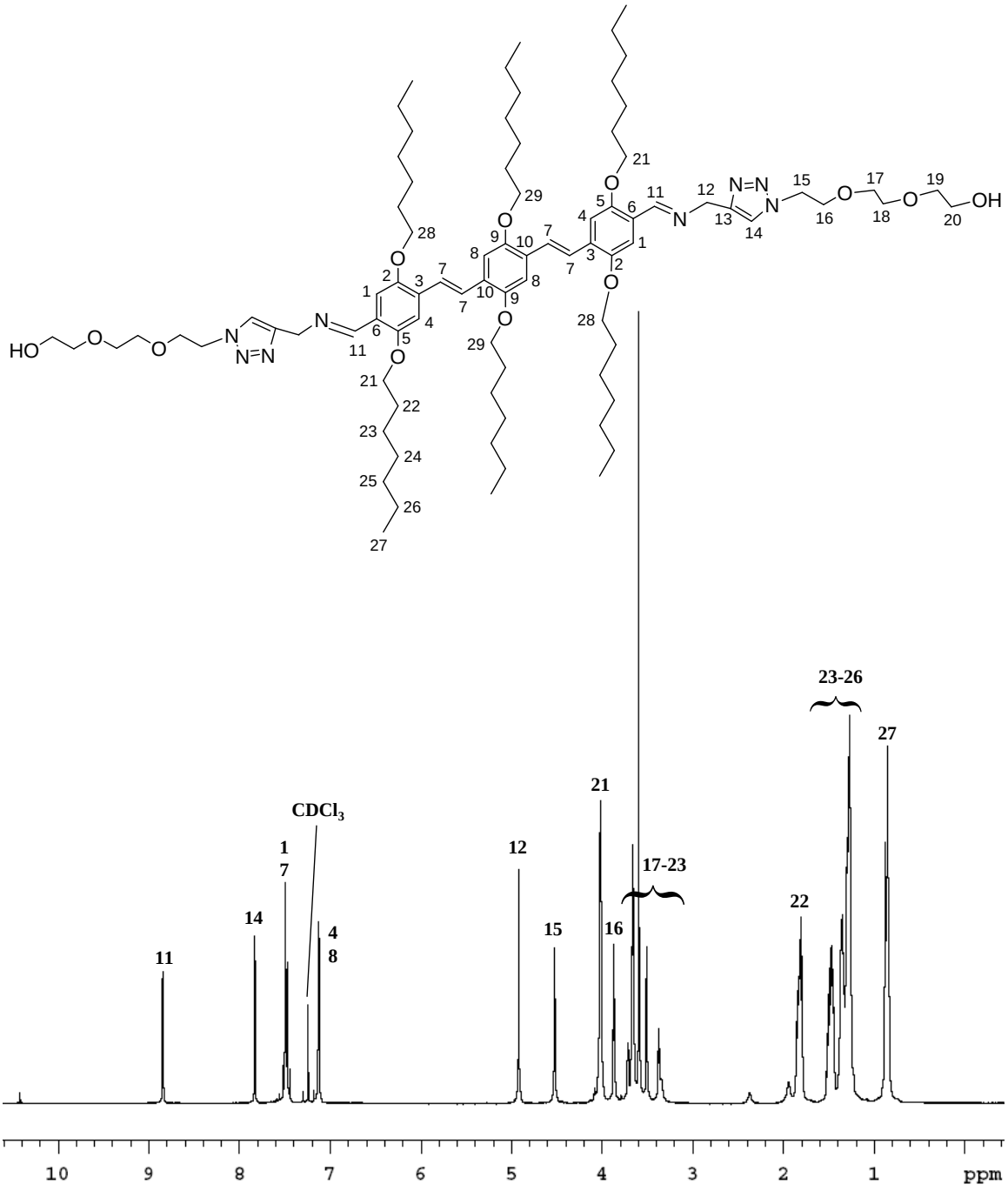

3.3.13.2. ^{13}C-NMR (150 MHz, $CDCl_3$) of 24 with assignments

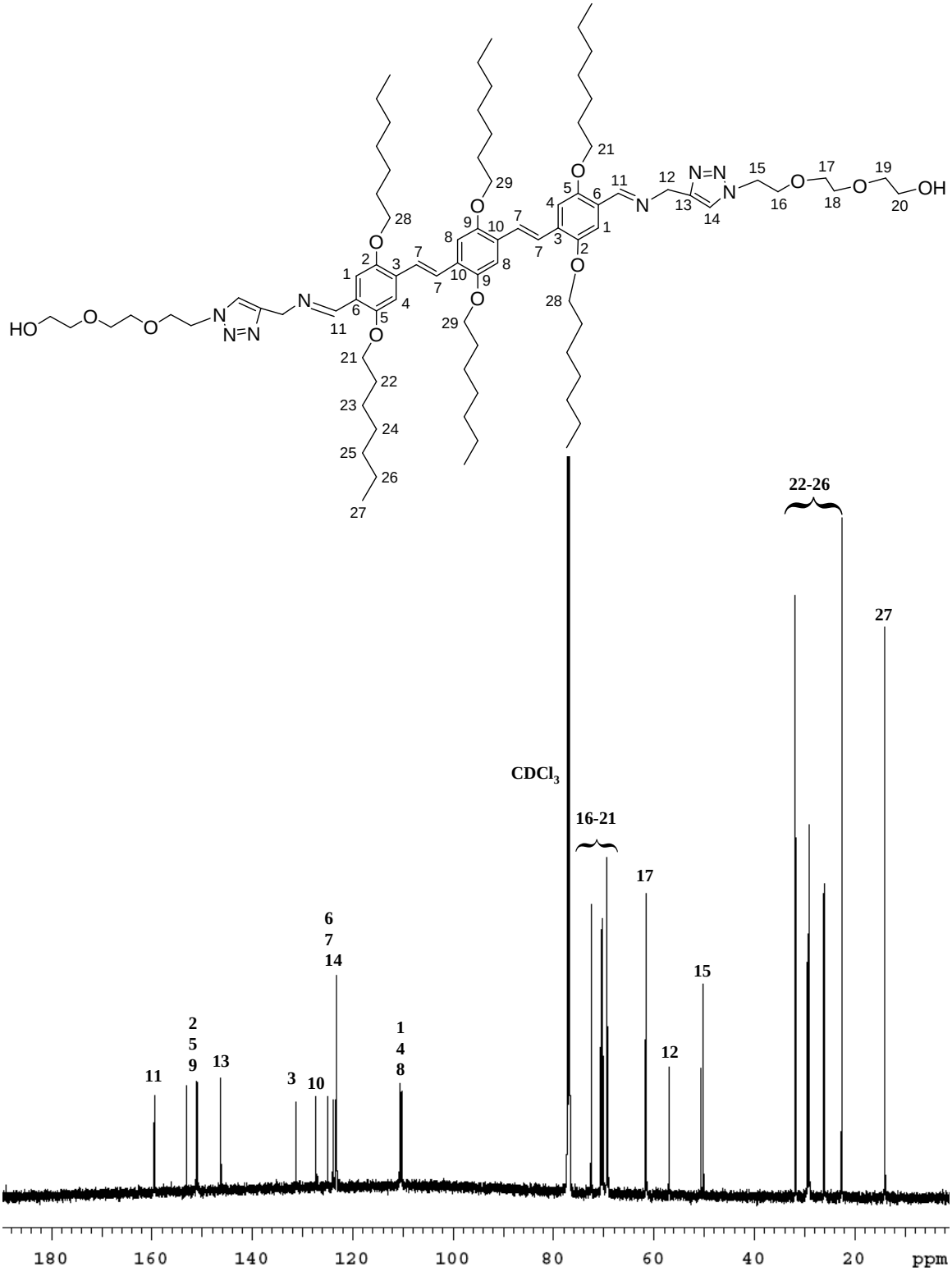

3.3.13.3. Table with NMR assignments of 24

Assignment	^{1}H (ppm)	^{13}C (ppm)
1	7.47 (s, 2H)	110.35
2		151.37
3		130.39
4	7.13 (s, 2H)	110.63
5		151.11
6		124.49
7	7.49 (s, 4H)	125.26
8	7.12 (s, 2H)	110.63
9		153.4
10		127.61
11	8.85 (s, 2H)	159
12	4.93 (s, 4H)	57.16
13		146.38
14	7.84 (s, 2H)	123.55
15	4.52 (t, 4H)	50.38
16	3.87 (t, 4H)	
17-20	3.65-3.48 (m, 16H)	61.77 (C17), 72.76-70.30 (C16 also)
21	4.02 (t, 12H)	69.62, 69.48, 69.43
22	1.80 (m, 12H)	
23-26	1.28 (m, 48H)	32.07-22.83 (C22 also)
27	0.84 (t, 18H)	14.31

3.3.13.4. HMQC and HMBC spectra of 24

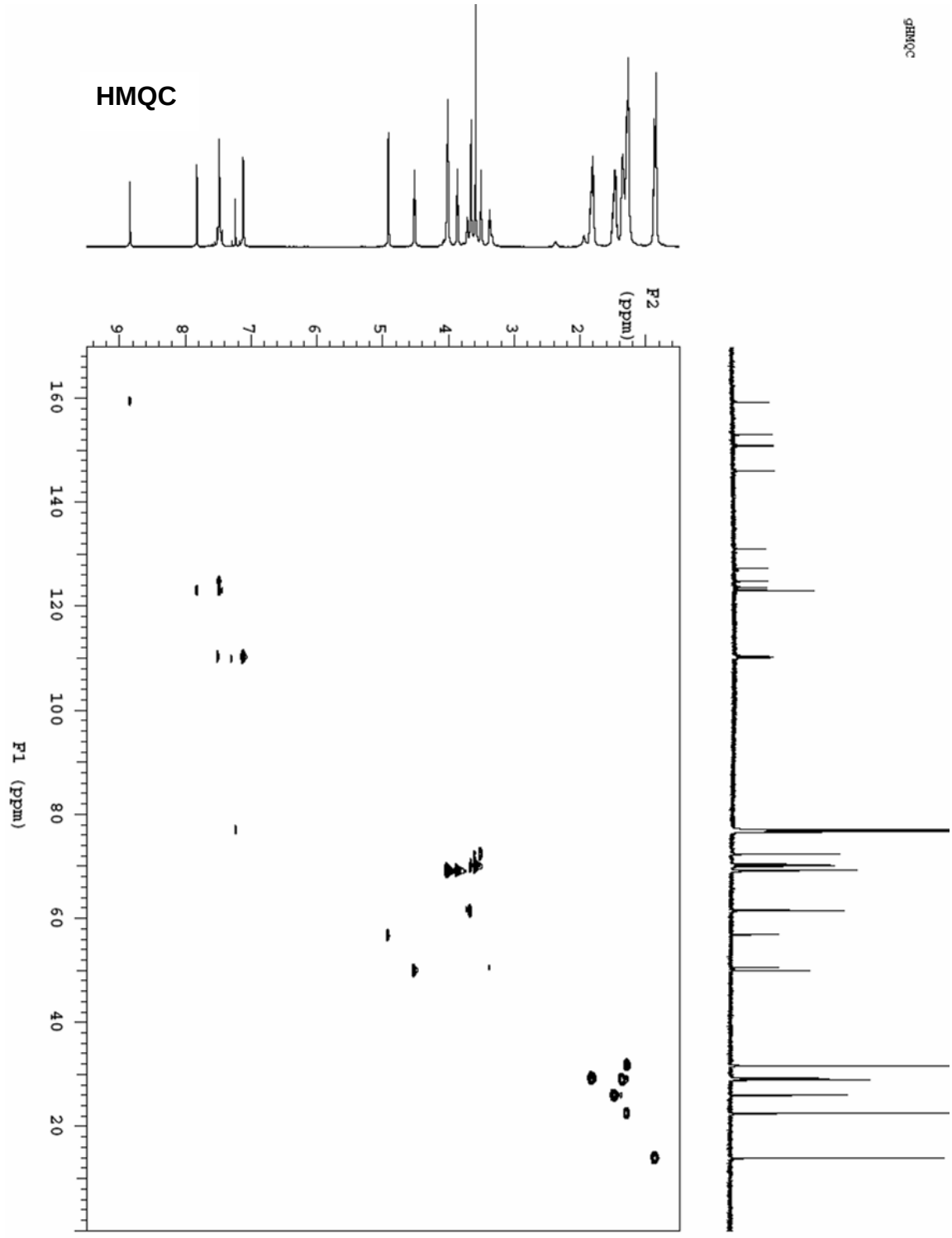

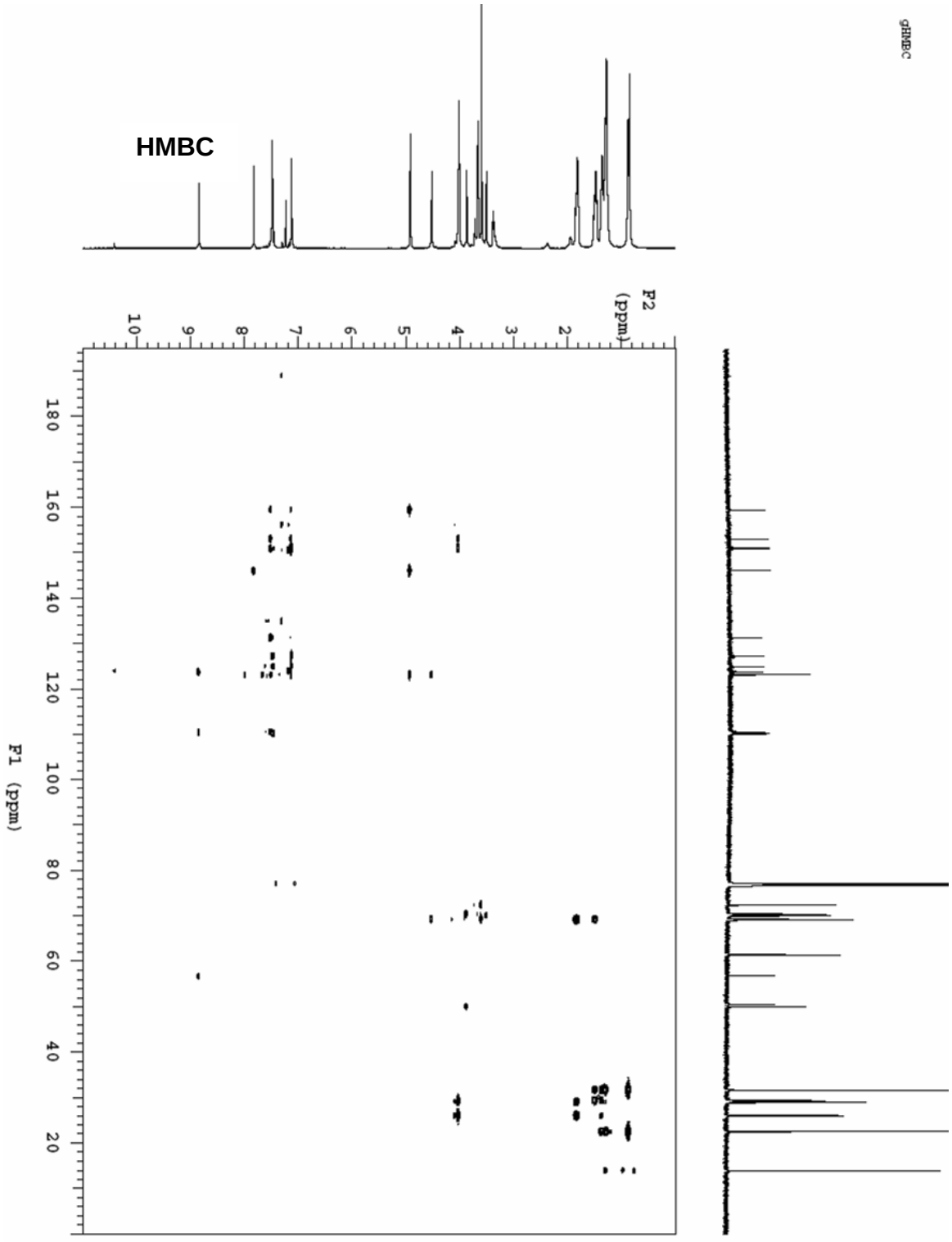
HMBC
F2 (ppm)
F1 (ppm)
gHMBC

3.3.13.5. Table with observed H-C couplings relevant to assigning the *anti-* geometry of the triazole ring

Correlation table of HMBC spectra of 24

HMBC	OPV 24			
	$C12_{57}$	$C13_{146.38}$	$C14_{123.55}$	$C15_{50}$
H12	x	√	√	x
H14	x	√	x	x
H15	x	x	√	x

√ : coupling expected and observed

x : no significant coupling observed

4. Functionalization of Si(100) and Si(111) surfaces with oligo(*p*-phenylene vinylene)s

4.1. Overview

A library of rigid-rod type conjugated oligo(*p*-phenylene vinylene)s (OPVs) (i.e., monomer, dimer, and trimer homologues, Scheme 4.1) featuring different side-chain substitutions have been attached to atomically flat surfaces of Si(100) and Si(111) via covalent Si-O-C bonds. The process involves the reaction of the respective –OH functional oligomers with Si-H and/or Si-Cl functional surfaces. Of the two –OH functionalities in one oligomer, only one reacts with the Si-surface while the other remains unchanged. To prove these residual –OH functionalities, a chemical derivatization has been used: The Si-OPV-CH_2OH surface (Surface 1, Scheme 4.2) subsequently readily reacts with *p*-tolyl isocyanate and forms urethane (U) links yielding Si-OPV-U-Ph monolayers (Surface 2, Scheme 4.2). The resulting monolayers are characterized by means of X-ray photoelectron spectroscopy (XPS), attenuated total reflection fourier transform infrared (ATR-FTIR), atomic force microscopy (AFM), and confocal fluorescence laser scanning microscopy (CFLSM).

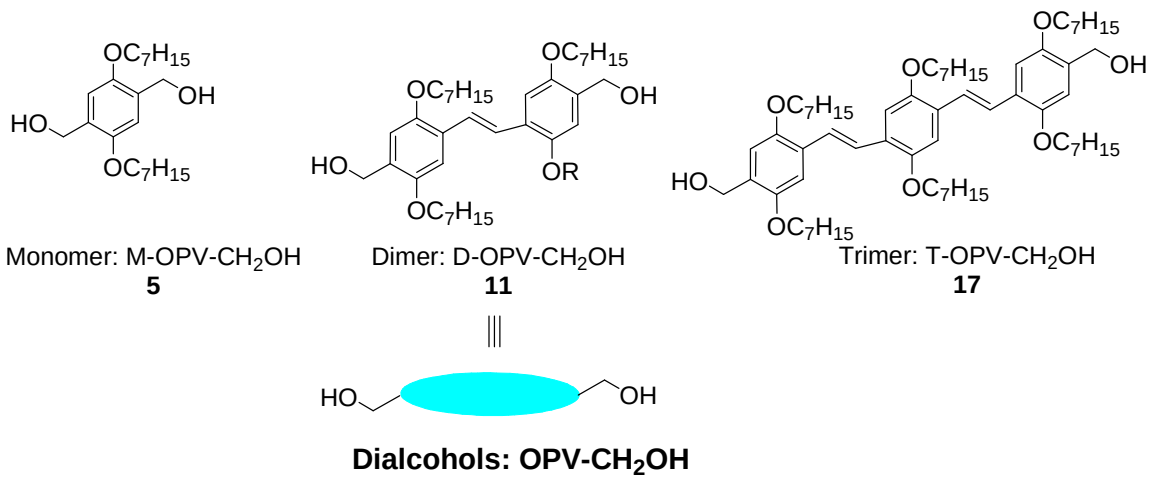

Scheme 4.1. Dihydroxy functional OPVs with varying side-chain lengths.

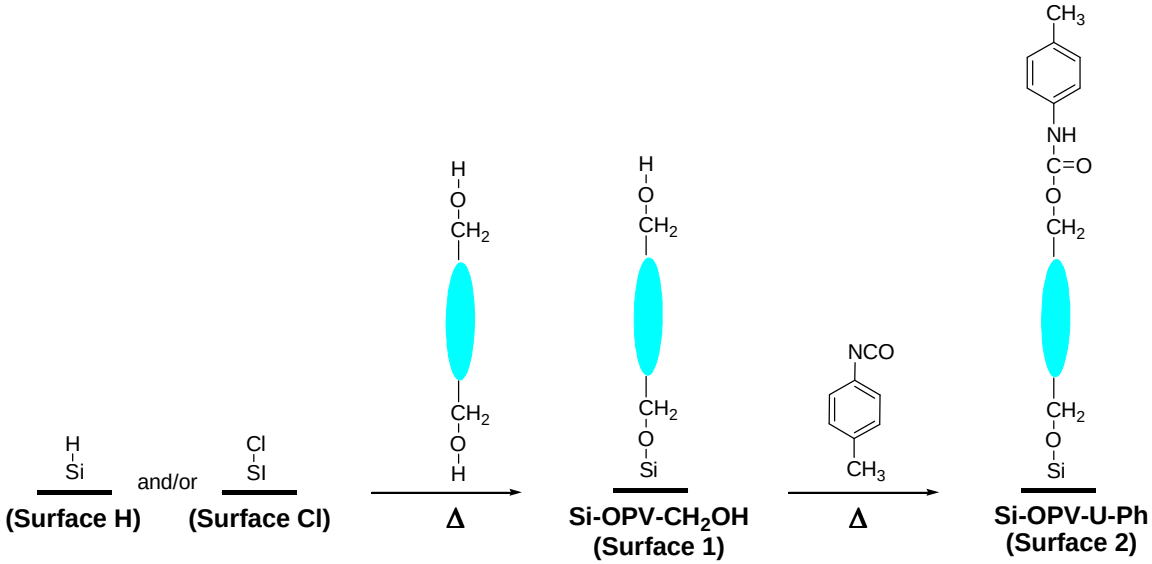

Scheme 4.2. Reactions of OPVs with Si-H and/or Si-Cl surfaces.

4.2. Surfaces: Results and discussion

4.2.1. Si-H and Si-Cl

The Si(100)-H and Si(111)-H surfaces were prepared according to literature.[123] X-ray photoelectron spectra (XPS), survey and narrow scans, of a representative Si-H functional surface are shown in figure 4.1. The small C (1s) peak at 285 eV

observed is reproducible, both in terms of energy and intensity, and can be attributed to minor contamination from carbon-containing sticky tabs (used to secure the sample in the XPS experiment). The small O (1s) peak at 533 eV can be attributed to traces of oxygen in the sample chamber or physisorbed on the Si-surface. The Si (2s) and Si (2p) peaks are detected at ~151 and ~99eV, respectively. The XPS narrow scan emphasizes the absence of a residual Si-peak from O-bound Si (SiO_x) at ~103eV, indicating an efficient etching process with subsequent hydride-functionalization.

Representative atomic force microscopy (AFM) images of the Si(100)-H and Si(111)-H surfaces discussed above are shown in figure 4.2, together with height traces of a respective cross-section. The scan direction is parallel to the x-axis. The surface roughness (RMS) of Si(100)-H and Si(111)-H are determined as 0.60 nm and 0.22 nm over areas of 1.0 μm^2 and 5.3 μm^2, respectively.

Si-Cl - terminated surfaces were made from freshly prepared respective Si-H surfaces in analogy to literature.[124] As indicated above, both, Si(100)-Cl and Si(111)-Cl surfaces, were used for further functionalization. However, there was no characterization of the Si-Cl surfaces before subsequent reactions. The available XPS is not connected to a dry-box or other inert gas chamber, and the Si-Cl surfaces are too reactive to handle in air.

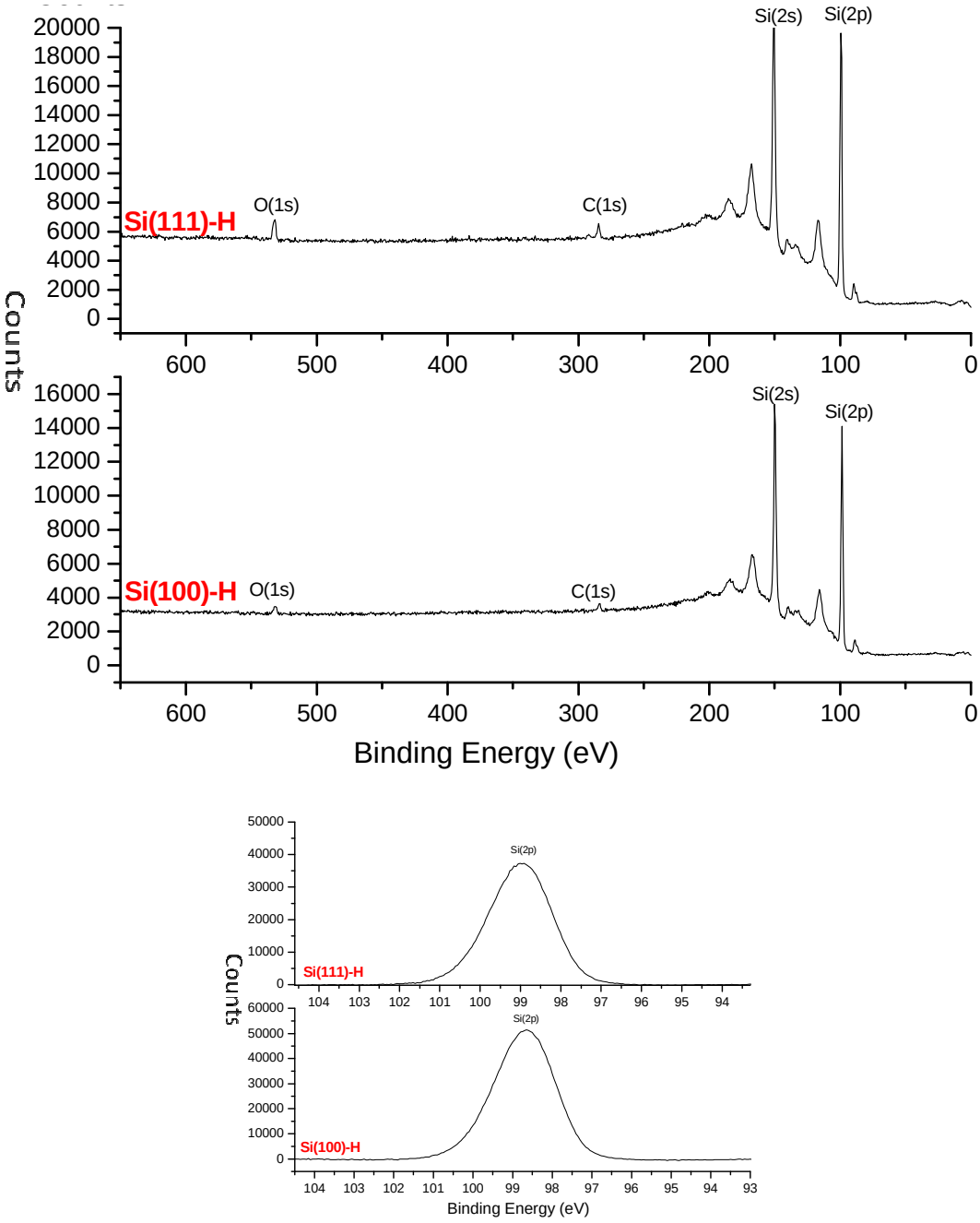

Figure 4.1. XPS spectra overlaid; survey scan (top) and narrow scan (bottom) of Si(100)-H and Si(111)-H surfaces.

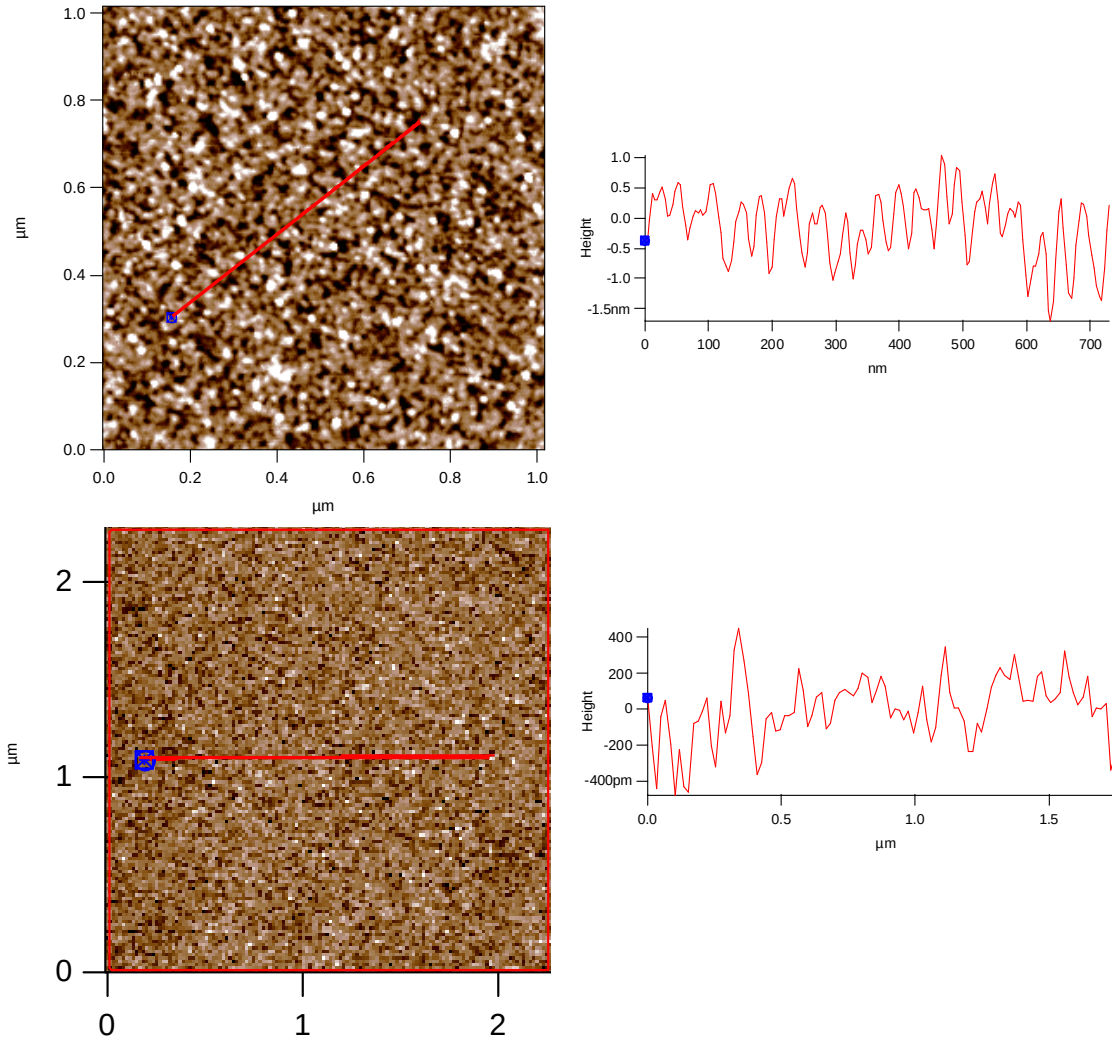

Figure 4.2. AFM images of Si(100)-H (top) and Si(111)-H (bottom) surfaces.

4.2.2. Dihydroxy-functional OPVs on Si(100)-H

The respective OPV (i.e. monomer-, dimer-, and trimer- dialcohols, Scheme 4.1) to the surface is layered on the freshly etched Si(100)-H surface under inert gas atmosphere. Under exclusion of light, the reaction flask is then heated to 80, 115, or 122^{o}C, for 4 days. The resulting Si-OPV-CH_2OH surfaces (Surfaces 1, Scheme 4.2) are subsequently sonicated in dry toluene (thereafter repeated twice with fresh toluene), and stored under argon.

The surfaces Si-OPV-CH_2OH are analyzed by means of XPS, ATR-FTIR, as well as AFM. Representative XPS spectra (Figure 4.3) detail the elemental surface analyses. The original silicon oxide surface, SiO_x, shows 2p and 2s peaks from silicon at 100-104 and 151-155 eV respectively. The etched and H-modified Si(100)-H functional surface shows 2s and 2p peaks from silicon at 151 and 99 eV respectively (Figure 4.3, left), with no residual Si-peak from O-bound Si (SiO_x) between 100 and 104 eV (Figure 4.3, right). The surfaces functionalized with the conjugated oligomers are distinctly different: The Si(100)-monomer spectrum, Si(100)-M-OPV-CH_2OH or Si(100)-**5,** shows 2s and 2p peaks of silicon at 151 and 99 eV, a Si-peak O-bound Si (SiO_x) at 103 eV, and the 1s peaks for carbon and oxygen at 285 and 533 eV respectively. The Si(100)-dimer spectrum, Si(100)-D-OPV-CH_2OH or Si(100)-**11**, a relatively less significant Si-peak O-bound Si (SiO_x) at 103 eV. The Si(100)-trimer spectrum, Si(100)-T-OPV-CH_2OH or Si(100)-**17**, lacks significant peaks for 2p and 2s of silicon entirely. The relative peak intensity for Si from Si-H decreases from Si(100)-monomer to Si(100)-dimer to Si(100)-trimer, as does the relative peak intensity for O-bound Si (SiO_x). This can be attributed to a more densely packed organic layer as well as an increase in layer thickness[125] with increasing size of the attached molecules. In the case of the dimer and trimer the aggregation tendency of the extended conjugated aromatic systems might also result in more densely packed monolayers.

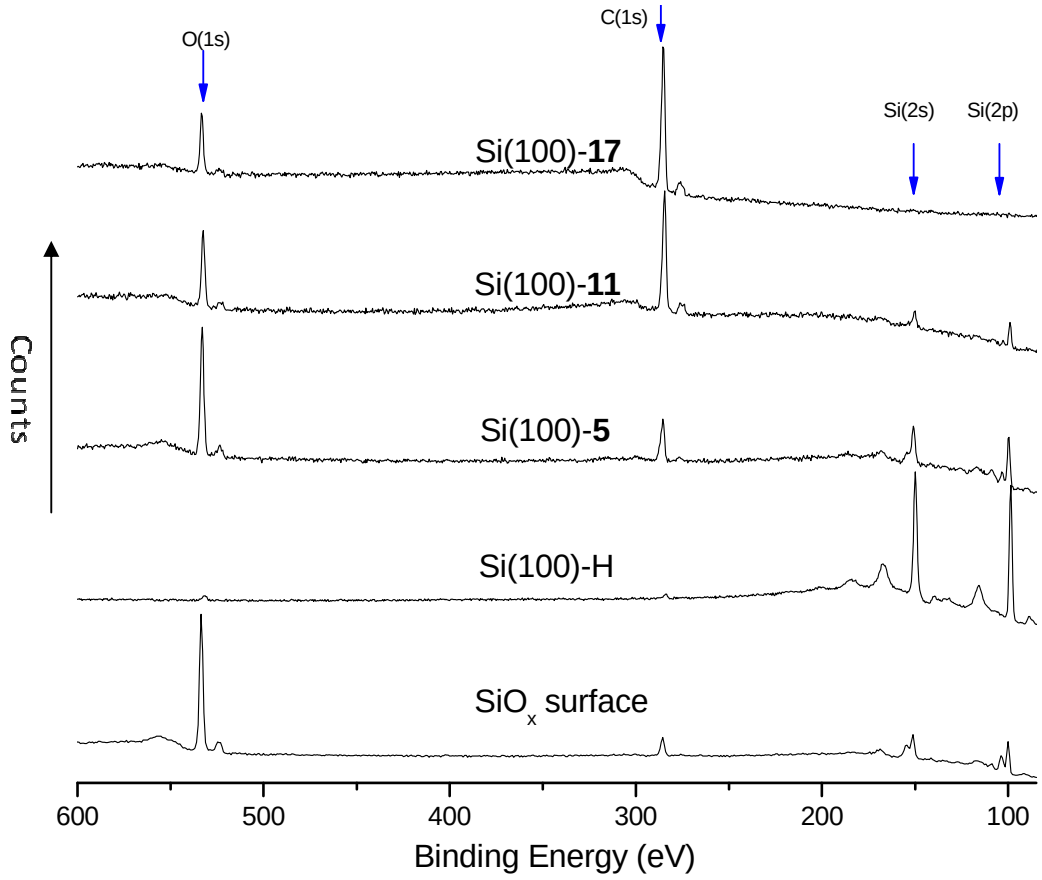

Figure 4.3. XPS spectra overlaid; survey scans of silicon wafer with SiO_x, Si(100)-H, Si(100)-**5**, Si(100)-**11** and Si(100)-**17** surfaces.

ATR-FTIR investigations of the monolayers show that the relative intensities of the asymmetric C-H_x (C-H, CH_2, and CH_3) stretching bands (at ~2954, 2928, 2857cm^{-1}), figure 4.4, increase from Si(100)-monomer to Si(100)-dimer to Si(100)-trimer, which is in agreement with the XPS results, indicating increasing surface coverage.

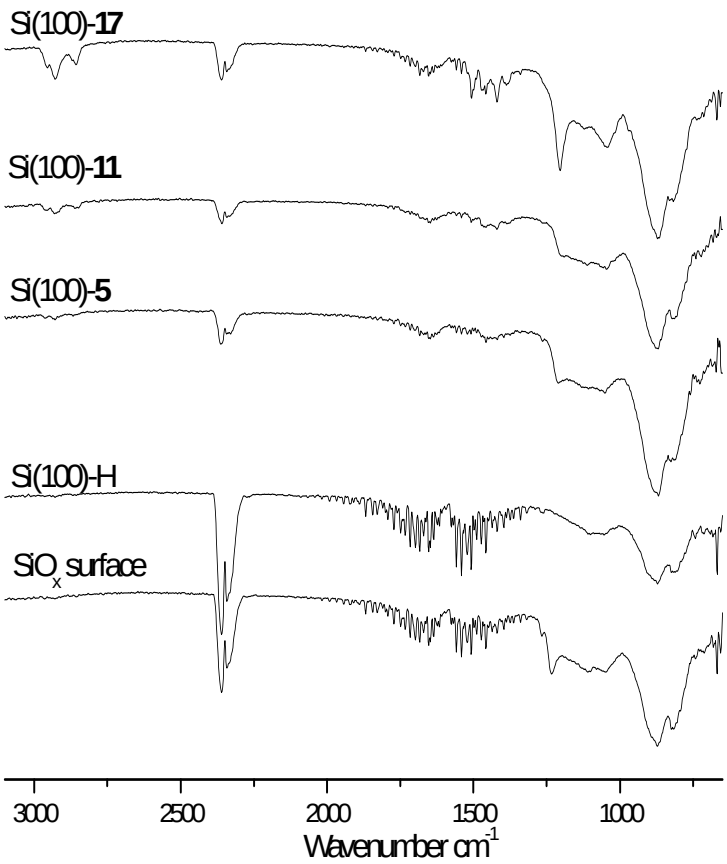

Figure 4.4. ATR-FTIR spectra overlaid; silicon wafer with SiO_x, Si(100)-H, Si(100)-**5**, Si(100)-**11**, and Si(100)-**17** surfaces.

In conclusion, the OH-functional monomer, dimer, and trimer homologues of OPV can be successfully attached to silicon Si(100)-H surfaces through Si-O-C bond formation. According to XPS and ATR-FTIR, the best results are obtained when trimer-OPV-CH_2OH is used. The following investigations thus focus on using trimer-OPVs.

4.2.3. Si(100)-OPV-CH_2OH

In the following trimer OPV homologues are discussed in detail regarding optimized reaction conditions for the surface functionalization and composition and structures of the resulting surfaces.

The freshly prepared Si(100)-H or Si(100)-Cl surfaces were reacted with solutions of T-OPV-CH_2OH (Scheme 4.1) in dried toluene or anhydrous chlorobenzene for 16-24 hours at 70-120^oC. Representative reaction conditions are summarized in table 4.1.

Table 4.1. Representative reaction conditions for Si(100)-OPV-CH_2OH surfaces.

Entry	Surface	T-OPV-CH_2OH (mg, mmol)	Solvent (mL)	Pyridine (mL)	Tem. (^oC)	Time (h)
1	**Si-H**	(50, 0.049)	Toluene (5)	n.a.	80	16
2		(10, 0.0097)	Toluene (0.3)		100	24
3					120	
4	**Si-Cl**	(100, 0.097)	Chlorobenzene (3)	n.a.	70	20
5		(20, 0.019)	Toluene (5)	0.5	80	24
6					90	

Overlaid XPS spectra of representative Si(100)-T-OPV-CH_2OH and Si(100)-H surfaces are shown in figure 4.5. The Si(100)-T-OPV-CH_2OH features 2s and 2p peaks of Si at ~151 and ~99eV respectively, and O-bound Si (SiO_x) at ~104 and

154eV. The C and O (1s) peaks from the attached molecules are observed at ~285 and 533eV respectively.

Compared to the Si(100)-H surface, the relative peak intensity of Si decreases and the relative peak intensities from O and C increase, indicating more surface coverage. A representative XPS narrow scan (Figure 4.5, bottom) of the surface generated from entry **6** in table 4.1. further supports this observation. The asymmetry of the peak at 285eV with a shoulder at ~287eV indicates the presence of C bound to O from either alcohol and/or ether (C-O-H and C-O-C), both present in the OPV molecule. The XPS-spectra of Si(100)-T-OPV-CH_2OH surfaces generated from Si-H and Si-Cl precursor surfaces show no significant differences. The AFM images, however, do show significant differences, however (see below).

A representative AFM image of the surfaces generated under conditions described in entry **2** is shown in figure 4.6. The scan direction is parallel to the x-axis. The surface roughness (RMS) of the T-OPV-functional surface is ~0.4nm over an area of 7.9μm^2. The chosen cross-section includes two of several visible "islands" in the AFM graph. The vertical heights of these islands are measured at ~ 2.50nm (difference between two blue markers in cross section). This value is in excellent agreement with the calculated molecular length of ~ 2.28nm (for details see experimental) and powder X-ray diffraction results of ~ 2.32nm.[117]

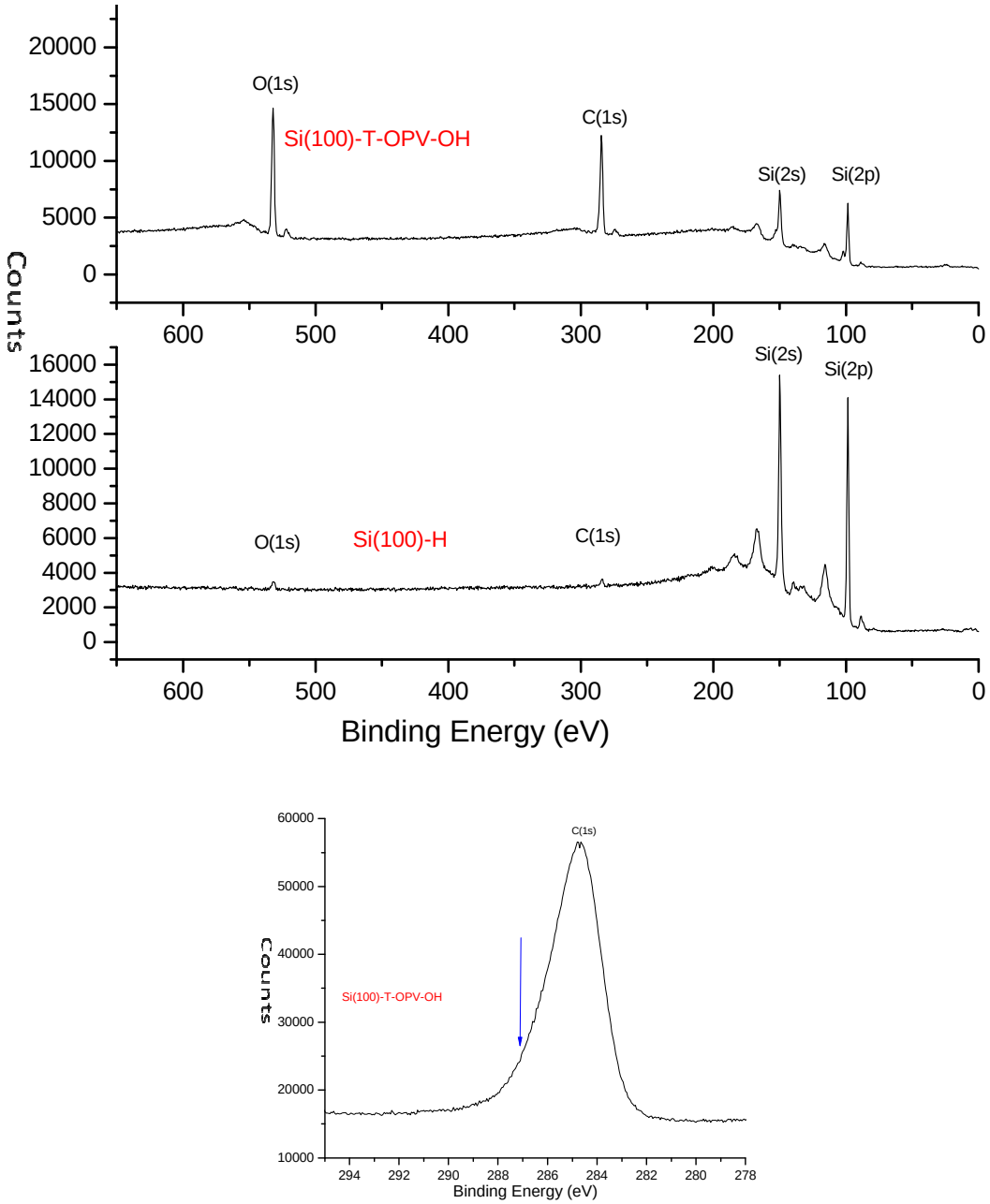

Figure 4.5. Representative XPS spectra overlaid; survey scans (top) of Si(100)-T-OPV-CH_2OH and Si(100)-H surfaces and narrow scan (bottom) spectrum of Si(100)-T-OPV-CH_2OH surface.

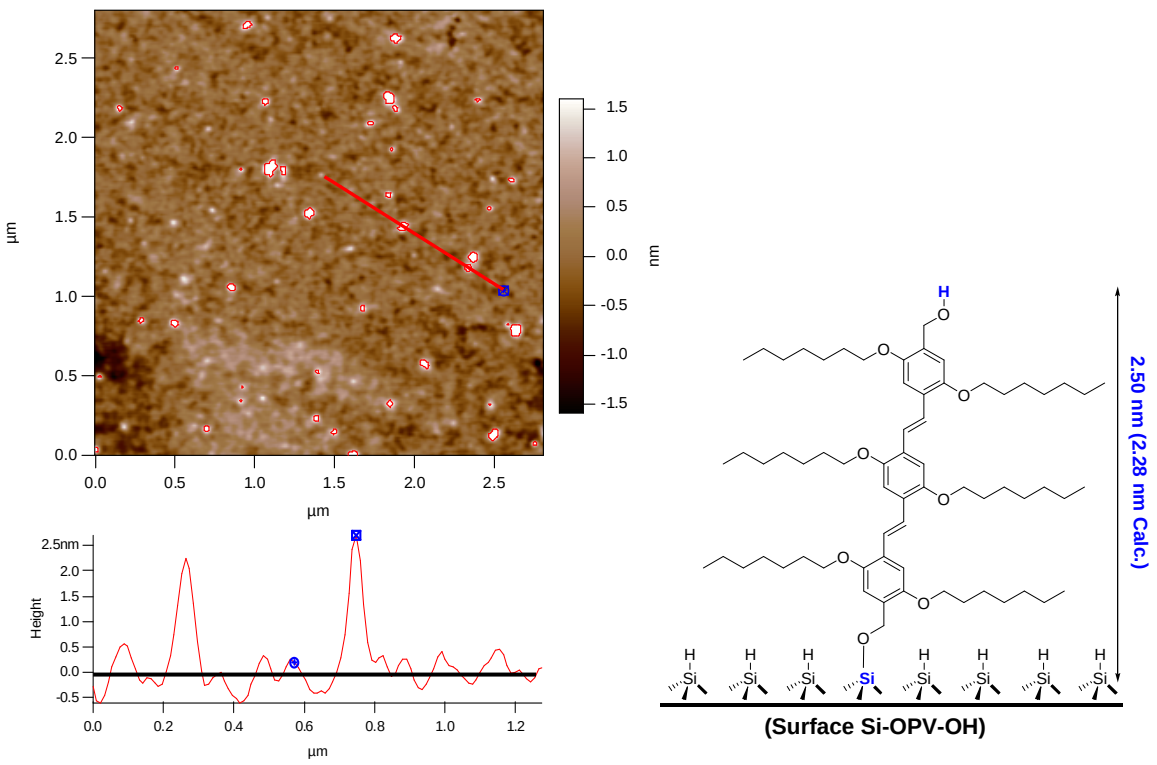

Figure 4.6. AFM image of Si(100)-OPV-CH_2OH surface (entries **2**).

4.2.4. Si(100)-T-OPV-U-Ph

As mentioned above, the residual OH-functionality at the main-chain terminus of the Si(100)-T-OPV-CH_2OH surface has been reacted with *p*-tolyl isocyanate. Three specific aims are addressed: 1. To provide proof of concept for a stepwise growth off a molecular monolayer in which the rigid-rod type oligomers stand perpendicular to the surface; 2. To introduce a selective label element N for the elemental surface analysis; and 3. To introduce a strong signature urethane vibrational mode for the FTIR analysis.

Representative reaction conditions are summarized in table 4.2. The freshly prepared Si(100)-T-OPV-CH_2OH surface is reacted with p-tolyl isocyanate at

room temperature or 45^{o}C for 24h or (4h or 8h), respectively under inert gas atmosphere.

Table 4.2. Representative reaction conditions for Si(100)-OPV-U-Ph surfaces.

Entry	Surface*	*p*-Tolyl isocyanate (mL)	Temp. (^{o}C)	Time (h)
1	Si(100)-OPV-CH_2OH	0.1	RT	24
2		1.5	45	4
3				8

* Made from Si(100)-Cl

According to XPS analyses, reactions carried out at room temperature for 24 hours lead to similar surfaces compared to reactions carried out at 45^{o}C for 8 hours. Representative overlaid XPS spectra of Si(100)-T-OPV-U-Ph and Si(100)-T-OPV-CH_2OH surfaces are shown in figure 4.7. The Si(100)-OPV-U-Ph features an additional peak from N (1s) at ~400eV (absent in Si(100)-T-OPV-CH_2OH). Compared to the Si(100)-T-OPV-CH_2OH surface, the relative peak intensities of C and O increase in Si(100)-OPV-U-Ph surface compared to Si. For comparison, a freshly prepared wafer with the Si(100)-OPV-CH_2OH surface is devided into two equal parts, one for the XPS characterization and the other to continue the reaction with *p*-tolyl isocyanate to afford the surface Si(100)-OPV-U-Ph. A representative overlay of XPS narrow scans is shown also (figure 4.7, bottom). The C 1s signal of the Si-T-OPV-U-Ph shows a pronounced shoulder and broader peak. The main peak centered at 285eV is characteristic of C in hydrocarbon environments (C-H, C-C, and C=C). The asymmetry of the peak with a shoulder at ~287eV signifies the presence of C bound to O in alcohols

and/or ethers (C-O-H and C-O-C, see also above), and the additional shoulder at ~289eV originates from a C in a urethane environment, i.e., O-C(O)-N and thus indicates the presence of the target structure.

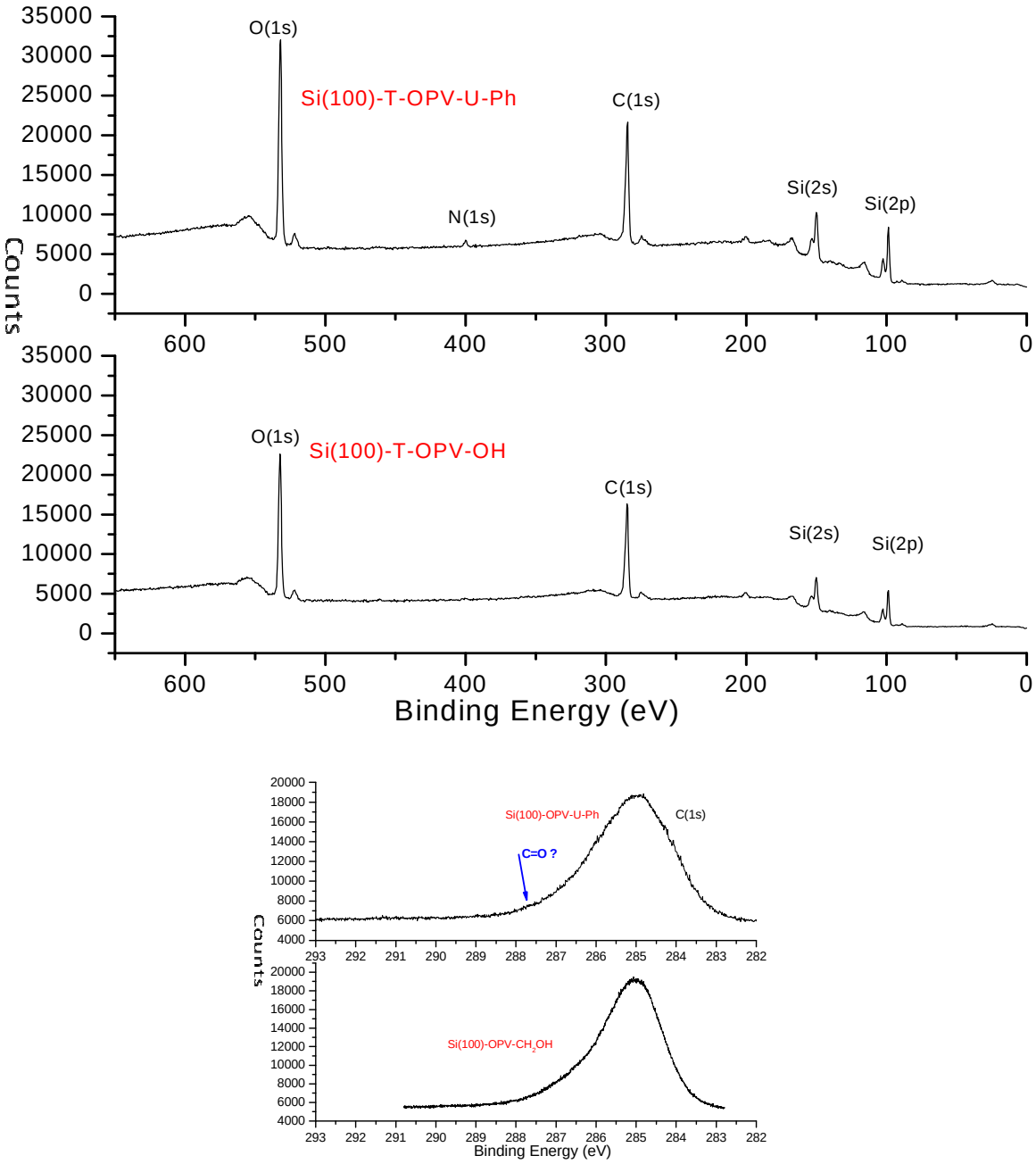

Figure 4.7. Representative XPS spectra overlaid; survey scans (top) and narrow scans (bottom) spectra of Si(100)-T-OPV-U-Ph and Si(100)-T-OPV-CH_2OH surfaces.

ATR-FTIR analyses using p-polarized incident beams (figure 4.8) reveal absorption bands from C-H stretching at 2929 cm^{-1}, C=O stretching at 1678 cm^{-1}, C-O (urethane bond) asymmetric stretching at 1261 cm^{-1}, and Si-O stretching at 1214 cm^{-1}. This strongly supports the attachment of *p*-tolyl isocyanate to Si via the Si(100)-T-OPV-CH_2OH surface.

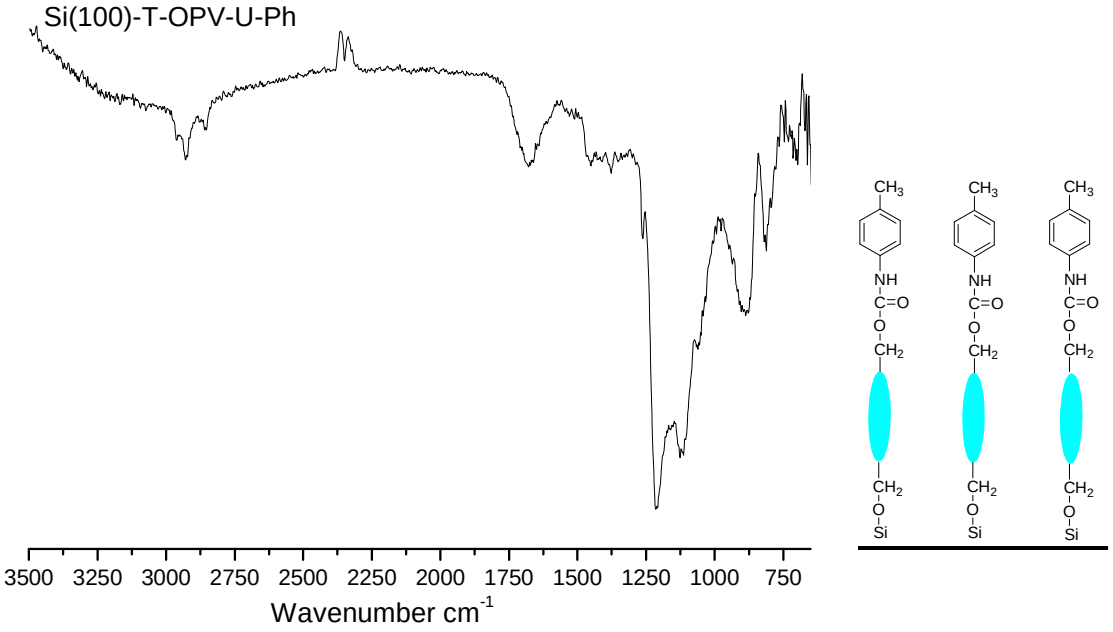

Figure 4.8. ATR-FTIR spectrum of Si(100)-OPV-U-Ph surface.

4.2.5. Si(111)-T-OPV-CH_2OH

Contrary to the Si(100)-H case, no significant reaction between T-OPV-CH_2OH (**17)** and Si(111)-H surfaces can be observed even at elevated temperatures (tested up to 120 Celsius). As mentioned above in more detail, compared to the Si(100)-H surface, Si(111)-H has only one reactive bond and less free space around Si for any reaction. Therefore, the more reactive and freshly prepared

Si(111)-Cl surfaces are used in the reaction with solutions of **17**. Representative reaction conditions are summarized in table 4.3.

Table 4.3. Representative reaction conditions for Si(111)-OPV-CH_2OH surfaces.

Entry	Surface	T-OPV-CH_2OH (mg, mmol)	Toluene (mL)	Pyridine (mL)	Temp. (^oC)	Time (h)
1	Si(111)-Cl	(12.5, 0.012)	5	0.5	90	24
2		(20.0, 0.019)			80	
3		(16.7, 0.016)			50	
4		(125, 0.12)			80	66

Overlaid XPS spectra of representative Si(111)-T-OPV-CH_2OH and Si(111)-H surfaces are shown in figure 4.9. Si(111)-T-OPV-CH_2OH surfaces feature 2s and 2p peaks of Si at ~151 and ~99eV respectively as well as O-bound Si (SiO_x) at ~104 and 154eV. The C and O (1s) peaks from the attached molecules are observed at ~285 and 533eV respectively. Compared to the Si(111)-H surface, the relative peak intensity of Si decreases and the relative peak intensities of O and C increase, indicating surface coverage. Comparing results from reactions **1** through **4**, the peak intensities of C increase from entry **4** to **2** to **1**, while the relative peak intensity of Si decreases. The peak intensity of O decreases from entry **4** to **2** to **1**, Comparing results from Si-Cl and Si-H surfaces, unreacted Si-Cl seem to be present after the reaction with T-OPV-CH_2OH and thus able to to convert to SiO_x upon exposure to the atmosphere. The higher the coverage with

T-OPV-CH_2OH, the less Si-Cl seem to remain, therefor showing less relative peak intensities from Si and O. The reaction of entry **4** shows the most coverage of T-OPV-dialcohol on the surface. A representative XPS narrow scan of **4** is also shown in figure 4.9. The C 1s signal at 285eV of the Si-T-OPV-CH_2OH shows a shoulder at ~287eV, from C bound to O in either alcohol and/or ether (C-O-H and C-O-C), both present in the OPV molecule.

Typical AFM images of representative surfaces Si(111)-T-OPV-CH_2OH (Entries **2** and **3**) are shown in figure 4.10. Comparing surfaces from entries **2** and **3**, the relative OPV-coverage is less in **3** indicating that higher temperatures lead to more surface coverage. The surface roughness (RMS) of surfaces prepared under conditions detailed in entries **3** and **2** are 0.40nm and 0.75nm over areas of 25 μm^2 and 2.4 μm^2 respectively. The value in the case of **3** is higher. A possible explanation for the higher value in the case of **3** could be that less surface coverage with organic molecules results in more unspecific hydrolysis of unreacted Si-Cl with subsequent oxidation, leading to an overall rougher surface. Height traces (cross-sections -solid red lines in the respective AFM images) on surfaces from entries **3** and **2** both consistently measure heights of ~2.6nm for the functionalized domains. These values are in excellent agreement with the values observed for Si(100)-TOPV-CH_2OH (2.50nm, see above) and, as discussed above, are confirmed by calculations and literature values from powder diffractograms.[117]

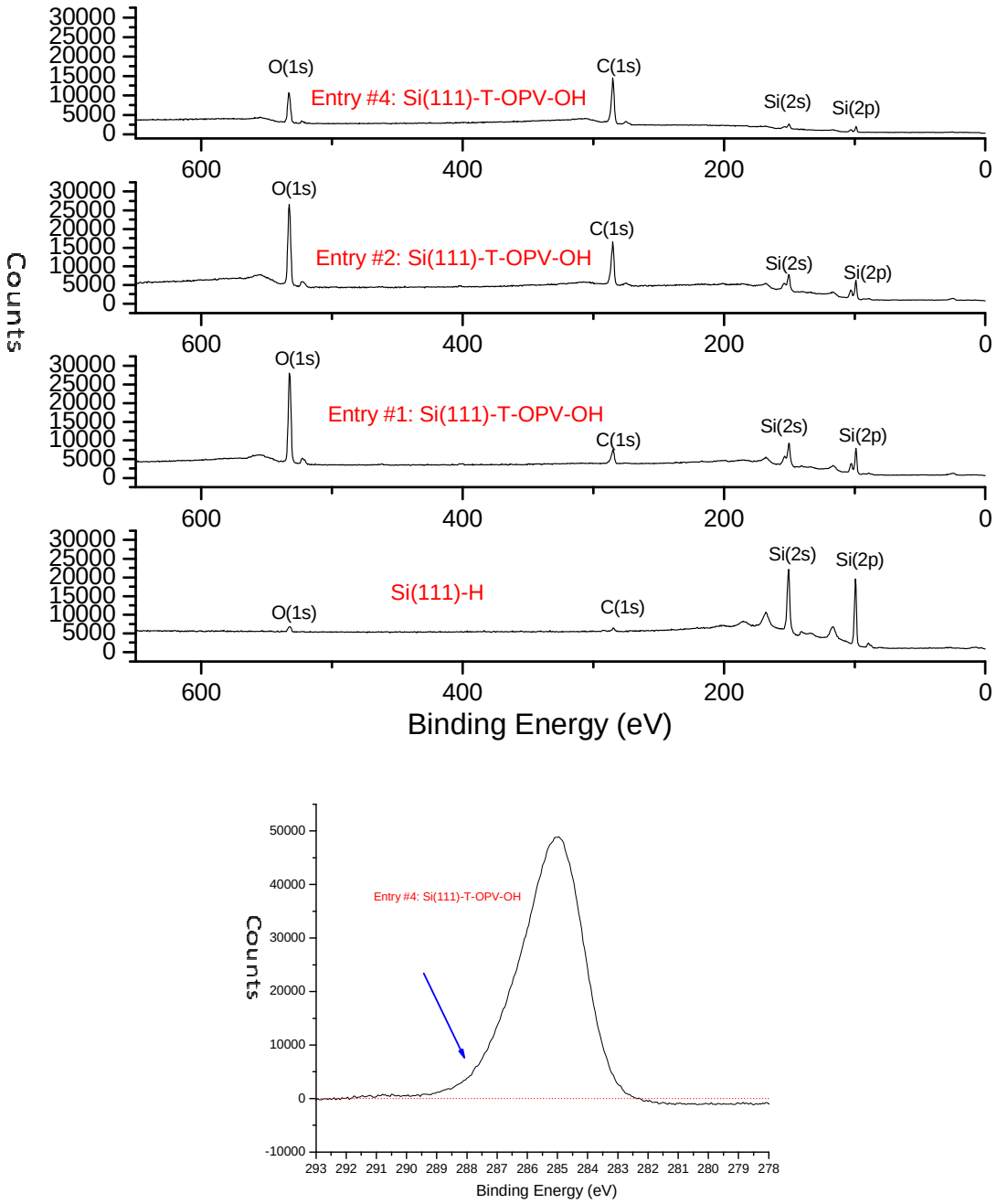

Figure 4.9. Representative XPS spectra overlaid; survey scans (top) of Si(111)-T-OPV-CH_2OH and Si(111)-H surfaces and narrow scan (bottom) of Si(111)-T-OPV-CH_2OH surface.

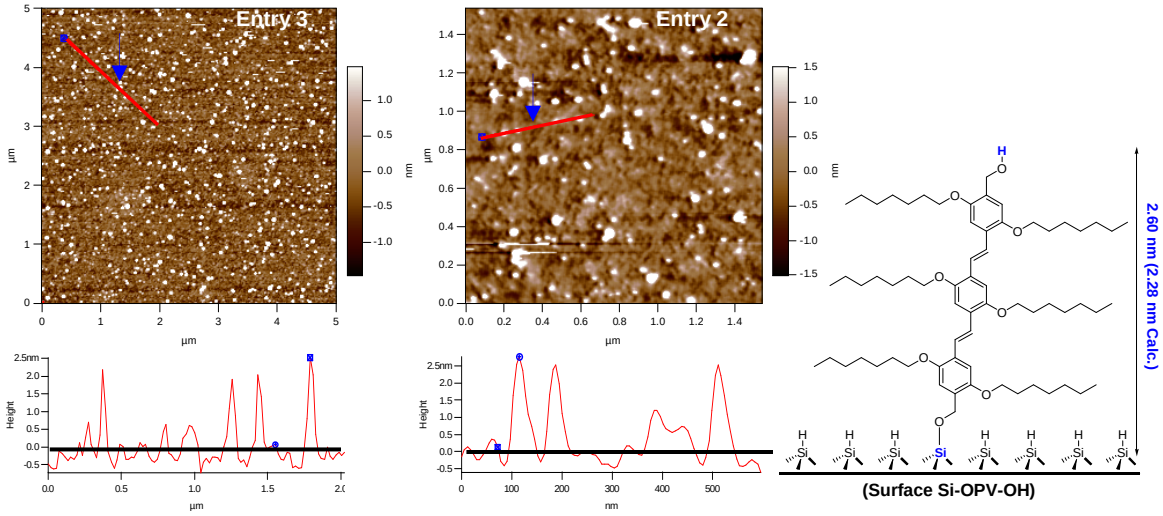

Figure 4.10. AFM images of Si(111)-T-OPV-CH_2OH surfaces (entry **2** and **3**).

4.2.6. Si(111)-T-OPV-U-Ph

A freshly prepared Si(111)-T-OPV-CH_2OH surface (prepared according to entry **4** in table 4.4) was reacted with p-tolyl isocyanate under inert gas atmosphere at 45^{o}C for 8h. Representative overlaid XPS spectra of the resulting surface Si(111)-T-OPV-U-Ph and the precursor surface Si(111)-T-OPV-CH_2OH are shown in figure 4.11. Si(111)-T-OPV-U-Ph features an additional peak from N (1s) at ~400eV (absent in Si(111)-T-OPV-CH_2OH; see also narrow scan, Figure 4.12, bottom left). Compared to the Si(111)-T-OPV-CH_2OH surface, the relative peak intensities of C and O increase in Si(111)-T-OPV-U-Ph surface compare to Si (see also Si(100)-OPV-U-Ph). A representative XPS narrow scan shown in figure 4.12 features a C 1s signal of the Si-T-OPV-U-Ph with a shoulder. As discussed above, the shoulder at ~287eV is attributed to C in alcohol and/or ether (C-O-H and C-O-C), and the shoulder at ~289eV to C in a urethane linkage O-C(O)-N, indicating the presence of the targeted structures.

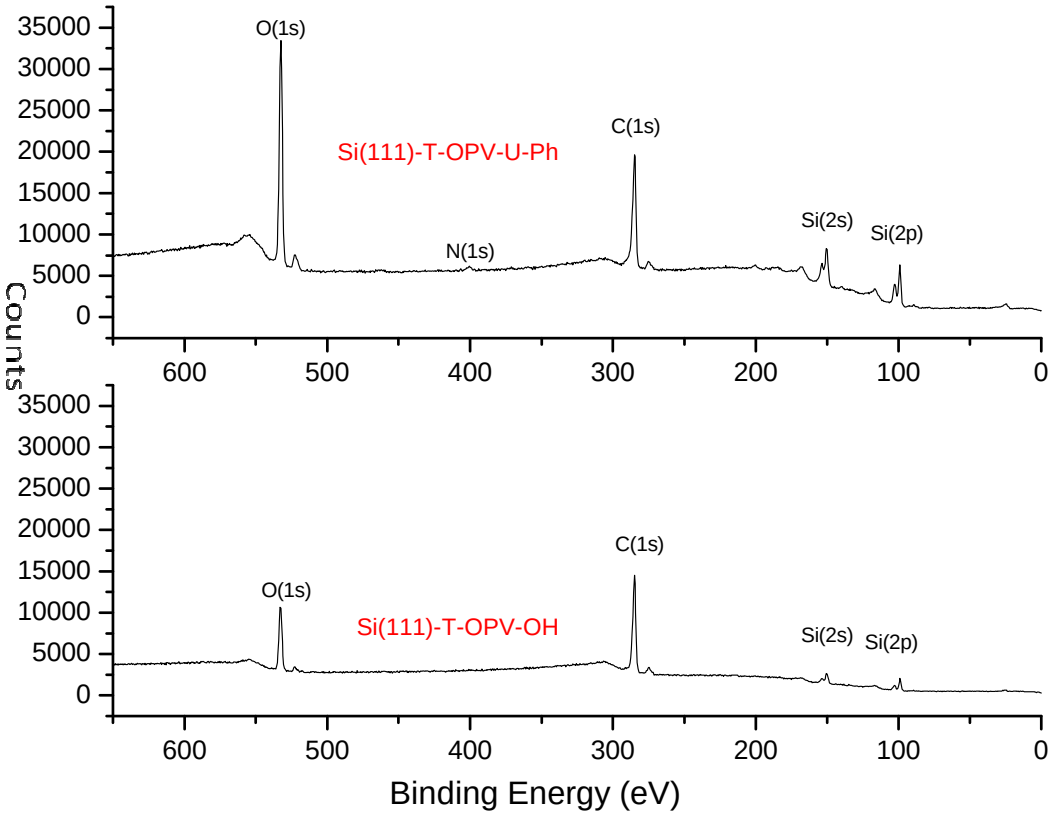

Figure 4.11. Representative XPS spectra overlaid; survey scans of Si(111)-OPV-CH_2OH and Si(111)-OPV-U-Ph surfaces.

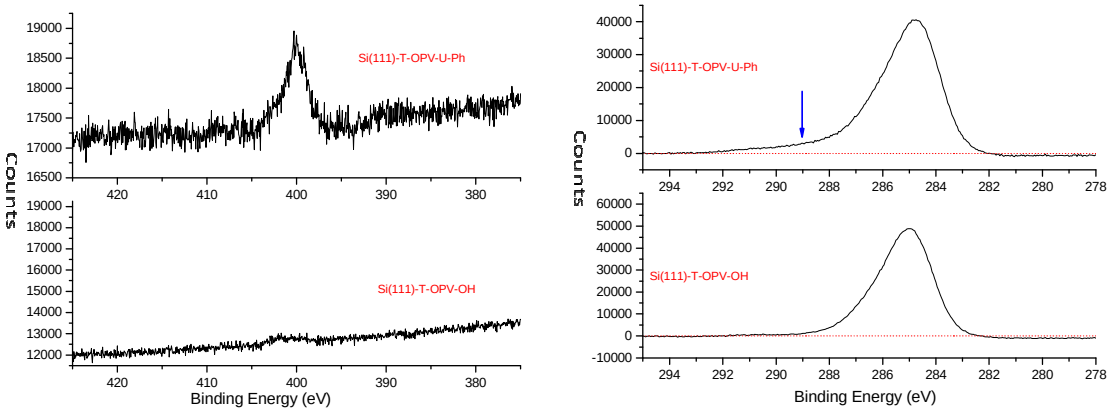

Figure 4.12. Representative XPS spectra overlaid; narrow scans of Si(111)-OPV-CH_2OH and Si(111)-OPV-U-Ph surfaces.

A typical AFM image of such a Si(111)-T-OPV-U-Ph is depicted in figure 4.13.

The surface roughness RMS after urethane formation is measured as 0.75nm

over a 34.5 μm^2 area. The depicted height trace (cross-section based on red line in the AFM image) of Si(111)-T-OPV-U-Ph measures the elevations of the attached monolayers as ~2.96nm . As shown in the scheme next to the AFM image, this value corresponds well with the expected step increase relative to the precursor surface Si(111)-T-OPV-CH_2OH and again is in excellent agreement with the calculated value of 2.90nm (see experimental).

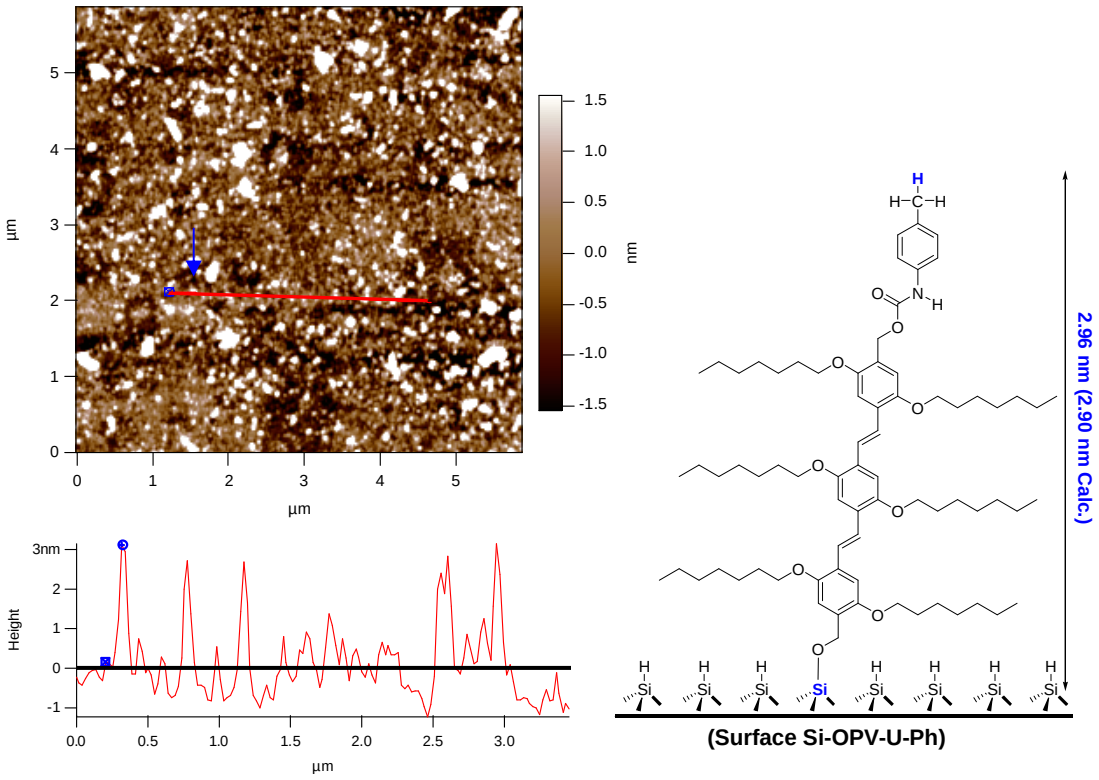

Figure 4.13. AFM image of Si(111)-OPV-U-Ph surface.

4.2.7. Optical properties

All surfaces were investigated in regard to their optical emission characteristics. To this end, excitation and emission spectra of the functionalized Si-surfaces were recorded with a confocal laser scanning microscope and compared to the

respective spectra of spin-coated oligomers or model-derivatives, and solutions thereof. Figure 4.14 (left) shows the normalized emission spectra of a T-OPV-CH_2OH **17** (with –OH end groups and –OHep side chains) in solution ($CHCl_3$), in a spin-cast film (T-OPV-CH_2OH spin coated on Si surface), and in a Si(111)-T-OPV-CH_2OH monolayer. The emission maxima are observed at λ_{max} = 462 nm (excited at 405 nm) in solution for the T-OPV-CH_2OH (concentration $3.7x10^{-8}$ M), λ_{max} = 486 nm (excited at 405 nm) for the monolayer in the surface Si-T-OPV-CH_2OH, and λ_{max} = 542 nm (excited at 405 nm) for a spin cast film (T-OPV-CH_2OH in $CHCl_3$, coated on Si-wafer). The gradual red shift is a consequence of aggregation. Figure 4.14 (right) shows the normalized emission spectra of a T-OPV-CH_2OH solution ($CHCl_3$) at different concentrations, illustrating the concentration effect on the aggregate emission (expecially at concentration of 3.7 x 10^{-6}M).

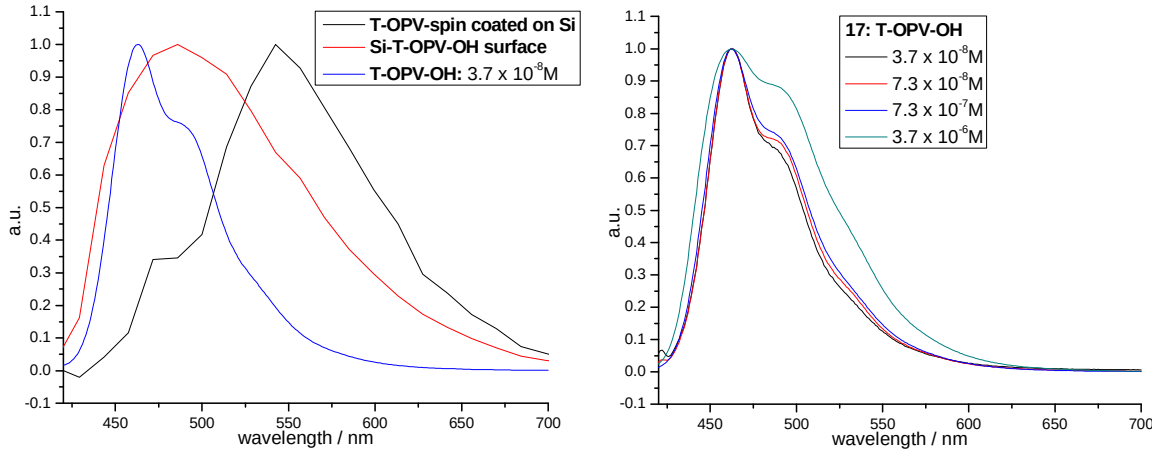

Figure 4.14. Normalized emission spectra of T-OPV-CH_2OH in solution ($CHCl_3$), T-OPV-CH_2OH spin-cast on SiO_x wafer, and Si(111)-T-OPV-CH_2OH surfaces.

Figure 4.15 illustrates the normalized emission spectra of a T-OPV-U-Ph (T-OPV-CH_2OH oligomers reacted with *p*-tolyl isocyanate) in solution ($CHCl_3$), a Si(111)-T-OPV-CH_2OH surface, a Si(111)-T-OPV-U-Ph surface, and a spin-cast film of T-OPV-U-Ph as control.

The emission maxima are observed at λ_{max} = 462 nm (excited at 405 nm) in solution for the T-OPV-U-Ph (concentration $4.5x10^{-8}$ M), λ_{max} = 486 nm (excited at 405 nm) for the monolayer in the surface Si-T-OPV-CH_2OH, λ_{max} = 528 nm (excited at 405 nm) for the monolayer in the surface Si-T-OPV-U-Ph, and λ_{max} = 552 nm (excited at 405 nm) the spin-cast film.

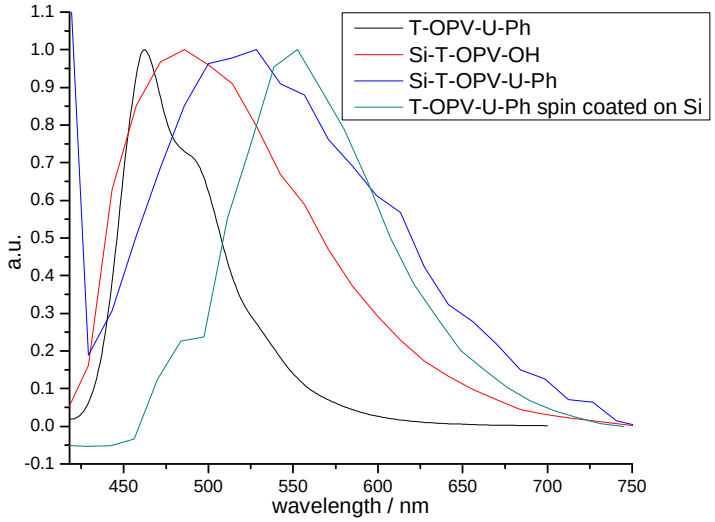

Figure 4.15. Normalized emission spectra of a T-OPV-CH_2OH in solution ($CHCl_3$), Si(111)-T-OPV-CH_2OH, a Si(111)-T-OPV-U-Ph, and a spin-cast on Si surfaces.

The red shift relative to Si-T-OPV-CH_2OH (λ_{max} = 486 nm, excited at 405 nm) to Si-T-OPV-U-Ph (λ_{max} = 528 nm, excited at 405 nm) is probably due to the added aromatic segment.

4.3. Experimental

4.3.1. General information

All experiments using air/moisture sensitive materials were carried out with high purity argon using standard Schlenk techniques. All glassware was cleared and dried for at least 24h in an oven at 120^{o}C prior to use.

4.3.2. Chemicals

Toluene (HPLC grade) and CH_2Cl_2 (HPLC grade) were purchased from Fisher Scientific. Anhydrous pyridine (99.8%, water <0.003%), anhydrous toluene (99.8%, water <0.003%), p-tolyl isocyanate (97%), and anhydrous chlorobenxene (99.8%, water <0.005%) were purchased from Sigma-Aldrich. Millipore (18.2MΩ-cm and 6 TOC) water was used for rinsing the samples (from Millipore system). All other solvents (THF, toluene, CH_2Cl_2, and hexanes) were dried and degassed, using a "Pure Solv" solvent purification system (using activated alumina, copper catalyst, molecular sieves columns) by Innovative Technology Inc. before use. Silicon wafer n-type Si(100) was donated by Dr. Bhanu Chauhan. Single-sided polished Si(111; n-type As-doped, 500 ± 25 μm thickness, 0.001-0.005 Ω.cm resistivity, 4^{o}±0.5^{o} off-cut), and double-side polished Si(111; float zone grade, n-type P-doped, 300 ± 25 μm thickness, 24-35 Ω.cm resistivity) were purchased from University WAFER.

4.3.3. Instrumentation

FTIR/ATR spectra were recorded on Bruker Tensor 27 spectrometer using Pike ATR or Harrick Seagull variable angle ATR accessory for characterizing samples

in bulk oligo-(*p*-phenylene vinylene)s and silicon surfaces before and after functionalization, respectively. All data were processed and analyzed by OPUS software.

An Atomic Force Microscope (AFM) from Asylum Research was used with an MFP-3D^{TM} SA extended head, 90μm XY scanner, TS 150 active vibration isolation table, and isolated in a Herzan AEK 2002 acoustic hood. Samples were scanned in contact mode with an Olympus cantilever. The images were processed and analyzed by IGOR Pro 6.03A/MFP3D080129. All images were routinely flattened.

X-ray photoelectron spectra (XPS) were recorded with an Omicron Surface Science Model 150 XPS spectrometer equipped with an Al or Mg Kα source (Omicron DAR 400) without monochromator, and with a concentric hemispherical analyzer (Omicron EA 125), and multichannel detector. No electron flood gun was employed. The pressure in the analytical chamber during analysis was approximately 5 x10^{-9} Torr.

Maximum emission was determined using a Leica SP2 AOBS spectral imaging confocal microscope.

4.3.4. Calculated molecular heights

In order to correlate the heights of molecular attachments on the Si-surfaces as determined by AFM with actual dimensions of the molecules used for attachment, the molecular structures were optimized in Chem3D Ultra 9.0 and used for distance calculations. Specifically, a model molecule for the surface

attachment was used: H_3Si-O-CH_2-Trimer-OPV-CH_2-OH, scheme 4.3**,** with calculated distances from Si to O and Si to H being 2.2nm and 2.28nm respectively. The calculated value for p-Tolyl isocyanate measured from H to C is 0.70nm. Therefore, the total length of Si-T-OPV-U-Ph is **2.9nm** (2.2nm + 0.70nm). The value 2.28nm is in excellent agreement with the studies by Ajayaghosh et al., measuring the length of $HOCH_2$-Trimer-OPV-CH_2OH **17** as 2.32nm, based on x-ray analyses of aggregates.[117]

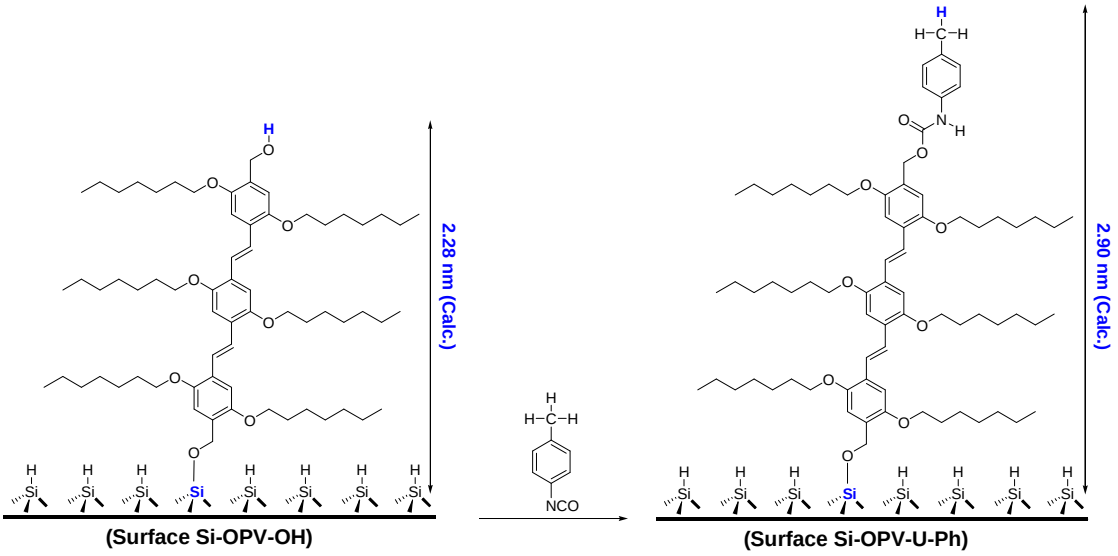

Scheme 4.3. Synthesis of model surface Si-OPV-U-Ph.

4.3.5. Si-H and Si-Cl surfaces: Hydrogen and chlorine-terminated surfaces

A wafer polished on one side and with native surface silicon oxide, SiO_x, was cut into pieces with dimensions of ca. 1.5x2 or 1x1 cm^2. The wafers were cleaned repeatedly with CH_3OH and H_2O and dried under nitrogen. Organic contaminants were removed through treatment in a boiling mixture of sulfuric acid and hydrogen peroxide (H_2SO_4:H_2O_2 = 2:1, v/v) for 1 hour. The wafer was rinsed

repeatedly with water and dried under argon. The silicon wafer was then etched in a 40% NH_4F solution (oxygen-free) for 30min and rinsed with oxygen-free water for 5 seconds. The resulting wafer was dried under nitrogen.

The reactive Si-Cl surface was made from freshly prepared Si-H surface using a three-neck round bottom reaction flask. The first neck was connected to a Cl_2 gas cylinder, the second neck was connected to the argon line, and the third neck was connected to an empty trap and the exhaust gas passed through the bottle of a KOH-solution KOH. The reaction flask was heated at 80^{o}C with a slow and steady Cl_2 gas flow for 20min. The reaction flask was cooled down to room temperature and purged with argon for at least 30 minutes. There was no characterization of the reactive Si-Cl surface before subsequent reactions.

4.3.6. Si(100)-M-OPV-CH_2OH surfaces from OPV-Monomer-Dialcohol, 5

The freshly prepared Si(100)-H surfaces were placed in a Schlenk reaction flask under argon. A solution of OPV-monomer-dialcohol **5** (~1x10^{-3} mmol) in dried toluene (3mL) was layered onto the Si-H wafer surface. Under exclusion of light, the reaction flask was heated and kept at 80^{o}C for 4 days. The modified Si(100) surfaces were sonicated in dry toluene for ~ 5 min (repeated twice with fresh toluene), and stored under argon.

4.3.7. Si(100)-D-OPV-CH_2OH surfaces from OPV-Dimer-Dialcohol, 11

The freshly prepared Si(100)-H surfaces were placed in a Schlenk reaction flask under argon. A solution of OPV-Dimer-Dialcohol **11** (~1x10^{-3} mmol) in dried

toluene (0.5mL) was layered onto the Si-H wafer surface. Under exclusion of light, the reaction flask was heated at 115^{o}C for 4 days. The modified Si(100) surfaces were sonicated in dry toluene for ~ 5 min (repeated twice with fresh toluene), and stored under argon.

4.3.8. Si(100)-T-OPV-CH_2OH surfaces from OPV-Trimer-Dialcohol, 17

The freshly prepared Si(100)-H surfaces were placed in a Schlenk reaction flask under argon. A solution of OPV-Trimer-Dialcohol **17** (~1x10^{-3} mmol) in dried toluene (0.5mL) was layered onto the Si-H wafer surface. Under exclusion of light, the reaction flask was heated at 120^{o}C for 4 days. The modified Si(100) surfaces were subsequently sonicated in dry toluene for ~ 5 min (repeated twice with fresh toluene), and stored under argon.

4.3.9. Si(100)-T-OPV-CH_2OH surfaces

The freshly prepared Si(100)-H or Si(100)-Cl surfaces were placed in a Schlenk reaction flask under argon. A solution of T-OPV-CH_2OH (50mg) in dried toluene (5mL) was degassed in three freeze-pump-thaw cycles and transferred to a Schlenk reaction flask via cannula. The mixture was heated at 80^{o}C for 16hours in the dark. After the reaction, the wafer was cleaned via sequentially sonicating in HPLC grade toluene and CH_2Cl_2 for a minimum of two cycles and then drying under vacuum.

4.3.10. Si(100)-T-OPV-U-Ph surfaces

The freshly prepared Si(100)-T-OPV-CH_2OH surface were placed in *p*-Tolyl isocyanate (1.5mL) in a Schlenk reaction flask under argon. The flask was heated at 45^oC for 8hours in the dark. After the reaction, the wafer was cleaned via sequentially sonicating in HPLC grade toluene and then CH_2Cl_2 for a minimum of two cycles and then dried under vacuum.

4.3.11. Si(111)-T-OPV-CH_2OH surfaces

A freshly prepared Si(111)-Cl surface was placed in a Schlenk reaction flask under argon. A solution of T-OPV-CH_2OH (12.5mg), dried toluene (5mL), and anhydrous pyridine (0.5mL) was degassed with argon for 60 min and transferred to the Schlenk reaction flask via a cannula. The flask was heated at 90^oC for 24hours in the dark. After the reaction, the wafer was cleaned via sequentially sonicating in HPLC grade toluene and then CH_2Cl_2 for a minimum of two cycles and then dried under vacuum.

4.3.12. Si(111)-T-OPV-U-Ph surfaces

The freshly prepared Si(111)-T-OPV-CH_2OH surface was placed in *p*-Tolyl isocyanate (1.5mL) and heated at 45^oC for 8 hours under argon and in the dark. After the reaction, the wafer was cleaned via sequentially sonicating in HPLC grade toluene and then CH_2Cl_2 for a minimum of two cycles and then dried under vacuum.

5. Stepwise functionalization of Si-H/Si-Cl surfaces using click chemistry

5.1. Overview

In an effort to explore the potential of using “click” type chemistry for surface functionalization (Scheme 5.1), 2-azidoethanol was reacted with Si-H and Si-Cl surfaces to afford ~N_3 functional surfaces Si~N_3.

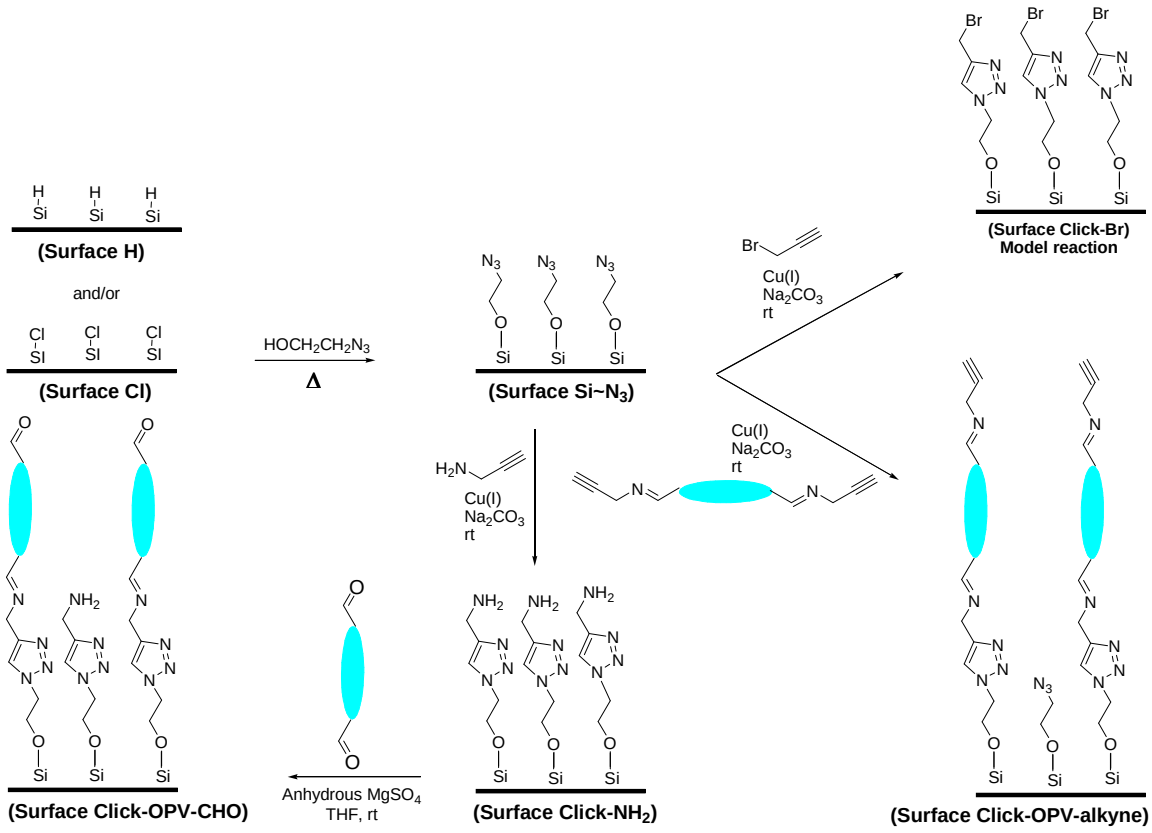

Scheme 5.1. Reactions of OPVs on Si-H and/or Si-Cl surfaces via click chemistry.

As a proof of principle reaction, propagyl bromide was used in a model reaction, as it is expected to display a signature Br-signal in the XPS analysis. The

reaction with propagyl bromide proceeds as expected and is confirmed by XPS. After optimizing reaction conditions, the analogous click-reaction of the Si-N_3 functional surfaces with T-OPV-dialkyne **19** (See chapter 2) affords Si-Click-OPV-alkyne functional surfaces (Scheme 5.1). In a prior step, trimer dialdehyde **16** (See chapter 2), was reacted with propargyl amide via Schiff base formation to produce dialkyne functional trimer OPV in quantitative yields (See chapter 3).[116] To further demonstrate the versatility of the "surface-clicking", this last reaction sequence is quasi inverted: First the Si~N_3 functional surface is reacted with propagyl amine. Then, the resulting Si-Click-NH_2 functional surface is reacted with the OPV-CHO, producing Si-Click-OPV-CHO functional surfaces via Schiff base formation. In summary, this report uses the Huisgen-"click"-cycloaddition for the efficient functionalization of Si~N_3 surfaces with modified OPV oligomers in multiple reaction sequences. The resulting monolayers were characterized by means of XPS, ATR-FTIR, AFM, and CFLSM.

5.2. Surfaces: Results and discussion

5.2.1. Si(100)[1]

5.2.1.1. Si(100)-H and Si(100)-Cl

The Si(100)-H and Si(100)-Cl surfaces were prepared as described above (Scheme 4.2, chapter 4).

[1] Single Side Polished

5.2.1.2. Si(100)~N_3

A freshly prepared Si(100)-H surface in an oxygen-free solution of 2-azidoethanol in dried toluene is heated at 80^{o}C for 72 hours. Representative XPS spectra of Si(100)~N_3 and Si(100)-H surfaces are overlaid in figure 5.1. The Si(100)-N_3 surface features 2s and 2p peaks of Si at ~151 and ~99eV, respectively and O-bound Si (SiO_x) at ~104 and 154eV. The (1s) peaks of the C and O in the attached molecules are observed at ~285 and 533eV, respectively. N (1s) is observed at ~400eV. Compared to the Si(100)-H surface, the relative peak intensity of Si decreases and the relative peak intensities for O and C increase, indicating attachment of the azido alcohol.

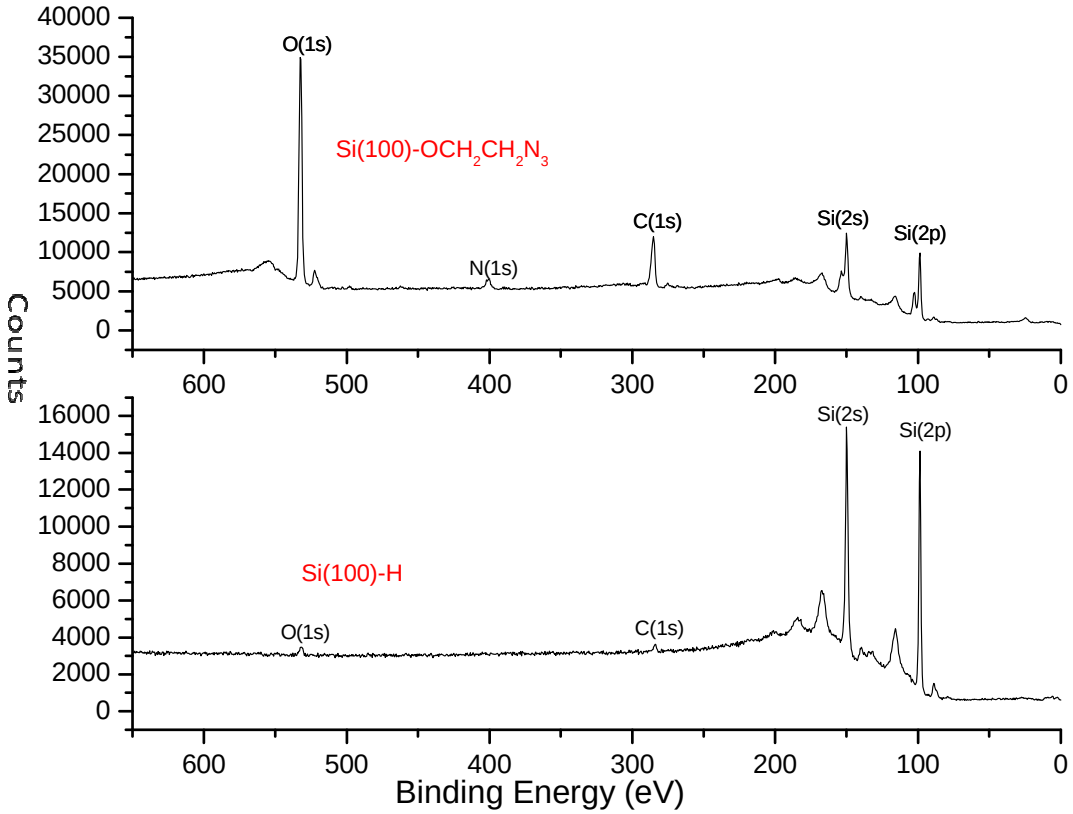

Figure 5.1. Representative XPS spectra overlaid; survey scans of Si(100)-H and Si(100)~N_3 surfaces.

Si~N_3 surfaces were also prepared from Si-Cl surfaces. Reactions were carried out in analogy. The XPS spectra showed no differences and are not discussed further.

5.2.1.3. Si(100)-Click-Br

Propagyl bromide is used in a subsequent step as a model reaction for “clicking” molecules to functional Si-surfaces. A freshly prepared Si(100)-N_3 surface is placed in a mixture containing propagyl bromide in toluene, tetrakis(acetonitrile) copper(I) hexafluoro phosphate, and Na_2CO_3 and kept at ambient temperature for 60 hours. Representative overlaid XPS spectra of Si(100)-Click-Br and Si~N_3 surfaces are shown in figure 5.2. The Si(100)-Click-Br surface features 2s and 2p peaks of Si at ~151 and ~99eV, respectively and O-bound Si (SiO_x) at ~104 and 154eV. The C and O (1s) peaks from the attached molecules are observed at ~285 and 533eV, respectively. N (1s) is observed at ~400eV. Br (3d) is observed in a narrow scan (Figure 5.2. bottom) at ~70eV. Compared to the Si(100)-N_3 surface, the relative peak intensities of Si and O decrease and the relative peak intensity of C increases, indicating more surface coverage consisting of C. These observations, together with the presence of Br are proof for an attachment of propagyl bromide to Si via the Si(100)~N_3 surface. Consequently, this “click” approach seems a promising for the analogous click-reactions of the Si~N_3 functional surface with the oligomeric T-OPV-dialkynes.

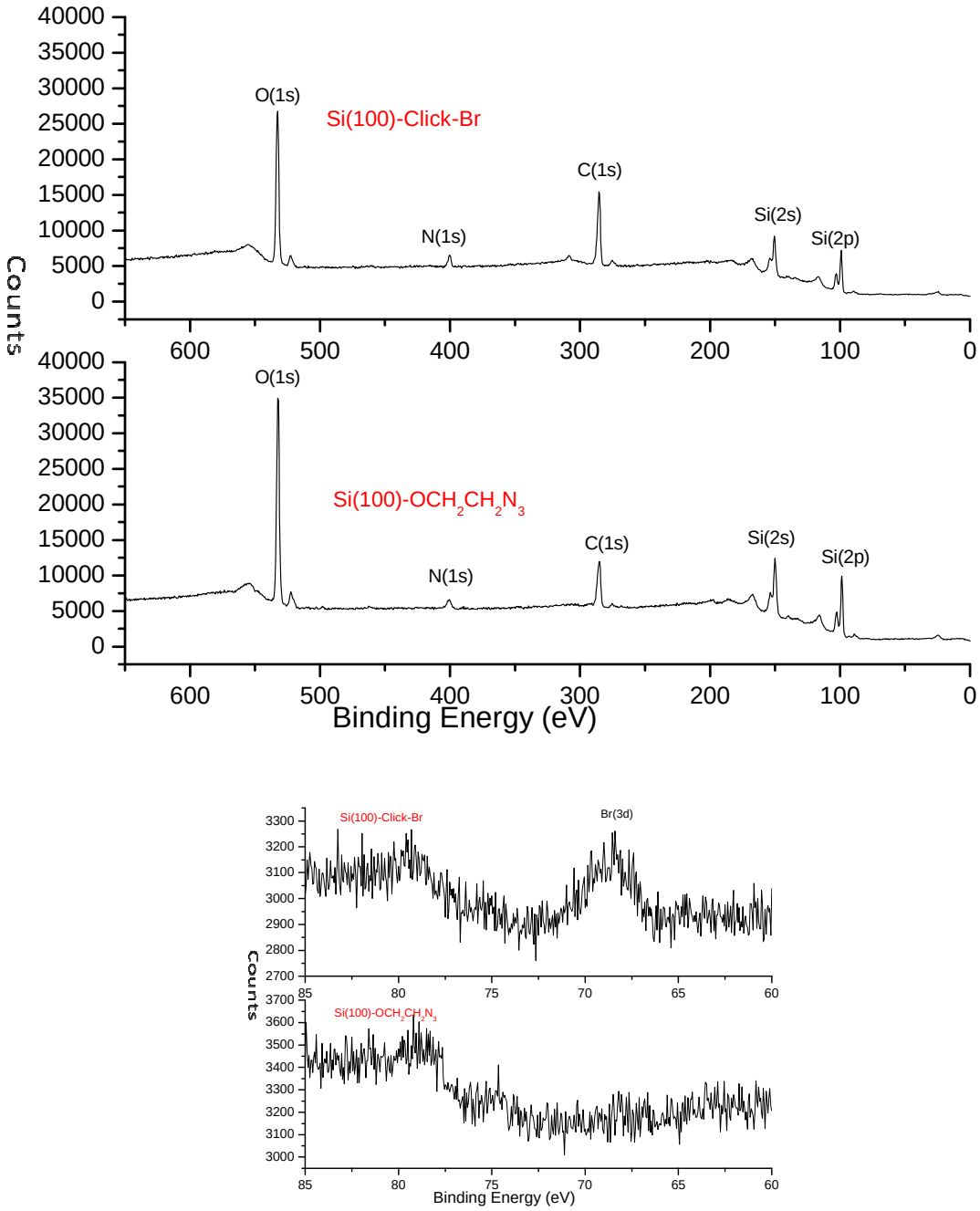

Figure 5.2. Representative XPS spectra overlaid; survey scans (top) and narrow scans (bottom) of Si(100)~N_3 and Si(100)-Click-Br surfaces.

A typical AFM image of the Si(100)-Click-Br surface is shown in figure 5.3 together with a cross-sectional height trace. The surface roughness (RMS) after reaction was determined as 0.62m over a 1μm^2 area. The height traces show

extended elevations of up to 1.5nm in height. The calculated values for these heights are ~0.82nm (see experimental). The difference of calculated vs. theoretical values is within the range of the surface roughness.

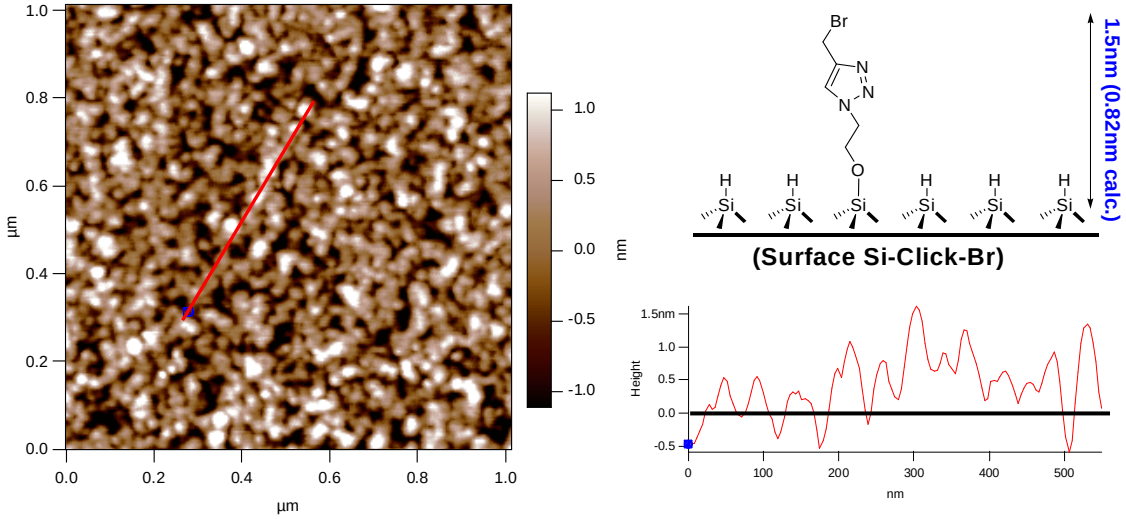

Figure 5.3. AFM image of Si(100)-Click-Br surface.

5.2.1.4. Si(100)-Click-OPV-alkyne

The preparation of a Si(100)-Click-OPV-alkyne surface is carried out in analogy to the preparation of a Si(100)-Click-Br surface. The reaction is continued at room temperature for 48 hours. Representative overlaid XPS spectra of Si(100)-Click-OPV-alkyne and Si(100)~N_3 are shown in figure 5.4. The Si(100)-Click-OPV-alkyne features 2s and 2p peaks of Si at ~151 and ~99eV, respectively and O-bound Si (SiO_x) at ~104 and 154eV. The (1s) peaks of the C and O from the attached molecules are observed at ~285 and 533eV, respectively. N (1s) is observed at ~400eV. Compared to the Si(100)~N_3 surface, the relative peak intensities of Si and O are less and the relative peak intensity of C is higher as

clearly shown in narrow scans (figure 5.5), indicating more surface coverage consisting of C. The relative peak intensity of N increases as two N are added per molecule OPV-dialkyne.

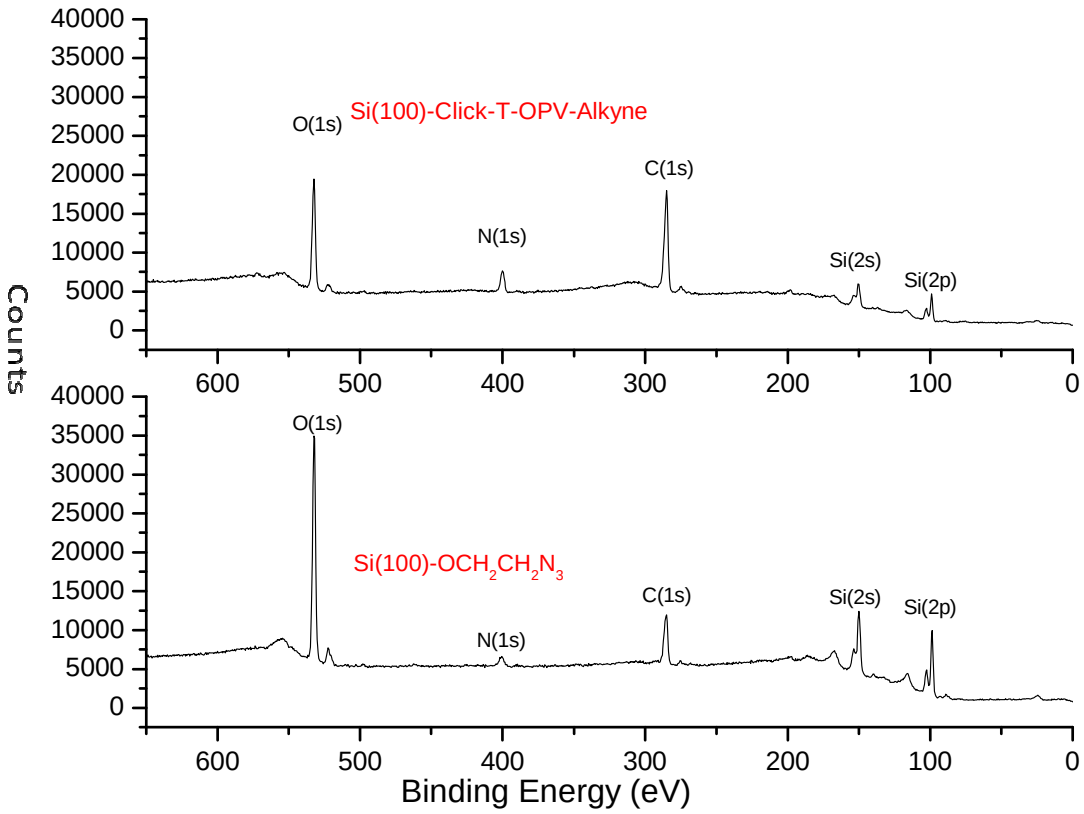

Figure 5.4. Representative XPS spectra overlaid; survey scans of Si(100)~N_3 and Si(100)-Click-OPV-alkyne surfaces.

A typical AFM image together with a cross-sectional height trace of the Si(100)-Click-OPV-alkyne surface (based on the solid red line) is shown in figure 5.6. The surface roughness RMS after reaction is determined as 0.76nm over a 1μm^2 area.

The height trace revealed elevations with heights of ~3.2nm which correspond the vertical height of a single perpendicular molecular length, as shown in the

figure next to the AFM image. The calculated value of 3.23nm (see experimental) is in excellent agreement.

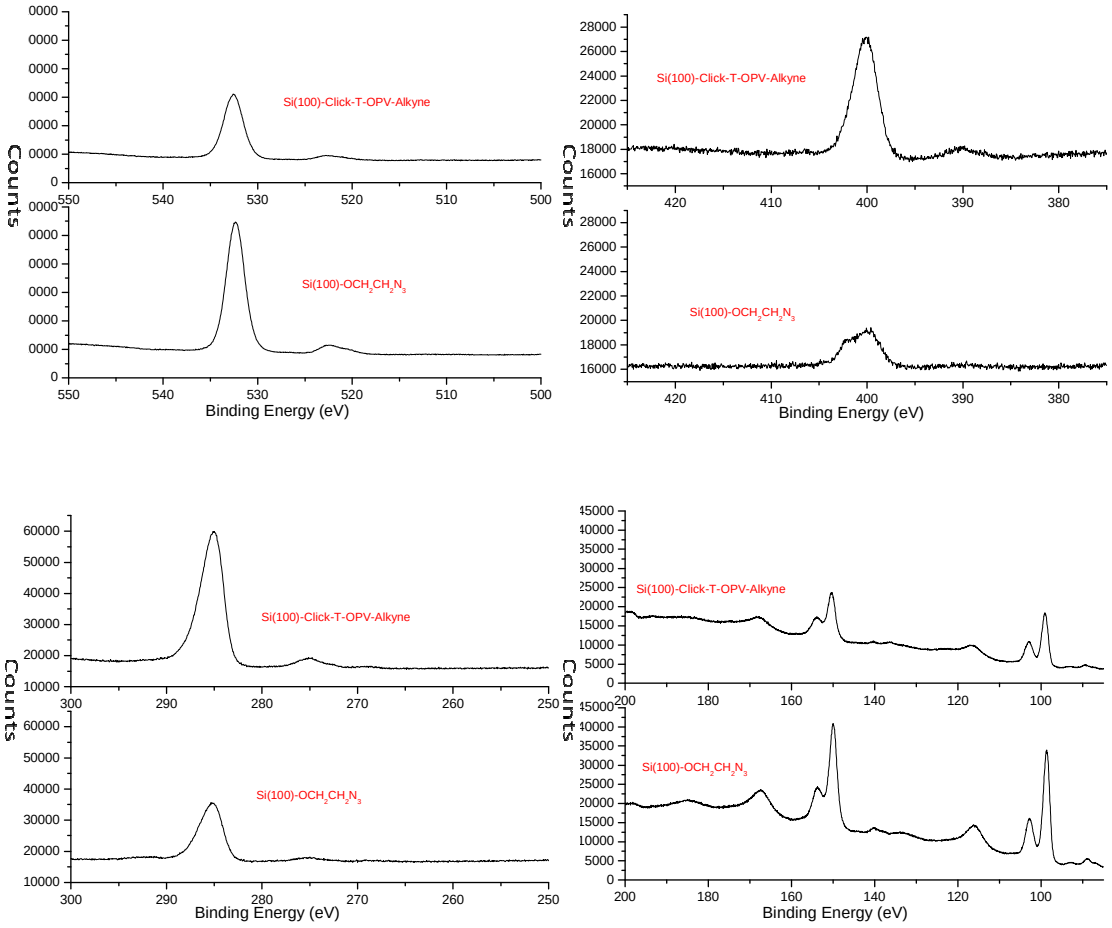

Figure 5.5. Representative XPS spectra overlaid; narrow scans of Si(100)~N_3 and Si(100)-Click-OPV-alkyne surfaces.

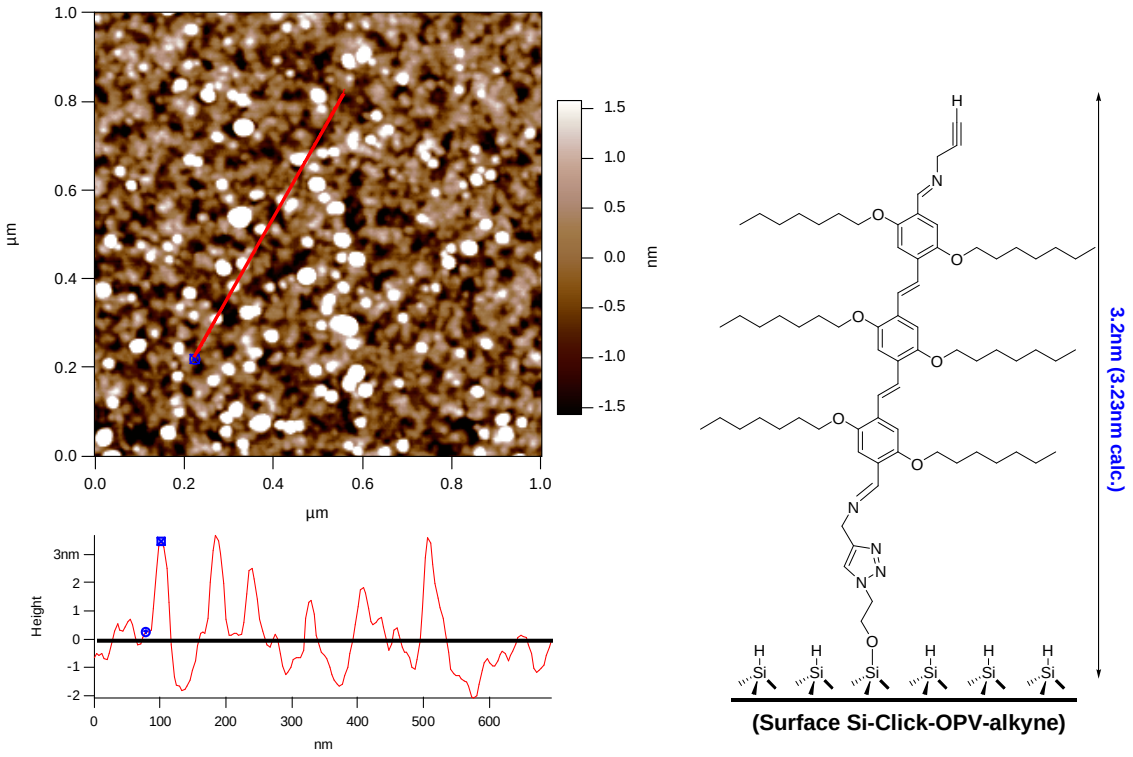

Figure 5.6. AFM image of Si(100)-Click-OPV-alkyne surface.

5.2.2. Si(111)[2]

5.2.2.1. Si(111)-H and Si(111)-Cl

The Si(111)-H and Si(111)-Cl surfaces were prepared as described above for the Si(100) surfaces (Scheme 4.2, chapter 4).

5.2.2.2. Si(111)~N_3

The preparation of a Si(111)~N_3 surface from Si(111)-H was carried out in analogy to the Si(100)~N_3 (see above). The total reaction time was 24 hours at 80^{o}C. The overlaid XPS spectra of the Si(111)~N_3 and Si(111)-H surfaces are shown in figure 5.7. The Si(111)-N_3 surface features 2s and 2p peaks of silicon at

[2] Single Side Polished

~151 and ~99eV, respectively and O-bound Si (SiO_x) at ~104 and 154eV. The (1s) peaks of C and O from the attached molecules are observed at ~285 and 533eV, respectively. N (1s) is observed at ~400eV. Compared to the Si(111)-H surface, the relative peak intensity of Si decreases and the relative peak intensities O and C increase. As in the Si(100)-N_3-case, these observations prove attachment of the azido alcohol to Si via the Si(111)-H surface. Compared to the Si(100)-N_3 surfaces, however, there seems to be less coverage, probably due to the higher reactivity of Si(100)-H toward the azido alcohol. In figure 5.7 the Si(100)-N_3 surface shows a lower relative peak intensity of Si compared to the peak intensities of O, N and C.

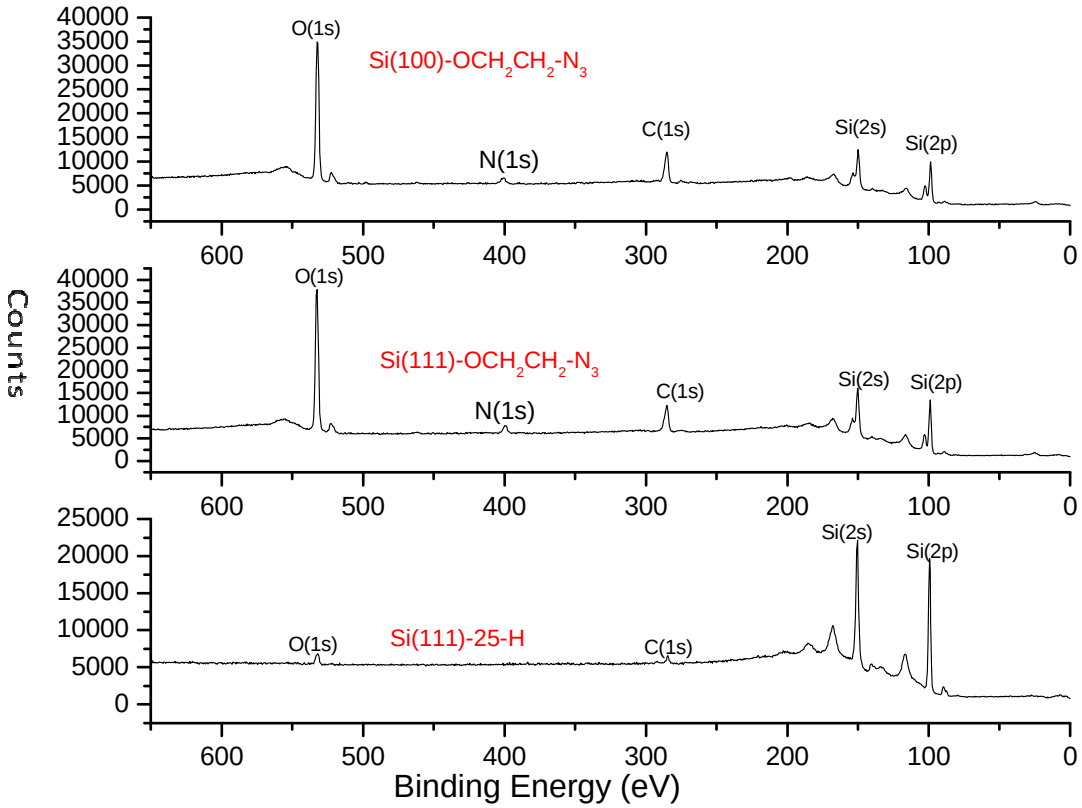

Figure 5.7. Representative XPS spectra overlaid; survey scans of Si(111)-H, Si(100)~N_3 and Si(111)~N_3 surfaces.

Si(111)~N_3 surfaces were prepared from Si(111)-Cl surfaces in order to compare them to Si(111)~N_3 surfaces made from Si(111)-H.

The preparation of a Si(111)~N_3 surface from Si(111)-Cl is performed in analogy to the Si(100)~N_3 (see above). The reaction time was 24 hours at 80^{o}C. Two representative overlaid XPS spectra of Si(111)~N_3 made from Si-Cl and Si(111)-N_3 made from Si-H surfaces are shown in figure 5.8. The Si(111)-N_3 made from Si-Cl features 2s and 2p peaks of Si at ~151 and ~99eV, respectively and O-bound Si (SiO_x) at ~104 and 154eV. The (1s) peaks of C and O from the attached molecules are observed at ~285 and 533eV, respectively. N (1s) is observed at ~400eV. Compared to the Si(111)-N_3 made from Si-H, the relative peak intensity of Si is less and the relative peak intensities O, N and C are higher, indicating more surface coverage. This allows the conclusion that reaction via Si-Cl is more efficient than via Si-H.

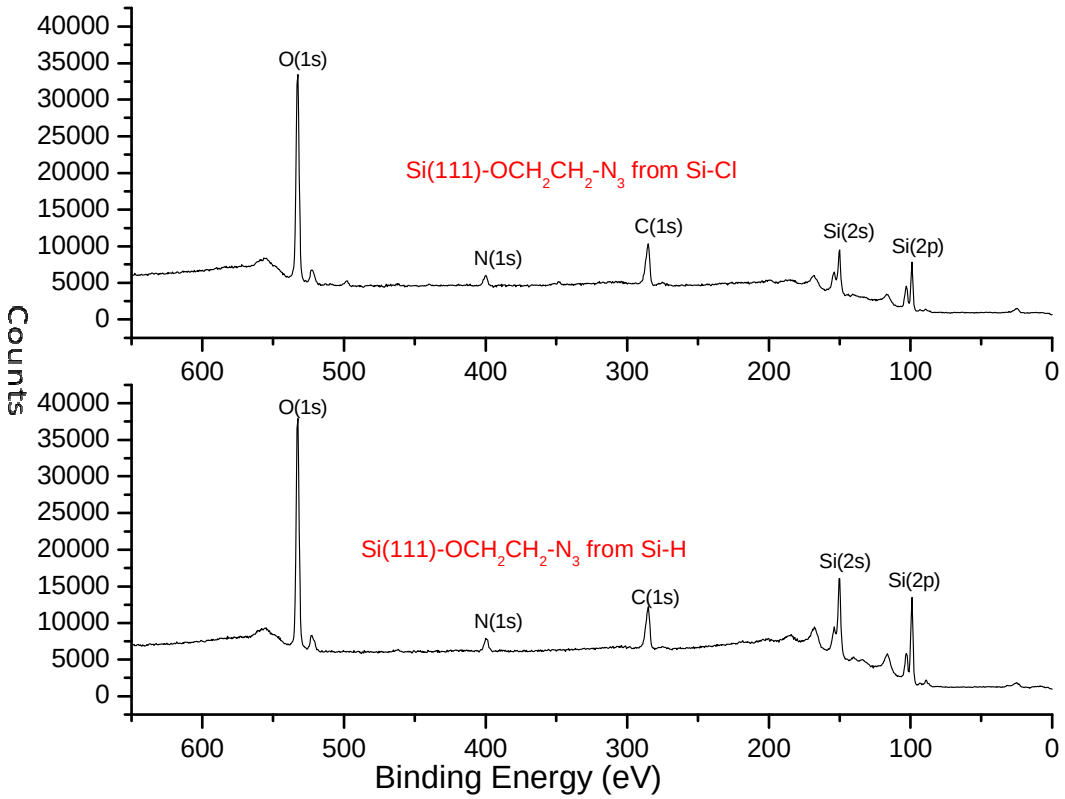

Figure 5.8. Representative XPS spectra overlaid; survey scans of Si(111)~N_3 from Si(111)-Cl and Si(111)-H surfaces.

5.2.2.3. Si(111)-Click-OPV-alkyne

The preparation of a Si(111)-Click-OPV-alkyne surface was carried out in analogy to the Si(100)-Click-OPV-alkyne surface using solutions of OPV-dialkyne **19** in dried toluene for 48 hours at room temperature. The overlaid XPS spectra of representative surfaces Si(111)-Click-OPV-alkyne and Si(111)~N_3 are shown in figure 5.9. The Si(111)-Click-OPV-alkyne surface features 2s and 2p peaks of Si at ~151 and ~99eV, respectively, and O-bound Si (SiO_x) at ~104 and 154eV. The (1s) peaks of C and O from the attached OPV dialkyne molecules are observed at ~285 and 533eV, respectively. N (1s) is observed at ~400eV. Compared to the Si(111)~N_3 surface, the relative peak intensity of Si is less and

the relative peak intensities of C and N are higher. This is also clearly discerned from a narrow scan (figure 5.10). The relative peak intensity of O is less relative to carbon, and based on different C/O ratios an additional indication of a successful attachment of T-OPV-dialkyne to Si via the Si~N_3 surface by click reaction.

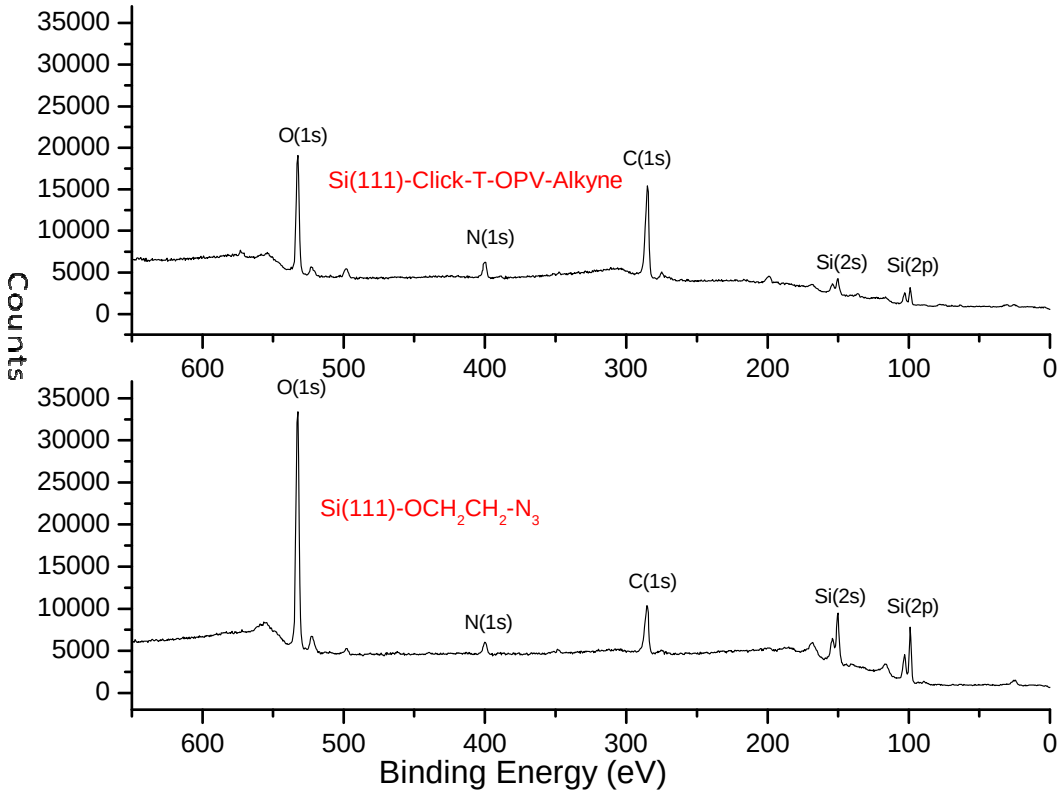

Figure 5.9. Representative XPS spectra overlaid; survey scans of Si(111)-H, Si(111)~N_3, and Si(111)-Click-OPV-alkyne surfaces.

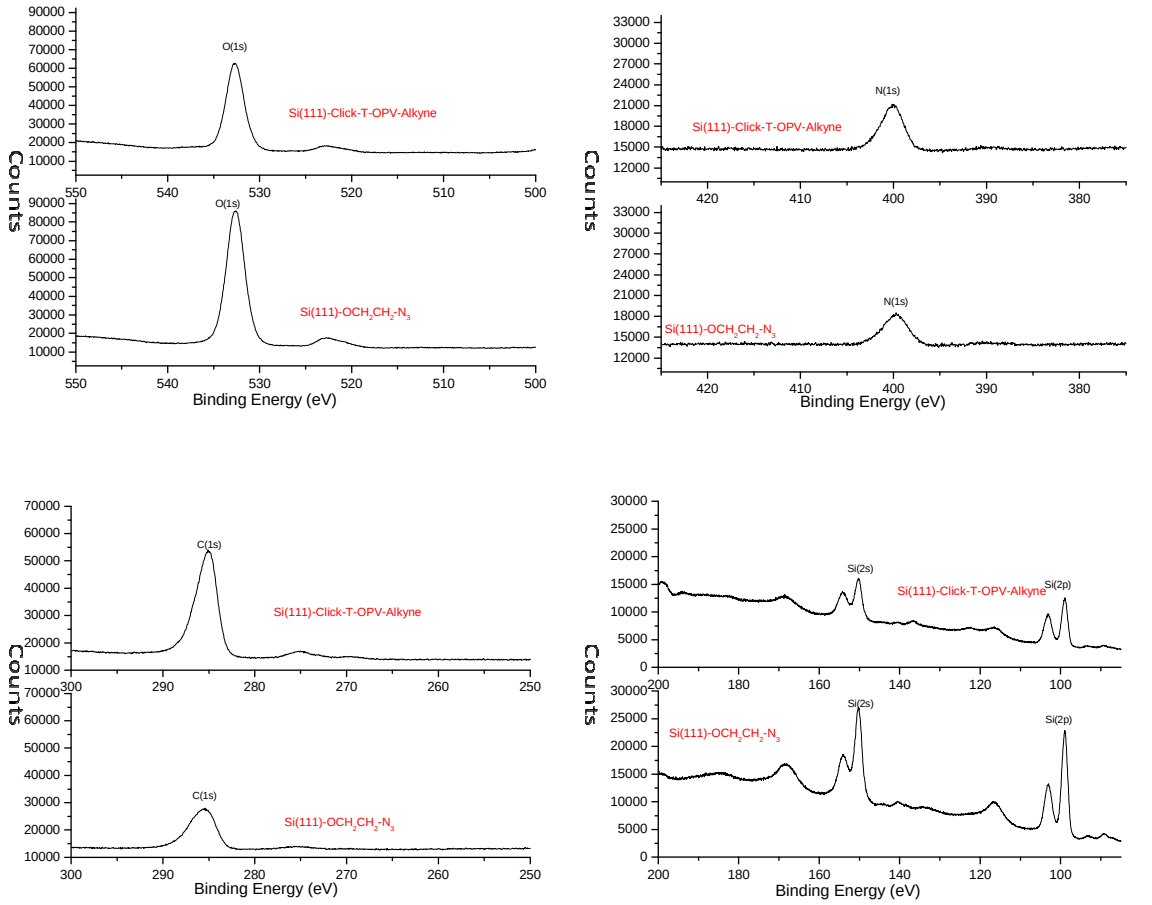

Figure 5.10. Representative XPS spectra overlaid; narrow scans of Si(111)~N_3 and Si(111)-Click-OPV-alkyne surfaces.

The Si(111)-Click-OPV-alkyne surfaces were investigated in regard to their optical emission characteristics.

Figure 5.11 shows a normalized UV/Vis absorption and emission spectra of T-OPV-alkyne in solution ($CHCl_3$) and an emission spectrum of a Si(111)-T-OPV-alkyne surface. The UV/Vis absorption maximum is measured at 437nm. The emission maxima are observed at λ_{max} = 494nm (excited at 405nm) in solution for the T-OPV-dialkyne (chapter 3) and λ_{max} = 514nm (excited at 405 nm) for the monolayer in the surface Si-T-OPV-alkyne. Compared the solution, a red shift

and broader emission are observed in the monolayer. These are strong indications of aggregation of the fluorophores on the surface.

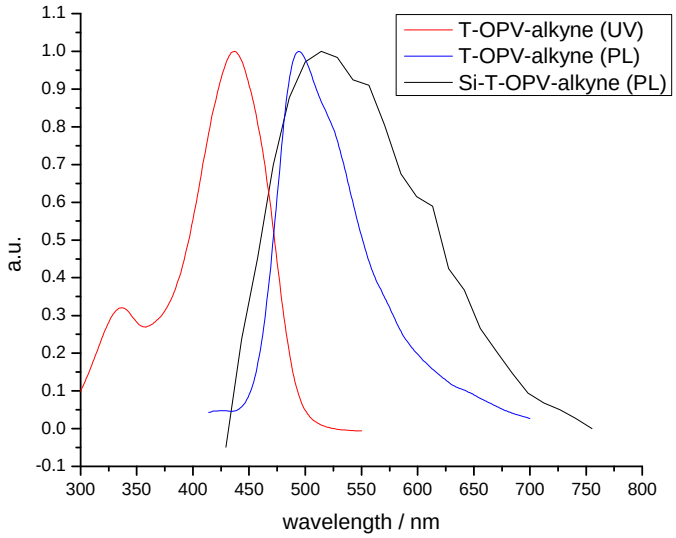

Figure 5.11. Normalized UV/Vis absorption spectrum of T-OPV-dialkyne in solution ($CHCl_3$, red) and normalized emission spectra of T-OPV-dialkyne in solution ($CHCl_3$, blue) and Si(111)-T-OPV-alkyne surface (black).

5.2.2.4. Si(111)-Click-NH_2

A $–NH_2$ functional Si-surface was prepared with propagyl amine for subsequent reaction with –CHO-functional OPV, using similar reaction conditions as in the homogenous reaction of –CHO-functional OPV with propargyl amine to produce dialkyne-functional OPV via Schiff base formation (See chapter 3).[116]

Representative overlaid XPS spectra of Si(111)-Click-NH_2 and Si(111)~N_3 surfaces are shown in figure 5.12. The Si(111)-Click-NH_2 surface features 2s and 2p peaks of silicon at ~151 and ~99eV, respectively and O-bound Si (SiO_x) at ~104 and 154eV. The (1s) peaks of C and O from the attached molecules are observed at ~285 and 533eV, respectively. The N (1s) peak is observed at

~400eV. Compared to the Si(111)-N_3 surface, the relative peak intensities of Si and O are less and the relative peak intensity from C is higher. As expected, the relative intensity of N (1s) is increased relative to Si, indicating presence of more N, indicating the presence of propagyl amine. However, unexpected peaks were observed at around 75 and 572eV. Although the propagyl amine is attached to the surface, it might not be in the anticipated fashion (see results below).

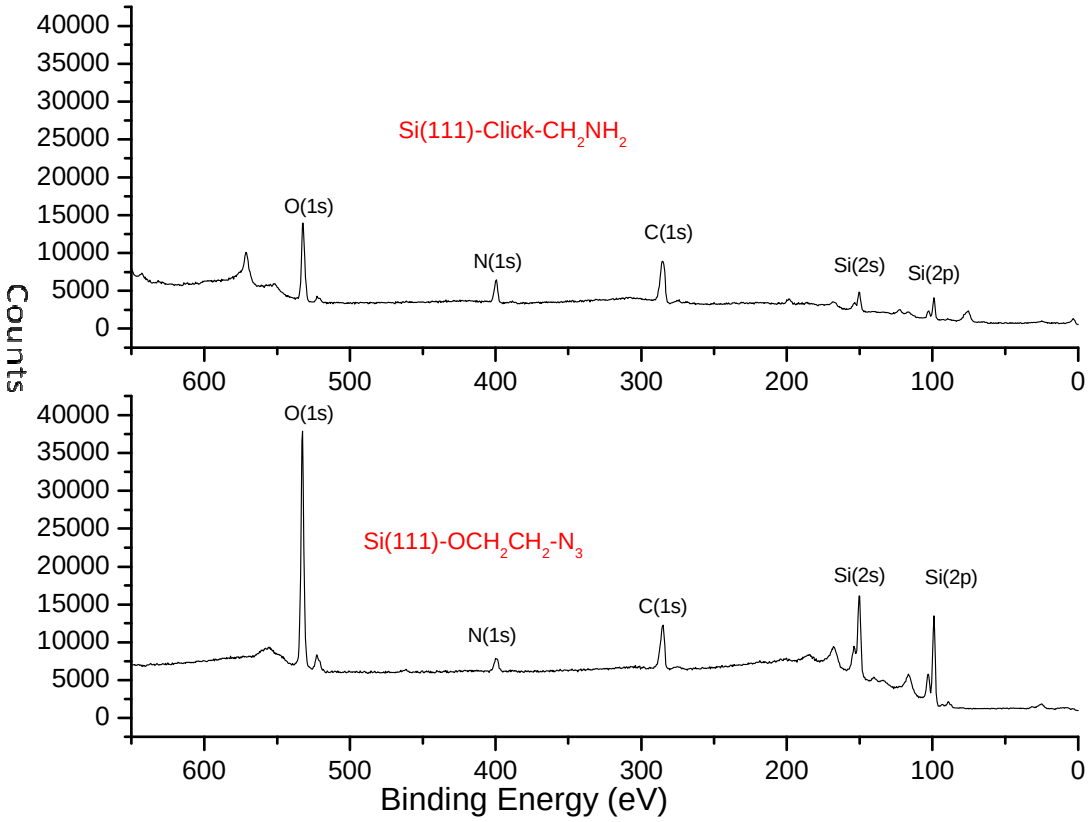

Figure 5.12. Representative XPS spectra overlaid; survey scans of Si(111)-Click-NH_2 and Si(111)~N_3 surfaces.

5.2.2.5. Si(111)-Click-OPV-CHO

The freshly prepared Si(111)-Click-NH_2 surface was placed in a mixture of trimer-OPV-CHO, anhydrous $MgSO_4$, and dried THF at room temperature for 30 hours.[116] The overlaid XPS spectra of Si(111)-Click-OPV-CHO and Si(111)-Click-

NH_2 surfaces are shown in figure 5.13. The XPS spectra show no differences before and after reaction, indicating no significant reaction. A possible explanation could be that in the prior reaction with propargyl amine, the mode of attachment did not proceed via the click-mechanism over the alkyne end, but by reaction of the NH_2-group in another mode.

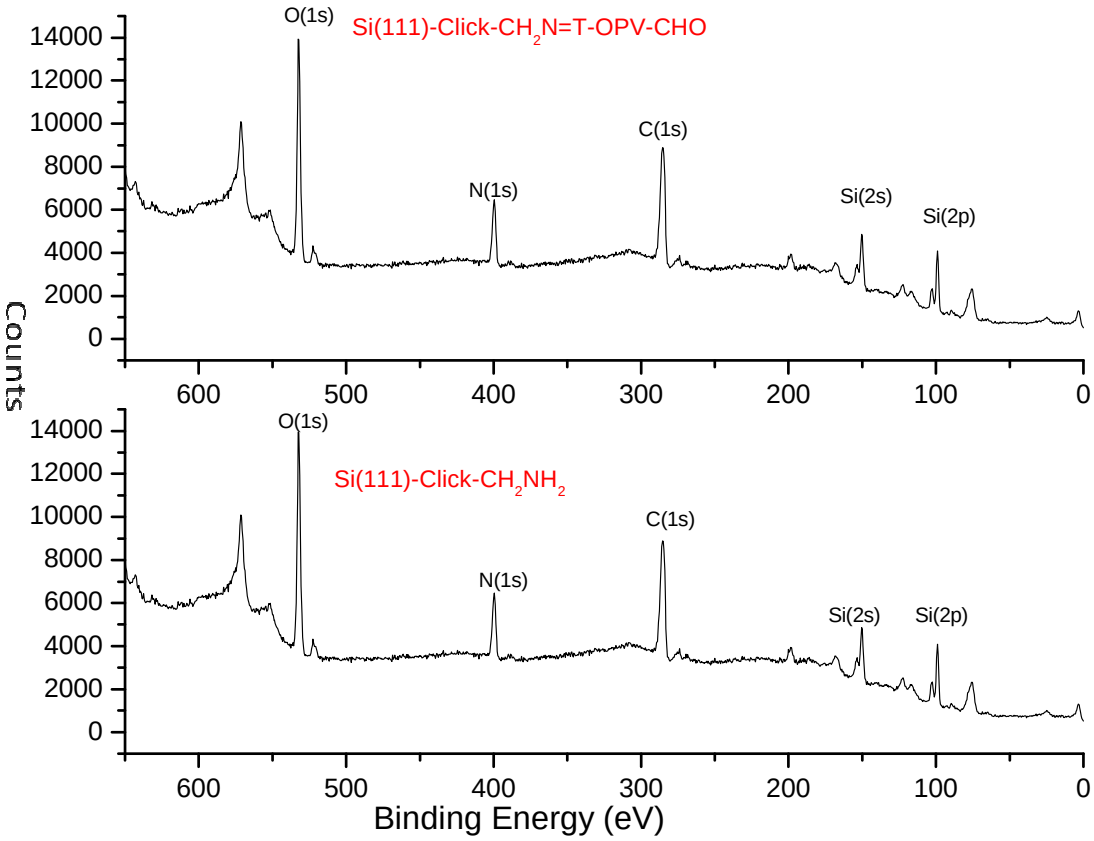

Figure 5.13. Representative XPS spectra overlaid; survey scans of Si(111)-Click-OPV-CHO and Si(111)-Click-NH_2 surfaces.

5.2.3. DSi(111): Double Side Polished Si(111)

5.2.3.1. DSi(111)O_x

A SiO_x covered silicon wafer, polished on both sides, was cleaned repeatedly with THF, H_2O, Acetone, CH_3OH, H_2O, CH_3OH, and H_2O, respectively and dried

under argon. This surface was used for a reference ATR-FTIR spectrum and background spectrum in several overlays.[126]

5.2.3.2. DSi(111)-H and DSi(111)-Cl

The DSi(111)-H and DSi(111)-Cl surfaces were prepared and used as described above (Scheme 4.2, chapter 4).

5.2.3.3. DSi(111)~N_3

The preparation of a DSi(111)~N_3 surface from DSi(111)-H was performed in analogy to the Si(100)~N_3 surface prepared from Si(100)-H (see above), with reaction times of 4, 24, and 48 hours at 80^{o}C. Representative overlaid XPS spectra of DSi(111)~N_3 and DSi(111)-H surfaces are shown in figure 5.14. The DSi(111)-N_3 surface features 2s and 2p peaks of Si at ~151 and ~99eV, respectively and O-bound Si (SiO_x) at ~104 and 154eV. The (1s) peaks of C and O from the attached molecules are observed at ~285 and 533eV, respectively. N (1s) is observed at ~400eV. Compared to the DSi(111)-H surface, the relative peak intensity of Si is lower and the relative peak intensities from O and C are higher.

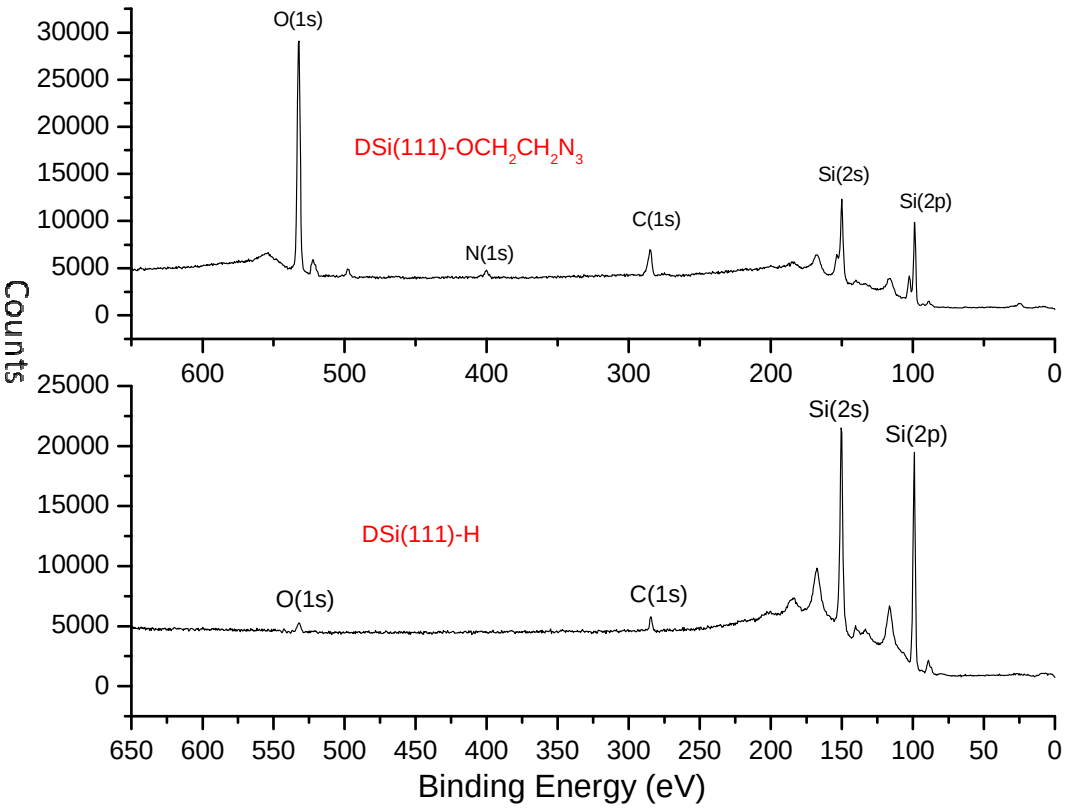

Figure 5.14. Representative XPS spectra overlaid; survey scans of DSi(111)-H and DSi(111)~N_3 surfaces.

DSi(111)~N_3 surfaces were prepared from DSi(111)-Cl surfaces in order to compare them to DSi(111)~N_3 surfaces made from DSi(111)-H.

The preparation of a DSi(111)-N_3 surface from DSi(111)-Cl was performed in analogy to the Si(100)~N_3 surface prepared from Si(100)-Cl (see above). In one approach, the reaction times were 17 and 24 hours at 80^{o}C, in another 24 hours at 50^{o}C. For the first approach, representative overlaid ATR-FTIR spectra of $DSiO_x$(111) (black), DSi(111)~N_3 (17 hours, green), and DSi(111)~N_3 (124 hours, purple) surfaces are shown in figure 5.15. No C-H stretching was observed for the SiO_x surface. For the DSi(111)~N_3 surfaces, the appearance of the C-H and N_3 stretching at 2950 and 2108 cm^{-1}, respectively, indicate the presence of the

azido alcohol. The relative stretching intensities from C-H and particularly the -N_3 group increase with longer reaction times (24 hours versus 17 hours), indicating more surface coverage containing C-H and N_3 units.

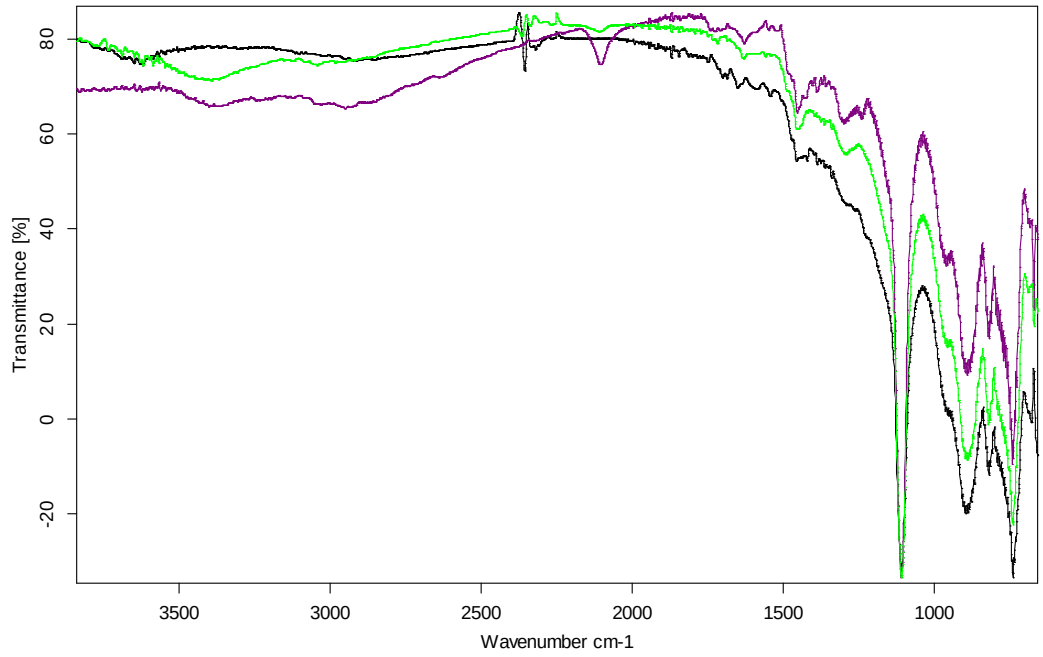

Figure 5.15. ATR-FTIR spectra of $DSiO_x$ (black), $DSi{\sim}N_3$ (17hours, green), and $DSi{\sim}N_3$ (24hours, purple) surfaces.

To evaluate the success of the second approach, representative overlaid XPS spectra of $DSi(111){\sim}N_3$ surfaces made from Si-Cl at 50^{o}C for 24h and from Si-H at 80^{o}C for 48h are shown in figure 5.16. The $DSi(111){\sim}N_3$ made from Si-Cl at 50^{o}C for 24h features 2s and 2p peaks of Si at ~151 and ~99eV, respectively and O-bound Si (SiO_x) at ~104 and 154eV. The (1s) peaks of C and O from the attachment molecules are observed at ~285 and 533eV, respectively. N (1s) is observed at ~400eV. Compared to the $DSi(111){\sim}N_3$ made from Si-H at 80^{o}C for 48h, the peak intensity of Si is less relative to peak intensities from O, N, and C. Attachment via Si-Cl seems more efficient than via the Si-H surface.

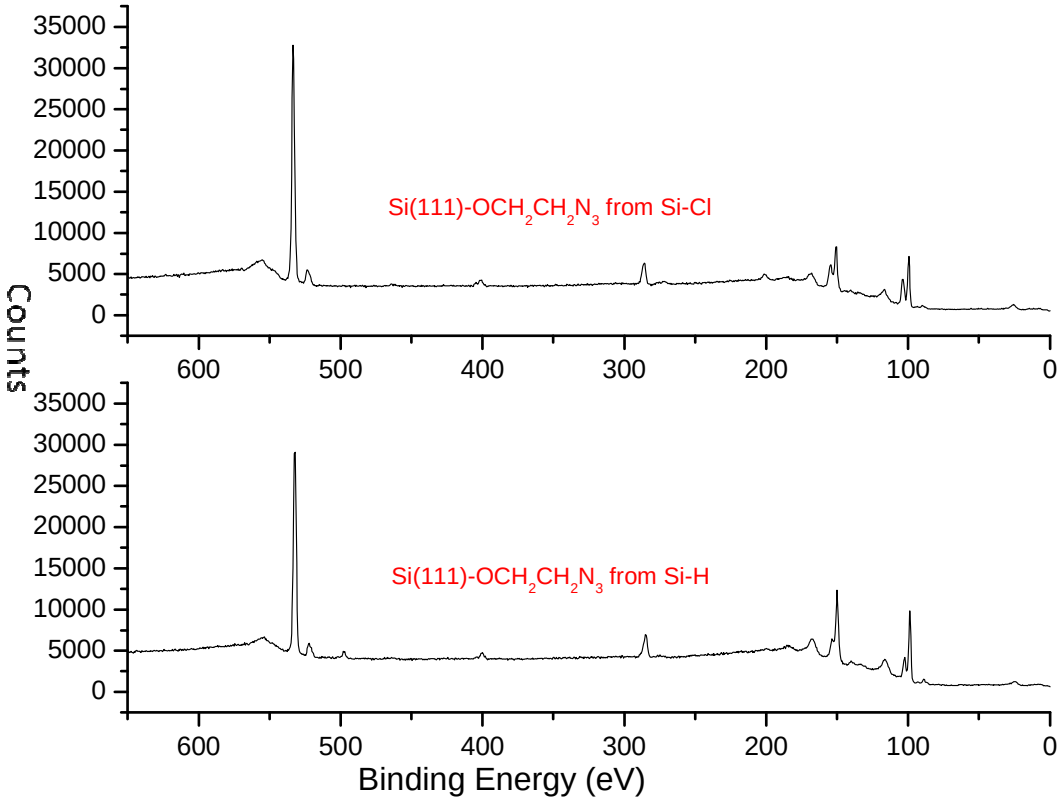

Figure 5.16. Representative XPS spectra overlaid; survey scans of DSi(111)~N_3 surfaces (from Si-H for 48h at 80^{o}C and from Si-Cl for 24h at 50^{o}C).

5.2.3.4. DSi(111)-Click-Br

Propagyl bromide was reacted with a Si~N_3 surface. The wafer used was polished on both sides, providing more surface for the reaction. Reaction conditions are described above.

The ATR-FTIR spectra of $HOCH_2CH_2N_3$ (bulk, red), DSi(111)~N_3 (made from Si-Cl at 80^{o}C for 17h, green), DSi(111)~N_3 (made from Si-Cl at 80^{o}C for 24h, purple), and DSi(111)-Click-Br (blue) surfaces are compared in figure 5.17. The DSi(111)-Click-Br (made from Si-Cl at 80^{o}C for 17h) surface features C-H stretching of triazole and alkane at 3345 cm^{-1} and 2950 cm^{-1}, respectively, C=C

stretching (triazole) at 1616 cm^{-1}, and disappearance of 2104 cm^{-1} (N_3 stretching). The DSi(111)-Click-Br shows a higher relative stretching intensity from C-H than DSi(111)~N_3 (17h from Si-Cl at 80°C). As a result and as discussed above also, this reaction proves to be a good model for the analogous click reaction of the DSi(111)~N_3 surface with OPV-dialkyne.

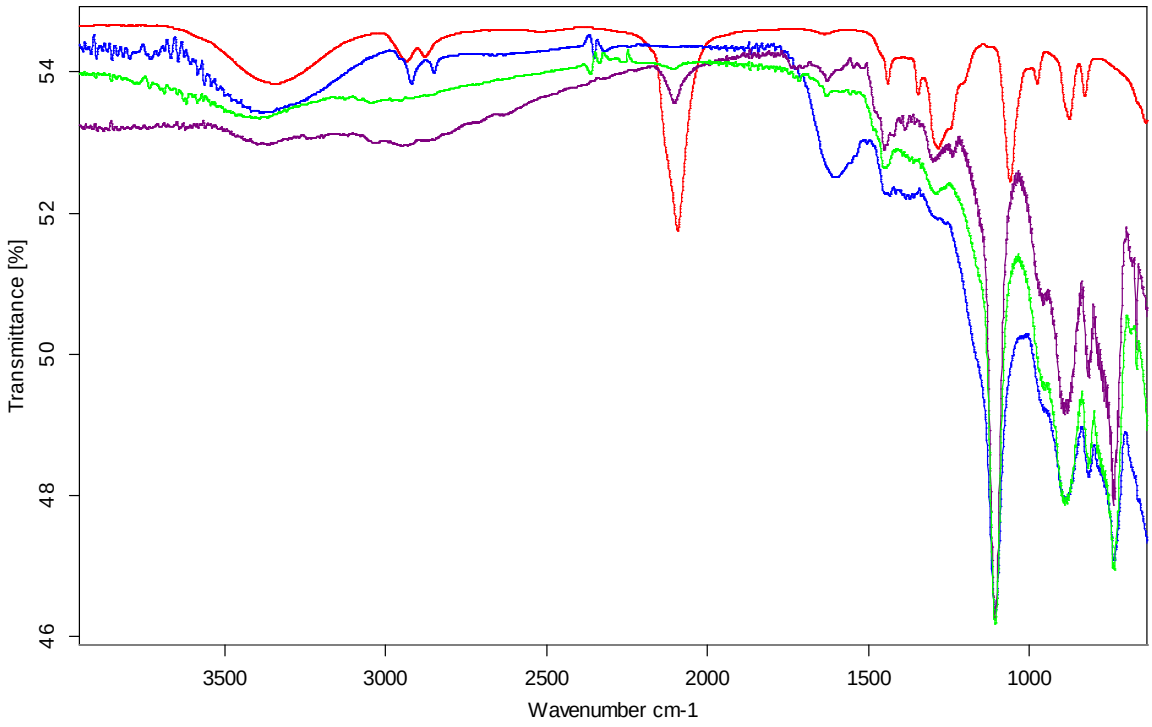

Figure 5.17. ATR-FTIR spectra of $HOCH_2CH_2N_3$ (bulk, red), and surfaces DSi(111)~N_3 (from Si-Cl for 17h at 80°C, green), DSi(111)~N_3 (from Si-Cl for 24h at 80°C, purple), and DSi(111)-Click-Br (blue).

5.2.3.5. DSi(111)-Click-OPV-alkyne

The preparation of a DSi(111)-Click-OPV-alkyne surface from DSi(111)~N_3 (made from Si-Cl at 80°C for 24h) was performed in analogy to the Si(100)-Click-OPV-alkyne surface (see above). The reaction was carried out for 48 hours at room temperature. Representative overlaid XPS spectra of DSi(111)-Click-OPV-alkyne and DSi(111)~N_3 surfaces are shown in figure 5.18. The DSi(111)-Click-

OPV-alkyne surface features 2s and 2p peaks of Si at ~151 and ~99eV, respectively and O-bound Si (SiO_x) at ~104 and 154eV. The (1s) peaks of C and O from the attached molecules are observed at ~285 and 533eV, respectively. N (1s) is observed at ~400eV. Compared to the DSi(111)~N_3 surface, the relative peak intensity of Si is less and the relative peak intensities of O, N, and C are higher. The relative peak intensity of N increases, as two N are added per molecule OPV-dialkyne. Moreover, the large OPV-dialkyne molecule will sterically prevent access to nearby N_3 functionalities on the surface, leaving many unreacted and detectable. Individually overlaid narrow scans of the respective peaks figure 5.19 make this clearer, indicating a successful reaction. The relative peak intensity of O decreases relative to C, due to the over-proportional addition of C rather than O per attachment of one T-OPV-dialkyne molecule.

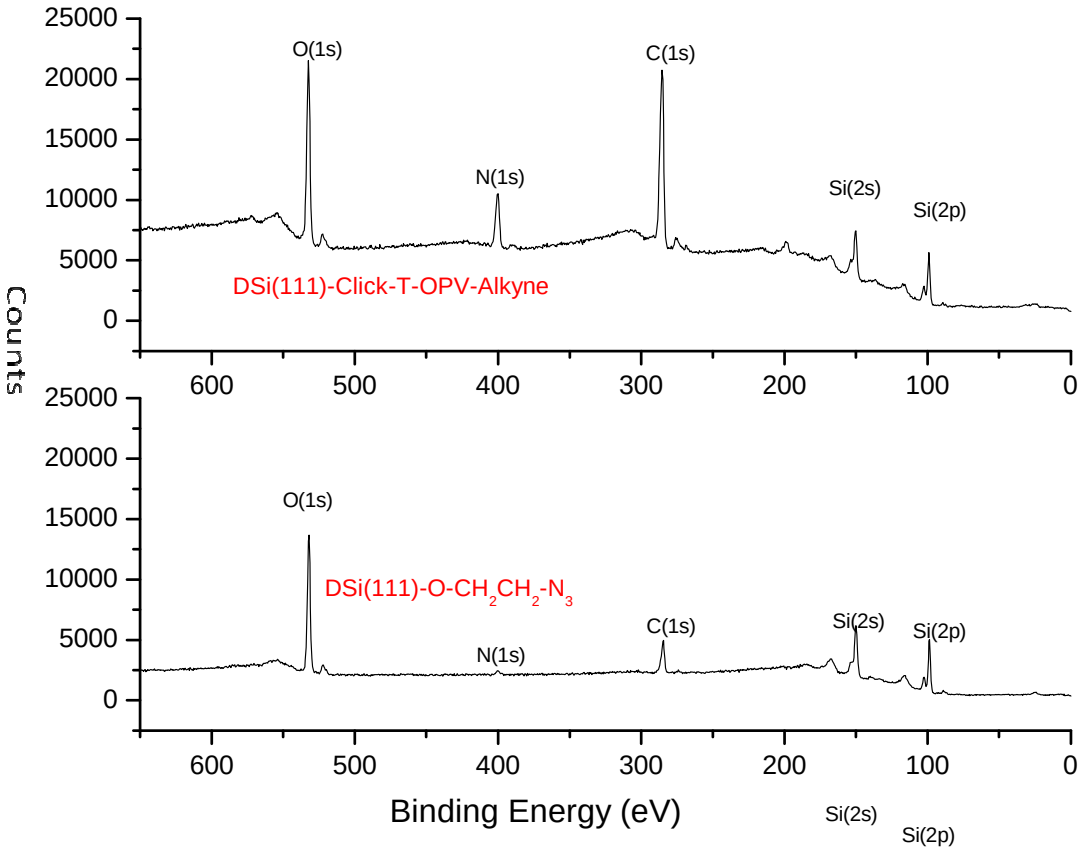

Figure 5.18. Representative XPS spectra overlaid; survey scans of DSi(111)-Click-OPV-alkyne and DSi(111)~N_3 (from Si-Cl for 24h at 80^{o}C) surfaces.

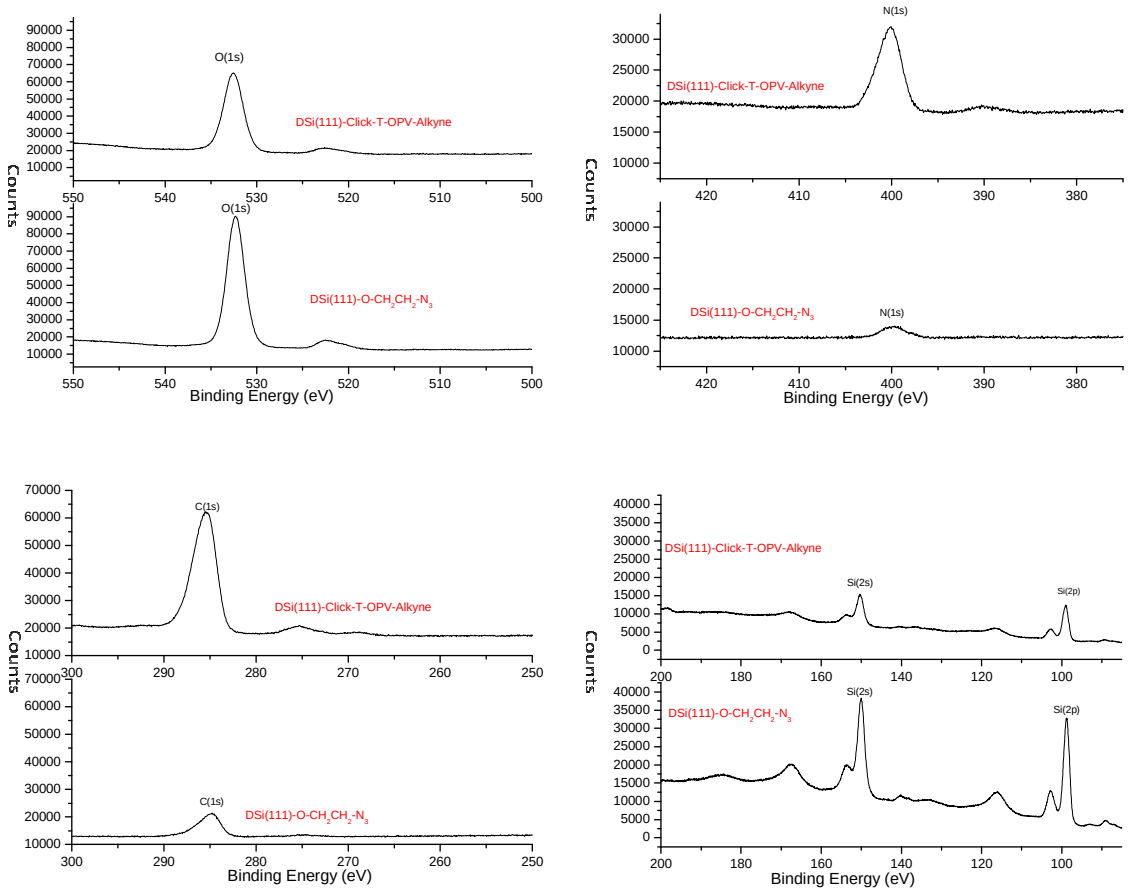

Figure 5.19. Representative XPS spectra overlaid; narrow scans of DSi(111)~N_3 and DSi(111)-Click-OPV-alkyne surfaces.

The observations are further supported by ATR-FTIR investigation. Overlaid ATR-FTIR spectra of a bulk trimer-OPV-dialcohol, surfaces DSi(111)O_x, DSi(111)~N_3 (made from Si-Cl at 80^{o}C for 24h), and DSi(111)-Click-OPV-alkyne are shown in figure 5.20. The DSi(111)-Click-OPV-alkyne surface features C-H stretching of triazole and alkane at 3345 cm^{-1} and 2950 cm^{-1}, respectively, C=C stretching (triazole) at 1616 cm^{-1}. Compared to the DSi(111)~N_3 surface, the DSi(111)-Click-OPV-alkyne surface ATR-FTIR shows a less intense N_3stretching peak . The relevant region of the spectrum has been enlarged and inserted into

the graph. The OPV-dialkyne molecules obviously did not react with all available N_3 groups on the Si~N_3 surface (see XPS discussion above). The FTIR results agree with the XPS results.

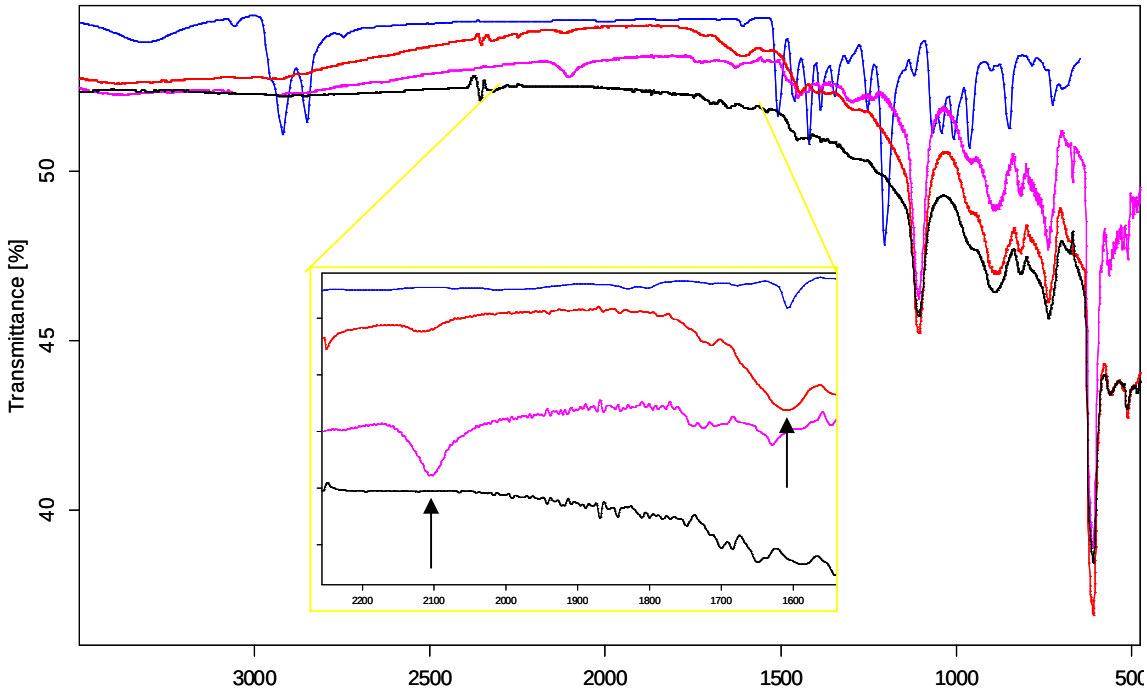

Figure 5.20. ATR-FTIR spectra of trimer-OPV-alcohol (bulk, blue), and surfaces DSi(111)O_x (black), DSi(111)~N_3 surface (from Si-Cl for 24h at 80^{o}C, purple), and DSi(111)-Click-OPV-alkyne (red).

A typical AFM image of a DSi(111)-Click-OPV-alkyne surface is shown in figure 5.21 together with a cross-sectional height trace (based on the solid red line). The surface roughness (RMS) is determined as 0.52nm over a 8.2μm^2 area.

The elevations with heights of ~3.3nm correspond to a single perpendicular molecular length, as shown in the figure next to AFM image. The calculated value of 3.23nm (see experimental) is in excellent agreement.

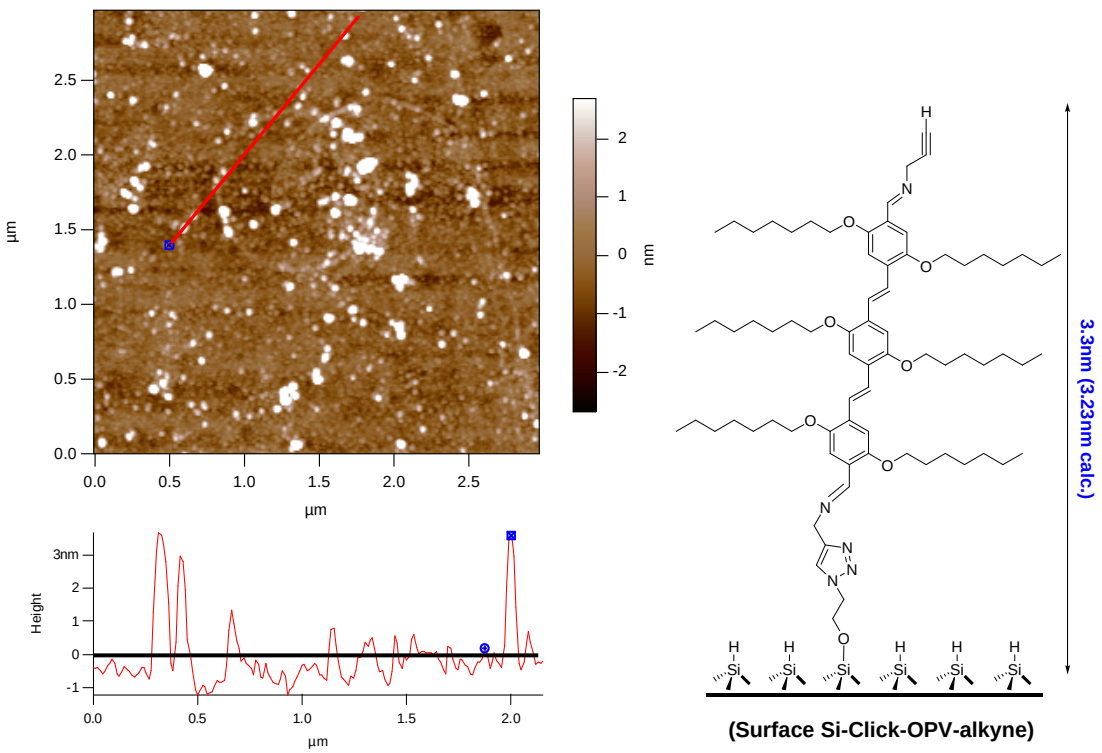

Figure 5.21. AFM image of DSi(111)-Click-OPV-alkyne surface.

5.3. Experimental

5.3.1. General information

All experiments using air/moisture sensitive materials were carried out with high purity argon using standard Schlenk techniques. All glassware was cleared and dried for at least 24h in an oven at 120^{o}C prior to use.

5.3.2. Chemicals

Sodium azide (Reagent Plus, 99.5%), 2-bromoethanol (95%), anhydrous pyridine (99.8%, water <0.003%), anhydrous toluene (99.8%, water <0.003%), anhydrous acetonitrile (99.8%, water <0.001%), anhydrous chlorobenzene (99.8%, water

<0.005%), anhydrous p-xylene (>99%, water <0.002%) were purchased from Sigma-Aldrich. Toluene (HPLC grade) and CH_2Cl_2 (HPLC grade) were purchased from Fisher Scientific. Millipore (18.2MΩ-cm and 6 TOC) water was used for rinsing the samples (from Millipore system). All other solvents (THF, toluene, CH_2Cl_2, and hexanes) were dried and degassed, using a "Pure Solv" solvent purification system (using activated alumina, copper catalyst, molecular sieves columns) by Innovative Technology Inc. before use. Silicon wafer n-type Si(100) was donated by Dr. Bhanu Chauhan. Single-sided polished Si(111; n-type As-doped, 500 ± 25 μm thickness, 0.001-0.005 Ω.cm resistivity, $4^o \pm 0.5^o$ off-cut), and double-side polished Si(111; float zone grade, n-type P-doped, 300 ± 25 μm thickness, 24-35 Ω.cm resistivity) were purchased from University WAFER.

5.3.3. Instrumentation

^1H and ^{13}C NMR spectra were recorded on Varian 200 MHz or 600 MHz spectrometers in $CDCl_3$ as an internal deuterium lock for ^1H-NMR.

FTIR/ATR spectra were recorded on Bruker Tensor 27 spectrometer using Pike ATR or Harrick Seagull variable angle ATR accessory for characterizing samples in bulk oligo(*p*-phenylene vinylene)s and silicon surfaces before and after functionalization, respectively. All data were processed and analyzed by OPUS software.

An Atomic Force Microscope (AFM) from Asylum Research was used with an MFP-3D^{TM} SA extended head, 90μm XY scanner, TS 150 active vibration isolation table, and isolated in a Herzan AEK 2002 acoustic hood. Samples were

scanned in contact mode with an Olympus cantilever. The scan direction was parallel to the x-axis. The images were processed and analyzed by IGOR Pro 6.03A/MFP3D080129. All images were routinely flattened.

X-ray photoelectron spectra (XPS) were recorded with an Omicron Surface Science Model 150 XPS spectrometer equipped with an Al or Mg Kα source (Omicron DAR 400) without monochromator, and with a concentric hemispherical analyzer (Omicron EA 125), and multichannel detector. No electron flood gun was employed. The pressure in the analytical chamber during analysis was approximately 5 $x10^{-9}$ Torr.

Maximum emission was determined using a Leica SP2 AOBS spectral imaging confocal microscope.

5.3.4. Calculated molecular heights

In order to correlate the heights of molecular attachments on the Si-surfaces as determined by AFM with actual dimensions of the molecules used for attachment the molecules structures were optimized in Chem3D Ultra 9.0 and distance were calculated. A model H_3Si-O-CH_2CH_2-N_3C_2H-CH_2-N=CH-Trimer-OPV-CH=N$CH_2C{\equiv}CH$ (Si-Click-OPV-dialkyne) was used and optimized in regard to structure, scheme **5.1**.

The calculated height for Si~N_3 was 0.73nm, measured from Si to N in H_3Si-O-CH_2CH_2-N_3. The calculated height for propagyl amine was 0.45nm, measured from H to N in $HC{\equiv}CCH_2NH_2$. The calculated height for Si(111)-EA-Click-Br was 0.82nm, measured from Si to H (Br) in H_3Si-O-CH_2CH_2-N_3C_2H-CH_2Br. The

calculated height for T-OPV-dialkyne was 1.96nm, measured from N to C (see scheme 5.2).

Therefore, the total calculated height for the Si-Click-OPV-dialkyne surface is **3.23nm** (0.45nm +0.82nm + 1.96nm).

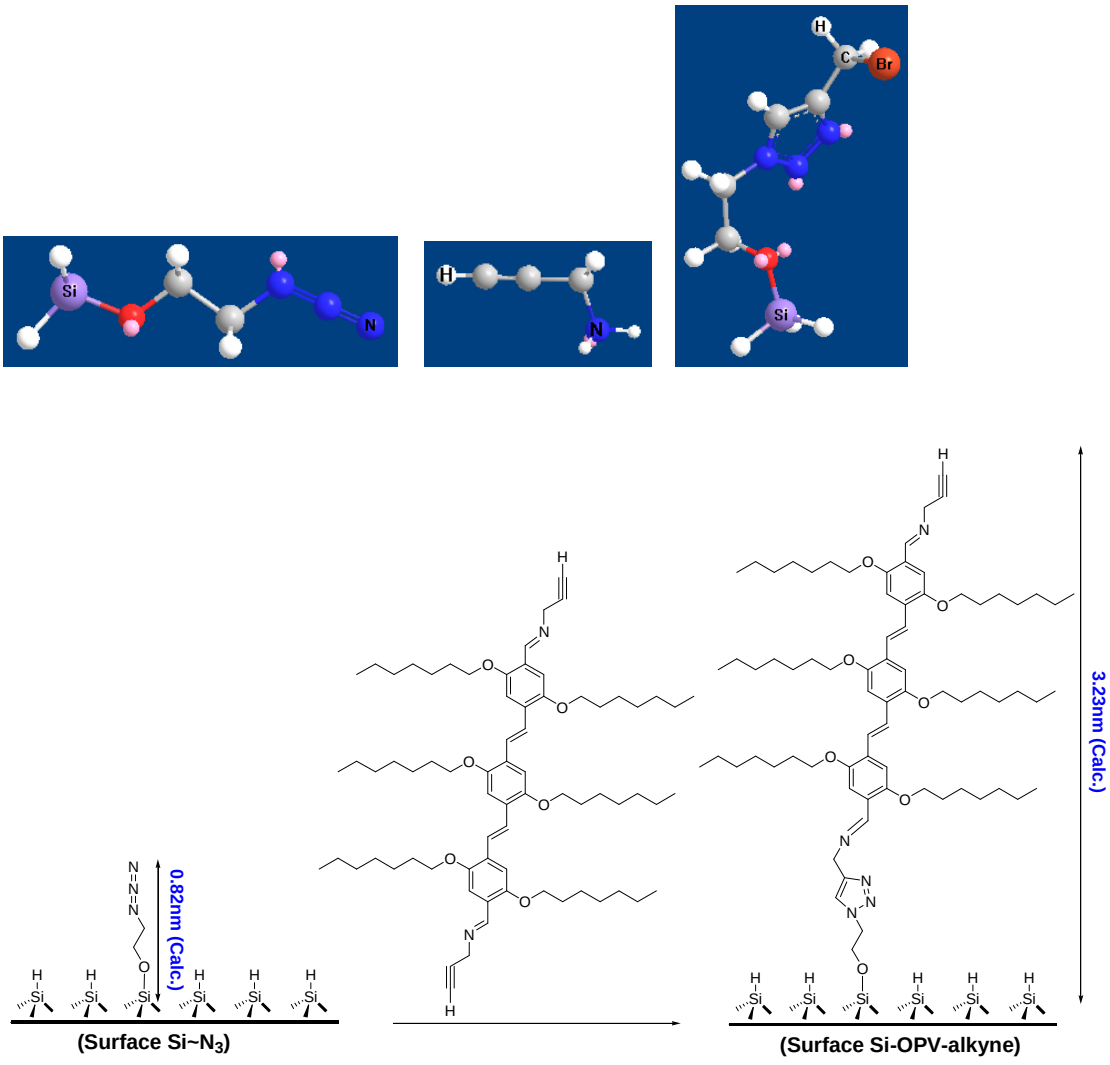

Scheme 5.2. Synthesis of model surface Si-Click-OPV-alkyne.

5.3.5. Synthesis of 2-azidoethanol

A solution of 2-bromoethanol (26.2g) and sodium azide (34.06g) were used to prepare 2-azidoethanol in analogy to literature.[127] First, the solid sodium azide

(20.5g) was added slowly to a vigorously stirred solution of 2-bromoethanol (26.2g) in distilled water (100 mL) at 0^{o}C. The solution was then allowed to warm to room temperature for 4 hours. Then, more solid sodium azide was added (13.56g) and was continued overnight at 80^{o}C. The 2-azidoethanol was extracted with diethyl ether (3 × 100mL), dried over $MgSO_4$, and filtered. The filtrate was concentrated by vacuum distillation, first at room temperature and then finally at 70^{o}C to afford 2-azidothanol in 74% yield as colorless oil.

^{1}H-NMR ($CDCl_3$, 600MHz) [ppm]: 3.801 (2H, t, -CH_2-O), 3.473 (2H, t, -CH_2-N_3), and 2.295 (1H, s, -OH). ATR-FTIR: 3346 cm^{-1}(O-H stretch), 2936 and 2879 cm^{-1} (C-H stretch), 2093 cm^{-1} (-N_3 stretch), and 1284 and 1061 cm^{-1} (C-O stretch).

5.3.6. Si(100) surface

5.3.6.1. Si(100)-H and Si(100)-Cl surfaces: Hydrogen and chlorine-terminated surfaces

A native silicon oxide, SiO_x, polished on one side, was cut into a dimension of ca. 1.5x2 or 1x1 cm^2 pieces. The wafer was cleaned repeatedly with CH_3OH and H_2O and dried under nitrogen. Organic contaminants were removed by treatment in a boiling mixture of sulfuric acid and hydrogen peroxide (H_2SO_4:H_2O_2 = 2:1, v/v) for 1 hour. The wafer was rinsed repeatedly with water and dried under argon. The silicon wafer was etched in a 40% NH_4F solution (oxygen-free) for 30min and rinsed with oxygen-free water for 5 seconds. The wafer was dried under nitrogen.

The reactive Si-Cl surface was made from freshly prepared Si-H surface using a Schlenk three-neck round bottom reaction flask. The first neck was connected to Cl_2 gas cylinder, the second neck was connected to the argon line, and the third neck was connected to the empty trap and passed through the bottle of solution of KOH for release and treated the excess of Cl_2 gas. The flask was heated at 80 ^oC with a slow and steady Cl_2 gas flow for 20min. The reaction flask was cooled down to room temperature and purged with argon for at least 30 minutes. There was no characterization of the reactive Si-Cl surface before subsequent reactions.

5.3.6.2. Si(100)~N_3 surface: Functionalization of Si(100)-H surface with 2-azidoethanol

A freshly prepared Si(100)-H surface was placed in a Schlenk reaction flask under argon. A mixture of 2-azidoethanol (1.5mL) and dried toluene (5.5mL) was degassed with argon for 60 min and transferred to the Schlenk reaction flask via a cannula. The reaction tube was heated at 80^oC for 72 hours. The wafer was cleaned via sequentially sonicating in HPLC grade toluene and then CH_2Cl_2 for a minimum of two cycles and then drying under vacuum.

5.3.6.3. Si(100)~N_3 surface: Functionalization of Si(100)-Cl surface with 2-azidoethanol

A freshly Si(100)-Cl surface was placed in a Schlenk reaction flask under argon. A mixture of 2-azidoethanol (1.5mL) in dried toluene (6mL) and anhydrous

pyridine (0.5mL) was degassed with argon for 60 min and transferred to the Schlenk reaction flask via a cannula. The flask was heated at 80^{o}C for 17 hours or 24 hours. The wafer was cleaned via sequentially sonicating in HPLC grade toluene and then CH_2Cl_2 for a minimum of two cycles and then drying under vacuum.

5.3.6.4. Si(100)-Click-Br surface: Click Si(100)~N_3 surface with propagyl bromide

A freshly prepared Si(100)-N_3 surface was placed in a Schlenk reaction flask under argon. A mixture of 80% solution of propagyl bromide in toluene, tetrakis(acetonitrile) copper(I) hexafluoro phosphate (2mg), and Na_2CO_3(6mg) ware added, just covering the silicon surface. The reaction was carried out at room temperature for 60 hours. The wafer was cleaned via sequentially sonicating in HPLC grade toluene and then CH_2Cl_2 for a minimum of two cycles and the drying under vacuum.

5.3.6.5. Si(100)-Click-OPV-alkyne surface: Click Si(100)~N_3 surface with T-OVP-dialkyne

A freshly prepared Si(100)~N_3 surface was placed in a Schlenk reaction flask under argon. A mixture of T-OPV-dialkyne (40mg), tetrakis(acetonitrile) copper(I) hexafluorophosphate (2mg), and Na_2CO_3(6mg) in dried toluene (7mL) was degassed with argon for 60 min and transferred to the Schlenk reaction flask via a cannula. The reaction was continued at room temperature for 48 hours. The

wafer was cleaned via sequentially sonicating in HPLC grade toluene and then CH_2Cl_2 for a minimum of two cycles and then drying under vacuum.

5.3.7. Si(111) surfaces

5.3.7.1. Si(111)-H and Si(111)-Cl surfaces: Hydrogen and chlorine-terminated surfaces

The preparation of Si(111)-H and Si(111)-Cl surfaces were performed in analogy to the preparation of Si(100) (see above). There was no characterization of the reactive Si-Cl surface.

5.3.7.2. Si(111)~N_3 surfaces: Functionalization of Si(111)-H surface with 2-azidoethanol

The preparation of a Si(111)~N_3 surface from Si(111)-H was performed in analogy to the Si(100)~N_3 surface from Si(100)-Cl (see above). The total reaction time was 24 hours at 80^{o}C. The wafer was cleaned via sequentially sonicating in HPLC grade toluene and then CH_2Cl_2 for a minimum of two cycles and then drying under vacuum.

5.3.7.3. Si(111)-N_3 surfaces: Functionalization of Si(111)-Cl surface with 2-azidoethanol

The preparation of a Si(111)~N_3 surface from Si(111)-Cl was performed in analogy to the Si(100)~N_3 surface from Si(100)-Cl (see above). The total reaction time was 24 hours at 80^{o}C. The wafer was cleaned via sequentially sonicating in

HPLC grade toluene and then CH_2Cl_2 for a minimum of two cycles and then drying under vacuum.

5.3.7.4. Si(111)-Click-OPV-alkyne surfaces: Click Si(111)~N_3 surface with OVP-dialkyne

The preparation of a Si(111)-Click-OPV-alkyne surface from Si(111)~N_3 was performed in analogy to the preparation of Si(100)-Click-OPV-alkyne from Si(111)~N_3 (see above). The wafer was cleaned via sequentially sonicating in HPLC grade toluene and then CH_2Cl_2 for a minimum of two cycles and then drying under vacuum.

5.3.7.5. Si(111)-Click-NH_2 surfaces: Click Si(111)~N_3 surface with propagyl amide

A freshly prepared Si(111)~N_3 surface was placed in a Schlenk reaction flask under argon. A solution of propagyl amide (3 drops), tetrakis(acetonitrile) copper(I) hexafluorophosphate (6mg), Na_2CO_3 (2-4mg), and HPLC grade DMSO (7ml) was degassed with argon for 30 min and transferred to the Schlenk reaction flask via a cannula. The reaction was continued at room temperature for 72 hours. The wafer was cleaned via sequentially sonicating in HPLC grade toluene and then CH_2Cl_2 for a minimum of two cycles and then drying under vacuum.

5.3.7.6. Si(111)-Click-OPV-CHO surface: Reaction of Si(111)-Click-NH_2 surface with OPV-dialdehyde

A freshly Si(111)-Click-NH_2 surface was placed in a mixture of trimer-dialdehyde-Hep (50mg), anhydrous $MgSO_4$ (200mg), and dried THF (3mL) in a Schlenk reaction flask. The reaction was continued at room temperature for 30 hours. The wafer was cleaned via sequentially sonicating in HPLC grade toluene and then CH_2Cl_2 for a minimum of two cycles and then drying under vacuum.

5.3.8. DSi(111) surfaces: Double side polished Si(111) surfaces

5.3.8.1. DSi(111)O_x surface: Original silicon wafer surface

A SiO_x covered silicon wafer, polished on both sides, was cleaned repeatedly with THF, H_2O, Acetone, CH_3OH, H_2O, CH_3OH, and H_2O, respectively and dried under argon. This surface was used for reference spectra and as background.

5.3.8.2. DSi(111)-H and DSi(111)-Cl surfaces: Hydrogen and chlorine-terminated surfaces

The preparation of DSi(111)-H and DSi(111)-Cl surfaces were performed in analogy to the preparation of Si(100)-H and Si(100)-Cl surfaces, respectively (see above). There was no characterization of the reactive Si-Cl surface.

5.3.8.3. DSi(111)~N_3 surfaces: Functionalization of DSi(111)-H surface with 2-azidoethanol

The preparation of a DSi(111)~N_3 surface from DSi(111)-H was performed in analogy to the Si(111)~N_3 and Si(100)~N_3 surfaces prepared from Si(111)-H and Si(100)-H (see above), with reaction times of 4, 24, or 48 hours. The functionalized wafer was cleaned via sequentially sonicating in HPLC grade toluene and then CH_2Cl_2 for a minimum of two cycles and then drying under vacuum.

5.3.8.4. DSi(111)~N_3 surface: Functionalization of DSi(111)-Cl surface with 2-azidoethanol

The preparation of a DSi(111)-N_3 surface from DSi(111)-Cl was performed in analogy to the Si(100)~N_3 surface prepared from Si(100)-Cl (see above). In one approach, the reaction times were 17 and 24 hours at 80^{o}C. In another approach, the reaction time was 24 hours at 50^{o}C.

5.3.8.5. DSi(111)-Click-Br surface: Click DSi(111)~ surface with propagyl bromide

The preparation of a DSi(111)-Click-Br surface from DSi(111)~N_3 surface (made from Si-Cl at 80^{o}C for 17 hours) was performed in analogy to the Si(100)-Click-Br surface (see above). The wafer was cleaned via sequentially sonicating in HPLC grade toluene and then CH_2Cl_2 for a minimum of two cycles and then drying under vacuum.

5.3.8.6. DSi(111)-Click-OPV-dialkyne surface: Click DSi(111)~N_3 surface with OVP-dialkyne

The preparation of a DSi(111)-Click-OPV-alkyne surface from the Si~N_3 surface (made from Si-Cl at 80^{o}C for 24hours) was performed in analogy to the preparation of Si(100)-Click-OPV-alkyne, with a reaction time of 48 hours at room temperature. The wafer was cleaned via sequentially sonicating in HPLC grade toluene and then CH_2Cl_2 for a minimum of two cycles and then drying under vacuum.

5.3.8.7. DSi(111)-Click-NH_2 surface: Click DSi(111)~N_3 surface with propagyl amine

The preparation of a DSi(111)-Click-NH_2 surface from Si~N_3 surface and propagyl amine was performed in analogy to the preparation of the Si(111)-Click-NH_2 surface (see above). The solvent was dried toluene (7mL). The wafer was cleaned via sequentially sonicating in HPLC grade toluene and then CH_2Cl_2 for a minimum of two cycles and then drying under vacuum.

6. Stepwise functionalization of Si-H/Si-Cl surfaces using urethane chemistry ("click-like")

6.1. Overview

This chapter highlights the reaction sequence of small, simple, and reactive molecules to build up reactive surfaces step-wise using "click-like" reaction. The rigid rod oligomerT-OPV-CH_2OH **17** is attached last.

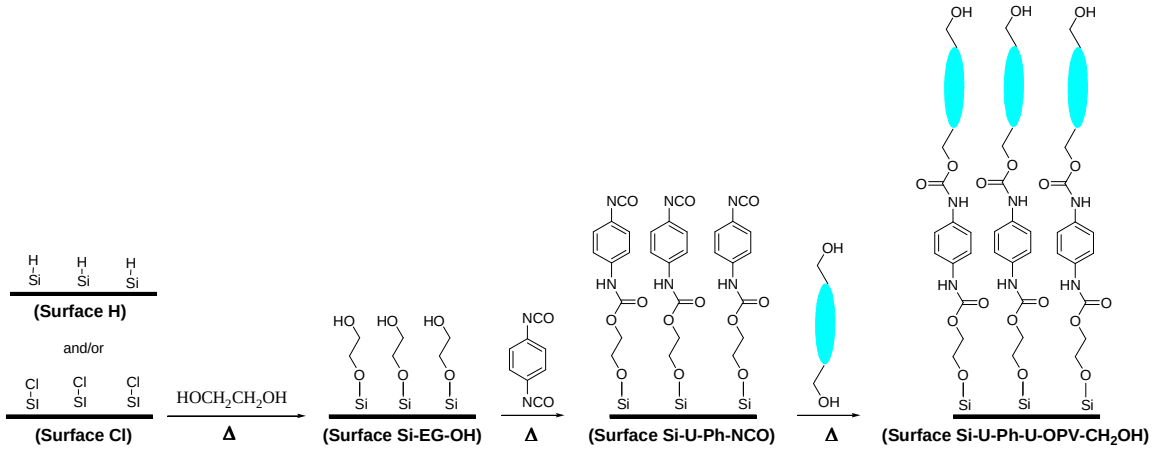

Scheme 6.1. Reactions of OPVs on Si-H and/or Si-Cl surfaces using ethylene glycol and 1,4-phenylene diisocyanate as linkers via "click-like" chemistry.

Specifically, this approach involves the synthesis of Si(111)-EG-OH functional surfaces (Scheme 6.1) from Si(111)-H and/or Si(111)-Cl surfaces with ethylene glycol ($HOCH_2CH_2OH$: HO-EG-OH), then using a "click-type" reaction (in this case urethane chemistry) to react the Si(111)-EG-OH functional surfaces with 1,4-phenylene diisocyanate (OCN-Ph-NCO) to afford Si(111)-U-Ph-NCO surfaces (Scheme 6.1). Subsequent reaction of the Si(111)-U-Ph-NCO surfaces

with an OH-functional OPV building block (T-OPV-CH_2OH **17**) affords Si(111)-U-Ph-U-OPV-CH_2OH surfaces (Scheme 6.1) in a “double click” approach. The resulting monolayers are characterized by means of XPS and AFM.

6.2. Surfaces: Results and discussion

6.2.1. Si(111)-H and Si(111)-Cl

The Si(111)-H and Si(111)-Cl surfaces were prepared as described above (Scheme 4.2, chapter 4).

6.2.2. Si(111)-EG-OH

6.2.2.1. Without Me_3SiCl

A freshly etched Si(111)-H was placed in anhydrous ethylene glycol (degassed at 95^oC with argon for 30 min) and heated at 160^oC for 48 hours. Representative overlaid XPS spectra of surfaces Si(111)-EG-OH and Si(111)-H are shown in figure 6.1 (top, green). The Si(111)-EG-OH features 2s and 2p peaks of Si at ~151 and ~99eV respectively and O-bound Si (SiO_x) at ~104 and 154eV. The (1s) peaks of C and O from the attached molecules are observed at ~285 and 533eV respectively. Compared to the Si(111)-H surface, the relative peak intensities of Si decrease and the relative intensities from C and O increase, indicating successful surface functionalization. However, the XPS also showed an unexpected peak at 496eV and O bound Si (SiO_x) at ~103eV (narrow scan, figure 6.1, green). Due to the high reaction temperature (160^oC), ethylene glycol might be condensing. Also, traces of water seem to be present and need to be

removed to afford higher surface coverage. As it is impossible to completely remove water traces from ethylene glycol by degassing, this water is most likely reacting with Si-H, resulting in the SiO_x peak (O bound Si).

6.2.2.2. With Me_3SiCl

Trimethylchlorosilane (Me_3SiCl) was used as a chemical scavenger in an attempt to remove trace amounts of water and fluorides. The byproducts formed are bis-trimethylsilyl ether and fluorotrimethylsilane, respectively. These are stable and do not react with the Si-H surface.[47]

The freshly etched Si-H surface was placed in anhydrous ethylene glycol with Me_3SiCl and heated at 95^oC for 24 hours under inert gas. Representative overlaid XPS spectra of Si(111)-EG-OH surfaces are shown in figure 6.1 (red). The narrow scan shows a shoulder at ~102eV (O-bound Si peak) that is is much smaller than in the case discussed above without using Me_3SiCl. However, there is a small shoulder peak from SiO_x.

6.2.2.3. With Me_3SiCl with additional degassing

An additional degassing step leads to success, indicated by absence of the peak at ~103eV (see overlaid spectra figure 6.1, blue).

A representative AFM image is shown in figure 6.2, together with a height trace of a respective cross-section. The roughness (RMS) of Si(111)-EG-OH is determined as 0.40nm over an area of 1.0μm^2, which is in agreement with the roughness (RMS) of Si(111)-H. The calculated height of an extended Si-CH_2CH_2-

OH is 0.60nm (see experimental part) and within the range of the surface roughness.

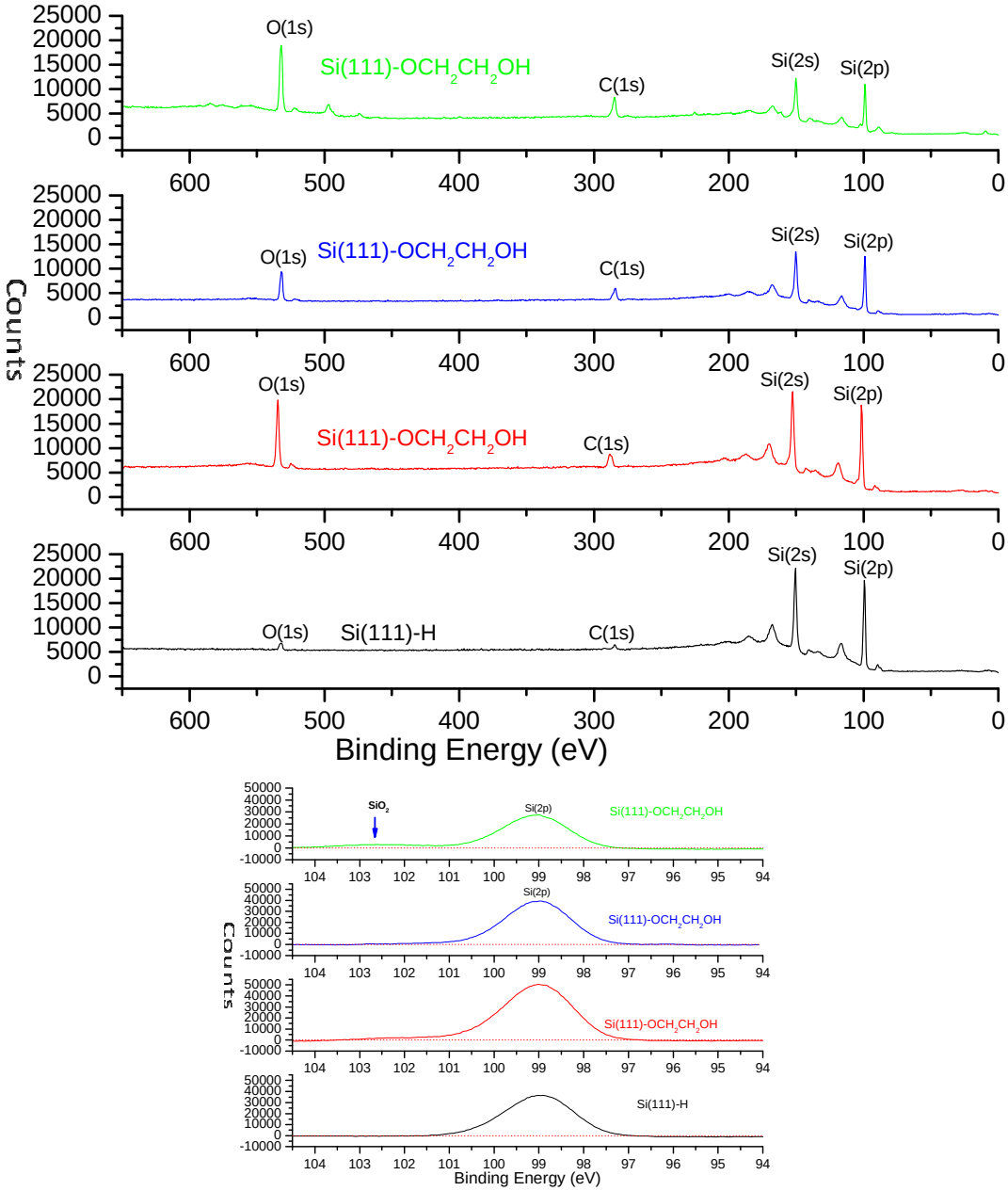

Figure 6.1. Representative XPS spectra overlaid; survey scans (top) and narrow scans (bottom) of Si(111)-EG-OH (green: without Me_3SiCl, blue: with Me_3SiCl with additional degassing, and red: with Me_3SiCl) and Si(111)-H surfaces (black).

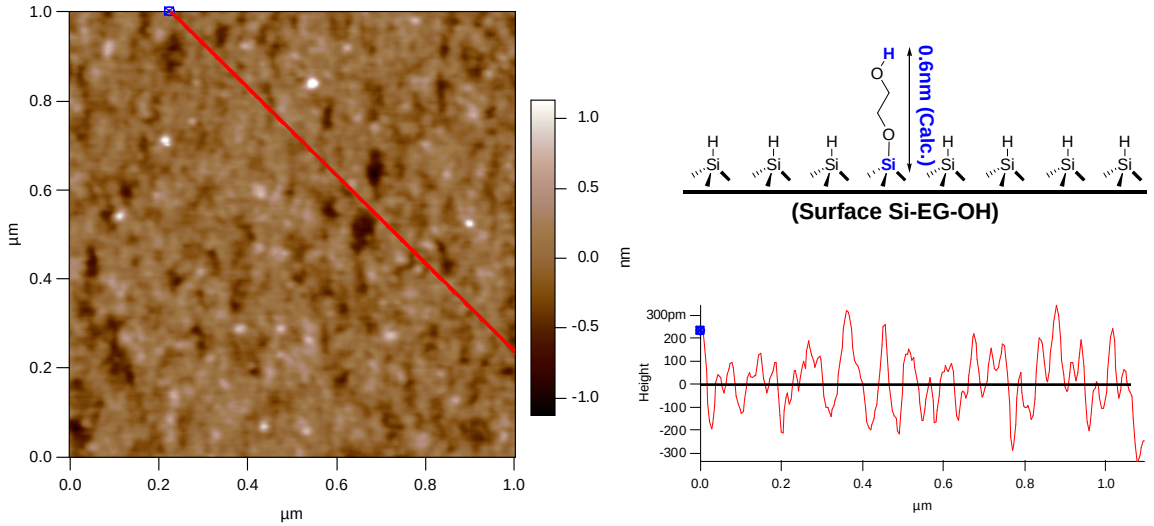

Figure 6.2. AFM image of Si(111)-EG-OH surface.

6.2.3. Si(111)-U-Ph-NCO

The Si(111)-EG-OH surface was placed in a suspension of 1,4-phenylene diisocyanate in dried toluene and heated at 50^{o}C or 70^{o}C for 8h or 24h, respectively, under inert gas atmosphere. The Si-U-Ph-NCO surface was removed and cleaned via sequential sonication in dried toluene and CH_2Cl_2 for a minimum of two cycles and then drying in a glove-box, before subjecting it to subsequent reaction steps.

6.2.4. Si(111)-U-Ph-U-OPV-CH_2OH

A freshly prepared Si(111)-U-Ph-NCO surface was placed in a solution of T-OPV-OH **17** in dried toluene and heated at 50^{o}C for 9 or 24 hours under inert gas atmosphere. Representative reaction conditions are summarized in table 6.1.

Table 6.1. Representative reaction conditions for Si(111)-U-Ph-U-OPV-CH_2OH surfaces.

Entry	T-OPV-OH (mg, mmol)	Toluene (mL)	T (^oC)	t (h)
1	(2.0, 1.9 x 10^{-3})	1.0	50	9
2	(4.0, 3.8 x 10^{-3})	8.0	50	24

Overlaid XPS spectra of representative surfaces Si(111)-U-Ph-U-OPV-CH_2OH (table 6.1. entry 1), Si(111)-EG-OH, and Si(111)-H are shown in figure 6.3. The Si(111)-U-Ph-U-OPV-CH_2OH feature 2s and 2p peaks of Si at ~151 and ~99eV respectively and O-bound Si (SiO_x) at ~103 and 154eV. The (1s) peaks of C and O from the attached molecules are observed at ~285 and 533eV respectively. N (1s) is observed at ~400eV. Compared to the Si(111)-EG-OH surface, the relative peak intensity of Si decreases and the relative intensities of C and O increase. Together with the appearance of the nitrogen peak and the AFM results (see below) this indicates successful attachment of T-OPV-OH. Narrow scans (Figure 6.3. bottom) reveal the presence of SiO_x at ~103eV on the Si(111)-U-Ph-U-OPV-OH surface, whereas this peak is insignificant in the Si(111)-EG-OH surface. A possible explanation is that the Si(111)-EG-OH surface contains unreacted Si-H that are “buried” under the flexible O-CH_2CH_2OH chains. Upon subsequent reactions, these chains stretch out, thus leaving uncovered Si-H and providing access for moisture and oxygen during the workup and subsequent sample handling.

Three AFM images of a surface Si(111)-U-Ph-U-OPV-CH_2OH (Table 6.1, entry 1) are shown in figure 6.4 together with cross-sectional height traces. Depicted are

three scans of the same area, using scan angles 0, 45, and 90 degrees relative to the x-axis. The different scan angles are used to avoid artefacts. The observed features change with scan angles, and hence can be considered as “real”. The roughness (RMS) is determined as 1.0nm over an area of 1μm^2.

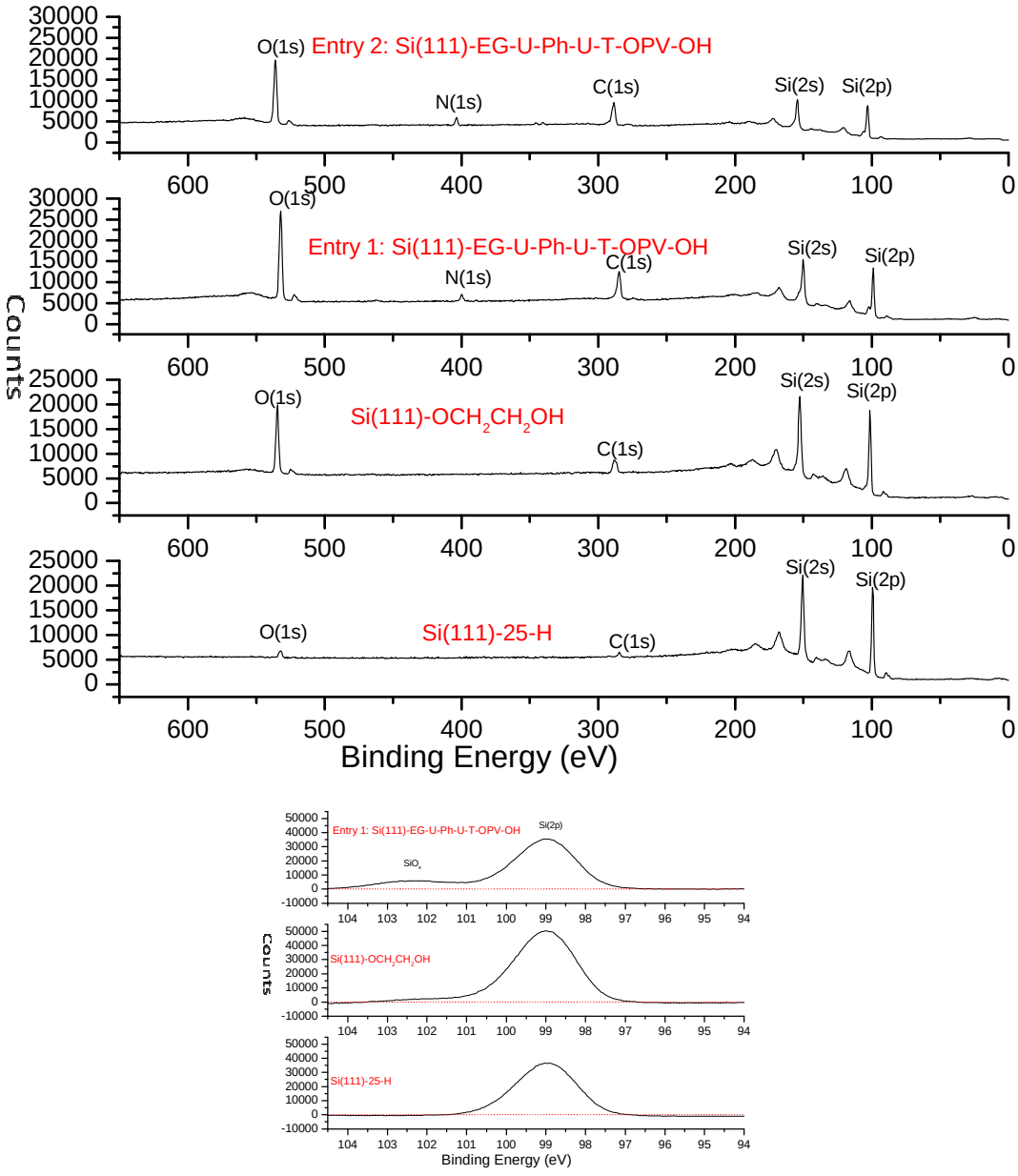

Figure 6.3. Representative XPS spectra overlaid; survey scans (top) and narrow scans (bottom) of Si(111)-U-Ph-U-OPV-CH_2OH, Si(111)-EG-OH, and Si(111)-H surfaces.

The height traces reveal elevations that consistently measure ~ 3.7nm. Assuming a stretched conformation, the distance from Si (anchor point) to the H of the unreacted -OH of the OPV fragment is calculated at 3.5 nm (schematic insert) and in excellent agreement.

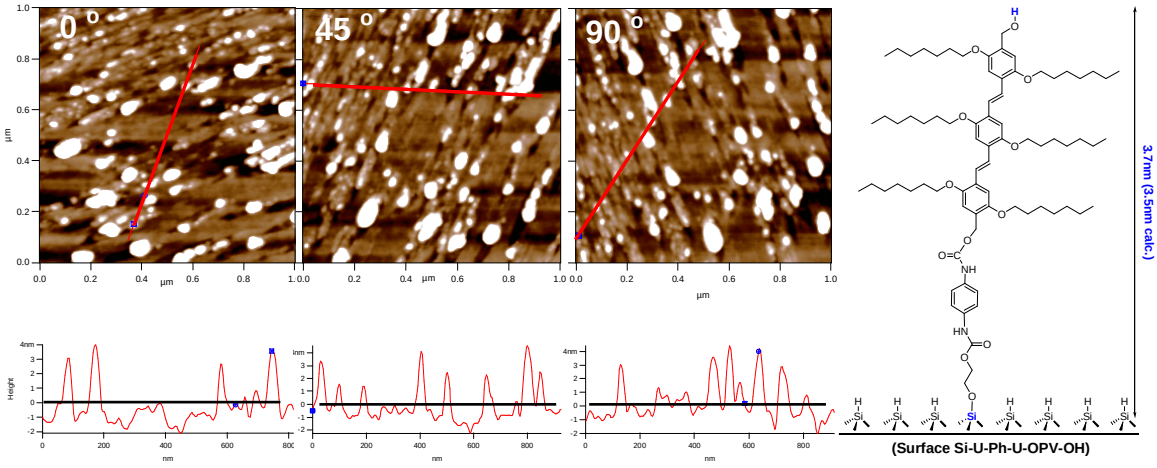

Figure 6.4. AMF images of Si(111)-U-Ph-U-OPV-CH_2OH surface (entry **1**) with different scan angles relative to x-axis.

Changing the reaction conditions (Table 6.1. entry 2), i.e. lowering the OPV concentration, and using higher solvent volume, together with increased reaction time, lead to more extended areas with functionalization. An AFM image of the surface from entry 2 is shown in figure 6.5, together with a cross-sectional height trace, revealing extended elevations with heights of ~3.64nm. The scan angle was 0 degree relative to the x-axis in the depicted AFM image. The surface roughness (RMS) was determined as 0.64nm over a 1.20μm^2 area.

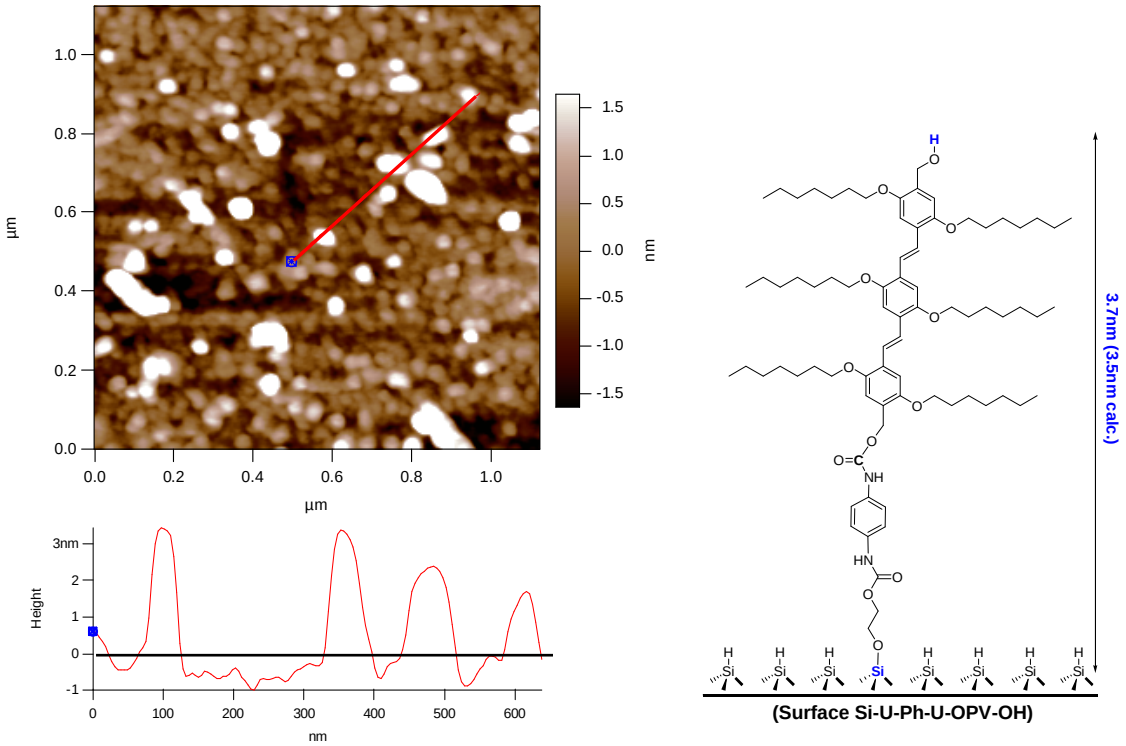

Figure 6.5. AFM image of Si(111)-U-Ph-U-OPV-CH_2OH surface (entry **2**).

Representative overlaid XPS spectra of Si(111)-U-Ph-U-OPV-CH_2OH surfaces are shown in figure 6.3. (top). Comparing the Si(111)-U-Ph-U-OPV-OH surfaces prepared at 50^{o}C for 9 hours (entry 1) and at 50^{o}C at 24 hours (entry 2) (Figure 6.3.) show higher surface coverage following longer reaction and reduction of the OPV concentration. It also seems that fewer random surface attachments are observed (number per unit are), rather that the aggregates grow preferentially next to existing attachments, indicating a templated growth. This could also explain the observation of higher surface coverage in the XPS, due to densely packed aggregates.

6.3. Experimental

6.3.1. General information

All experiments using air/moisture sensitive materials were carried out with high purity argon using standard Schlenk techniques. All glassware was cleared and dried for at least 24h in an oven at 120^{o}C prior to use.

6.3.2. Chemicals

Anhydrous ethylene glycol 99.8% (water constant <0.003%) and 1,4-phenylene diisocyanate 99% were purchased from Sigma-Aldrich. Trimethylchlorosilane was purchased from Gelest. HPLC grade methanol, ethanol, toluene, and dichloromethane were purchased from Fisher Scientific. Millipore (18.2MΩ-cm and 6 TOC) water was used for rinsing the samples (from Millipore system). All other solvents (THF, toluene, CH_2Cl_2, and hexanes) were dried and degassed, using a "Pure Solv" solvent purification system (using activated alumina, copper catalyst, molecular sieves columns) by Innovative Technology Inc. before use. Single-sided polished Si(111; n-type As-doped, 500 $\pm$ 25 μm thickness, 0.001-0.005 Ω.cm resistivity, 4$^{o}\pm$0.5^{o} off-cut), and double-side polished Si(111; float zone grade, n-type P-doped, 300 $\pm$ 25 μm thickness, 24-35 Ω.cm resistivity) were purchased from University WAFER.

6.3.3. Instrumentation

An Atomic Force Microscope (AFM) from Asylum Research was used with an MFP-3D^{TM} SA extended head, 90μm XY scanner, TS 150 active vibration

isolation table, and isolated in a Herzan AEK 2002 acoustic hood. Samples were scanned in contact mode with an Olympus cantilever. The scan direction was parallel to the x-axis. The images were processed and analyzed by IGOR Pro 6.03A/MFP3D080129. All images were routinely flattened.

X-ray photoelectron spectra (XPS) were recorded with an Omicron Surface Science Model 150 XPS spectrometer equipped with an Al or Mg Kα source (Omicron DAR 400) without monochromator, and with a concentric hemispherical analyzer (Omicron EA 125), and multichannel detector. No electron flood gun was employed. The pressure in the analytical chamber during analysis was approximately 5 $x10^{-9}$ Torr.

6.3.4. Calculated molecular heights

In order to correlate the heights of molecular attachments on the Si-surfaces as determined by AFM with actual dimensions of the molecules used for attachment, the molecules structures were optimized using Chem3D Ultra 9.0 and distances were calculated.

Models H_3Si-O-CH_2-CH_2-OH (A), H_3Si-OCH_2CH_2-O-CONH-Ph-NCO (B), and HO-CH_2-T-OPV-CH_2-OH (C) were used and optimized in regard to structure of height trace of the Si-EG-UrethaneT-OH-Hep surface.

For Si-CH_2CH_2-OH the height trace distance from Si to H (as highlighted with color) was calculated as 0.6nm, which is within the measured surface roughness. The corresponding value height trace for the Si-EG-Urethane (as highlighted with color) was calculated as 1.4nm, using the distance Si and C (the reaction of

isocyanate with alcohol occurred) in the model $H_3Si\text{-}OCH_2CH_2\text{-}O\text{-}CONH\text{-}Ph\text{-}NCO$. The calculated height trace for $HO\text{-}CH_2\text{-}T\text{-}OPV\text{-}CH_2\text{-}OH$ from O to H is 2.1nm. Therefore, the total height trace of $Si\text{-}U\text{-}Ph\text{-}U\text{-}OPV\text{-}CH_2OH$ is 3.5nm (1.4nm + 2.1nm), as shown in scheme 6.2.

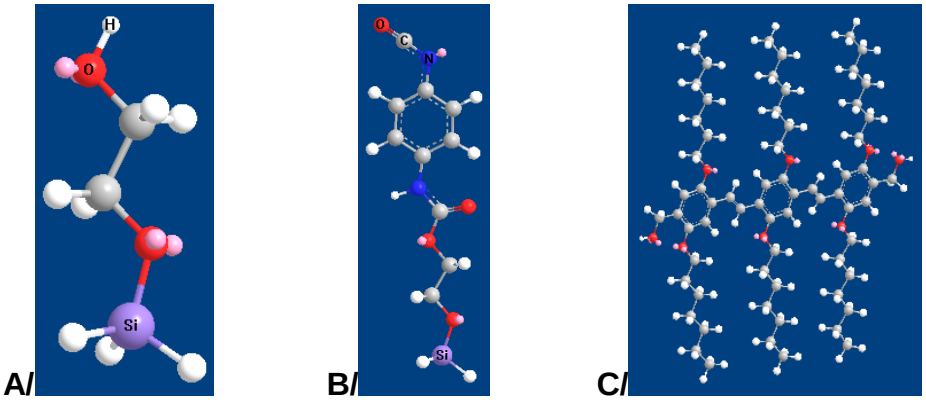

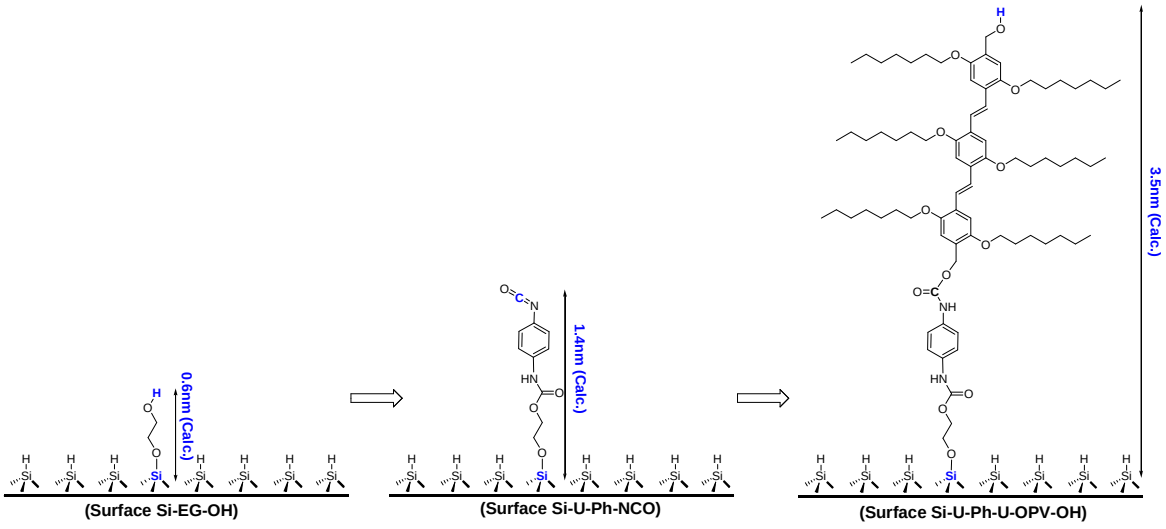

Scheme 6.2. Synthesis of model surface $Si\text{-}U\text{-}Ph\text{-}U\text{-}OPV\text{-}CH_2OH$.

6.3.5. Si(111)-EG-OH surface: Functionalization of Si(111)-H surface with ethylene glycol

6.3.5.1. Without Me_3SiCl

A freshly prepared Si(111)-H was placed in a Schlenk reaction flask under argon. Anhydrous ethylene glycol (20mL) was degassed at 95^{o}C with argon for 30 min and transferred to the Schlenk reaction flask via a cannula. The flask was heated at 160^{o}C for 48 hours. The wafer was removed and cleaned via sequentially sonicating in HPLC grade CH_3OH, CH_3CH_2OH, and water for a minimum of two cycles and then drying under vacuum.

6.3.5.2. With Me_3SiCl

A freshly prepared Si(111)-H was placed in a Schlenk reaction flask under argon. Anhydrous ethylene glycol (20mL) was degassed by three freeze-pump-thaw cycles. Trimethylchlorosilane (1mL) was added and degassed with nitrogen for another 15min. The Si-H surface was placed in the reaction flask and the reaction continued at 95^{o}C for 24 hours. The wafer was removed and cleaned via sequentially sonicating in HPLC grade CH_3OH for a minimum of four cycles and then drying under vacuum.

6.3.5.3. With Me_3SiCl with additional degassing

A freshly prepared Si(111)-H was placed in a Schlenk reaction flask under argon. Anhydrous ethylene glycol (30mL) was degassed by three freeze-pump-thaw cycles. Trimethylchlorosilane (2mL) was added and degassed with nitrogen for

another 15min. The Si-H surface was placed in the reaction flask and degassed with argon for another 30min to remove any trace of oxygen on the surface and the reaction was performed at 90^{o}C for 20 hours. The wafer was removed and cleaned via sequentially sonicating in HPLC grade CH_3OH for a minimum of four cycles and then drying under vacuum.

6.3.6. Si(111)-U-Ph-NCO: Functionalization of Si(111)-EG-OH surface with 1,4-phenylene diisocyanate

A suspension of 1,4-phenylene diisocyanate (0.025g) in dried toluene (5mL) was prepared in a glove box. The Si(111)-EG-OH surface was placed in the mixture in a reaction vessel and heated at 50^{o}C or 70^{o}C for 8h or 24h, respectively. The wafer was removed and cleaned via sequentially in dried HPLC grade of toluene and CH_2Cl_2 for a minimum of two cycles and then drying in glove box. The reactive isocyanate surface was not characterized and further functionalized with T-OPV-CH_2OH.

6.3.7. Si(111)-U-Ph-U-OPV-CH_2OH surface: Functionalization of Si(111)-U-Ph-NCO surface with T-OPV-CH_2OH

A freshly prepared Si(111)-U-Ph-NCO surface was placed in a solution of T-OPV-CH_2OH (2mg) in dried toluene (1mL) in a reaction vessel under argon. The reaction vessels were heated at 50^{o}C for 9 and 24 hours. The wafer was removed and cleaned via sequentially sonicating in HPLC grade of toluene and CH_2Cl_2 for a minimum of two cycles and then drying under vacuum.

7. References

1. Waltenburg, H. N.; Yates, J. T. *Chem. Rev.* **1995**, *95*, 1589.

2. Hamers, R. J.; Wang, Y. *Chem. Rev.* **1996**, *96*, 1261.

3. (a) Buriak, J. M. *Chem. Rev.* **2002**, *102*, 1271. (b) Stewart, M. P.; Buriak, J. M. *Comments Inorg. Chem.* **2002**, *23*, 179. (c) Stewart, M. P.; Buriak, J. M. *Adv. Mater.* **2000**, *12***,** 859. (d) Buriak, J. M. *Chem. Commun,.* **1999**, 1051. (e) Wayner, D. D. M.; Wolkow, R. A. *J. Chem. Soc., Perkin Trans. 2*, **2002**, 23. (f) Sieval, A. B.; Linke, R.; Zuilhof, H.; Sudholter, E. J. R. *Adv. Mater.* **2000**, *12*, 1457. (g) Claland, G.; Horrocks, B.R.; Houlton, A. *J. Chem. Soc. Faraday Trans.,* **1995**, *91*, 4001.

4. (a) Hu, D. Q.; MacPherson, C. D.; Leung, K. T. *Surf. Sci.* **1992**, *273*, 21. (b) MacPherson, C. D.; Hu, D. Q.; Doan, M.; Leung, K. T. *Surf. Sci.* **1994**, *310*, 231.

5. Albert, K. J.; Lewis, N. S.; Schauer, C. L.; Sotzing, G. A.; Stitzel, S. E.; Vaid, T. P.; Walt, D. R. *Chem. Rev.* **2000**, *100*, 2595.

6. Freeman, W. M.; Robertson, D. J.; Vrana, K. E. *Biotechniques* **2000**, *29*, 1042.

7. Hansen, K. M.; Ji, H. F.; Wu, G. H.; Datar, R.; Cote, R.; Majumdar, A.; Thundat, T. *Anal. Chem.* **2001**, *73*, 1567.

8. Zee, F.; Judy, J. W. *Sensor Actuators B* **2001**, *72*, 120.

9. Birkinshaw, K. *Int. Rev. Phys. Chem.* **1996**, *15*, 13.

10. Eijkel, J. C. T.; Prak, A.; Cowen, S.; Craston, D. H.; Manz, A. *J. Chromatogr. A* **1998**, *815*, 265. Drott, J.; Lindstrom, K.; Rosengren, L.; Laurell, T. *J. Micromech. Microeng.* **1997**, *7*, 14.

11. Weigl, B. H.; Yager, P. *Science* **1999**, *283*, 346.

12. Maboudian, R. *Surf. Sci. Rep.* **1998**, *30*, 209.

13. Higashi, G. S.; Chabal, Y. J.; Trucks, G. W.; Raghavachari, K. *Appl. Phys. Lett.* **1990**, *56*, 656.

14. Higashi, G. S.; Becker, R. S.; Chabal, Y. J.; Becker, A. J. *Appl. Phys. Lett.* **1991**, *58*, 1656.

15. Newton, T. A.; Boiani, J. A.; Hines, M. A. *Surf. Sci.* **1999**, *430*, 67.

16. Hessel, H.E.; Feltz, A.; Reiter, M.; Memmert, U.; Behm, R.J. *Chem. Phys. Lett.* **1991**, *186*, 275.

17. Allongue, P.; Henry de Villeneuve, C.; Morin, S.; Boukherroub, R.; Wayner, D.D.M. *Electrochim. Acta*, **2000**, 45, 4591.

18. Arima, K.; Endo, K.; Kataoka, T.; Oshikane, Y.; Inoue, H.; Mori, Y. *Appl. Phys. Lett.* **2000**, 76, 463.

19. Chabal, Y.J. Higashi, G.S.; Raghavachari, K,; Burrows, V.A. *J. Vac. Sci. Technol., A.* **1989**, 7, 2104.

20. Bansal, A.; Li, X.; Lauermann, I.; Lewis, N. S.; Yi, S. I.; Weinberg, W. H. *J. Am. Chem. Soc.* **1996**, *118*, 7225.

21. He, J.; Patitsas, S. N.; Preston, K. F.; Wolkow, R. A.; Wayner, D. D. M. *Chem. Phys. Lett.* **1998**, *286*, 508.

22. Zhu, X.-Y.; Boiadjiev, V.; Mulder, J. A.; Hsung, R. P.; Major, R. C. *Langmuir* **2000**, *16*, 6766.

23. Luo, H.; Chidsey, C. E. D.; Chabal, Y. *Mater. Res. Soc. Proc.* **1997**, *477*, 415.

24. Bansal, A.; Li, X.; Lauermann, I.; Lewis, N. S.; Yi, S. I.; Weinberg, W. H. *J. Am. Chem. Soc.* **1996**, *118*, 7225.

25. Bansal, A.; Lewis, N.S. J. Phys. Chem. B 1998, 102, 1067. (c) Bansal, A.; Lewis, N.S. J. Phys. Chem. B **1998**, *102*, 4058.

26. Boukherroub, R.; Bensebaa, F.; Morin, S.; Wayner, D.D.M. Langmuir **1999**, *15*, 3831.

27. Linford, M. R.; Chidsey, C. E. D. *J. Am. Chem. Soc.* **1993**, *115*(26), 12631.

28. Linford, M. R.; Fenter, P.; Eisenberger, P. M.; Chidsey, C. E. D.; *J. Am. Chem. Soc.,* **1995**, *117(11)*, 3145.

29. Chatgilialoglu, C. *Acc. Chem. Res.* **1992**, 25*(4)*, 188.

30. Labinger, J. A. *In Comprehensive Organic Synthesis*, Trost, B. M., Fleming, I.; Eds.; Pergamon: New York, **1991**, *8*, 699.

31. Fleming, I. *In Comprehensive Organic Chemistry*; Jones, N., Ed.; Pergamon: New York, **1979**, *3*, 568.

32. (a) Terry, J.; Linford, M. R.; Wigren, C.; Cao, R.; Pianetta, P.; Chidsey, C. E. D. *Appl. Phys. Lett.* **1997**, *71*, 1056. (b) Terry, J.; Mo, R.; Wigren, C.; Cao, R.; Mount, G.; Pianetta, P.; Linford, M. R.; Chidsey, C. E. D. *Nucl. Instrum. Methods Phys. Res., Sect. B* **1997**, *133*, 94. (c) Terry, J.; Linford, M. R.; Wigren, C.; Cao, R.; Pianetta, P.; Chidsey, C. E. D. *J. Appl. Phys.* **1999**, *85*, 213.

33. Cicero, R. L.; Linford, M. R.; Chidsey, C. E. D. *Langmuir* **2000**, *16*, 5688.

34. Sieval, A. B.; van den Hout, B.; Zuilhof, H.; Sudhölter, E. J. *Langmuir* **2000**, *16*, 2987.

35. Sieval, A. B.; van den Hout, B.; Zuilhof, H.; Sudhölter, E. J. R. *Langmuir* **2001**, *17*, 2172.

36. Zhang, L.; Wesley, K.; Jiang, S. *Langmuir* **2001**, *17*, 6275.

37. Henry de Villeneuve, C.; Pinson, J.; Bernard, M. C.; Allongue, P. *J. Phys. Chem. B* **1997**, *101*, 2415.

38. Allongue, P.; Delamar, M.; Desbat, B.; Fagebaume, O.; Hitmi, R.; Pinson, J.; Saveant, J.-M. J. Am. Chem. Soc., **1997**, *119*, 201.

39. Allongue, P.; Henry de Villeneuve, C.; Pinson, J.; Ozanam, F.; Chazalviel, J.N. Wallart, X. Electrochim. Acto, **1998**, *43*, 2791.

40. Brook, M. A. *Silicon in Organic, Organometallic, and Polymer Chemistry*; Wiley: New York, **2000**.

41. *The Chemistry of Organic Silicon Compounds*; Patai, S., Rappoport, Z., Eds.; John Wiley and Sons: New York, **1989**.

42. Faucheur, A.; Yang, F.; Allongue, P.; Henry de Villeneuve, C.; Ozanam, F.; Chazalviel, J.-N. *Appl. Phys. Lett.* **2006**, *88*, 193123.

43. Sung, M.M.; Kluth, G.J.; Yauw, O.W.; Maboudian R. *Langmuir*, **1997**, *13*, 6164.

44. Dusciac, D.; Chazalviel, J.-N.; Ozanam, F.; Allongue, P.; Henry de Villeneuve, C. Surface science, **2007**, *601*, 3961.

45. Cleland, G.; Horrocks, B. R.; Houlton, A. *J. Chem. Soc., Faraday Trans.* **1995**, *91*, 4001.

46. Effenberger, F.; Gotz, G.; Bidlingmaier, B.; Wezstein, M. *Angew. Chem., Int. Ed.* **1998**, *37*, 2462.

47. Boukherroub, R.; Morin, S.; Sharpe, P.; Wayner, D. D. M.; Allongue, P. *Langmuir* **2000**, *16,* 7429.

48. Allongue, P.; Costa-Kieling, V.; Gerischer, H. *J. Electrochem. Soc.* **1993**, *140*, 1018.

49. Wagner, P.; Nock, S.; Spudich, J.; Volkmuth, W. D.; Chu, S.; Cicero, R. L.; Wade, C. P.; Linford, M. R.; Chidsey, C. E. D. *J. Struct. Biol.* **1997**, *119*, 189.

50. Cicero, R. L.; Wagner, P.; Linford, M. R.; Hawker, C. J.; Waymouth, R. M.; Chidsey, C. E. D. *Polym. Prepr.* **1997**, *38*, 904.

51. Sieval, A.B.; Demirel, A.L.; Nissink J.W.M.; Linford, M.R.; Maas, J.H.v.d. Jeu, W.H.d.; Zuilhof, H.; Sudholter, E.J.R. *Langmuir* **1998**, *14*, 1759.

52. Boukherroub, R.; Wayner, D. D. M. *J. Am. Chem. Soc.* **1999**, *121*, 11513.

53. Strother, T.; Cai, W.; Zhao, X.; Hamers, R.J.; Smith, L.M. *J. Am. Chem. Soc.* **2000**, *122*, 1205.

54. Strether, T.; Hamers, R.J.; Smith, L.M. *Nucleic Acids Res.* **2000**, *28*, 3535.

55. Bocking, T.; Kilian, K.; Gaus, K.; Gooding, J. J. *Langmuir* **2006**, *22*, 3494.

56. Voicu, R.; Boukherroub, R.; Bartzoka, V.; Ward, T.; Wojtyk, J.T.C.; Wayner, D.D.M. *Langmuir*, **2004**, *20*, 11713.

57. (a) Drefahl, G.; Plötner, G. *Chem. Ber.* **1958**, *91*, 1274. (b) Drefahl, G.; Plötner, G. *Chem. Ber.* **1961**, *94*, 907.

58. Müllen, K.; Wegner, G. (Eds.), *Electronic Materials: The Oligomer Approach*, Wiley-VCH, Weinheim, **1998**.

59. Burroughes, J. H.; Bradley, D. D. C.; Brown, A. R.; Marks, R. N.; Mackay, K.; Friend, R. H.; Burn, P. L.; Holmes, A. B. *Nature*, 1990, **347**, 539.

60. Schenk, R.; Gregorius, H.; Meerholz, K.; Heinze J.; Müllen, K. *J. Am. Chem. Soc.* **1991**, *113*, 2634.

61. Braun, D.; Heeger, A. J. *Appl. Phys. Lett.* **1991**, *58*, 1982.

62. Sakamoto, A.; Furukawa, Y.; Tasumi, M. *J. Phys. Chem.* **1994**, *98*, 4635.

63. Burn, P. L.; Holmes, A. B.; Kraft, A.; Bradley, D. D. C.; Brown, A. R.; Friend, R. H.; Gymer, R. W. *Nature* **1992**, *356*, 47.

64. Hilberer, A.; Brouwer, H. J.; Van der Scheer, B. J.; Wildeman, J.; Hadziioannou, G. *Macromolecules* **1995**, *28*, 4525.

65. Samuel, I. D. W.; Rumbles, G.; Collison, C. J. *Phys. Rev. B* **1995**, *52*, 11573.

66. Van Hutten, P. F.; Krasnikov, V. V.; Hadziioannou, G. *Acc. Chem. Res.* **1999**, *32*, 257.

67. Braun, D.; Staring, E. G. J.; Demandt, R. C. J. E.; Rikken, G. L. J.; Kessener, Y. A. R. R.; Venhuizen, A. H. J. *Synth. Met.* **1994**, *66*, 75.

68. Greenham, N. C.; Samuel, I. D. W.; Hayes, G. R.; Phillips, R. T.; Kessener, Y. A. R. R.; Moratti, S. C.; Holmes, A. N.; Friend, R. H. *Chem. Phys. Lett.* **1995**, *241*, 89.

69. Cao, Y.; Parker, I. D.; Yu, G.; Zhang, C.; Heeger, A. J. *Nature* **1999**, *397*, 414.

70. Thorn-Csányi, E.; Kraxner P. *macromol. Rapid. Commun.* **1995**, 16, 147.

71. Stalmach, U.; Kolshorn, H.; Brehm I.; Meier, H. *Liebigs Ann.* **1996**, 1449.

72. Oelkrug, D.; Tompert, A.; Egelhaaf, H.-J.; Hannack, M.; Steinhuber, E.; Hohloch, M.; Meier, H.; Stalmach, U. *Synth. Met.* **1996**, *83*, 231.

73. Chua, B.S.; Cacialli, F.; Davies, J. E.; Feeder, N.; Friend, R. H.; Holmes, A. B.; Marseglia, E. A.; Moratti, S. C.; Brédas, J. –L.; dos Santos, D. A. *New luminescent PPV derivatives for LED applications***.** *Mat Res Soc Symp Proc: Symposium J.* **1998**, *488***,** 87.

74. Peeters, E; Marcos Ramos, A.; Meskers, S. C. J. Janssen, R. A. J. *J. Chem. Phys.* **2000**, *112*, 9445.

75. van Hal, P. A.; Beckers, E. H. A.; Peeters, E.; Apperloo, J. J.; Janssen, R. A. J. *Chem. Phys. Lett.* **2000**, *328*, 403.

76. Grozema, F. C.; Candeias, L. P.; Swart, M.; van Duijnen, P. T.; Wildeman, J.; Hadziiannou, G.; Siebbeles, L. D. A.; Warman, J. L. *J. Chem. Phys.* **2002**, *117*, 11366.

77. Granier, T.; Thomas, E. L.; Karasz, F. E. *J. Polym. Sci., Polym. Phys. Ed.***1988**, *26*, 65.

78. Granier, T.; Thomas, E. L.; Gagnon, D. R.; Lenz, J. R. W.; Karasz, F. E. *J. Polym. Sci., Polym. Phys. Ed.* **1986**, *24*, 2793.

79. Bradley, D. D. C.; Friend, R. H.; Hartmann, T.; Marseglia, E. A.; Sokolowski, M. M.; Townsend, P. D. *Synth. Met.* **1987**, *17*, 473.

80. Chen, D.; Winokur, M. J.; Masse, M. A.; Karasz, F. E. *Polymer* **1992**, *33*, 3116.

81. Mao, G.; Fischer, J. E.; Karasz, F. E.; Winokur, M. J. *J. Chem. Phys.* **1993**, *98*, 712.

82. Friend, R. H.; Gymer, R.W.; Holmes, A. B.; Burroughes, J. H.; Marks, R.N.; Taliani, C.; Brad-ley, D. D. C.; Dos Santos, D. A.; Brédas, J. L.; Lögdlund, M.; Salaneck, W.R. *Nature* **1999**, *397*, 121.

83. Granström, M.; Berggren, M.; Inganäs, O. *Science* **1995**, *267*, 1479.

84. Malls, J. J. M.; Walsh, C. A.; Greenham, N. C.; Marseglia, E. A.; Friend, R. H.; Moratti, S. C.; Holmes, A. B. *Nature* **1995**, *376*, 498.

85. Kaino, T. ; Kurihare, T.; Saito, S.; Tsutsui, T.; Tokito, S. *Appl. Phys. Lett.* **1989**, *54*, 1619.

86. (a) Karasz, F. E.; Wnek, G. E.; Chien, J. C.; Liilya, C. P. *Polymer* **1979**, *20*, 1441. (b) Brédas, J. L.; Beljonne, D.; Shuai, J.; Toussaint, J. M. *Synth. Met.* **1991**, *43*, 3743. (c) Dai, L.; Winkler, B.; Dong, L.; Tong L.; Mau, A. W. H. *Adv. Mater.* **2001**, *13*, 915. (d) Burroughes, J. H.; Bradley, D. D. C.; Brown, A. R.; Marks, R. N.; MacKay, K. Friend, R. H., Burn P.L., Holmes, A. B. *Nature,* **1990**, *347*, 539. (e) Bernius, M. T.; Inbasekaran, M.; O'Brien, J.; Wu, W. *Adv. Mater.* **2000**, *12*, 1737. (f) Fumitomo, H.; Maria, A. D-G.; Schwartz, B. J.; Heeger, A. J. *Acc. Chem. Res.* **1997**, *30*, 430.

87. Hoffman, A. S. *Clin. Chem.* **2000**, *46*, 1478.

88. Duncan, R. *Nat. Rev. Drug Discovery,* **2003**, *2*, 347.

89. Delair, T.; Charles, M.-H.; Cros, P.; Laayoun, A.; Mandrand, B.; Pichot, C. *Polym. Adv. Technol.* **1998**, *9*, 349.

90. Lue, R. Y.; Chen, G. Y.; Hu, Y.; Zhu, Q.; Yao, S. Q. *J. Am. Chem. Soc.* **2004**, *126*, 1055.

91. Ashraf, S. S.; Benson, R. E.; Payne, E. S.; Halbleib, C. M.; Gron, H. *Protein. Expr. Purif.* **2004**, *33*, 238.

92. Chen, I.; Howarth, M.; Lin, W.; Ting, A. *Nat. Methods,* **2005**, *2*, 99.

93. Tan, J. F.; Ravi, P.; Too, H. P.; Hatton, T. A.; Tam, K. C. *Biomacromolecules,* **2005**, *6*, 498.

94. Salem, A. K.; Cannizzaro, S. M.; Davies, M. C.; Tendler, S. J. B.; Roberts, C. J.; Williams, P. M.; Shakessheff, K. M. *Biomacromolecules,* **2001**, *2*, 575.

95. Marek, M.; Kaiser, K.; Gruber, H. J. *Bioconjugate Chem.* **1997**, *8*, 560.

96. Huisgen, R. *1,3-Dipolar Cycloaddition Chemistry* ed.: A. Padwa, Wiley, New York, 1984, pp. 1–176.

97. Kolb, H. C.; Finn, M. G.; Sharpless, K. B. *Angew. Chem. Int. Ed.* **2001**, *40*, 2004.

98. Rostovtsev, V. V.; Green, L. G.; Fokin, V. V.; Sharpless, K. B. *Angew. Chem. Int. Ed.* **2002**, *41*, 2596.

99. Bock, V. D.; Hiemstra, H.; van Maarseveen, J. H. *Eur. J. Org. Chem.* **2006**, 51.

100. Gupta, S. S.; Kuzelka, J.; Singh, P.; Lewis, W. G.; Manchester, M.; Finn, M. G. *Bioconjugate Chem.* **2005**, *16*, 1572.

101. Kolb, H. C.; Sharpless, K. B. *Drug Discovery Today,* **2003**, *8*, 1128-1137.

102. Hawker, C. J.; Wooley, K. L. *Science,* **2005**, *309*, 1200.

103. Agard, N. J.; Baskin, J. M.; Prescher, J. A.; Lo, A.; Bertozzi, C. R. *ACS Chem. Biol.* **2006**, *1*, 644.

104. Beatty, K. E.; Xie, F.; Wang, Q.; Tirrell, D. A. *J. Am. Chem. Soc.* **2005**, *127*, 14150.

105. Wu, P.; Feldman, A. K.; Nugent, A. K.; Hawker, C. J.; Scheel, A.; Voit, B.; Pyun, J.; Frechet, M. J.; Sharpless, K. B.; Fokin, V. V. *Angew. Chem. Int. Ed.* **2004**, *43*, 3928.

106. Such, G. K.; Quinn, J. F.; Quinn, A.; Tjipto, E.; Caruso, F. *J. Am. Chem. Soc.* **2006**, *128*, 9318.

107. Nandivada, H.; Chen, H.; Bondarenko, L.; Lahann, J. *Angew. Chem. Int. Ed.* **2006**, *45*, 3360.

108. Gao, H.; Matyjaszewski, K. *Macromolecules,* **2006**, *39*, 4960.

109. Riva, R.; Schmeits, S.; Stoffelbach, F.; Jerome, C.; Jerome, R.; Lecomte, P. *Chem. Commun.* **2005**, *42*, 5334.

110. van Steenis, Dirk Jan V. C.; David, Olivier R. P.; van Strijdonck, Gino P. F.; van Maarseveen, Jan H.; Reek, Joost N. H. *Chem. Commun.* **2005**, *34*, 4333.

111. Englert, B. C.; Bakbak, S.; Bunz, U. H. F. *Macromolecules,* **2005**, *38*, 5868.

112. Punna, S.; Diaz, D. D.; Li, C.; Sharpless, K. B.; Fokin, V. V.; Finn, M. G. *Polymer Preprints,* **2004**, *45*, 778.

113. Gupta, S. S.; Raja, K. S.; Kaltgrad, E.; Strable, E.; Finn, M. G. *Chem. Commun.* **2005**, *34*, 4315.

114. Brennan, J. L.; Hatzakis, N. S.; Tshikhudo, T. R.; Dirvianskyte, N.; Razumas, V.; Patkar, S.; Vind, J.; Svendsen, A.; Nolte, R. J. M.; Rowan, A. E.; Brust, M. *Bioconjugate Chem.* **2000**, *17*, 1373.

115. Kohn, M.; Wacker, R. Peters, C.; Schroder, H.; Soulere, L.; Breinbauer, R.; Niemeyer, C. M.; Waldmann, H. *Angew.Chem. Int. Ed.* **2003**, *42*, 5830.

116. Vundyala, N.; Sun, C.; Sidime, F.; Shi, W.; L'Amoreaux, W.; Raja, K. S.; Peetz, M. R. *Tetrahedron Letters*, **2008**, *49 (45)*, 6386.

117. George, S.J. and Ajayaghosh A. *Chem.Eur.J.* **2005**, 11, 3217.

118. Wang, B.; Wassielewski, M.R. *J. Am. Chem. Soc.* **1997**, *119*, 12.

119. Peetz, R. M.; Strachota, A.; Thorn-Csanyi, E. *Macromol. Chem. Phys.*, **2003**, *204*, 1439.

120. Narwark, O. Dissertation, University of Hamburg, **2002**.

121. Peetz, R. M.; Strachota, A.; Thorn-Csányi, E. *Macromol.Chem.Phys.,* **2003**, *204*, 1439.

122. Sen Gupta, S.; Raja, K. S.; Kaltgrad, E.; Strable, E.; Finn, M. G. *Chem. Commun.* **2005**, *34*, 4315.

123. Sakaue H.; Fujiwara S.; Shingubara S.; Takahagi T. *Appl. Phys.Lett.* **2001**, *78*, 309.

124. Zhu, X.-Y.; Boiadjiev, V.; Mulder, J. A.; Hsung, R. P.; Major, R. C. *Langmuir* **2000**, *16*, 6766.

125 Xu, F. J.; Cai, Q. J.; Kang, E. T.; Neoh, K. G. *Langmuir* **2005**, *21(8)*, 3221.

126. Hacker, A. C.; Anderson, A. K.; Richter, J. L.; Richter, A. C. *Langmuir* **2005**, *21*, 882.

127. Hooper, N.; Beeching, L. J.; Dyke, J. M.; Morris, A.; Ogden, J. S.; Dias, A. A.; Costa, M. L.; Barros, M. T.; Cabral, M. H.; Moutinho, A. M. C. *J. Phys. Chem. A,* **2002**, *106 (42)*, 9968.